http://researchcommons.waikato.ac.nz/

Research Commons at the University of Waikato

Copyright Statement:

The digital copy of this thesis is protected by the Copyright Act 1994 (New Zealand).

The thesis may be consulted by you, provided you comply with the provisions of the Act and the following conditions of use:

- Any use you make of these documents or images must be for research or private study purposes only, and you may not make them available to any other person.
- Authors control the copyright of their thesis. You will recognise the author's right to be identified as the author of the thesis, and due acknowledgement will be made to the author where appropriate.
- You will obtain the author's permission before publishing any material from the thesis.

Hypsometry of New Zealand estuaries

A thesis submitted in partial fulfilment

of the requirements for the degree

of

Masters of Science

in Earth Sciences

at

The University of Waikato

by

Berengere Dejeans

The University of Waikato

2016

THE UNIVERSITY OF
WAIKATO
Te Whare Wānanga o Waikato

Abstract

Estuarine morphology is constantly changing because of continual sediment transport mainly driven by tidal asymmetry and wind waves. For modelling purposes, intertidal areas have often been simplified to relatively semi-circular basins. Although suitable for providing a preliminary understanding of processes, this approach does not take into account the real curvature of natural basins. One way of studying the morphology of an estuary is to use its hypsometry. This quantity, often represented as a curve, describes the area-weighted distribution of depth and therefore includes the uneven form of a basin. Overseas studies have shown that the shape of the hypsometric curve of an estuary can be used as a measure of its state of infilling.

The present study focuses on the morphology of New Zealand estuaries by comparing their hypsometric curves and examining the relative contribution of various forcing factors towards the shape of these curves and consequently towards the development of the morphology. I applied the hypsometric relationship defined by Boon & Byrne (1981) in order to assess how well it describes New Zealand estuaries and what factors influence the shape of the hypsometric curve. Their equation introduces the empirical parameter γ which controls the concavity of the curve. Area-depth curves were computed using bathymetric data for the 22 studied estuaries. The best fitting curves relative to Boon & Byrne's relationship were determined by minimising the error between the modelled and observed curves and provided a measure of γ for each site. This relationship appeared to be relatively satisfactory (error of less than 5%) for most estuaries. A database was created where the tidal range, the length of the longest fetch, the length of the fetch along the direction of most common winds, the wind speed and the significant wave height were stored for each study estuary. The impact of each parameter was estimated using statistical clustering analysis. No clear correlation could be identified. Conversely the results suggest that estuaries with the same environmental conditions could present very different values of γ. Current data, sedimentation accumulation rates and proportion of intertidal area at high water were also collected which enabled to observe that for some study sites the value of γ seems to be a reasonable indicator of the degree of infilling.

However there were exceptions and some sites with higher γ were in an advanced state of infilling. This suggests that even though Boon & Byrne's relationship provides a reasonable representation of the hypsometry of New Zealand estuaries, the parameter γ does not seem to be a satisfactory measure of infilling of New Zealand estuaries. The present study also showed that when comparing with studies conducted in the United Kingdom and in the United Stated it appeared that the values of γ estimated for New Zealand estuaries are in the whole higher than overseas. This could be attributed to the fact that New Zealand basins are relatively young systems but also could be due to other specificities of those basins such as the influence of the geology.

Acknowledgements

I first would like to express my sincere gratitude and thanks to my supervisor Associate Professor Karin Bryan for all her guidance and support all along this project. I particularly appreciated her patience, encouragement and enthusiasm. Her help has truly been invaluable.

Besides my supervisor I would like to thank Steve Hunt for all his help during my thesis not only for providing data but also for taking time to exchange about the interpretation.

I also want to thank NIWA and especially Dr Malcolm Green and Glen Reeve for their time and for sharing bathymetric data.

I also want to thank the Waikato Regional Council and especially Dr Cathy Liu and Dr Hannah Jones for taking the time and sharing bathymetric data necessary to this project.

I also wish to thank ECoast and MetOcean and especially Dr Shaw Mead (ECoast), Dougal Greer (ECoast), Dr Sarah Gardiner (MetOcean) and Juliana Miranda (MetOcean) for taking the time to meet me and letting me access their bathymetric data to compute the corresponding hypsometry.

I also want to thank Dr Terry Hume for the data he provided.

I also would like to thank Bradley Monahan for providing bathymetric data for Tauranga.

I also wish to acknowledge Dirk Immenga for the provided current data for Raglan estuary.

Finally I wish to address my personal thanks to my friends and fellow students for their welcome when I arrived in New Zealand and their support throughout the past year and a half.

Table of Contents

List of Figures

List of Tables

List of Symbols

Symbol	Unit	Description
γ		Empirical coefficient
γ_1		Value of γ estimated with the first model
$\gamma_{2,h}$		Value of γ estimated with the second model for the part of the basin below MHWS
$\gamma_{2,l}$		Value of γ estimated with the second model for the part of the basin below MLWS
$\gamma_{2,m}$		Value of γ estimated with the second model for the part of the basin below the average tidal level
$\gamma_{3,h}$		Value of γ estimated with the third model for the part of the basin below MHWS
$\gamma_{3,l}$		Value of γ estimated with the third model for the part of the basin below MLWS
$\gamma_{3,m}$		Value of γ estimated with the third model for the part of the basin below the average tidal level
ε_1	[%]	RMSE (Root-Mean Square Error) for the first model
$\varepsilon_{2,h}$	[%]	RMSE for the second model for the part of the basin below MHWS
$\varepsilon_{2,l}$	[%]	RMSE for the second model for the part of the basin below MLWS
$\varepsilon_{2,m}$	[%]	RMSE for the second model for the part of the basin below the average tidal level
$\varepsilon_{3,h}$	[%]	RMSE for the third model for the part of the basin below MHWS
$\varepsilon_{3,l}$	[%]	RMSE for the third model for the part of the basin below MLWS

$\varepsilon_{3,m}$	$[\%]$	RMSE for the third model for the part of the basin below the average tidal level
a	$[m^2]$	Area above elevation contour at elevation h
a_n		Dimensionless area a
A_{min}	$[m^2]$	Minimum area of basin
$A = A_{max}$	$[m^2]$	Cumulative basin area above lowest point of the basin
C	$[m.s^{-1}]$	Velocity of the tide
d	$[m]$	Constant depth (taken as an average of the depth of the flats)
F	$[m]$	Length of fetch
g	$[m.s^{-1}]$	Gravitational acceleration
h	$[m]$	Height above lowest point of the basin
h_n		Dimensionless height h
H	$[m]$	Height between lowest and highest points of the basin
H_w	$[m]$	Wave height
L	$[m]$	Tidal wavelength
r		Empirical coefficient giving the curvature of the basin
r_1		Value of r estimated with the first model
$r_{2,h}$		Value of r estimated with the second model for the part of the basin below MHWS
$r_{2,l}$		Value of r estimated with the second model for the part of the basin below MLWS
$r_{2,m}$		Value of r estimated with the second model for the part of the basin below the average tidal level
T	$[s]$	Tidal period
U_A	$[m.s^{-1}]$	Average wind speed
V	$[m^3]$	Volume of the basin

Chapter 1

Introduction

1.1. Introduction

According to Pritchard's (1967) definition, an estuary is a 'semi-enclosed coastal body of water which has a free connection with the open sea and within which sea water is measurably diluted with fresh water derived from land drainage'. They are at the interface between land and ocean and between fresh and salt water and so are exposed to conditions such as salinity variations, swell and intermittent flooding. This makes them highly valuable in terms of ecology (unique habitats) but also gives them economic (e.g tourism, species of commercial value) as well as cultural (e.g. recreational activities, support for scientific knowledge; Potter, 2001) significance.

Estuaries are dynamic environments whose morphology mostly results from the long-term net sediment transport coming both from the land and the coast. The main factors influencing estuarine morphology are the type of sediments and the combination of river, waves and tidal processes whose importance varies from an estuary to the other. On the long time scale, sediments accumulate in estuaries until they are completely infilled (Dronkers, 1986; Masselink *et al.*, 2014).

One way of describing the morphology of a basin is to calculate its hypsometry, which describes the distribution of horizontal surface with respect to elevation. Hypsometry can be particularly useful for modelling since it describes the curvature of a shoreline with more accuracy than a simple linear function would do (Boon & Byrne, 1981). Over the years, several formal relationships have been developed to describe hypsometry (e.g. Strahler, 1952; Wang *et al.*, 2002). The present study focuses on a relationship derived by Boon (1975) and Boon & Byrne (1981), which uses two empirical coefficients to give the hypsometric curves a sigmoidal shape. The first coefficient, referred to as r, gives the curvature of the basin. The second coefficient, γ, has been used as a measure

of infilling for estuaries in various studies (e.g. Boon & Byrne, 1981; Gardiner *et al.*, 2011; Hunt *et al.*, 2015; Moore *et al.*, 2009). Boon & Byrne's relationship has notably been used by Townend (2008) who showed it gave a reasonable representation of estuaries in the United Kingdom.

1.2. Research aim and objectives

The aim of this thesis is to determine whether New Zealand estuaries are well-described by Boon & Byrne's equation. More precisely three objectives are pursued:

1. Can Boon & Byrne's equation fit the observed hypsometry of New Zealand estuaries?

2. What is the relative role played by external factors (waves, tidal range) in controlling the shape of the hypsometric curve? More precisely can external forcing parameters explain the variation in values of γ?

3. Can the value of γ be used as a measure of infilling for New Zealand estuaries?

1.3. Thesis outline

The next chapter, **Chapter Two**, is a literature review which gives some background regarding the theory of estuarine infilling which shapes the morphology of estuaries. It also describes how hypsometry has been used in past studies including some details of the methods adopted to compute this quantity, with a particular focus on the study conducted by Boon & Byrne in 1981. A quick overview of more recent findings regarding factors influencing hypsometry is also given.

Chapter Three details the methodology adopted in order to compute the hypsometric data. More precisely it describes the development of a Graphical User Interface (GUI) which aimed to help a user generate hypsometric curves from a gridded bathymetry.

Chapter Four shows the hypsometry distribution of the study sites. First the observed hypsometries are presented and used to find the combination of the two empirical parameters that give the best fit of Boon & Byrne's relationship to the observed hypsometry.

Different forcing factors which are likely to have an influence on the shape of hypsometric curves are presented **Chapter Five**. Statistical clustering analyses was conducted in order to identify potential correlations between the values of the study forcing factors and the values of γ estimated in Chapter Four.

In **Chapter Six,** the degree of infilling of the study sites is estimated in order to assess whether it can be correlated to the values of γ. To do so, sedimentation accumulation rates, current data and proportion of intertidal are calculated or derived from previous studies.

Chapter Seven summarizes and discusses the results presented in the previous chapters. Some limitations of the study are also noted. The final section of this chapter gives an overview of the findings of the present study.

Chapter 2

Literature review

This chapter overviews the background literature on estuarine morphology. More precisely, it focuses on the estuarine infilling 'traditional' theory and introduces the concept of hypsometry including some examples of application.

2.1. Introduction

New Zealand's estuaries started to form at the end of the postglacial marine transgression, about 6 500 years ago, which was caused by the sea level rise associated with global warming. Sea level has risen approximately 150 meters and flooded the land (Hume & Swales, 2003; Masselink *et al.*, 2011). Estuaries are complex systems and very different from one to the other, due to the association of coastal processes (interaction between tides, waves and river) and other processes, such as flocculation (Masselink *et al.*, 2011). One classification was proposed by Hume *et al.* in 2007, called Estuary Environment Classification (EEC), where different levels are defined, each one focusing on particular aspects of such features (global scale processes, hydrodynamics processes and catchment processes). Figure 2.1 shows the distribution of estuaries in New Zealand, according to hydrodynamic processes (Hume *et al.*, 2007). This classification particularly shows that there are various types of estuaries in New Zealand which are often characterised by different morphologies. Estuarine morphology is greatly influenced by external factors and especially the tide and the waves which in turn are functions of the morphology (Dronkers, 1986).

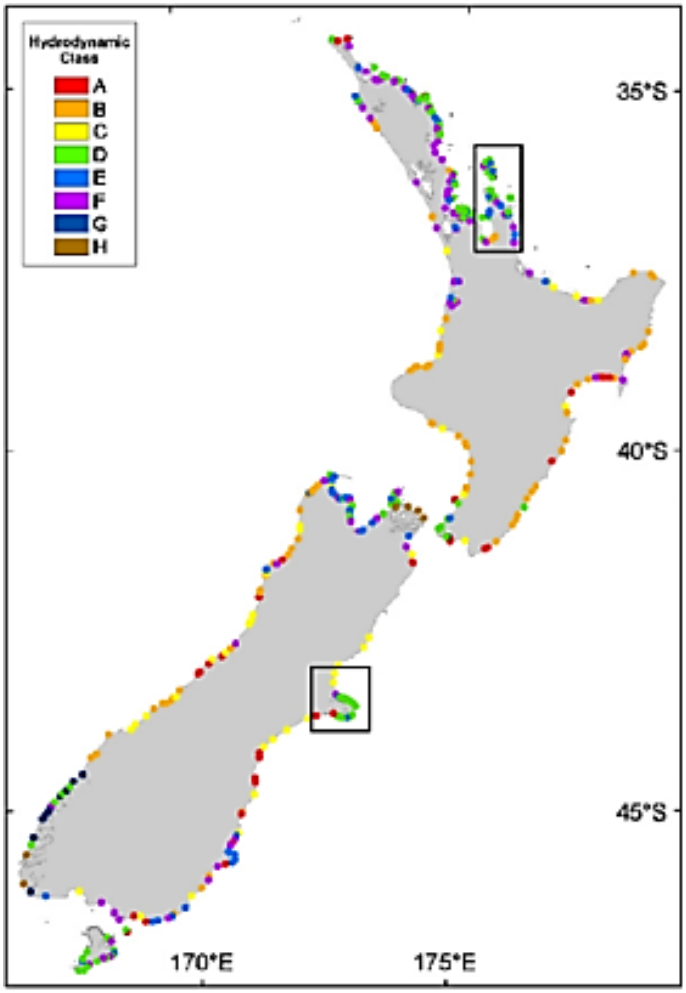

Figure 2. 1: Location of some estuaries in New Zealand and their classification at Level 2 (i.e. according to hydrodynamic processes) of the EEC, i.e. regarding hydrodynamic processes (Hume *et al*., 2007).

2.2. Evolution of estuarine morphology

Estuaries constantly evolve in shape, and progressively infill with sediments - a process which Hume & Swales (2003) call "aging". They reach temporary equilibrium states, but will keep filling up with sediments, with input from the sea and the land, until they eventually "die" (Dronkers, 1986; Hume & Swales, 2003). Morphology of estuaries results from the combination of tidal currents, waves, basin geometry, variations in relative sea level and sediment

supply (source, grain size and volume of sediments; Harris, 1988). Other factors also play a role in the morphodynamics of estuaries, for instance biological and anthropic activity (Friedrichs, 2011).

2.2.1 Estuary infilling theory

The morphology of an estuary is mostly shaped by the net sediment transport which mainly results from the differences of both magnitude and duration of the currents during the ebbing tide and the flooding tide. These are controlled by the distortion of the tide as it propagates within an estuary, and is often referred to the 'tidal asymmetry' (Dronkers, 1986). The tide behaves like a shallow-water wave. In particular, its velocity C can be expressed by the following equation (Equation 2.1; Masselink *et al.*, 2011):

$$C = \sqrt{gh} = \frac{L}{T} \qquad (Equation\ 2.1)$$

where g is the gravitational acceleration, h the water depth, L the tidal wavelength and T the tidal period.

Tidal distortion is especially common and important in the first stages of evolution (as the basin fills up with sediments) of estuaries. The ebb tide has then often a longer duration than the flood tide. The wave front steepens as it propagates inside the estuary (Figure 2.2; Masselink *et al.*, 2011). During the flooding tide, the water level increases so that the water depth under the crest is much larger than under the trough especially in the deep areas of the basin (e.g. channel). Therefore, as described by Equation 2.1, the crest will travel much faster than the trough (Figure 2.3; Masselink *et al.*, 2011). Yet, the discharge volume is conserved over a tidal cycle, which means the magnitude of the current will be higher during flood than during ebb to "compensate" for its smaller duration (Figure 2.4). This stage is called flood-dominance and results in an import of sediments, which increases the elevation of the intertidal part relative to the channels (Figure 2.4; Masselink *et al.*, 2011; Hunt *et al.*, 2015). This deposit of sediments makes the flats more and more shallow. This change of morphology

causes the average water depth to be larger at high tide than low tide (Figure 2.4c). The trough will therefore travel faster whereas the crest will slow down. The velocity of the flooding tide will decrease and its duration will increase. Consequently because of the conservation of the volume discharge mentioned before the ebb will in turn have a shorter duration and higher velocities (Figure 2.6; Masselink *et al.*, 2011).

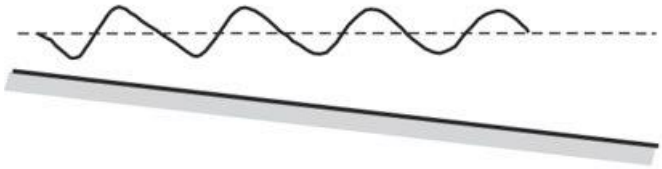

Figure 2. 2: Distortion (steepening) of the tidal wave as it progresses along the estuary (Masselink *et al.*, 2011).

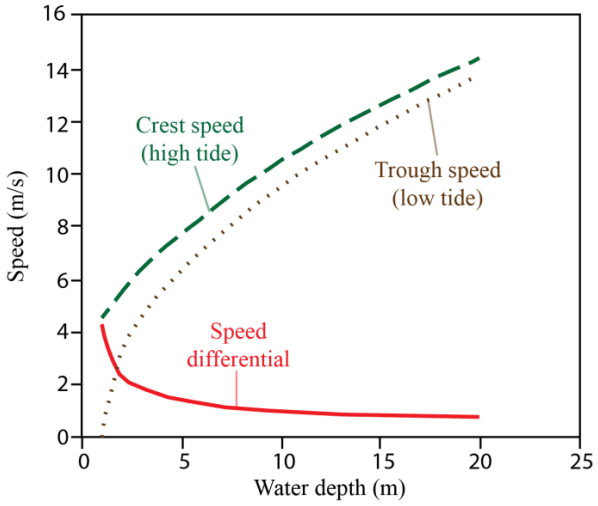

Figure 2. 3: Velocity of the crest (high tide) and trough (low tide) of a shallow water depth along with the differential of the two (Masselink *et al.*, 2011).

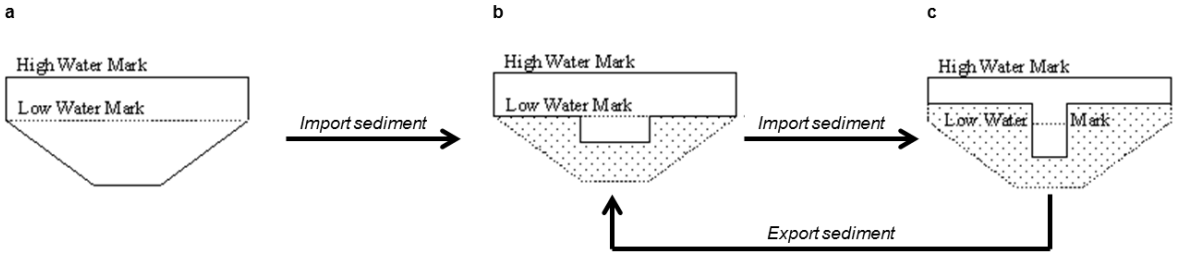

Figure 2. 4: Estuary infilling theory (modified from Pethick, 1994).

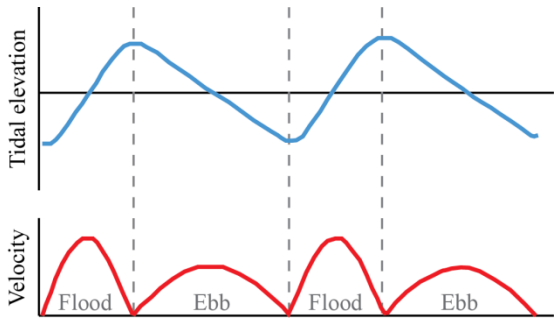

Figure 2. 5: Tidal water level and current velocity when flood-dominance which occurs when an estuary reaches the configuration shown in Figure 2.4b. Scales are arbitrary (Masselink *et al.*, 2011).

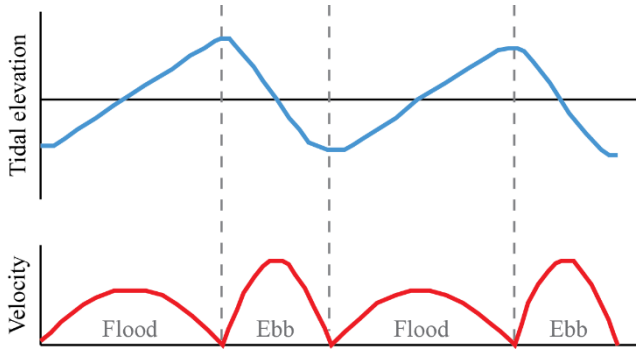

Figure 2. 6: Tidal water level and current velocity when ebb-dominance occurring when the basin is infilled (configuration shown in Figure 2,4c). Scales are arbitrary (Masselink *et al.*, 2011).

2.2.2 Factors controlling the net sediment supply (and therefore the estuarine morphology)

Estuarine morphology is a function of sediment supply, which (along with catchment input) is determined by tidal forcing and waves, which, reciprocally, depend upon the morphology of the estuary (Figure 2.7; Friedrichs, 2011). As stated above, the morphology of estuaries is in perpetual evolution and estuaries are progressively filling with sediments. Infilling is however uneven over time and space. Indeed, the deposition of sediments is a function of many various

parameters and varies both in terms of nature of deposited materials and deposition rate. On the one hand, the quantity of accumulated sediments will be limited by the amount of sediments available, the shape and size of the basin (and, more precisely, the estuarine depth) as well as the subsidence, caused by local rises of sea level. On the other hand, the rate or pattern of infilling will be mainly defined by the tides, the waves and the sediments type, which will influence the intensity of transport mechanisms (Perillo, 1995; Wang *et al.*, 2002; Hume & Swales, 2003).

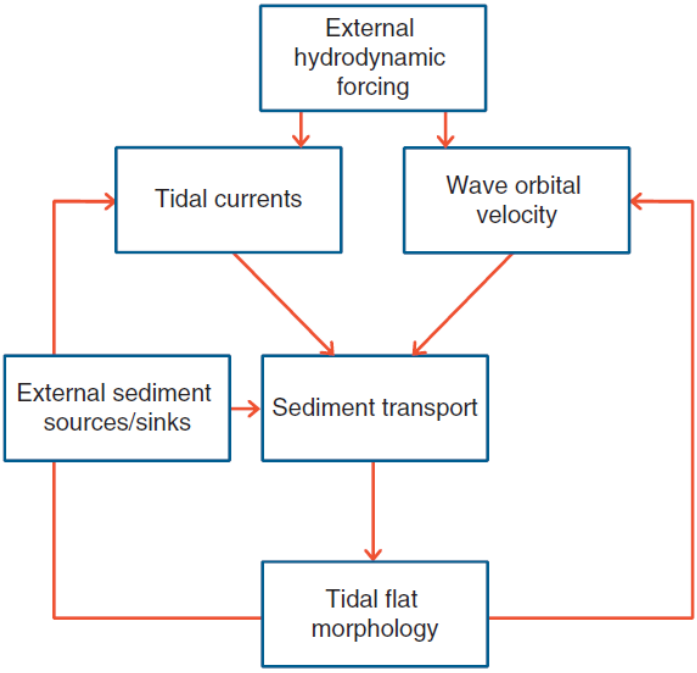

Figure 2. 7: Simplified morphodynamic components influencing tidal flat evolution (Friedrichs, 2011).

2.2.2.1 Tidal asymmetries

Tidal asymmetry is one of the most important parameter that controls the net sediment transport. It can be divided into two types, which are temporal and spatial asymmetries (Friedrichs, 2011). The temporal asymmetries, also called Eulerian effects, refer to the differences in velocities between the flood and the ebb tidal currents, which are notably caused by the distortion of the tidal wave both as it enters and spreads inside the estuary (Dronkers, 1986 ; Friedrichs &

Aubrey, 1988 ; Hunt *et al.*, 2015). Spatial asymmetries (or Lagrangian effects) mainly stem from the combination of fluctuations of hydrodynamic energy and time lags between bed stress and depth-integrated suspended sediment concentration. First, the tide will mobilize particles from an area of high concentration to an area of a lower concentration (Figure 2.8). However, the particles will need time to deposit on the bed, causing an excess of sediments. Conversely, the tide will then take the sediments to an area of a higher concentration (Figure 2.8), but the resuspension of the particles will not be immediate either, hence a deficit of sediments. These two time lags result in a net transport of sediment toward areas of lower energy (Friedrichs, 2011). When describing the asymmetry-induced sediment transport in estuaries, Dronkers (1986) divided sediments into two categories: coarse (diameter of about 200 µm or more) and fine (usually particles between 1 and 10 µm that can combine and form aggregates). For both categories, he also distinguishes between bed load and suspended transport. Thus, tides do not affect all types of sediments the same way. Indeed, the bed load transport of the coarse portion will not be altered a lot by tidal asymmetry, since those particles mainly move by rolling, sliding and saltating, and remain very close to the bottom of the ocean. More importantly, they respond immediately to the current orientation, direction and velocities of the area. The suspended portion, however, does not only depend on the current characteristics but is also affected by the vertical concentration of sediments (Ridderinkhof, 1997). The bigger the current velocity is, the more important the saturation load of sediment will be. Therefore, when ebb duration is shorter than flood duration, bigger velocities are reached during ebb compared to flood, and the suspended coarse sediments will globally be exported rather than deposited (Dronkers, 1986 ; Hunt *et al.*, 2015). On the other hand, fine sediments tend to deposit around the slack water periods, whose duration will therefore affect the transport. More precisely, the suspended portion will depends upon the slack duration, which refers to the period of time when the depth-averaged velocity is too small to mobilize sediments (Dronkers, 1986 ; Hunt *et al.*, 2015).

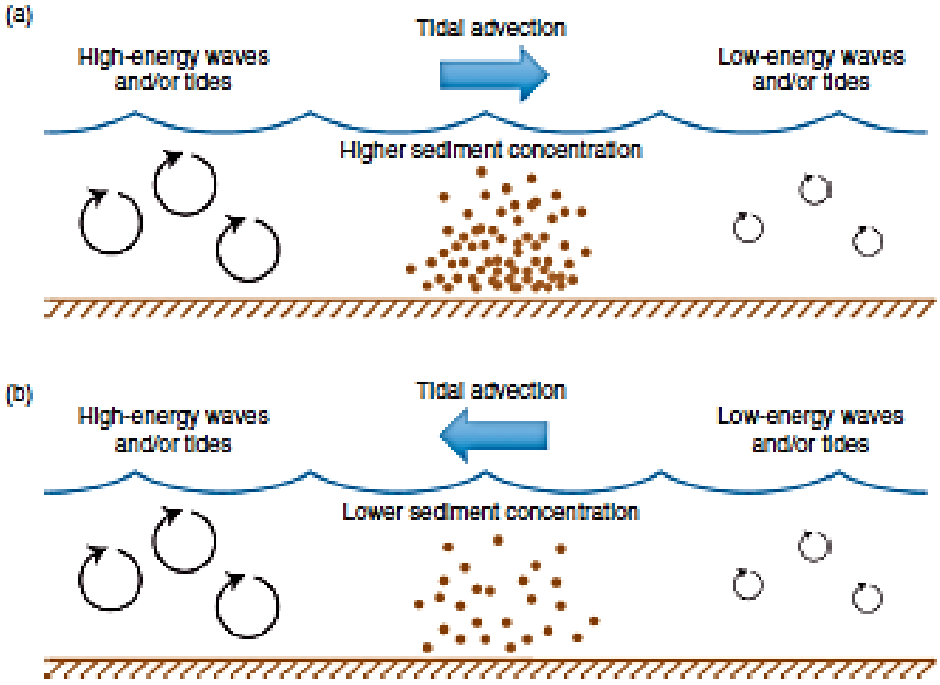

Figure 2. 8: Because suspended sediments concentration lag behind instantaneous bottom stress, a) tidal currents moving away from areas of higher energy will carry more sediment than b) tidal currents moving away from areas of lower energy (Friedrichs, 2011).

2.2.2.2 Wind waves

It is now well-established that tidal asymmetries play a great role in the net sediment transport in estuaries, but another major factor influencing this phenomenon is the wind-induced waves ("wind waves"; Green *et al.*, 1997; Hunt *et al.*, 2015). The contribution of wave to net sediment transport has been studied and proven to be significant (Green & Coco, 2007; Hunt *et al.*, 2015). Indeed, they are responsible for erosion of tidal flats, which provides a source of suspended sediments. They can then be exported from the estuary during ebb. To reuse the earlier distinction, the finer the sediments, the longer they will be transported seaward. Yet, even if the coarse sediments are transported less far during ebb, the flood flow will not be able to mobilize and carry them landward as easily. Consequently, wind waves tend to favor a net export of both fine and coarse sediments from estuaries to the oceans (Dronkers, 1986). Waves and wave-

related processes are not constant over a tidal cycle and, like tidal asymmetries, are reciprocally linked to the estuarine morphology. Green *et al.* (1997) divided the variations in waves "intensity" and "kind". Indeed, the water depth relative to the wavelength of waves enables the emergence and submergence of intertidal regions, which leads to variations in the fetch, directly influencing the waves intensity, and especially their height. Besides, the turbid fringe that arrives causes a variation in the relationship linking turbidity to wave-orbital velocity, hence an evolution of dynamics (Green *et al.*, 1997).

2.3. Hypsometry

2.3.1. General interest: Why study hypsometry?

Topography, or shape, is a critical parameter when studying drainage basins in general and estuaries in particular, hence the need to describe and quantify it (Langbein, 1947). As described in the previous section, estuarine morphologies are constantly evolving. The changes being spatially unevenly distributed and cause tidal asymmetries, which take part in the evolution of the morphology in question (Figure 2.9, Friedrichs, 2011).

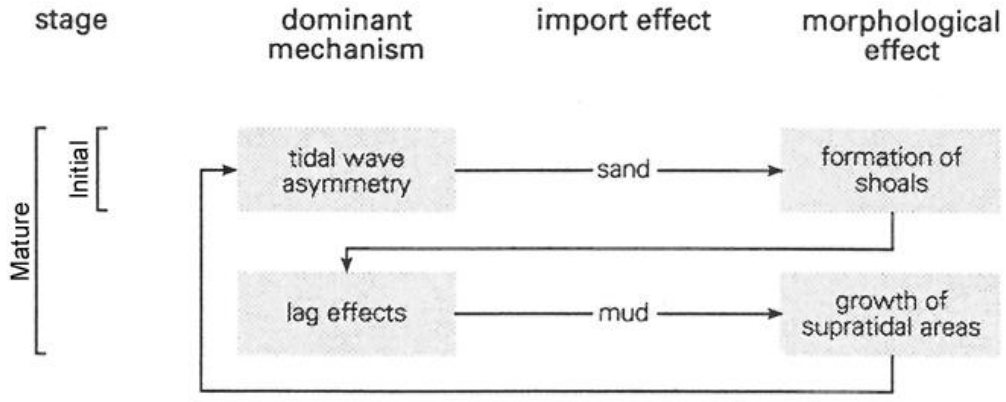

Figure 2. 9: Reciprocal effects of tidal asymmetry on morphology (Nordstrom & Roman, 1996).

One interesting measure that can provide insight into how estuarine morphology developed is its hypsometry. A large number of studies conducted in the early 80s or before assumed that estuary basins were a mere reservoir where sediments could accumulate, which, although an appropriate approximation in some cases, leaves aside the uneven shape of the estuary. More particularly, the basin surface was often considered as a steady quasi-semicircular plan (Keugelan, 1967). The tide distortion, mainly due to the basin form, was therefore not taken into account. However, according to Seelig & Sorensen (1978), considering the surface area as a function of height has led to different results regarding the temporal distribution of flow rates. As a result, studying the hypsometry, namely the "distribution of horizontal surface area with respect to elevation" (Friedrichs & Aubrey, 1996), allows inclusion of the geomorphology of estuarine basins more accurately. In 1952, Strahler describes how hypsometry has been and could be used in varied fields, such as hydrology, soil erosion and sedimentation, as well as military science.

2.3.2. Hypsometric curves: Principle and some examples

2.3.2.1. Hypsometric curves: Principle

The most convenient way of expressing hypsometry is to plot the hypsometric curves (Langbein, 1947). Strahler was the first to define this concept of hypsometry in terms of geomorphology, in 1952. The plot is a cumulative curve, where the y-axis represents the elevation and the y-axis is for the area ("horizontal slices of the topography at any given elevation" (Strahler, 1952)). He distinguishes hypsographic curves, which use data in absolute units of measure from hypsometric curve, where the data are made dimensionless. This was to allow easy comparison of two basins even when they have very different size. The plotted values will therefore vary between 0 and 1 in both abscissa and ordinates (Figure 2.10). Strahler (1952) explains that a basin, whose volume is V, may be

compared to k (k natural number) horizontal slabs, which are piled vertically. Each slab i ($i \in [\![1 ; k]\!]$) has a volume ΔV_i and a thickness Δh_i (Figure 2.11).

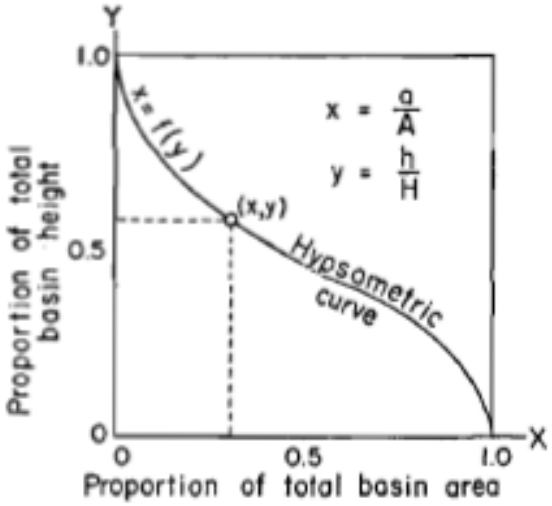

Figure 2. 10: Example of hypsometric curve (Strahler, 1952).

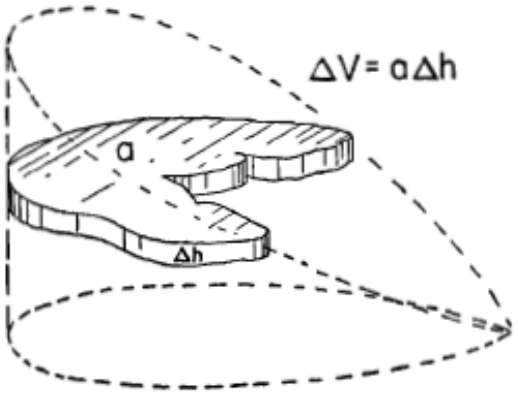

Figure 2. 11: Division of a basin (Strahler, 1952).

The question that arises then is that of the function which best describes the relationship between the basin area and height. A simple linear relationship would assume that the contours of the basin are parallel and constant (Boon & Byrne, 1981). Strahler (1952) observed the hypsometry of drainage basins and derived the relationship given in Equation 2.2, whose symbols are defined in

Table 2.1. The parameters used are dimensionless so that comparisons of the hypsometry of various environments can be made. Equation 2.2 describes a curve whose sinuosity fluctuates a lot; in particular, it is concave if the upper parts (smallest areas of the basin) and convex in the lower parts (largest areas). The degree of curvature is quantified with the value of r: high values of r corresponds to curve with a small degree of sinuosity. Examples of curves generated by Equation 2.2 given different values of z are given in Figure 2.12.

$$\frac{h}{H} = \left[\frac{A_{max} - a}{a} \cdot \frac{A_{min}}{A_{max} - A_{min}}\right]^z \quad with\ r = \frac{a}{A_{max}} \qquad (Equation\ 2.2)$$

Table 2. 1 : Parameters used to define the hypsometry of estuaries

Symbol	Parameter
a	Basin area above elevation h
$A_{max} = A$	Maximum basin area
A_{min}	Minimum basin area
h	Height above minimum basin elevation
H	Interval between peak and minimum basin elevation
r	Amount of basin curvature regarding slope at the point of inflection (determined empirically)
z	Positive exponent controlling relative volume of solids in basin (area below hypsometric curve)
$\frac{1}{z} = \gamma$	Exponent determining the general location of the curve (determined empirically)

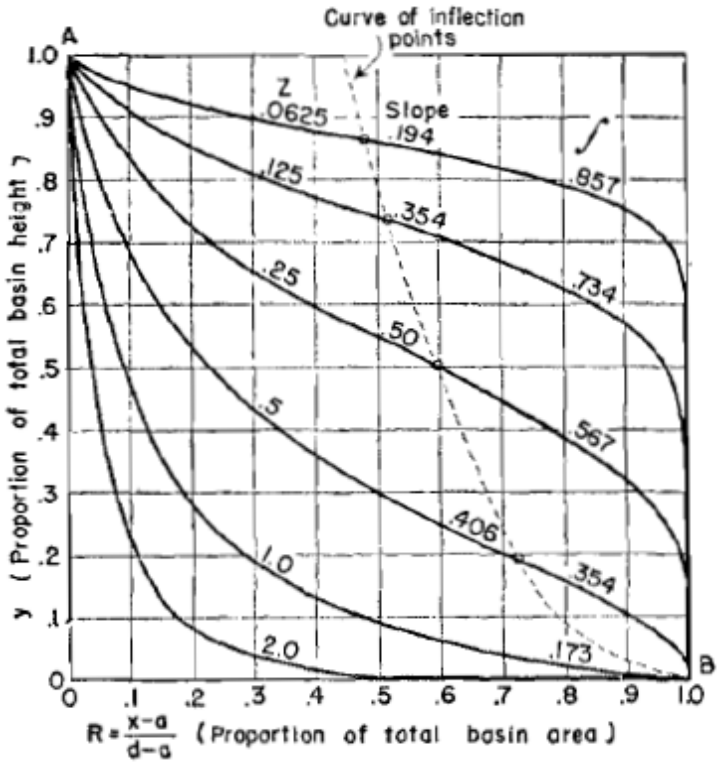

Figure 2. 12: Examples of a family of curves for a particular value of r = 0.1 (Strahler, 1952).

In 1975, Boon defined a new formula for hypsometry (Equations 2.3 and 2.4), derived from Strahler's one (Equation 2.2). Details of the symbols are given in Table 2.1 and Figure 2.13).

$$\frac{a}{A} = \frac{G}{[r + G(1-r)]} \qquad (Equation\ 3)$$

$$\text{with } G = \left(1 - \frac{h}{H}\right)^{\gamma} \qquad (Equation\ 4)$$

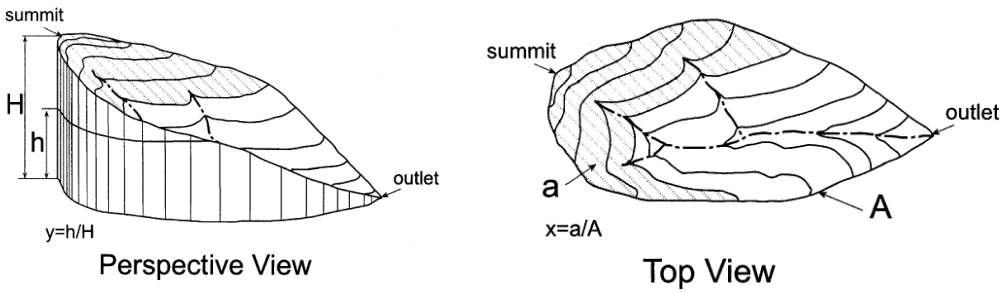

Figure 2. 13: Parameters h, H, a and A (Luo, 1998).

The shape of the hypsometric curve can be affected by the curvature of the studied shoreline (Figure 2.14, Boon & Byrne, 1981), the tidal range, wind-induced waves and whether the net sediment transport is positive (accretion) or negative (erosion; Table 2.2; Friedrichs & Aubrey, 1988). Moreover, the area below the curve (dependent on γ) gives the volume of sediment in the basin, and therefore provides information regarding its maturity. Thus, a small (respectively large) γ will correspond to a large (respectively small) volume of sediments within the intertidal zone, hence a mature (respectively young), ebb-dominant (respectively flood-dominant) estuary (Dronkers, 1986; Hunt *et al.*, 2015).

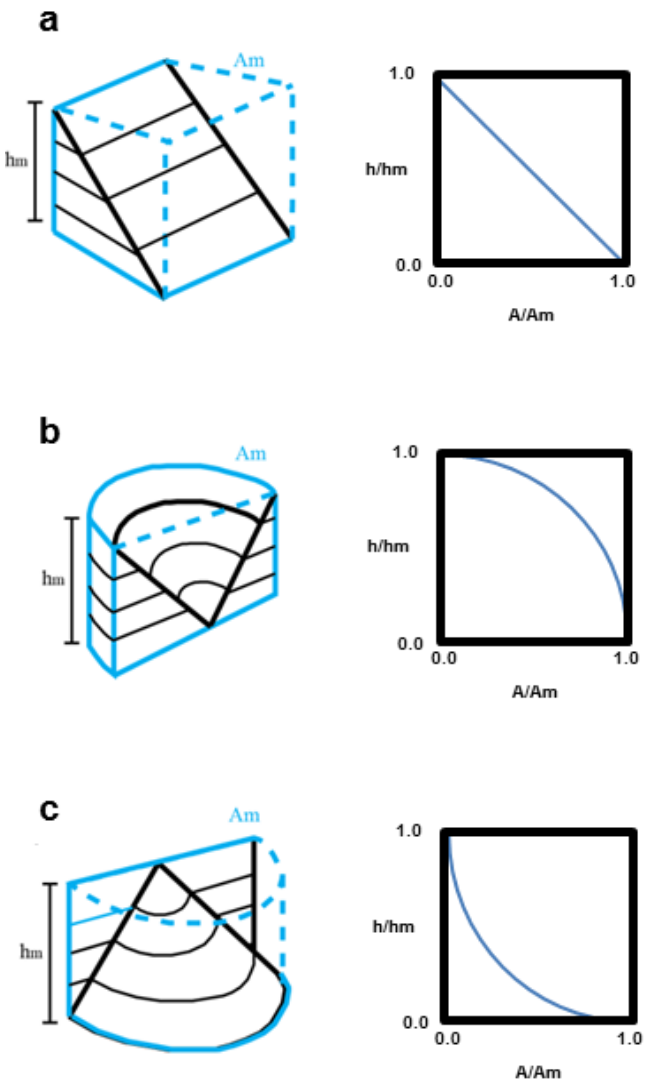

Figure 2. 14: Block diagrams of topographies giving the global shape of the hypsometric curve of a) a straight shoreline (linear hypsometry), b) an embayed shoreline (convex hypsometry) and c) a lobate shoreline (concave hypsometry; modified from Friedrichs & Aubrey, 1988).

Table 2. 2: Rough relationship between factors and concavity.

Factor	**Hypsometry**		**Source**
	More concave	***More convex***	
Shoreline curvature	Lobate	Embayed	Boon & Byrne (1981)
Tidal range	Lower	Higher	Dieckmann *et al*. (1987)
Long-term sediment transport dynamic	Erosion	Accretion	Kirby (1992)
Exposure to wind wave activity	More important	Little important	Wells & Park (1992)
"Maturity"	Immature, unfilled estuary	More mature, infilled estuary	Boon & Byrne (1981)

Friedrichs & Aubrey (1996) grouped the tidal currents and wind waves together by computing the ratio of tidal to wave activity. A high ratio will favour a convex hypsometry and, conversely, a low ratio will correspond to a concave hypsometry. Comparison between several studies (Dieckmann *et al.*, 1987, Wells & Park, 1992) however showed that this relationship depends on the environment and, in particular, on how the tidal ranges and wave activity vary.

2.3.2.2. Some examples of applications of hypsometry

Hypsometry has been widely used in studies involving the geomorphology and can serve different purposes. Indeed, one of its main advantages is that such approach provides a good approximation of the geomorphology (Boon & Byrne, 1981). It allows assessment of the effects of external factors the shape of study areas in different environments, such as mountains (e.g. Masek *et al*., 1994). A lot of work on drainage basins involves hypsometric analysis in order to study hydrodynamics and morphodynamics (e.g. Boon & Byrne, 1981; Eiser & Kjerfve, 1986), as well as for ecology and environmental considerations (Kirby, 2000; Oertel, 2001). For instance, in 1947, Langbein carried out a quantitative analysis

of the river flows in about 340 drainage basins in the northeastern United States, to estimate the relative contribution of several potential factors of river floods, including climate, soil, vegetation and topography. When they focused on the slope of the basins, they plotted the altitude with regard to sea level in some places, and then interpolated the hypsometric curves. They notably used these curves for snow surveys to approximate the mean depth of covering snow.

The use of hypsometry and especially its accuracy have improved a lot since the first studies with the development of technologies (e.g. Lidar) and computing tools enabling collection of more accurate topographic data (Townend, 2008). Indeed to get the hypsometric data, Strahler (1952) used topographic maps. Once the drainage basins were selected, he measured the area of the basin and the areas between each two consecutive topographic lines (contours), using a planimeter. He then determined the distance between the basin mouth and the summit point and the height of each contour. After calculating the ratios (dimensionless areas and heights), he plotted them and drew a smooth curve linking all points. As stated in his paper, the accuracy of his results is mainly dependent upon the maps' scale and precision. Boon & Byrne (1981) carried out an hypsometric analysis to study the tide propagation and the flow in a tidal marsh environment. They used planimetering to get the elevations and corresponding areas of the study site. Once they plotted the dimensionless data, they used the formula modified by Boon (1975) to define possible fitting hypsometric curves and adjusted them (i.e. they "chose" the parameters r and γ that would best represent real conditions) by trial and error. Then, they used these parameters in a numerical model that was forced with a sinusoidal M2 tide (whose amplitude was based on tidal measurements) for different stages of development of their basin. Their studied proved the use of hypsometry was a more realistic approximation of the geomorphology, especially useful when modelling hydraulic response of a basin. The access to more accurate data has particularly helped Townend (2008) to 'test' Boon & Byrne's equation on UK estuaries showing their relationship gave a satisfactory representation of the observed hypsometry of his study sites.

Another point particularly relevant for the present study is that hypsometry is particularly used to get an indication of the degree of infilling of estuaries. This notion was seems to have been first introduced by Boon & Byrne (1981) who

related the values of γ (which defines the relative position of the hypsometric curve) to the stage of infilling (and therefore maturity) of their study site. More precisely they used higher values of γ to simulate earlier stage of development. In other words a young basin (unfilled) corresponds to low values of γ and as the estuary infills with sediments the value of γ increases. Boon & Byrne's relationship and was used in different studies (e.g. Gardiner *et al*., 2011; Hunt *et al*, 2015; Moore *et al*., 2009) which also used the corresponding value of γ as an indicator of the maturity of their study estuary usually considering that $\gamma \in [3.5,5]$ characterised a relatively young basin (little infilled) whereas $\gamma \in]0,2.5]$ characterised a more mature one (more infilled).

2.4. Concluding remarks on the literature review

Estuaries are in perpetual evolution and progressively infilling with sediments. Their morphology is mainly shaped by tidal asymmetries and wind-induced waves, which are, in turn, influenced by the morphology of the basin. A convenient way of studying the geomorphology of an environment is to define its hypsometry, which is the distribution of the horizontal surface with regard to elevation. Past studies proved hypsometry provided information regarding shoreline curvature, tidal range, long-term sediment transport, exposure to wind wave activity and maturity of a basin. Plotting such a curve for various environments using dimensionless parameters enables easy comparison between each other. It seems, however, that such comparisons have not been done on a large scale.

Different mathematical relationships have been developed and over the years to describe the hypsometry. Among them Boon & Byrne's (1981) seems to have been relatively widely used and proven satisfactory particularly in the US (e.g. Boon, 1975; Boon & Byrne, 1981) and in the UK (e.g. Townend, 2008). It is all the more convenient that one of the two fitting coefficients it introduces seems to be a measure of the maturity (degree of infilling) of an estuary.

Chapter 3

Methodology of Data Collection: Creation and Deployment of the Graphical User Interface Hypsometric tool

3.1 Introduction

This chapter describes the conception and the implementation of a Graphical User Interface (GUI), which was developed with the aim of collecting hypsometric data of New Zealand estuaries. It describes how the interface was created and how it works. The testing phase and the final deployment are then presented.

3.2 Aim of the tool: Collecting hypsometric data

In order to facilitate the collection of hypsometric data, an interface was created with MATLAB to read a model grid and calculate the corresponding hypsometry. Indeed, an easy way to compute the hypsometry of a basin is to use a gridded bathymetry; however such data often have a commercial value which prevents the raw model grids from being easily accessed. The purpose of making an interface was therefore for the user to be able to generate the hypsometry of a site with ease, even if he or she is not familiar with this quantity, and share it without having to provide the raw model grid. The tool was also required to meet three criterion: to be easy to use; to be understandable (which means the user needs to be able to directly understand what he or she is expected to do); and to anticipate every possible scenario regarding the user behaviour.

3.3. Structure of the interface

The GUI was built with MATLAB. A GUI is ‘a graphical display in one or more windows containing controls, called *components*, that enable a user to perform interactive tasks’ (The MathWorks, Inc., 2015a). The final interface is basically a window which contains components (e.g. push buttons, check boxes), each of which calls for an external code (a callback) which instructs the computer to undertake a specific action. The GUI is run with MATLAB but does not require the user to have any previous knowledge of coding. Such an interface can be developed either interactively, which calls on both a figure window to display the component and a code file to define the callbacks, or programmatically, which means everything is defined within the code. The interactive approach was chosen, because it is easier when creating a moderately complex GUI (The MathWorks, Inc., 2015a). Indeed, it is based on the Graphical User Interface Development Environment (GUIDE), a development environment which contains tools that help lay out and program the GUI. This interactive approach relies on two main stages: the design, which is the layout of the GUI and the implementation, which refers to the connection of each component to a callback. A blank template of the interface was chosen to start with, which corresponds to a new blank figure window where components can be added (Figure 3.1). For this particular project, four different objects were chosen:

- Static texts: The texts are meant to give information to the user regarding what they need to do and simply explain the main actions of the GUI;
- Push buttons: When those buttons are pushed, one or several separate windows appear;
- Edit texts: Those components are editable by the user, who is required to provide a certain information; and
- Check boxes: Those components are displayed when the user needs to choose between two predefined options.

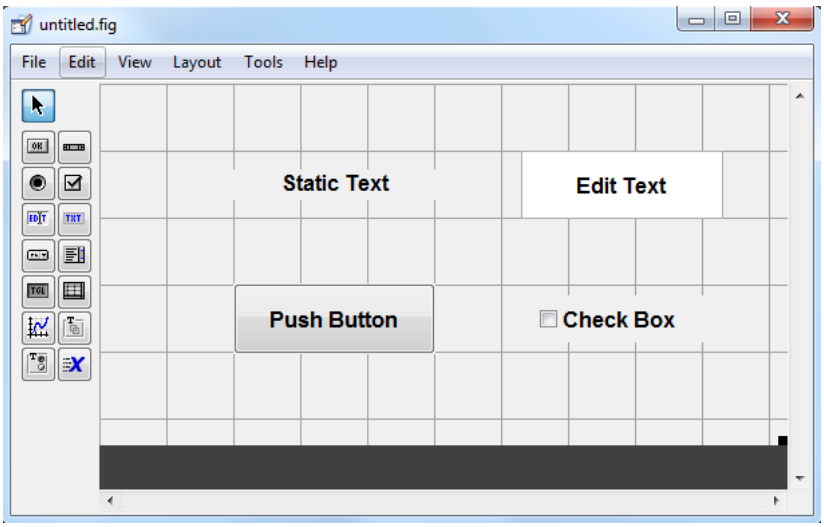

Figure 3. 1: GUI template and the four used components.

Each component is associated with a unique combination of properties (e.g. background color, size of the font), which can be modified (Figure 3.2). One key property is the 'tag': it corresponds to a string of characters which must be unique for each component (it works as an identifier of the component). This tag can then be used in the callback to refer to the element and particularly to get its handles. This will enable the user code the way he or she wants the component to behave hence the importance of this property. Once it is done, the figure can be saved, during which process the GUI generates two files: a FIG-file (.fig; Figure 3.3) corresponding to the layout and a code file (.m) which contains the MATLAB code (the callbacks) which will govern the behaviour of the GUI. At this stage, the M-file consists of an initialization code and a framework for every callback - the callbacks are still blank which means no action is performed yet when a component is triggered. Any modification of the code will be applied to the FIG-file, and vice versa. The next phase is therefore the implementation, which means coding the expected behaviour of each component (i.e. write the callbacks). All the components have a different identifier, referred to as a graphic handle. This handle is used, within the code, to get the properties of the corresponding object, and altering them if necessary (Glaze, 1998; The MathWorks, Inc., 2015a).

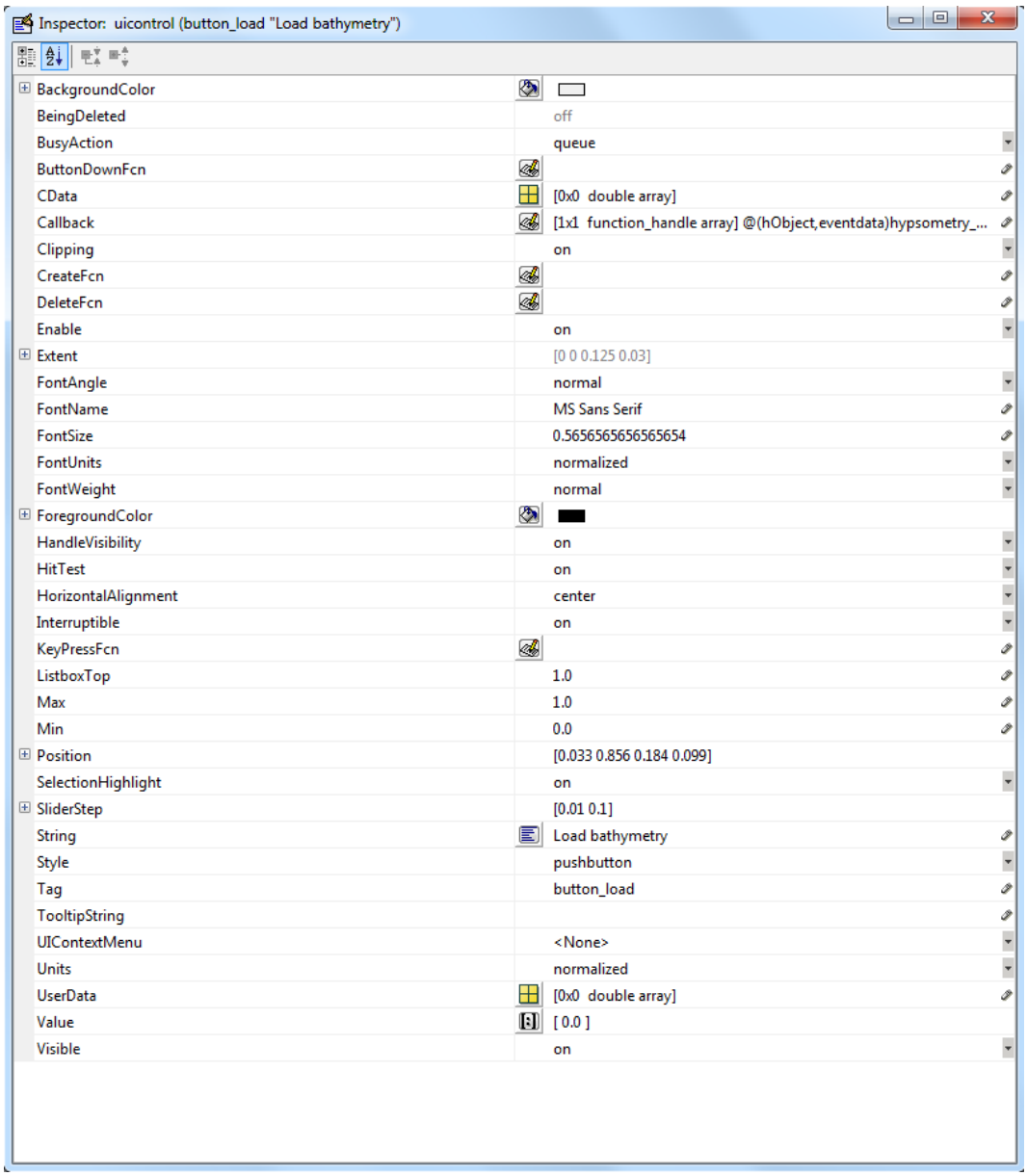

Figure 3. 2: Properties of GUI components - Example of a push button.

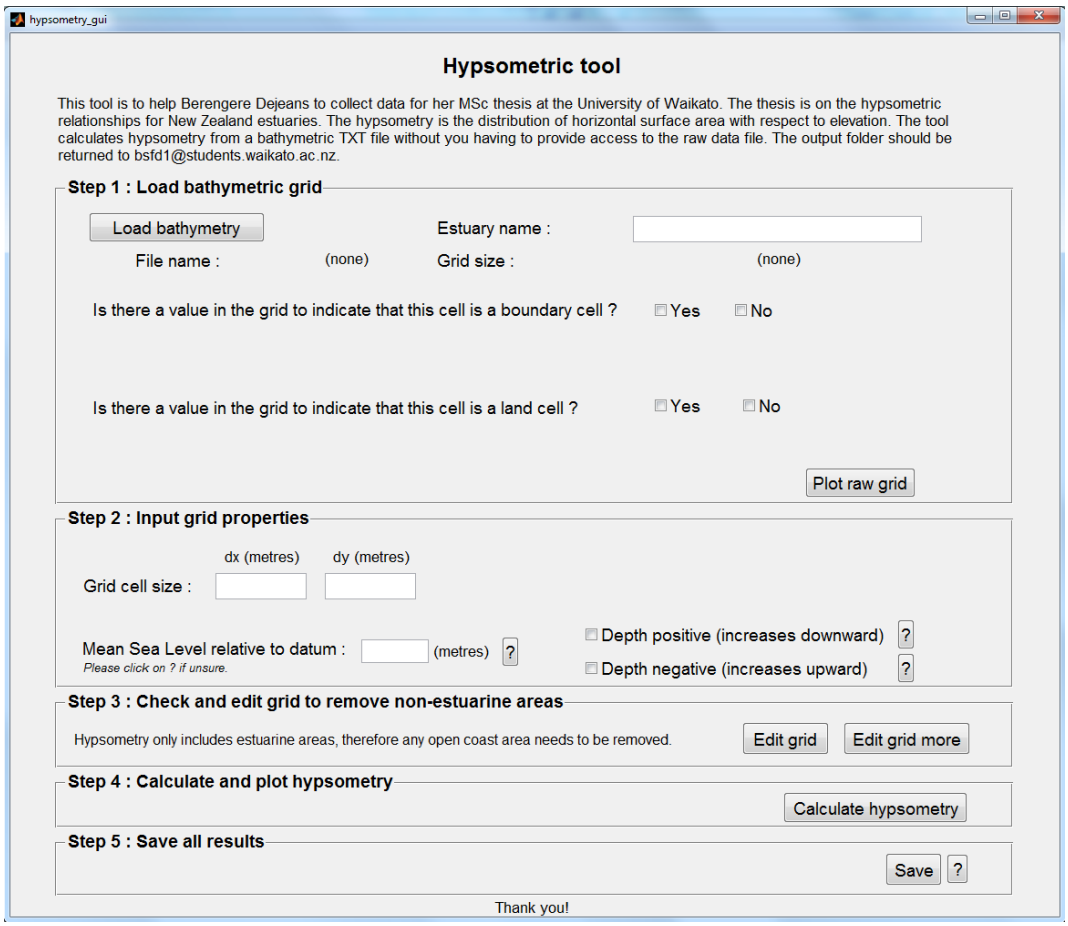

Figure 3. 3: Figure of the final GUI.

The final version of the interface contains 47 components (Figure 3.3) and its global structure is given in Figure 3.4. Basically, all the steps the user must follow can be grouped together into five main stages. First, the grid needs to be loaded and the user needs to specify the name of the site and the values of boundary and land cells if the grid has them. To be able to be processed, the grid needs to be rectangular (Step 1). Then, the properties of the grid need to be given, namely the size of the grid cells, the elevation of the bathymetry relative to Mean Sea Level (MSL) and the orientation of the grid (Step 2). An example of those two completed steps is presented on Figure 3.5. Afterwards, the user can modify the grid, in case it encompasses an area larger than the estuary. More precisely, the push buttons enable the user to have the grid plotted and he/she can 'adjust' it by clicking around the areas to be removed. In terms of code, the values of the grid cells in question are replaced by not-a-number NaN (Step 3, Figure 3.6), which is the Matlab missing number identifier. The next step is the computation

of the hypsometry. At this stage, the user only has to push a button and the hypsometric curve is generated. The corresponding callback mainly consists of the creation of an elevation vector h, ranging from the minimum value of the grid to the maximum one and whose increment is 0.01. Then, for each element h_i of the vector, the number of cells with a value below or equal to h_i is counted and multiplied by the grid cell size previously stored, which gives the corresponding area a_i (Step 4). The last step is to save the data. Pushing the 'Save' button creates two figures to JPEG, representing the bathymetry of the estuary and the hypsometric curve generated and an ASCII file where the properties given by the user are written (name of the site, grid cell sizes, orientation of the bathymetry and elevation to MSL) respectively. Those three files are contained in a new empty folder created at the beginning of this 'Save' button callback (Step 5). Tasks are expected to be taken in a certain order since some of them are dependent upon others (e.g. the area cannot be plotted if the user has not provided the values for boundary and land cells or the grid cell size). Therefore, error message boxes were also added to pop up whenever a previous step was not completed, requiring to anticipate every possibility of how a user might use the interface.

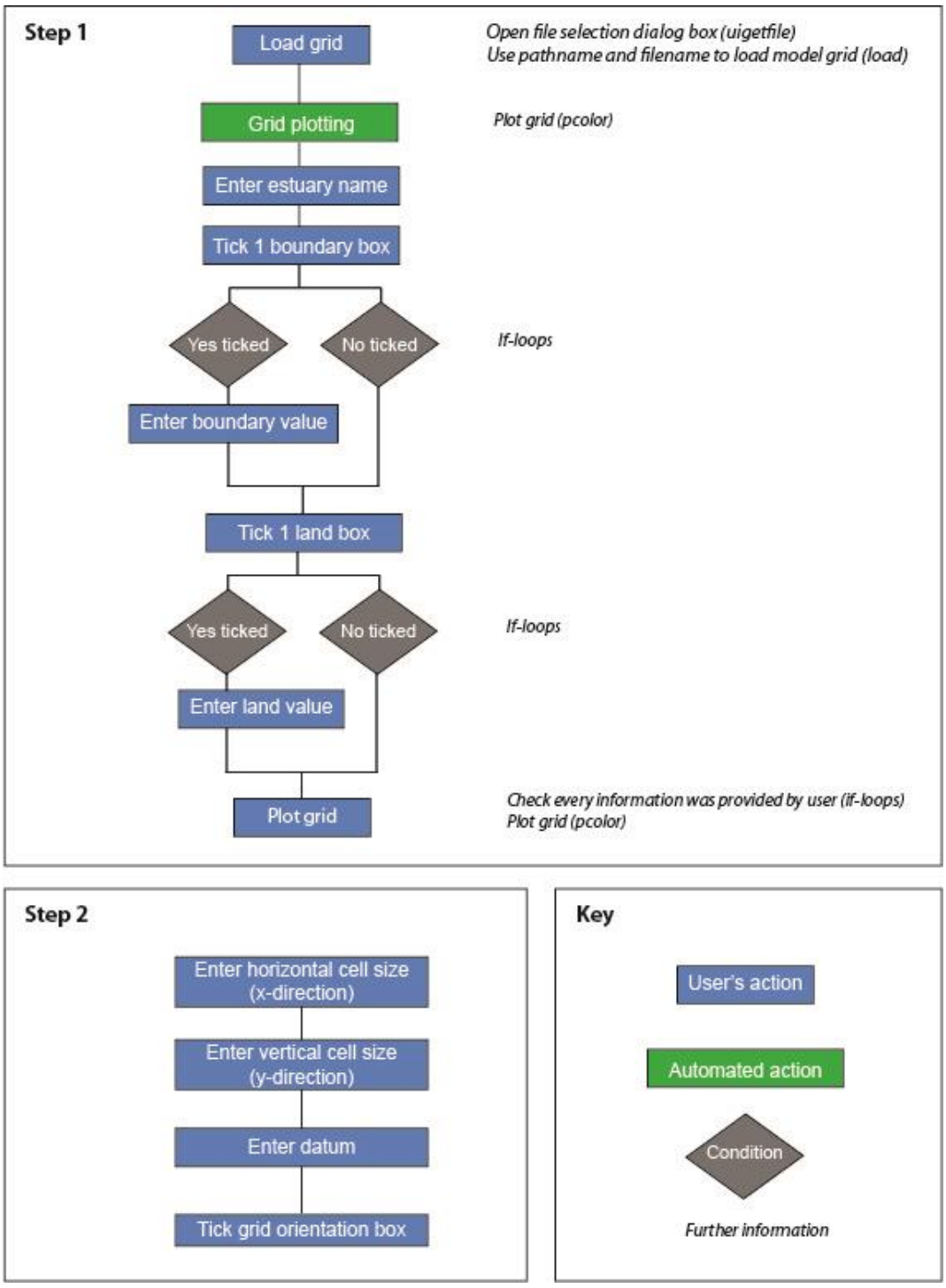
Step 1
Load grid
Open file selection dialog box (uigetfile)
Use pathname and filename to load model grid (load)
Grid plotting
Plot grid (pcolor)
Enter estuary name
Tick 1 boundary box
Yes ticked
No ticked
If-loops
Enter boundary value
Tick 1 land box
Yes ticked
No ticked
If-loops
Enter land value
Plot grid
Check every information was provided by user (if-loops)
Plot grid (pcolor)
Step 2
Enter horizontal cell size (x-direction)
Enter vertical cell size (y-direction)
Enter datum
Tick grid orientation box
Key
User's action
Automated action
Condition
Further information

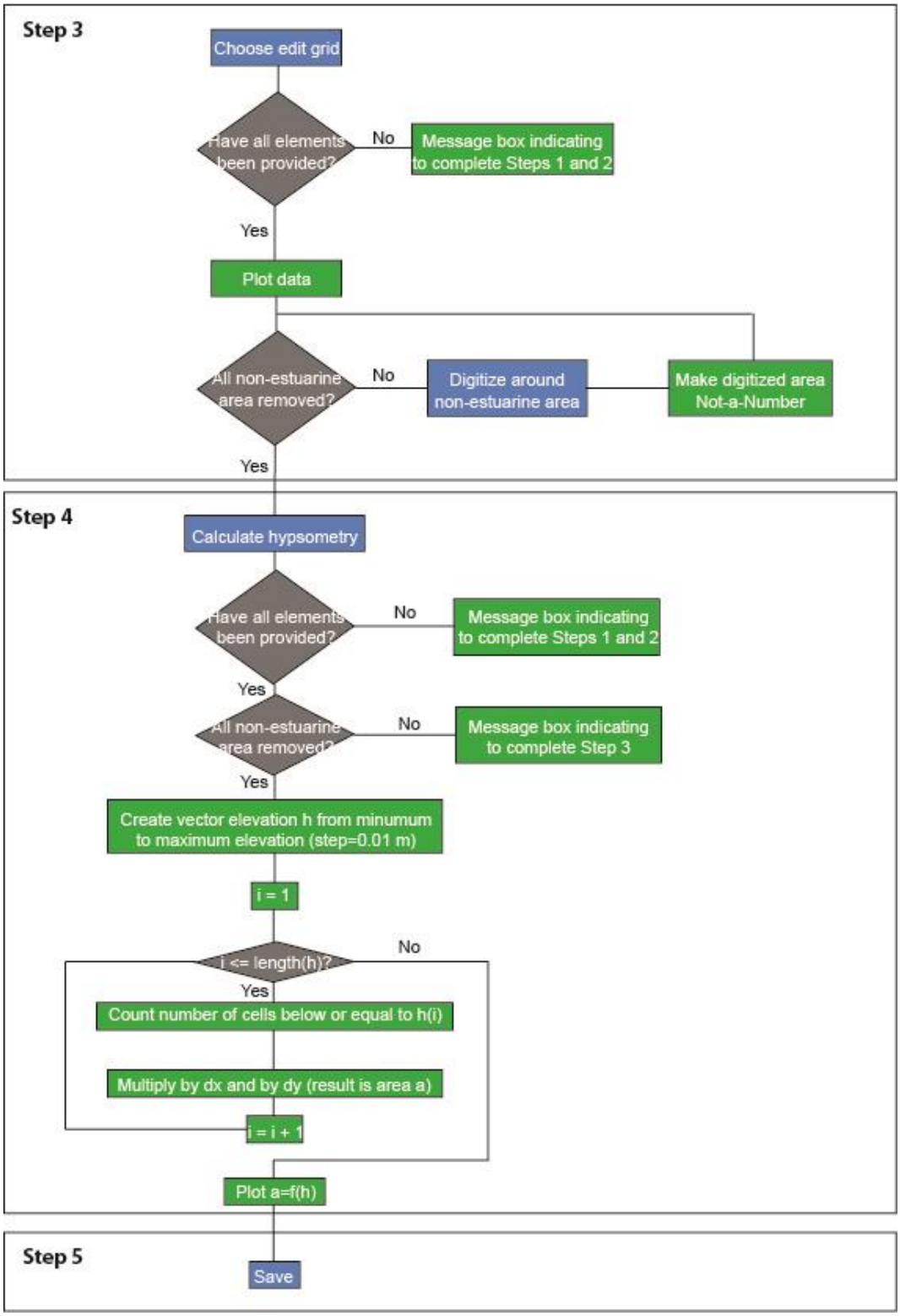

Figure 3. 4: Structure of the final GUI

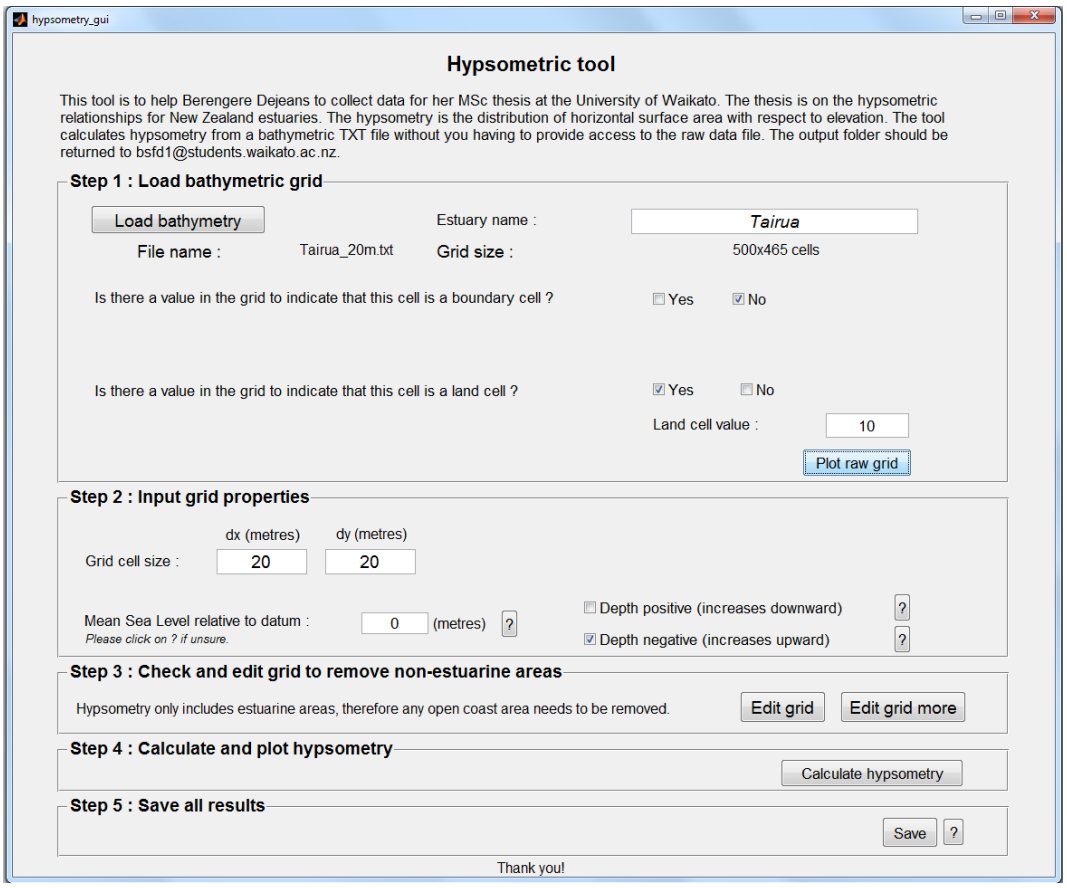

Figure 3. 5: Example of the steps 1 and 2 for the model grid of Tairua.

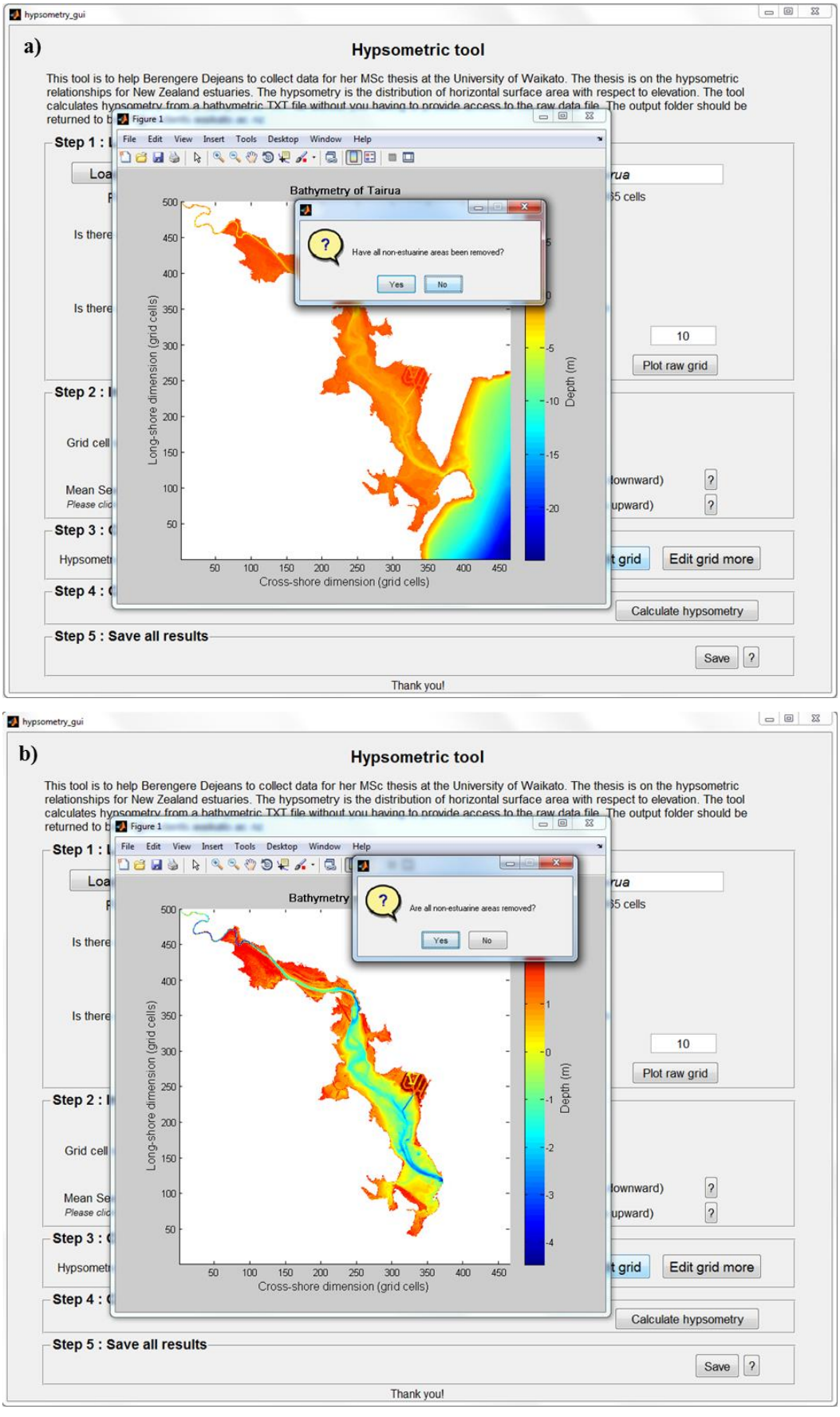

Figure 3. 6: Example of 'Step 3' of the GUI for the model grid of Tairua a) before editing (i.e. raw grid) and b) after editing (i.e. estuarine area of the grid).

3.4. Testing

Once operational and before deployment, the user interface required testing. The aim of this phase is to appreciate how a user perceives the GUI, and more precisely to make sure it is understandable, easy to use and that every possibility of interpretation from the user has anticipated. Thus, 5 people who had not been involved in the creation process were asked to test the GUI and give feedback. As an example, at first, testers tended to be confused by the order they were meant to perform the tasks. The messages boxes indicating a step was missed were not enough, and the components of the GUI were therefore displayed in a different way: the components were grouped into five main sets (Figure 3.4) which were all accompanied by a short description. Another common source of confusion was where the user needed to provide the datum (more precisely the elevation of the bathymetry relative to MSL) and specify the orientation of the bathymetry. Hence the addition of a push button 'Help' which opened a new window displaying an explaining figure (Figure 3.7) was added. Overall, the feedback helped improve the GUI, both in terms of design (modification of the layout, increase of the font sizes) and in terms of clarity (modification of the wording of some components and addition of dialog boxes and figure giving more information to the user) making it easier to manipulate and clearer.

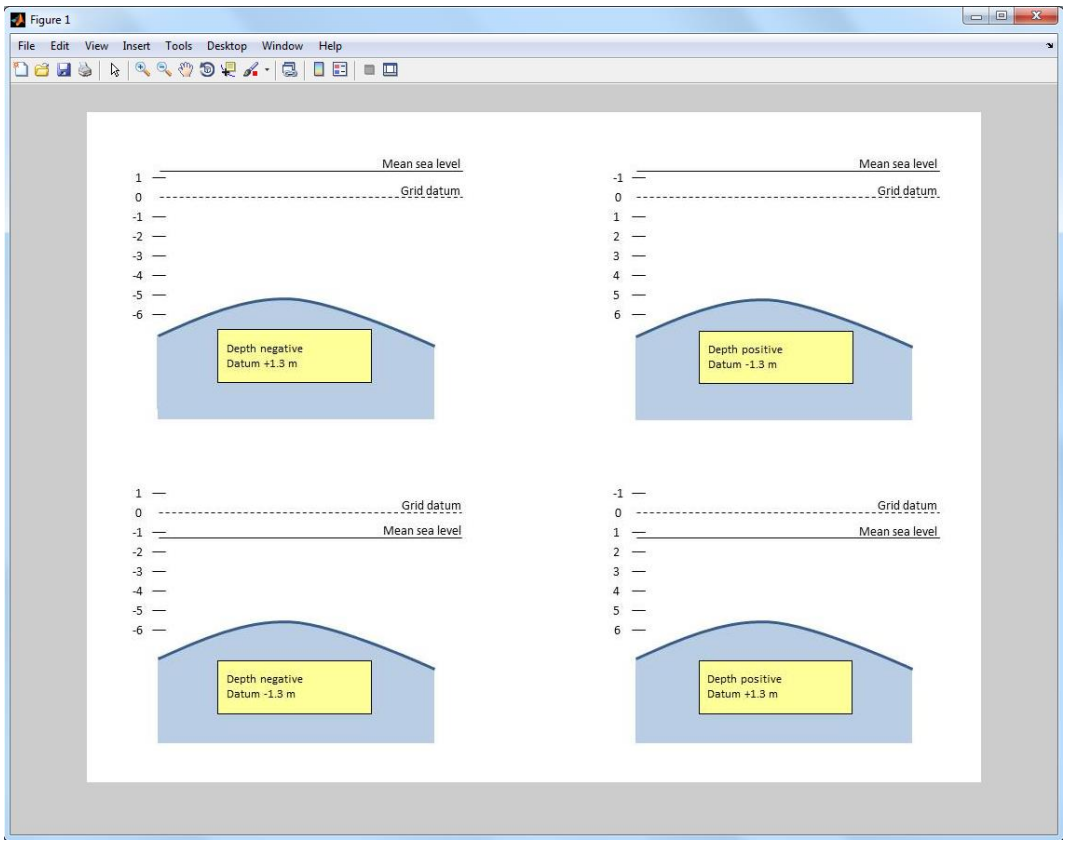

Figure 3. 7: 'Help' window created to appear when the user clicks on the '?' button in order to clarify the meaning of the bathymetry orientation.

3.5. Final implementation

3.5.1. Hypsometry collection

The GUI was finally deployed in five different organizations: the Waikato Regional Council (WRC), the Crown Research Institute National Institute of Water and Atmospheric Research (NIWA), the consulting and research company ECoast Ltd, the consultancy MetOcean Solutions Ltd which specialises in oceanography and meteorology and the University of Waikato (UoW) which resulted in the collection of the hypsometry of 22 different estuaries (Table 3.1). The gridded bathymetries gathered at WRC had been made from LIDAR data,

multibeam echo-soundings (MES) and single beam echo-soundings. Some of the grids had been computed by the program MIKE 21, a 2D coastal modelling tool developed by DHI and the other ones came from a 3-dimensional explicit finite difference model 3DD. NIWA provided grids made with MIKE21 from multibeam data. The grids supplied by MetOcean Solutions Ltd were computed using a combination of multibeam data (for the channels), singlebeam data and chart data from the LINZ (Land Information New Zealand) website (for the intertidal parts) and LIDAR data where it was relevant.

The bathymetry data collected within the University of Waikato were developed using a variety of different techniques. The bathymetry of Maketu comes from the MSc thesis of Nigel David Goodhue (2007) and was produced from the combination of historic data from 1995-1997 (for the southern and the western part of the estuary), a RTK (Real Time Kinetic) survey (for the most critical area, namely the entrance of the estuary and some of the main channels) and a video-based survey which involved image rectification (for the central part of the estuary (not covered by the RTK) which was more complex particularly due to the presence of shallow sand banks) (details are provided in the thesis). He gridded the bathymetry in SURFER^{TM}. The bathymetry of Raglan was produced by Steve Hunt using the Delft3D hydrodynamic numerical modelling software (Hunt *et al.*, 2015). The model grid of Tauranga was developed by Bradley Monahan for his PhD thesis. He used a combination of multibeam data from the Port of Tauranga, LIDAR and echo sounder data (Monahan *et al.*,in preparation). He also used the Delft3D software and performed a triangular interpolation on a combination of multibeam echosounders (MBES), LIDAR data and data from LINZ.

Table 3. 1: Sites for which the hypsometry was collected and their source.

Source	Site	Date of collection	Grid cell size (m)		Datum relative to MSL (m)
			x-direction	*y-direction*	
WRC	Firth of Thames	27/07/2015	50	50	0
	Tairua		20	20	0
	Whangamata		20	20	0
	Whitianga		20	20	0
NIWA	Kaipara	17/08/2015	20	20	0
	Manukau*		20	20	0
	Okura		20	20	0
ECoast	Mahurangi	10/09/2015	25	25	0
	Matakana		25	25	0
	Okura		25	25	0
	Waitemata		25	25	0
	Whangateau		25	25	0
	Whitford		25	25	0
MetOcean	Avon	1/10/2015	25	25	0
	Bay of Islands		20	20	0
	Bluff		25	25	0
	Firth of Thames		20	20	0
	Lyttelton		25	25	0
	Otago		25	25	0
	Wellington		10	10	0
	Whangarei		50	50	0
UoW	Maketu		15	15	0
	Raglan		50	50	0
	Tauranga		20	20	0

**Collected as a shapefile*

Since estuaries are rather complex features, particularly in terms of geometry, I decided to study the hypsometry of some sub-estuaries within the main estuarine bodies. Indeed, in some cases the gridsizes used for the whole estuary were too large to resolve the sub-basins within a site, and so a new hypsometry of those subsets was also generated. Practically, the user used the GUI as described before but classified the sub-estuaries as full basins, and removed the surrounding area using the tool. Overall, 13 sub-basins were

considered from 6 different estuaries (Table 3.2). Their location is given the next chapter.

Table 3. 2: Sub-basins included in the analysis.

Site	Number of studied sub-basins
Bay of Islands	2
Kaipara	1
Manukau	3
Okura	1
Raglan	2
Tauranga	4

The bathymetry of some additional sites was not available directly as model grid and therefore required conversion in order to be processed with the GUI. One of them, namely Manukau, was collected at NIWA as a shapefile, and converted into a rectangular grid with ArcGIS® using the kriging method for the interpolation. The model grid of Tauranga collected was a 20 x 20 meter grid which seems appropriate at the scale of the whole basin. However, in order to study sub-basins of this estuary, the Delft3D software was also used to regrid the original point cloud database at a better scale to resolve the sub-basins. More precisely, the grid was cut into sub-basins and refined to a 5 x 5 metres grid (Figure 3.14). Then, for each 'sub-grid', a triangular interpolation was made on the MBES, LIDAR and LINZ point cloud data.

3.5.2. Comments regarding the implementation

The main limitation was that the GUI required the input grid to be rectangular, which is the not the only type of grids that are commonly used. Non-rectangular (e.g. curvilinear or flexible mesh grids) may be more appropriate for certain modelling purposes, but can be, however, harder to deal with and especially to handle with MATLAB and would require more complicated coding within the GUI. That is why only rectangular grids were included in this project.

Another point worth noticing is the delineation of the seaward limit of the basins. In the absence of a clear description of how Boon (1975) or Boon & Byrne

(1981) outlined their sites, the estuaries were cut at the narrowest part of the mouth for the sake of consistency.

3.6. Concluding remarks

Since gridded bathymetries are valuable commercial data which are not easily accessed, a Graphical User Interface was developed with MATLAB to enable a user to compute the hypsometry of an estuary share the hypsometric data without having to provide the raw model grid. The GUI design tools provided by MATLAB facilitated the creation of such an interface by providing an efficient approach. This GUI was deployed within five organizations: the Waikato Regional Council; the National Institute of Water and Atmospheric Research; ECoast Ltd; MetOcean Solutions Ltd and the University of Waikato. The inclusion of a function enabling the bathymetry to be edited, i.e. to interactively remove parts of the grid if it contained non-estuarine areas, also allowed computation and collection of hypsometries of sub-basins within 6 estuaries. Thus, even though the GUI only worked with rectangular grids, the hypsometries of 22 estuaries and 13 sub-basins were gathered.

Chapter 4

Hypsometry distribution

4.1. Introduction

This chapter presents the hypsometry of estuaries which were calculated for each estuary and their comparison to a model defined by Boon & Byrne in 1981. The aim of this section is to assess whether the relationship, which has been previously tested overseas, particularly in the United States (Boon, 1975; Boon & Byrne, 1981) and in the United Kingdom (Townend, 2008), can also be used to describe the hypsometry of New Zealand estuaries.

4.2. Collected sites

The deployment of the GUI resulted in the collection of 22 estuaries (Figure 4.1). Most of the sites (18) were located in the North Island and the remaining 4 were in the South Island. The bathymetric map and corresponding hypsometry (i.e. the output of the GUI) of all of those sites are presented in Appendix A. In addition, 13 sub-estuaries were considered, which were contained within 6 of the study estuaries. Their location is given in Figures 4.2, 4.3, 4.4, 4.5, 4.6, 4.7 and 4.8.

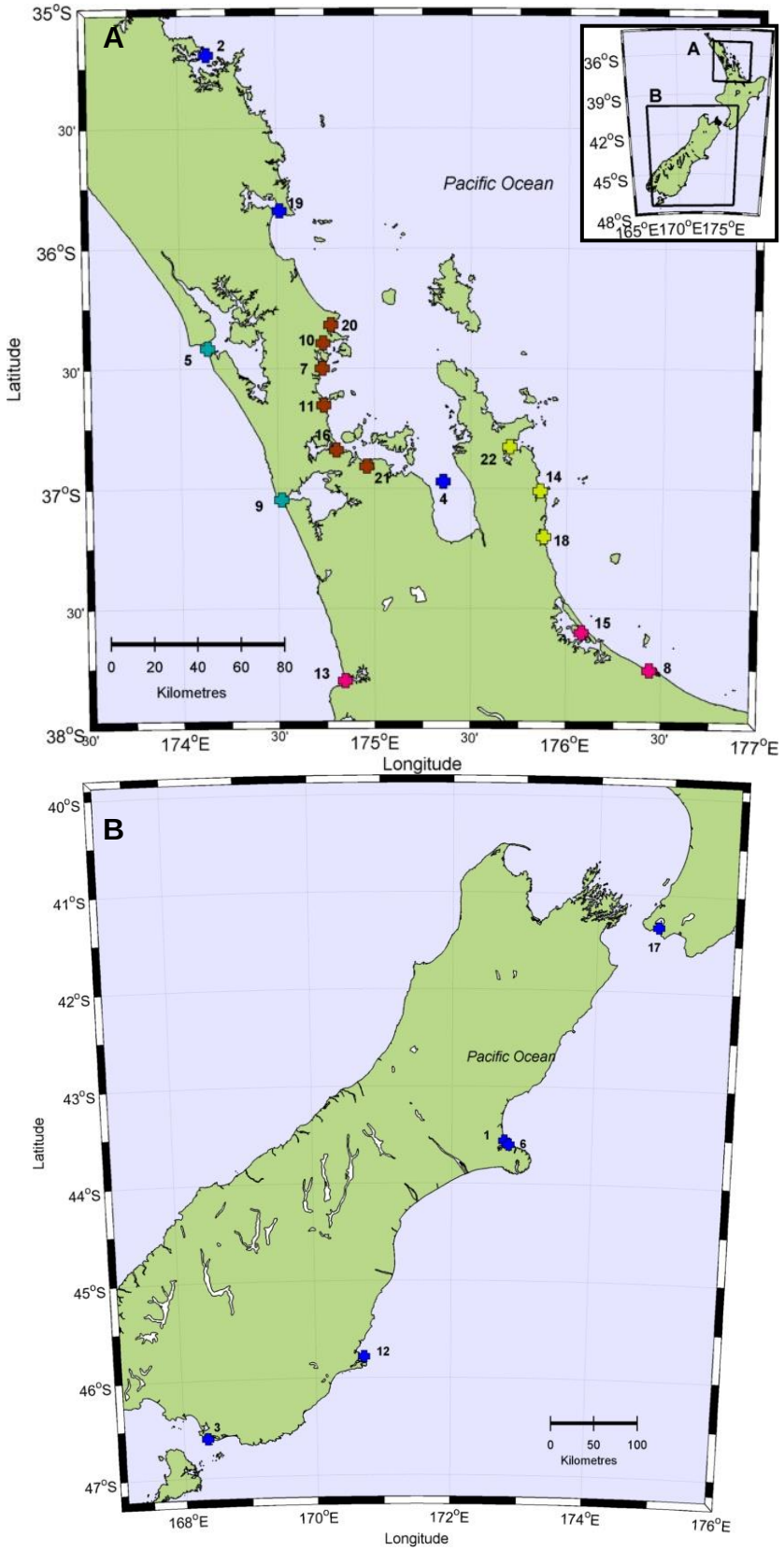

Figure 4. 1: Location of the sites of the (A) North and (B) South Islands where hypsometric data have been collected from ECoast (brown), MetOcean (blue), NIWA (green), the University of Waikato (pink) and the Waikato Regional Council (yellow).

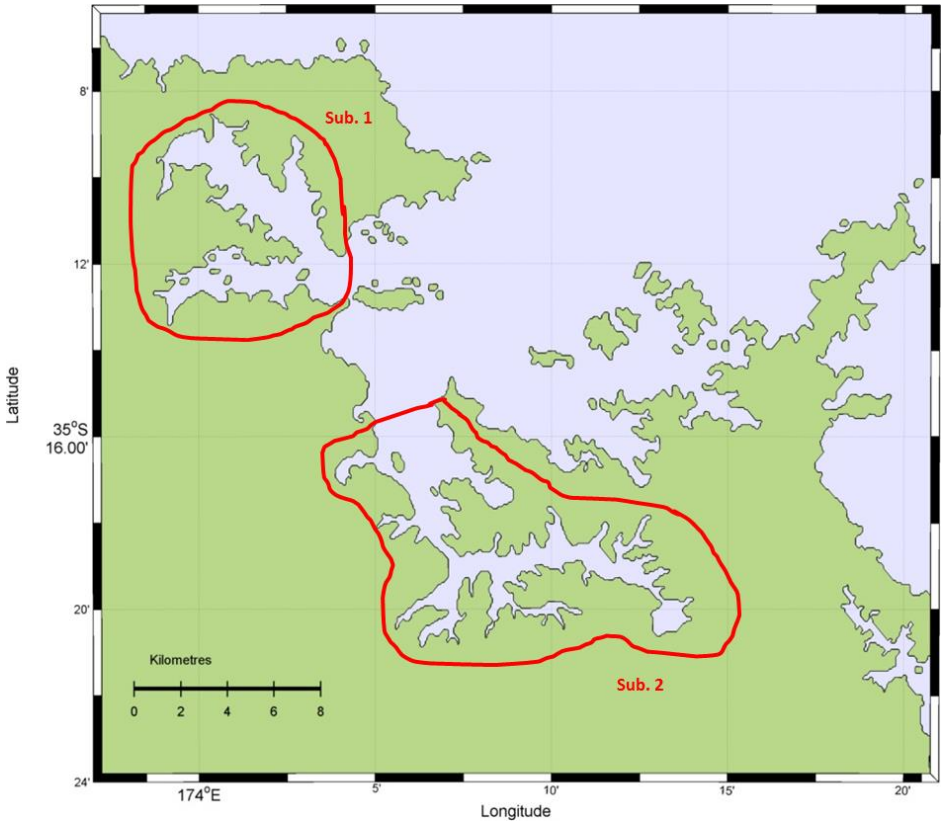

Figure 4. 2: Sub-estuaries considered in Bay of Islands.

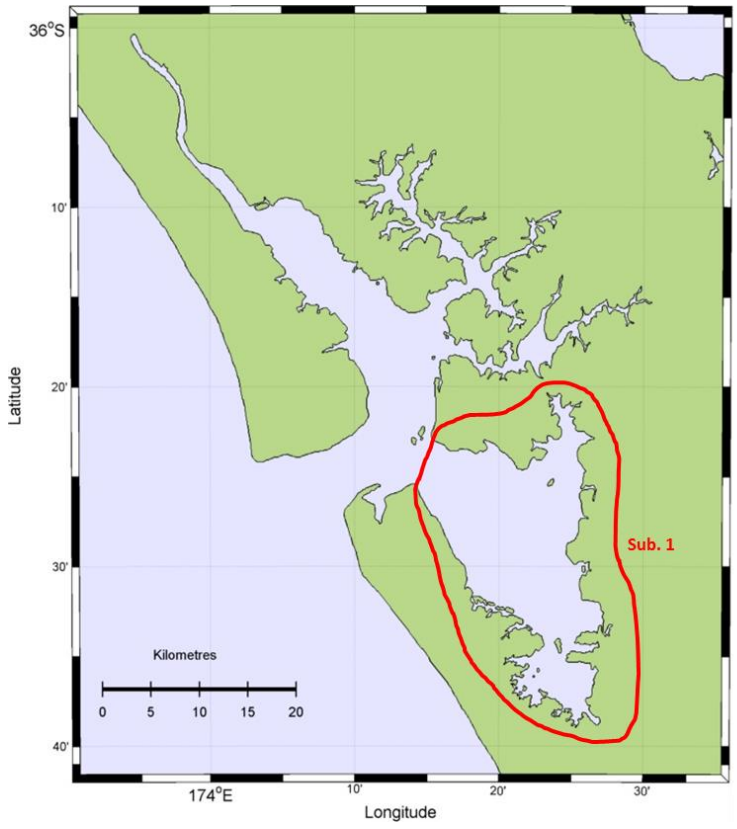

Figure 4. 3: Sub-estuaries considered in Kaipara.

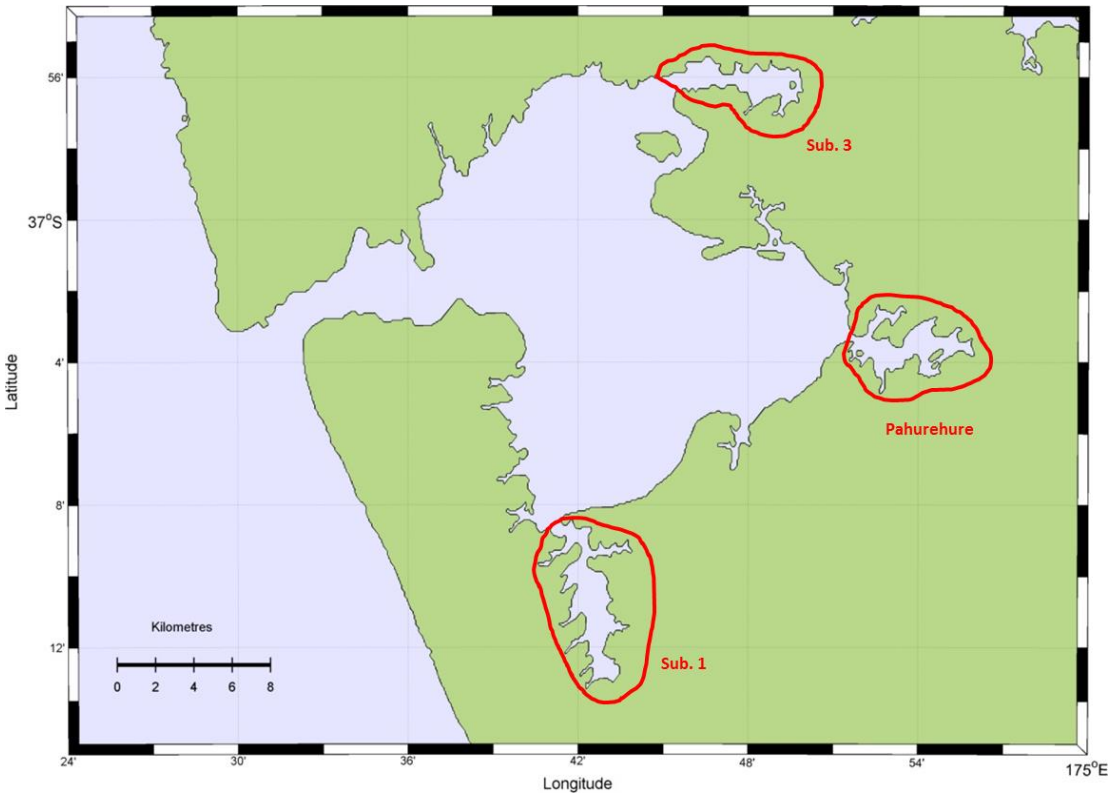

Figure 4. 4: Sub-estuaries considered in Manukau.

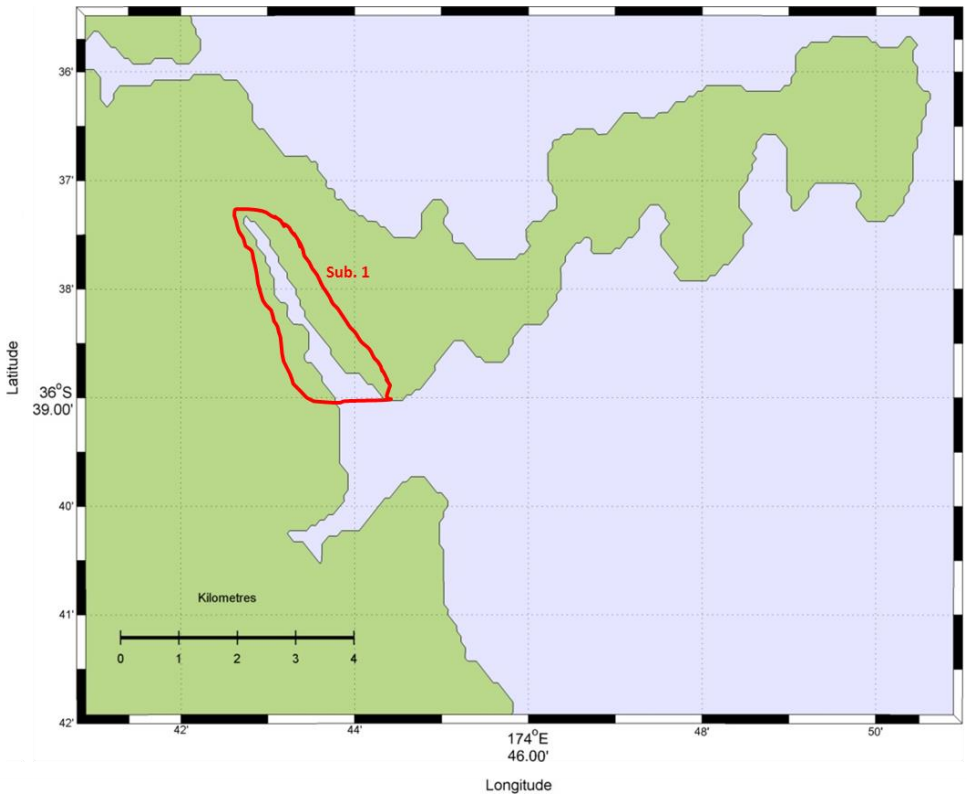

Figure 4. 5: Sub-estuary considered in Okura.

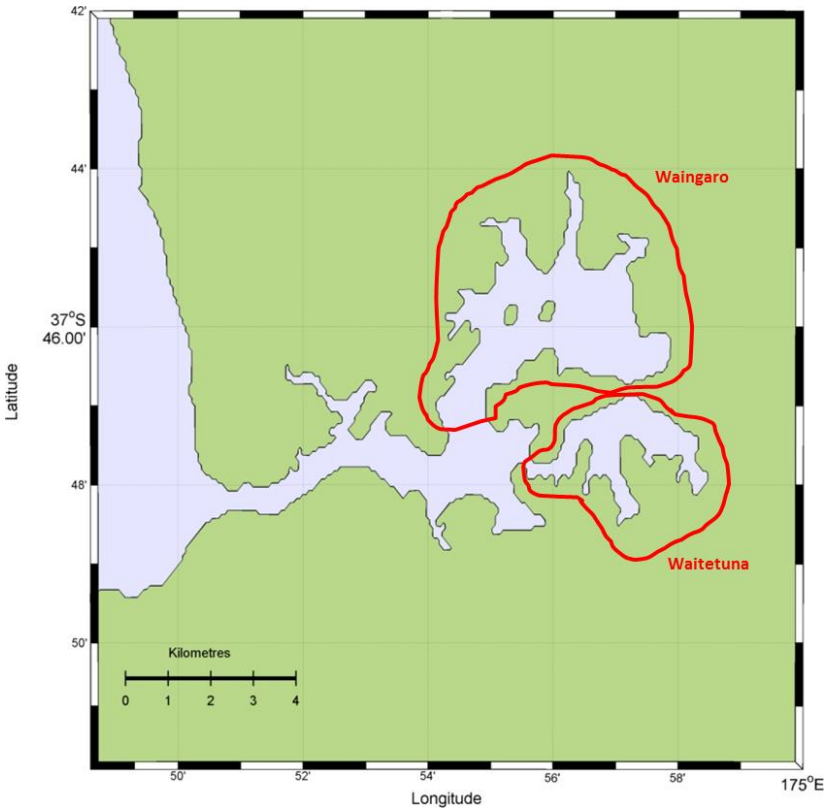

Figure 4. 6: Sub-estuaries considered in Raglan.

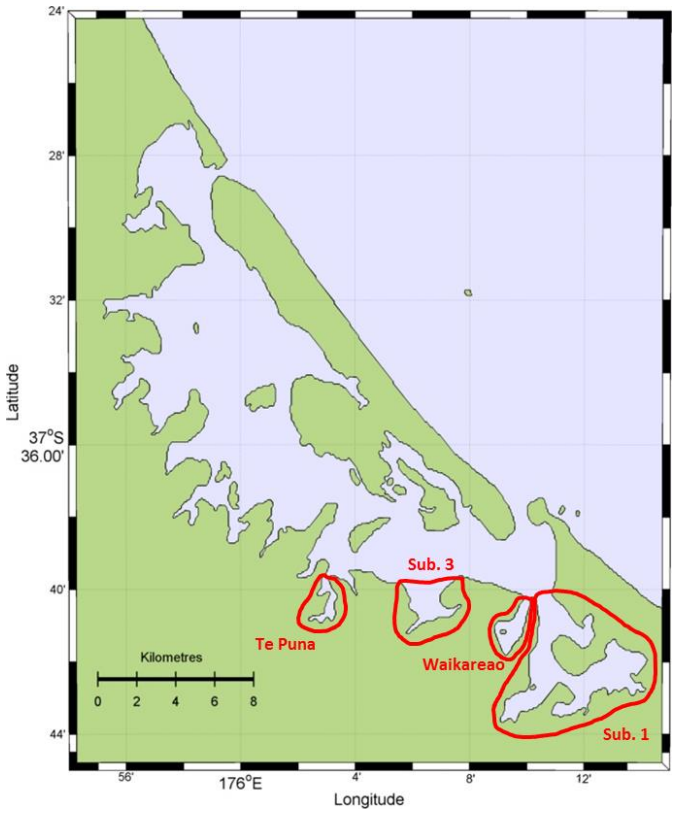

Figure 4. 7: Sub-estuaries considered in Tauranga.

The majority of hypsometries have the characteristic sigmoidal shape (i.e. have an 's-shape') that Boon and Bryne (1981) predicted, with an unique point of inflection separating a concave upper part (highest elevations) from a convex lower part (lower elevations). However, the sinuosities and area below the curve differ largely between estuaries (Figures 4.8, 4.9, 4.10 and 4.11). Moreover, two of the hypsometric curves, namely the ones of Bay of Islands and Lyttelton (Figure 4.8b and 4.8f), do not appear to have clear points of inflection; simply put, their global shape is essentially convex rather than sigmoidal. As for the Bay of Islands, there is no clear change of slope in the lower part of the basin is due to the absence of narrow drainage channels (a drainage network) within the basin as a whole (Figure A.2 in Appendix A). The hypsometry of sub-sections of this bay will be considered later. The hypsometry of Lyttelton, on the other hand, has been computed from a bathymetry made after the estuary was dredged (dredging has been conducted in Lyttelton Harbour since 1876 in order to develop a shipping channel to facilitate navigation (Lyttelton Port of Christchurch (LPC), 2012)). The bathymetry collected for this site is therefore not representative of natural conditions. Regarding the curves of the 20 other basins, the slopes are relatively smooth in the intertidal region with the elevation decreasing more rapidly either just before (e.g. Mahurangi (Figure 4.9a), Maketu (Figure 4.9b), Matakana (Figure 4.9d)) or within the subtidal area (e.g. Manukau (Figure 4.9c), Otago (Figure 4.9f), Tauranga (Figure 4.10c)). For the sites where the highest water is well below the highest mapped elevation (e.g. Mahurangi (Figure 4.9a), Matakana (Figure 4.9d), Raglan (Figure 4.11a)), the slope of supra-tidal part of the curve is steep and tends to decrease in the intertidal part of the basin (apart from Wellington Harbour where the slope remains steep until approximately twenty meters below MSL and decreases only beyond this point).

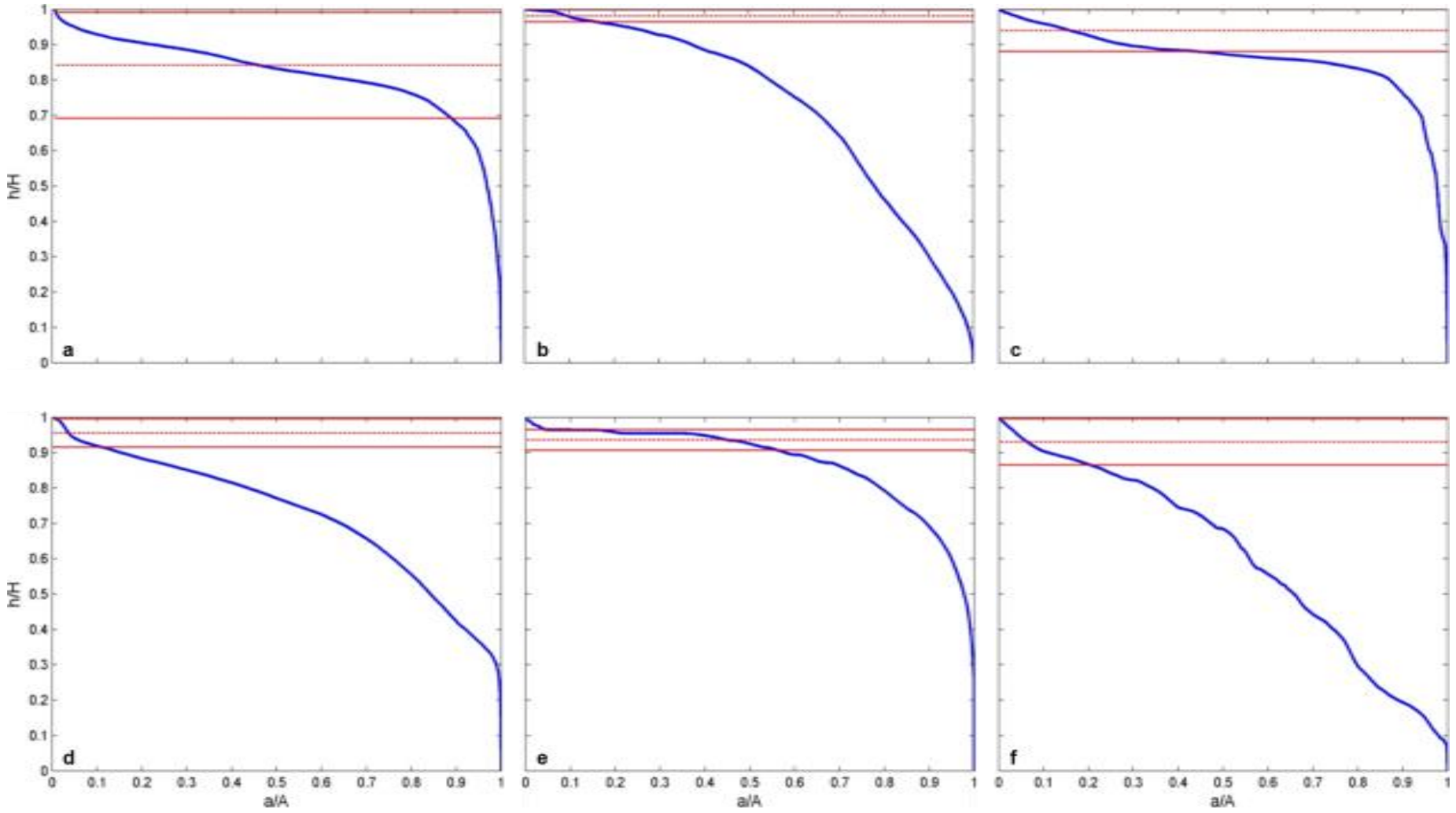

Figure 4. 8: Observed hypsometric curves after normalization (i.e. division by the max area of the estuary) of a) Avon, b) Bay of Islands, c) Bluff, d) Firth of Thames, e) Kaipara and f) Lyttelton. The upper red line corresponds to the water level at high tide during a spring tide, the lower red line to the water level at low tide during a psring tide and the dotted red line is the average of the two.

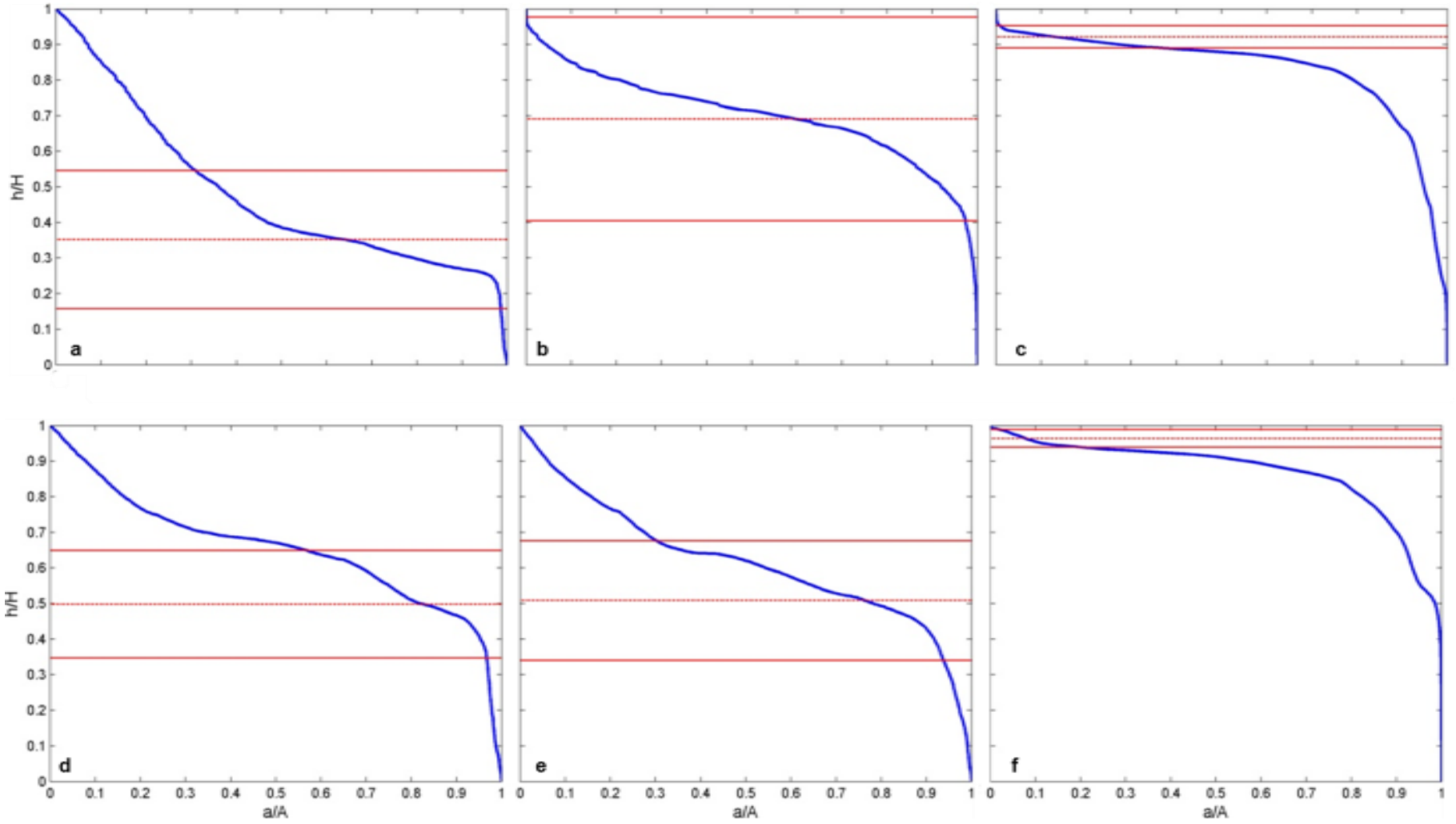

Figure 4. 9: Observed hypsometric curves after normalization (i.e. division by the max area of the estuary) of a) Mahurangi, b) Maketu, c) Manukau, d) Matakana, e) Okura and f) Otago. The upper red line corresponds to the water level at high tide during a spring tide, the lower red line to the water level at low tide during a spring tide and the dotted red line is the average of the two.

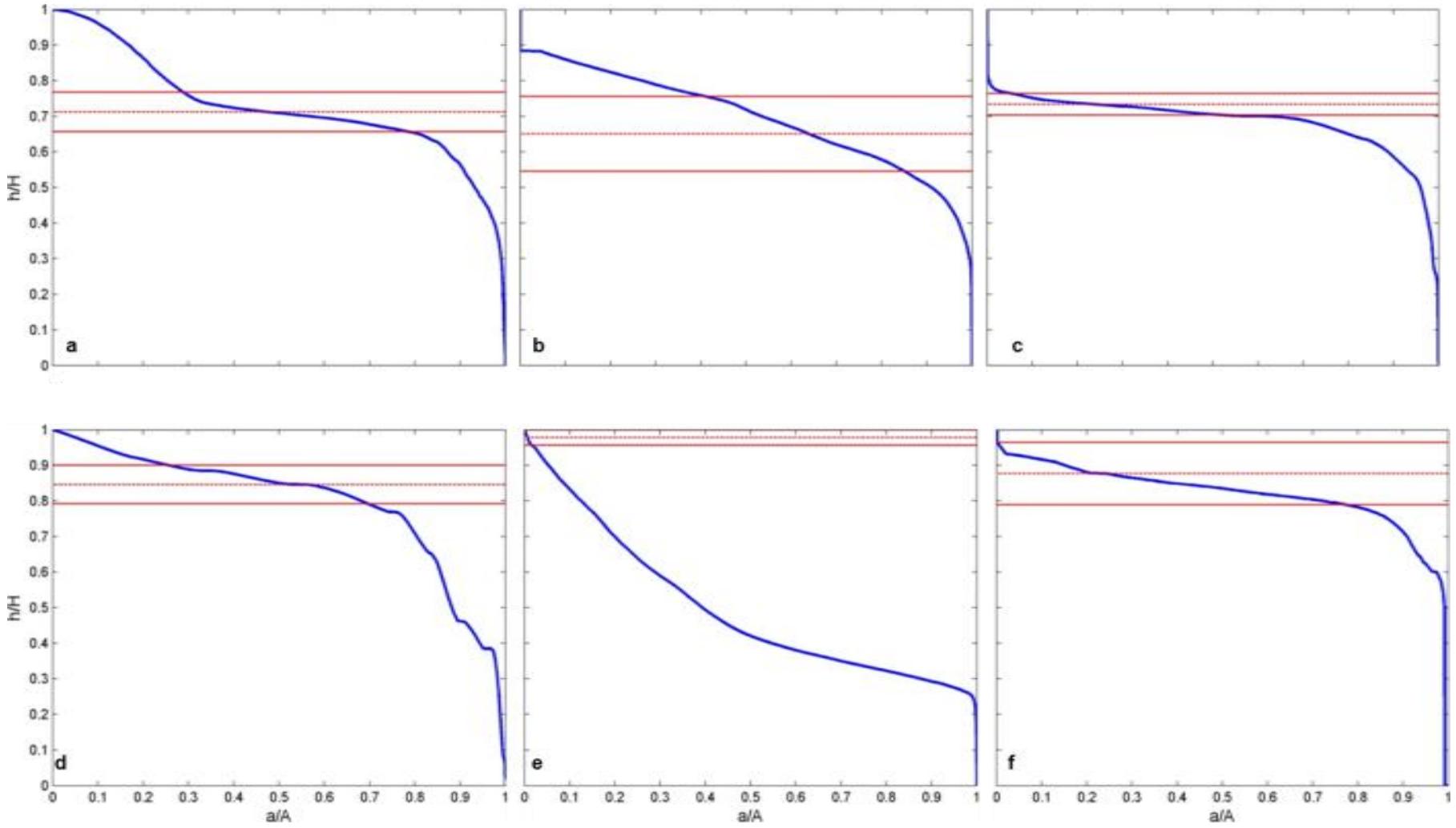

Figure 4. 10: Observed hypsometric curves after normalization (i.e. division by the max area of the estuary) of a) Raglan, b) Tairua, c) Tauranga, d) Waitemata, e) Wellington and f) Whangamata. The upper red line corresponds to the water level at high tide during a spring tide, the lower red line to the water level at low tide during a psring tide and the dotted red line is the average of the two.

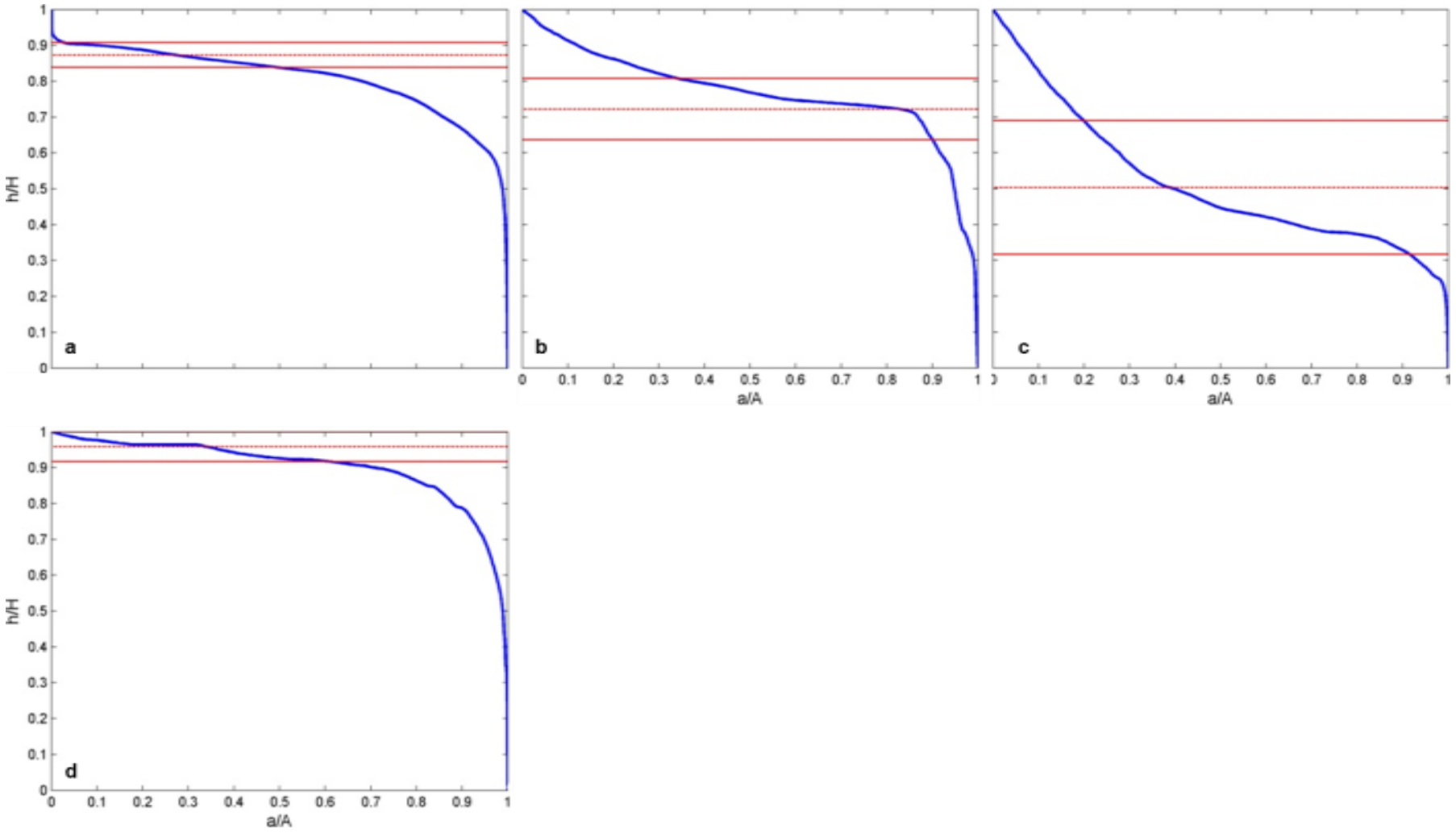

Figure 4. 11: Observed hypsometric curves after normalization (i.e. division by the max area of the estuary) of a) Whangarei, b) Whangateau, c) Whitford and d) Whitianga. The upper red line corresponds to the water level at high tide during a spring tide, the lower red line to the water level at low tide during a psring tide and the dotted red line is the average of the two.

4.3. Application of Boon & Byrne's relationship

4.3.1. Estimations of r- and γ-values

Once the hypsometries were collected, the formula defined by Boon (1975) and Boon and Byrne in 1981 was used to model the shape of the curves. This relationship defines the dimensionless cumulative area *a* below every elevation h (Equation 4.1):

$$\frac{a}{A} = \frac{G}{r + G\,(1-r)} \quad \text{where } G = \left(1 - \frac{h}{H}\right)^{\gamma} \qquad \text{(Equation 4.1)}$$

where A is the maximum basin area and H is the vertical distance between the maximum and minimum basin elevation. The coefficients r and γ are defined empirically. Boon (1975) refers to r as the curvature coefficient since controls the curvature of the basin. The value of the exponent γ determines the relative position of the curve, i.e. the relative volume of sediment in the basin (Boon & Byrne, 1981).

Every hypsometry was processed in MATLAB to ensure the same protocol was used for all sites. Each of the 22 estuaries was processed independently. The first step was to normalize the areas and elevations collected, dividing them respectively by the largest area and the overall depth of the estuary. The way Boon (1975) and Boon & Byrne (1981) defined the maximum basin area A was not clearly presented in their paper. Indeed, they do not specify whether A corresponds to the maximum area of the whole basin or the area of the basin which was below high tide (and in that case, which tide (mean high water spring, mean high water neap, highest astronomical tide, etc.)).

4.3.1.1. First application of the hypsometry model

As a first attempt, for each site, the value of A was chosen as being the largest area of the basin, which corresponded to the area at the highest mapped elevation. The shape of the normalized observed hypsometric curve remained the same but the dimensionless areas a_n and dimensionless elevations h_n now ranged between 0 and 1. The optimum values of r and γ were calculated by iterating through a range of values $(r, \gamma)_i$ and finding the values that provided the minimum root-mean-square error (RMSE) ε_i (expressed as a percentage) between observed hypsometry and modelled hypsometry $a_{nm,i}$.

$$\varepsilon_i = 100\, x \sqrt{\frac{1}{n} \sum_{i=1}^{n} \left(a_{nm,i} - a_n\right)^2} \quad \text{(Equation 4.2)}$$

where n is the numbered of observed points considered.

In past studies, the curvature factor r was constrained between 0.01 and 3.181 and γ between 0.9737 and 5 (Boon & Byrne, 1981; Townend, 2008; Moore *et al.*, 2009; Table 4.1). In order to improve model fit, r was varied between 0.001 and 15 with steps of 0.001 and γ between 0.1 and 30 with steps of 0.1. The r and γ values considered to give the best fit to the Boon & Byrne formula (Equation 4.1) compared to the observed hypsometry were the ones corresponding to the smallest error ε_i (Table 4.2). The resulting hypsometric curves for each site are presented in Appendix A.

Table 4. 1: Examples of r- and γ -values found in past studies using Boon & Byrne's equation.

Location	Environment(s)	r- value	γ-value	Source
United States	Tidal marsh creek	0.016	2	Boon (1975)
United States	Inlet lagoon	0.01	[1.8, 5.0]	Boon & Byrne (1981)
New Zealand	Barrier-enclosed estuary	0.01	[1.8, 4.0]	Hunt *et al.* (2015)
United Kingdom	Saltmarsh estuary	-	[1.5, 3.5]	Moore *et al.* (2009)
United Kingdom	Estuaries, creeks, tidal inlets	[0.044, 1.301]	[0.9737, 3.9370]	Townend (2008)
	Tidal embayment	0.04	1.47	Van Maanen *et al.* (2013)

Table 4. 2: First estimates of r-values, γ-values and the corresponding error.

Site	r_1	γ_1	ε_1 (%)
Avon	0.004	3	1.19
BOI	0.332	0.8	1.37
Bluff	0.001	3.3	2.59
FOT	0.055	2	1.88
Kaipara	0.019	1.6	2.29
Lyttelton	0.383	1.2	2.25
Mahurangi	0.187	3	8.04
Maketu	0.005	4.2	1.43
Manukau	0.004	2.7	3.14
Matakana	0.015	3.8	3.24
Okura	0.024	3.8	3.85
Otago	0.006	2.2	2.13
Raglan	0.006	3.9	6.09
Tairua	0.013	3.4	2.27
Tauranga	0.001	5.7	5.04
Waitemata	0.028	1.9	2.68
Wellington	0.125	3.3	7.60
Whangamata	0.001	3.8	1.41
Whangarei	0.002	3.5	1.76
Whangateau	0.003	3.8	3.46
Whitford	0.054	4.3	7.29
Whitianga	0.006	1.9	1.17

4.3.1.2. The second application of the hypsometry model

This first fitting of Boon & Byrne's relationship gave values of r between 0.001 (Bluff, Tauranga and Whangamata) and 0.383 (Site Lyttelton) and values of γ between 0.8 (Bay of Islands) and 5.7 (Tauranga). Unfortunately, the *r* values for Bluff, Tauranga and Whangamata: where at the endpoint of the interval of the values considered which renders this fitting questionable. Moreover, the values differed extensively to those provided in past studies, particularly the γ-values which would all be expected to remain below 5 (e.g. van Maanen *et al.*, 2013; Hunt *et al.*, 2015). Moreover, the computed errors ε_i (and accordingly

the presence of gaps between of the modelled hypsometric curve and the observed one, Table 4.2, Figure 4.12) show that this first trial did not fit the data very well at some sites (e.g. Mahurangi, Raglan, Whangateau, Whitford). Usually the largest differences were observed at the highest elevations and/or around the upper part of the channels where the slope locally steepens. The first adjustment to fitting technique was to remove areas that were higher than high tide (only taking into account the part of the estuaries affected by hydrodynamic parameters. In order to appreciate the difference in terms of hypsometry, three different levels of the tide were considered: the mean high water springs and mean low water springs levels (MHWS and MLWS respectively) and the average of the two. In the following, the quantities corresponding to the bathymetry below MHWS (respectively MLWS and the average of the two) will be annotated h (respectively l and m). Those sea level values were taken from the tide predictions accessible on the LINZ website when available and the details are presented in Appendix B (Land Information New Zealand (LINZ), 2015). For the two sites that were not in the LINZ tables, Whangamata and Whitford, the sea levels were extracted from the NIWA tide forecaster (National Institute of Water and Atmospheric Research (NIWA), 2015). The process to find the new values $r_{2,i}$ and $\gamma_{2,i}$, (where $i \in (h, l, m)$) was otherwise the same as previously described. The new values $r_{2,i}$, $\gamma_{2,i}$ and the corresponding $\varepsilon_{2,i}$ are given in Table 4.3 and the modelled curves are given in Appendix A.

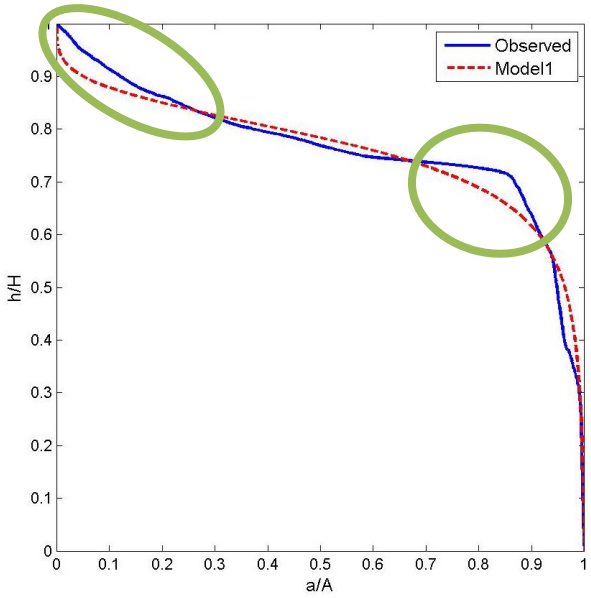

Figure 4. 12: Location of the largest errors (green circle) – Example of Whangateau.

Table 4. 3: Second estimates of r-values, γ-values and their corresponding errors.

Site	Below MHWS			Below MLWS			Below average tidal level		
	$r_{2,h}$	$\gamma_{2,h}$	$\varepsilon_{2,h}$ (%)	$r_{2,l}$	$\gamma_{2,l}$	$\varepsilon_{2,l}$ (%)	$r_{2,m}$	$\gamma_{2,m}$	$\varepsilon_{2,m}$ (%)
Avon	0.005	2.8	1.27	0.11	1.1	1.55	0.024	1.4	0.56
Bay of Islands	0.337	0.8	1.38	0.487	0.7	1.35	0.367	0.8	1.42
Bluff	0.001	3.3	2.59	0.02	1.2	1.21	0.003	2.3	2.06
Firth of Thames	0.054	2	1.89	0.084	1.5	2.49	0.069	1.7	2.12
Kaipara	0.047	1.1	2.32	0.042	1.4	2.56	0.038	1.4	2.19
Lyttelton	0.441	1.1	2.22	0.74	0.8	2.11	0.665	0.8	1.98
Mahurangi	0.013	4.2	4.84	3.096	0.6	4.79	0.015	2.2	4.28
Maketu	0.007	3.7	1.64	0.08	1.6	2.17	0.046	1.4	2.68
Manukau	0.011	1.8	2.06	0.072	0.9	0.83	0.026	1.3	1.61
Matakana	0.046	1.7	4.12	1.353	1	2.58	0.197	0.7	3.32
Okura	0.049	1.7	2.44	0.414	1.1	1.53	0.191	0.9	1.53
Otago	0.009	1.9	2.06	0.037	1.1	1.51	0.017	1.5	1.62
Raglan	0.009	2.1	1.76	0.084	1.2	3.10	0.037	1.2	1.36
Tairua	0.023	2.1	3.11	0.024	1.7	2.28	0.02	1.9	2.08
Tauranga	0.006	2	1.33	0.048	1	2.18	0.016	1.4	1.28
Waitemata	0.102	1	2.48	0.3	0.9	5.29	0.278	0.7	3.36
Wellington	0.125	3.3	7.60	0.121	3.2	7.74	0.127	3.2	7.69
Whangamata	0.002	3.4	1.51	0.023	1.4	4.30	0.005	1.9	1.57
Whangarei	0.013	1.7	1.77	0.026	1.4	2.88	0.019	1.5	1.98
Whangateau	0.013	1.7	3.17	0.182	1.2	4.75	0.202	0.9	3.32
Whitford	0.014	4.3	4.77	0.014	2.1	2.71	0.01	2.9	2.99
Whitianga	0.006	1.9	1.18	0.033	1.4	1.62	0.011	1.6	1.27

Overall, those new estimated values give a better fit of Boon & Byrne's equation to the observed hypsometry. The cases which had the largest error using the first model ($\varepsilon_{1,i} \geq 5\ \%$), were improved regardless of the tidal level used in this second model (e.g. Manukau, Raglan, Tauranga) except in the case of Wellington where the errors remains above 7 %. However, most of the errors are larger when considering the basin below the

average tidal level $(0.56\ \% < \varepsilon_{2,m} < 7.69\ \%)$ and even more so below MLWS $(0.83 < \varepsilon_{2,l} < 7.74)$ than when considering the basin below MHWS $(1.18\ \% < \varepsilon_{2,h} < 7.60)$. In the last case (the basin below MHWS), all r –values $r_{2,h}$ slightly increased (up to 0.074 for Waitemata) or remained the same, apart from Mahurangi and Whitford (where r decreased to 0.174 and 0.119 respectively, Table 4.3). However, in general terms, the new range of r-values was much more similar and within the range of past studies ($0.001 \leq r_{2,i} \leq 3.09$ than the values calculated for model 1. With regard to the γ-values in the three cases using different tidal levels,, they almost all decrease (up to 4.4) or do not change. Mahurangi is the only site for which the γ-value increased (increase of 1.2) but only when the part of the estuary below MHWS is considered. Overall the new γ-values are now below 5 (the highest, $\gamma = 4.3$, being estimated at Whitford) which conforms better with previous work (Boon & Byrne, 1981; Townend, 2008). Generally speaking, this second model, applied by considering the part of the basin affected by the tide (below high water springs), gives a better fit between Boon & Byrne's equation and the observed hypsometries.

4.3.1.3. Third application the hypsometry model

Past studies usually referred to the curvature factor r as the ratio of the 'minimum basin area' by the 'maximum basin area' but usually either computed it empirically (using it as a fitting parameter; Townend, 2008) or used the same value in all simulations (e.g. Boon & Byrne, 1981). Therefore, following Boon & Byrne (1981) and Hunt *et al.* (2015), a third set of curves was generated by setting $r = 0.01$. Hence, a new estimation of γ-values, $\gamma_{3,i}$, was made considering again the basin below MHWS, MLWS and the average of the two and the resulting values are given in Figure 4.13.

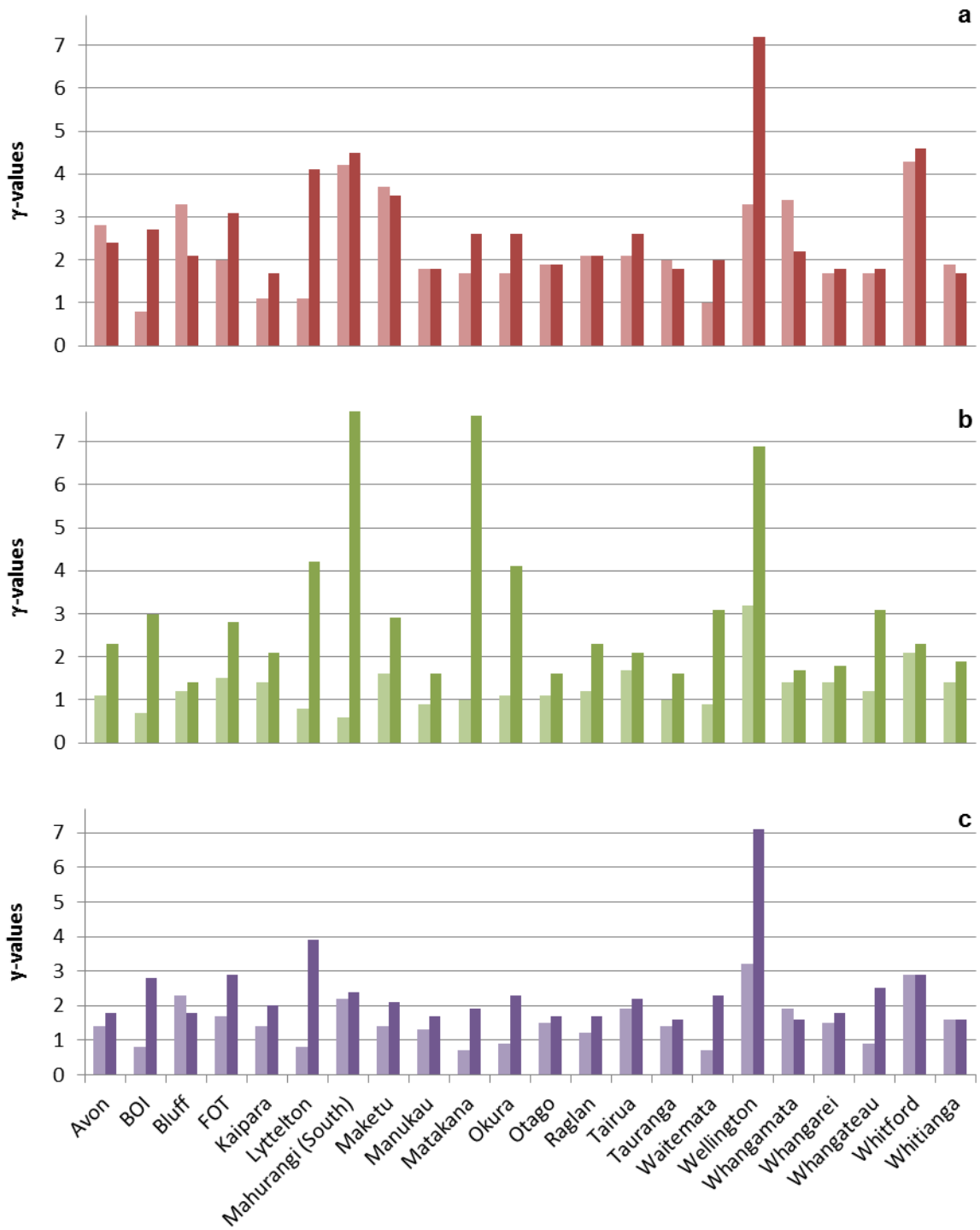

Figure 4. 13: The γ-values resulting from the 3rd application of the hypsometry model (dark bars) compared to the second model (light bars). The part of the basin below (a) MHWS, below (b) MLWS and below (c) the average of the two is considered.

This third fitting leads to changes in γ-values from +3.9 to -1.2 ([0.2,8.2] and [-0.5,3.9] respectively) when comparing with the second application of the model and the part of the basin below MHWS (below MLWS and below the average tidal level respectively). The values of the errors tend to be larger than for the second model. By only comparing the error between the observed hypsometry and this third model, a classification into three main groups can be proposed regarding how well the Boon & Byrne's equation fits the data: very good to good fit ($\varepsilon_{3,i} \leq 5\ \%$), relatively poor fit ($5\ \% < \varepsilon_{3,i} \leq 10\ \%$) and very poor fit ($\varepsilon_{3,i} > 10\ \%$) (Table 4.4). When considering the part of the basin below MHWS this classification appears to be satisfactory because the errors are relatively well distributed along the curve (there is no local big gap). Nevertheless, Mahurangi does not fit very well in this classification since, despite a relatively small error, the modelled hypsometry clearly does not match the observed one at all when considering the basin below MLWS (Figure 4.14). Overall, apart from Bluff and Whitford, the third model fits best for the hypsometry of the basin below MHWS, then next best for the model using the average of the tidal level and finally worst for the model using MLWS. For three sites, namely Bay of Islands, Lyttelton and Wellington, this fitting is however very poor even when considering the part below MHWS. The observed hypsometry of Bay of Islands and Lyttelton was already highlighted as relatively 'unusual' compared to the ones of the other study sites in that they do not have a very clear sigmoidal shape. Regarding Wellington, the model particularly fails to match the observations at the highest elevations where the observed hypsometry is nearly linear. Furthermore, different institutions extrapolate and interpolate their bathymetries during gridding using different protocols. The fitting errors are consistently higher for some institutions. In these cases, the model seems to fail to represent the transition between the flats and the channels (e.g. Figure 4.15). In the absence of information regarding how the bathymetric data have been computed, it may be hypothesized that the poor fit of the model with the observations results from the way the bathymetries have been interpolated. To sum up, the third model offers a relatively good fit with the observed hypsometries of most of the study sites but is not satisfactory for all estuaries.

Table 4. 4: Comparison of the goodness of fit of the third model to the observed hypsometry estimated according to the RMSE between the hypsometry predicted by Boon & Byrne's relationship and the observed hypsometry.

Site	RMSE for the part of the basin below MHWS (%)		RMSE for the part of the basin below MLWS (%)		RMSE for the part of the basin below average tidal level (%)	
Avon	2.29	Good	7.91	Poor	2.22	Good
BOI	12.45	Very poor	13.45	Very poor	12.99	Very poor
Bluff	4.52	Good	2.06	Good	3.26	Good
FOT	5.69	Poor	7.45	Poor	6.61	Poor
Kaipara	4.59	Good	4.72	Good	4.26	Good
Lyttelton	14.16	Very poor	15.94	Very poor	15.40	Very poor
Mahurangi	4.90	Good	19.42	Very poor	4.38	Good
Maketu	2.11	Good	6.75	Poor	5.12	Poor
Manukau	2.26	Good	5.45	Poor	2.99	Good
Matakana	5.97	Poor	17.12	Very poor	8.63	Poor
Okura	5.08	Poor	13.34	Very poor	9.76	Poor
Otago	2.07	Good	3.45	Good	1.95	Good
Raglan	1.99	Good	6.88	Poor	3.79	Good
Tairua	3.68	Good	3.52	Good	2.95	Good
Tauranga	1.77	Good	4.51	Good	1.74	Good
Waitemata	7.39	Poor	12.67	Very poor	11.27	Very poor
Wellington	10.66	Very poor	10.61	Very poor	10.70	Very poor
Whangamata	4.22	Good	4.79	Good	2.18	Good
Whangarei	1.90	Good	3.64	Good	2.55	Good
Whangateau	3.17	Good	11.15	Very poor	10.27	Very poor
Whitford	4.82	Good	2.88	Good	2.99	Good
Whitianga	1.68	Good	3.41	Good	1.41	Good

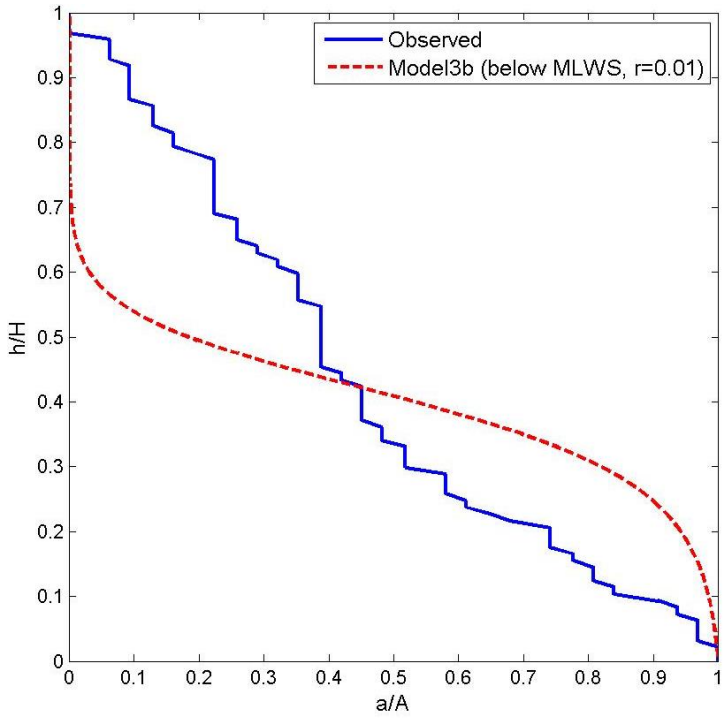

Figure 4. 14: Third modelled vs. observed hypsometry of Mahurangi below MLWS.

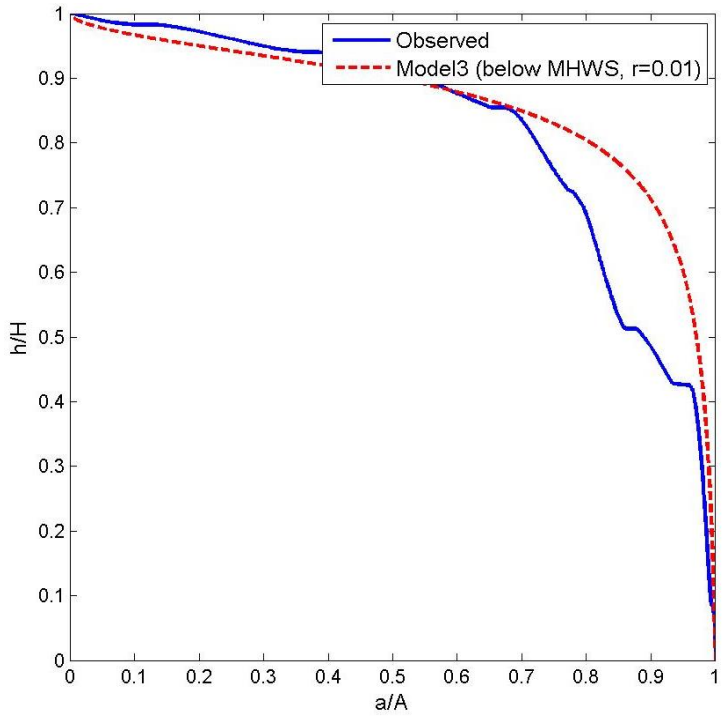

Figure 4. 15: Third model vs. observed hypsometry of Waitemata.

4.3.1.4. Application of Boon & Byrne's relationship to sub-estuaries

As previously indicated, 13 sub-estuaries have also been considered and their hypsometry compared to Boon & Byrne's equation. The hypsometry of more than half of the sub-basins behaved similarly to a whole basin and their hypsometric curves are given in Figures 4.16, 4.17 and 4.18. The model appears to fit the data relatively well except for the sub-estuaries of Bay of Islands and the third sub-estuary of Tauranga when considering the part of the site below MHWS. As for Bay of Islands' two sub-basins, their hypsometries are relatively well represented by the first and second model but not by the third as was the full bay. Indeed, their hypsometric curves have also a relatively convex shape rather than sigmoidal, hence the 'failure' of the third fitting method. Regarding Tauranga's third sub-estuary, unlike previously, the third model seems to well represent the hypsometry when considering the part below MLWS but not below MHWS. This may be explained by the lack of precision of the tidal levels (the level taken as the low water MLWS would actually be closer to the high water MHWS for this sub-part of Tauranga). Otherwise the estimations of r- and γ-values give the same ranges, which means that γ remains below 5 for the second and third model (Tables 4.5, 4. 6 and 4.7).

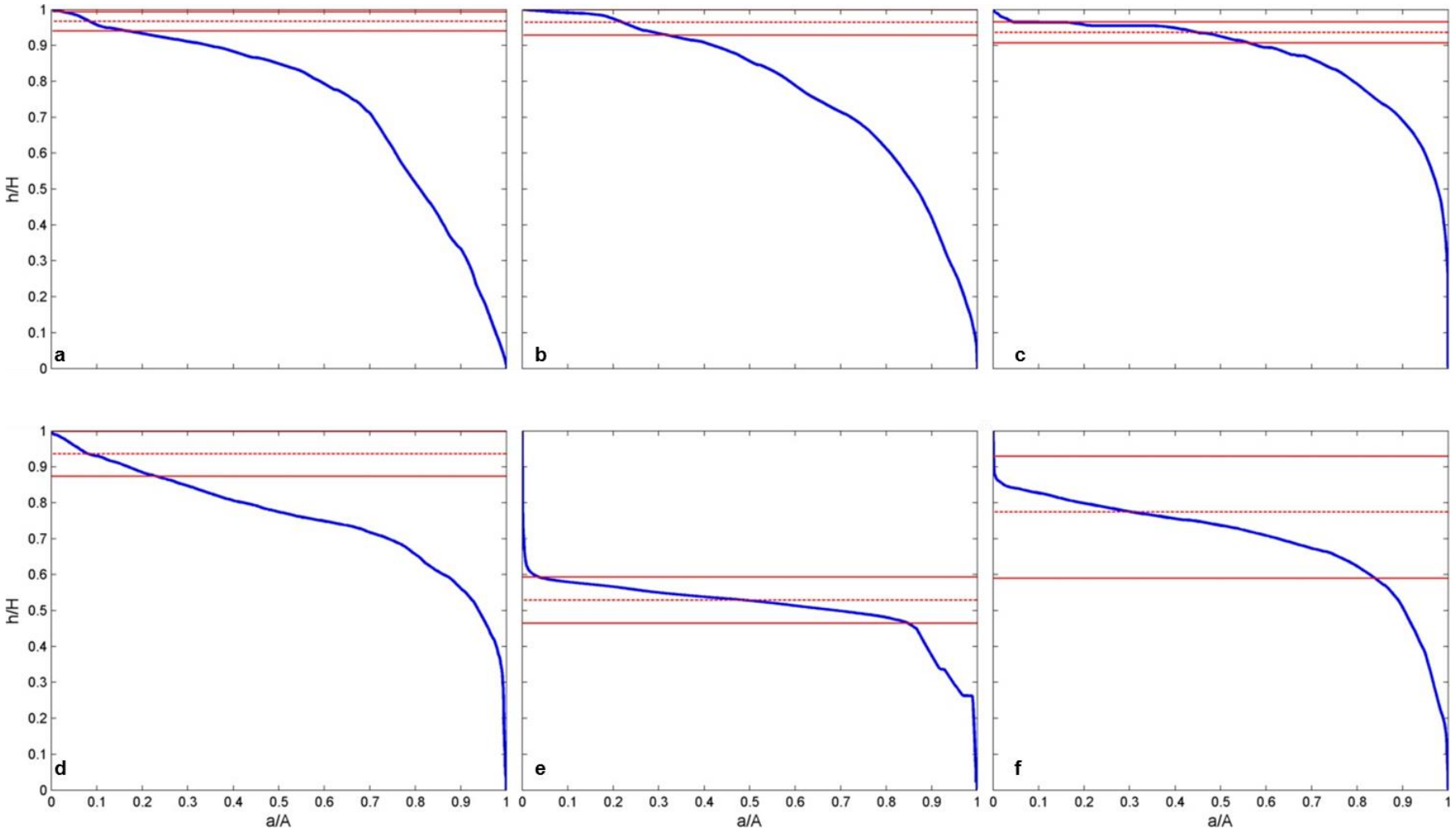

Figure 4. 16: Observed hypsometric curves of the study sub-estuaries after normalization of Bay of Islands' a) sub-basin 1 and b) sub basin 2, c) Kaipara's sub-basin and Manukau's d)sub-basin 1, e) sub-basin 2 (Pahurehure) and f) sub-basin 3.

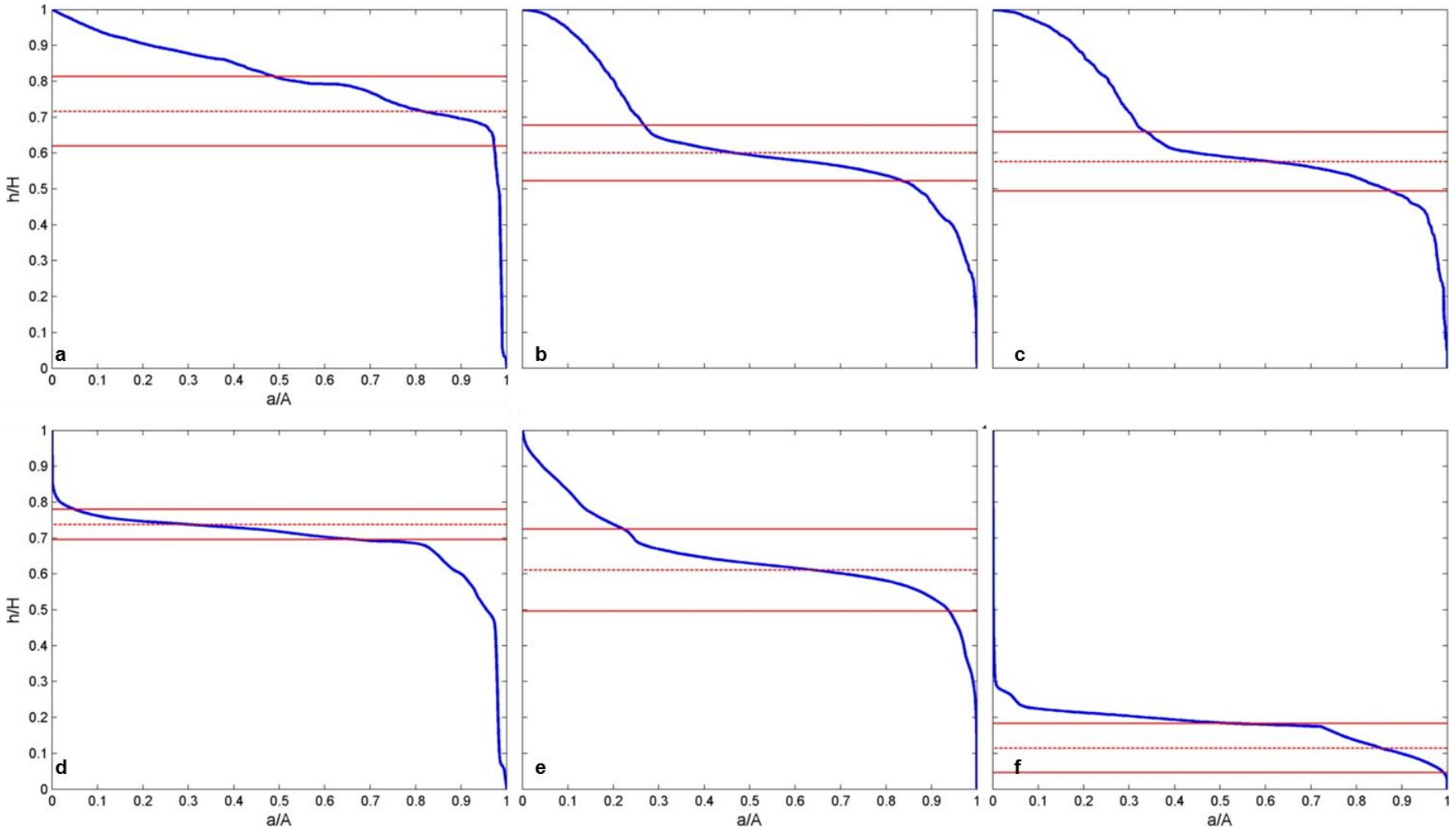

Figure 4. 17: Observed hypsometric curves of the study sub-estuaries after normalization of Okura's a) sub-basin, Raglan's b) sub basin 1 (Waingaro) and c) sub-basin2 (Waitetuna), and Tauranga's d) sub-basin 1, e) sub-basin 2 (Waikareao) and f) sub-basin 3.

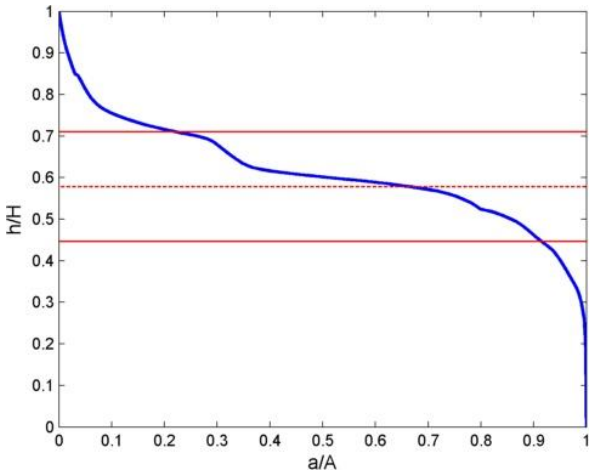

Figure 4. 18: Observed hypsometric curves after normalization of Tauranga's sub-basin 4 (Te Puna).

Table 4. 5: Estimation of r- and γ-values of sub-basins according to model 1.

Estuary	Sub-estuary	r_1	γ_1	ε_1 (%)
BOI	BOI 1	0.166	1.1	2.46
	BOI 2	0.199	0.9	1.47
Kaipara	Kaipara 1	0.006	1.7	3.01
Manukau	Manukau 1	0.015	2.7	2.18
	Manukau 2	0.001	9.4	4.37
	Manukau 3	0.005	4.1	2.04
Okura	Okura 1	0.005	3	3.27
Raglan	Waingaro	0.011	4.6	7.90
	Waitetuna	0.029	3.4	9.31
Tauranga	Tauranga1	0.001	5.5	5.19
	Waikareao	0.001	6.7	4.56
	Tauranga3	0.003	28.8	2.44
	Te Puna	0.004	5.7	2.98

Table 4. 6: Estimation of r- and γ -values of sub-basins according to model 2.

Estuary	Sub-estuary	Below MHWs			Below MLWS			Below average tide		
		$r_{2,h}$	$\gamma_{2,h}$	$\varepsilon_{2,h}$ (%)	$r_{2,l}$	$\gamma_{2,l}$	$\varepsilon_{2,l}$ (%)	$r_{2,m}$	$\gamma_{2,m}$	$\varepsilon_{2,m}$ (%)
BOI	BOI 1	0.203	1.0	2.51	0.374	0.7	1.70	0.239	0.9	2.20
	BOI 2	0.163	1.0	1.46	0.186	1.1	1.34	0.175	1.1	1.11
Kaipara	Kaipara 1	0.025	1.0	1.91	0.028	1.8	4.10	0.058	1.1	3.56
Manukau	Manukau 1	0.015	2.7	2.18	0.039	1.5	1.82	0.018	2.3	2.10
	Pahurehure	0.012	2.0	1.94	0.048	2.2	5.81	0.061	1.1	2.82
	Manukau 3	0.01	3.0	1.39	0.209	1.1	2.44	0.07	1.2	0.84
Okura	Okura 1	0.008	1.8	3.56	1.937	0.6	11.20	0.042	0.9	4.23
Raglan	Waingaro	0.006	2.7	1.57	0.075	1.4	3.07	0.035	1.3	1.15
	Waitetuna	0.005	2.7	1.33	0.135	0.9	1.89	0.036	1.3	1.56
Tauranga	Tauranga1	0.004	2.2	1.91	0.132	0.7	2.93	0.02	1.3	2.06
	Waikareao	0.002	3.3	1.25	0.059	1.6	3.89	0.027	1.3	0.99
	Tauranga3	0.5	0.6	4.91	0.054	1.5	1.17	0.078	1.7	3.01
	Te Puna	0.008	2.8	2.52	0.028	1.7	2.98	0.036	1.5	2.81

Table 4. 7: Estimation of r- and γ-values according to model 3.

Site		Below MHWs			Below MLWS			Below average tide		
Estuary	***Sub-estuary***	$r_{3,h}$	$\gamma_{3,h}$	$\varepsilon_{3,h}$ ***(%)***	$r_{3,l}$	$\gamma_{3,l}$	$\varepsilon_{3,l}$ ***(%)***	$r_{3,m}$	$\gamma_{3,m}$	$\varepsilon_{3,m}$ ***(%)***
BOI	BOI 1	0.01	2.6	9.98	0.01	2.5	12.27	0.01	2.5	11.06
	BOI 2	0.01	2.5	9.30	0.01	2.8	9.84	0.01	2.8	9.37
Kaipara	Kaipara 1	0.01	1.3	2.53	0.01	2.4	5.16	0.01	1.8	6.20
Manukau	Manukau 1	0.01	3.0	2.47	0.01	2.2	4.16	0.01	2.6	2.70
	Manukau 2	0.01	2.1	1.99	0.01	3.4	7.36	0.01	1.8	5.77
	Manukau 3	0.01	3.0	1.39	0.01	3.0	10.50	0.01	2.1	5.49
Okura	Okura 1	0.01	1.7	3.59	0.01	4.9	27.18	0.01	1.3	5.14
Raglan	Waingaro	0.01	2.5	2.07	0.01	2.5	6.58	0.01	1.8	3.50
	Waitetuna	0.01	2.4	2.17	0.01	2.0	7.70	0.01	1.9	3.43
Tauranga	Tauranga1	0.01	1.8	2.66	0.01	1.7	7.68	0.01	1.5	2.63
	Waikareao	0.01	2.4	3.65	0.01	2.6	6.84	0.01	1.7	2.82
	Tauranga3	0.01	2.8	14.05	0.01	2.4	4.95	0.01	3.1	7.08
	Te Puna	0.01	2.7	2.83	0.01	2.2	4.20	0.01	2.1	4.43

4.3.2. Discussion of the models

Generally Boon & Byrne's equation is a good representation of the hypsometry of some of the study estuaries provided some considerations are taken into account. The very first estimation of r- and γ-values did not give a very good fit overall. However when removing the part of the bathymetry which is not affected by the tide (above MHWS) the model appeared more satisfactory, with reduced errors and values of γ in better accordance with the ones found in the literature. Despite the lack of details regarding the way Boon (1975) and Boon & Byrne (1981) computed the hypsometry of their study site it would seem that they also focused on the part of the basin affected by the tide and did not include the most upper part of the basin. Since hypsometry is here used as a way of describing the morphology of estuaries it makes sense to take the highest tide as the upper limit since wave and tides are the forcing with the greatest influence on the morphology (Friedrichs, 2011). The influence of the tides and the waves will be

studied more closely in Chapter 5 and Chapter 6. The goodness of the model however generally decreases when considering the basin below the average tidal level and even more so when considering the estuary below MLWS. A third evaluation of γ-values was conducted setting the curvature factor r to 0.01, as was done by Boon & Byrne (1981). This last model also appears satisfactory in a general way. However it does not represent the hypsometry well at the sites where the observed hypsometry does not have a sigmoidal shape but are rather convex (namely Bay of Islands and Lyttelton). Indeed the curvature factor r defines the inflection of the curve and imposing $r = 0.01$ will therefore force a certain shape to the curve. The hypsometries collected at some institutions are also less well represented by this third model which might be due to the interpolated method they used to compute the model grids. Furthermore the hypsometry of Wellington seems to be relatively aside in that the values obtained for γ are much higher than at any other site. Furthermore applying Boon & Byrne's equation to the sub-basins considered has proven to give similar results as when considering the full basin.

4.4. Concluding remarks

Taken as a whole, Boon & Byrne's relationship gives a good representation of the hypsometry of some of the sites (e.g. Maketu, Avon) but does not appear to fit well the observed hypsometry of other basins (e.g. Bay of Islands, Wellington). The optimal fit is obtained by considering the part of the estuary affected by the tide and especially the depth below MHWS. Setting the curvature factor r to 0.01 obviously reduces the goodness of the model (since there is one less coefficient, namely γ, used as a fitting parameter) but still gives a relatively good representation of the hypsometry of the studied estuaries apart from Bay of Islands and Lyttelton and Wellington. All in all, the third model

which has the advantage of having only one fitting coefficient, namely γ is relatively satisfactory and the γ-values will be kept. In the following chapter, we will attempt to relate those values to external parameters.

Chapter 5

Physical parameters and assessment of their potential influence on the value of γ

The aim of this section is to explain the cause of variation in the γ-values established in the previous chapter, by investigating potential external drivers. To do so, the values of physical parameters, namely the tidal range, the wind speed, the length of fetch and the significant wave height, were gathered for each study estuary and a statistical analysis was conducted first using a k-means clustering method and then by neural network clustering. The goal of the analysis is to identify group of estuaries which behave similarly and possibly explain the corresponding values of γ. The k-means clustering enables clustering of the the study sites for each forcing factor considered here. The neural network is meant to supplement it by grouping sites using combinations of the forcing factors.

5.1. Introduction

Previous works have shown that hypsometry was influenced by some forcing parameters. For instance Dieckmann *et al.* (1987) showed that more concave hypsometric curve corresponded to higher tidal range. Similarly Friedrichs and Aubrey (1996) observed that the hypsometric curves tended to be more convex when the tidal range was large , when long-term accretion occurred and/or when the wave activity was low (with the reverse occurring in the case of concave curves). This is why in this chapter some forcings are collected for each of the study sites and compared to the values of $\gamma_{3,h}$ estimated in Chapter 4 in order to identify a potential correlation.

5.2. Physical parameters

For each of the 22 studied basins and the 13 sub-estuaries, a set of forcing parameters including the tidal range, the wind speed, the length of longest fetch, the length of the fetch along the direction of the most common winds and the significant wave height were collected in order to assess their potential influence on the hypsometry. This section describes the sources and the distribution of the values of those factors.

5.2.1. Tidal range

The tidal ranges were obtained from the LINZ website (Appendix B). For each study site, the spring tidal range has been computed as the difference between the mean high water springs (MHWS) and the mean low water springs (MLWS) and the neap tidal range as the difference between the mean high water neaps (MHWN) and the mean low water neaps (MLWN). The average tidal range (i.e. the average of the two) was also calculated (Table 5.1). A shoreline classification based on tidal ranges was proposed by Davies in 1964 and reused by Hayes in 1975 and divides the estuaries into three main groups: microtidal (tidal range < 2 m), mesotidal (tidal range between 2 m and 4 m) and macrotidal (tidal range > 4 m). According to this classification, 12 of the 35 study sites (which include both the estuaries and the sub-estuaries) are microtidal, 3 are mesotidal and the rest are microtidal during neap tides but mesotidal during spring tides.

Table 5. 1: Tidal ranges of the study estuaries (the location of the sites is given in the previous chapter in Figures 4.1 to 4.7).

Site		Spring range (m)	Neap range (m)	Mean range (m)	Tidal classification
Estuary	***Sub-basin***				
Avon	**-**	2.2	1.3	1.75	Mesotidal/Microtidal
Bay of Islands	**-**	2.1	1.2	1.65	Mesotidal/Microtidal
	Sub. 1	1.8	1.4	1.6	Microtidal
	Sub. 2	2.1	1.3	1.7	Mesotidal/Microtidal
Bluff	**-**	2.3	1.4	1.85	Mesotidal/Microtidal
Firth of Thames	**-**	3.7	1.9	2.8	Mesotidal/Microtidal
Kaipara	**-**	2.9	1.9	2.4	Mesotidal/Microtidal
	Sub. 1	3.7	2.3	3.0	Mesotidal
Lyttelton	**-**	2.3	1.4	1.85	Mesotidal/Microtidal
Mahurangi	**-**	2.4	1.5	1.95	Mesotidal/Microtidal
Maketu	**-**	1.5	1.0	1.25	Microtidal
Manukau	**-**	2.9	1.7	2.3	Mesotidal/Microtidal
	Sub. 1	2.9	1.7	2.3	Mesotidal/Microtidal
	Pahurehure	3.5	2.1	2.8	Mesotidal
	Sub. 3	3.8	2.1	2.95	Mesotidal
Matakana	**-**	2.4	1.5	1.95	Mesotidal/Microtidal
Okura	**-**	2.8	1.7	2.25	Mesotidal/Microtidal
	Sub. 1	2.8	1.7	2.25	Mesotidal/Microtidal
Otago	**-**	1.7	1.2	1.45	Microtidal
Raglan	**-**	3.2	1.7	2.45	Mesotidal/Microtidal
	Waingaro	3.2	1.7	2.45	Mesotidal/Microtidal
	Waitetuna	3.2	1.7	2.45	Mesotidal/Microtidal
Tairua	**-**	1.8	1.2	1.5	Microtidal
Tauranga	**-**	1.8	1.2	1.5	Microtidal
	Sub. 1	1.8	1.2	1.5	Microtidal
	Waikaraeo	1.8	1.2	1.5	Microtidal
	Sub. 3	1.8	1.2	1.5	Microtidal
	Te Puna	1.9	1.3	1.6	Microtidal
Waitemata	**-**	2.8	1.8	2.3	Mesotidal/Microtidal
Wellington	**-**	1.4	0.7	1.05	Microtidal
Whangamata	**-**	2.0	1.0	1.5	Microtidal
Whangarei	**-**	2.3	1.5	1.9	Mesotidal/Microtidal
Whangateau	**-**	2.5	1.7	2.1	Mesotidal/Microtidal
Whitford	**-**	3.0	1.6	2.3	Mesotidal/Microtidal
Whitianga	**-**	1.8	1.2	1.5	Microtidal

5.1.2. Wind speed and fetch length

5.1.2.1. Average wind speed

The second factor that was considered was the wind. Wind data were obtained from the New Zealand's National Climate Database. This database, developed by the National Institute of Water and Atmospheric Research (NIWA), comprises climate observations from about 6500 climate stations overall and whose oldest observations date from 1850. The data are available on the CliFlo website which provides, among other data, hourly observations of surface wind. The quantity of observations (i.e. the period of time for which CliFlo provides data) is dependent upon the station going from 1 year (Kaipara's sub-basin, corresponding to station 1380) to 38 years (Pahurehure, corresponding to station 1965). Thus the data from the station the closest to each study estuary were downloaded and the corresponding wind rose was plotted (Appendix C). The direction of the most common winds was extracted and both the strongest and the average strength of the winds in that direction were derived. The direction of the most common winds and the strongest and average wind speed are given in Table 5.2.

Table 5. 2: Direction and speed of most common winds observed at the study sites. (Site locations are provided in the previous chapter Figures 4.1 to 4.7.)

Site		Direction of most common winds (°)	Along direction of most common winds
Estuary	***Sub-basin***		***Average speed of winds*** $(m.s^{-1})$
Avon	**-**	10	4.43
Bay of Islands	**-**	270	4.15
	Sub. 1	270	4.15
	Sub. 2	270	4.15
Bluff	**-**	180	6.78
Firth of Thames	**-**	290	4.16
Kaipara	**-**	180	3.34
	Sub. 1	50	3.75
Lyttelton	**-**	30	4.91
Mahurangi	**-**	200	3.73
Maketu	**-**	240	1.39
Manukau	**-**	260	9.17
	Sub. 1	260	9.17
	Pahurehure (Sub. 2)	270	5.14
	Sub. 3	220	3.38
Matakana	**-**	270	4.12
Okura	**-**	200	4.90
	Sub. 1	200	4.90
Otago	**-**	180	4.13
Raglan	**-**	180	5.72
	Waingaro	180	5.72
	Waitetuna	180	5.72
Tairua	**-**	210	4.91

Tauranga	**-**	240	7.00
	Sub. 1	200	2.34
	Waikareao	180	3.33
	Sub. 3	240	7.00
	Te Puna	240	7.00
Waitemata	**-**	210	7.29
Wellington	**-**	270	4.94
Whangamata	**-**	220	4.34
Whangarei	**-**	160	5.09
Whangateau	**-**	270	4.12
Whitford	**-**	230	2.51
Whitianga	**-**	220	2.97

5.1.2.2. Longest fetch and fetch along direction of most common winds

Another parameter considered was the fetch length. For each site, two measures were taken: the longest fetch of the estuary and the longest fetch according to the direction of the most common winds. They were measured on satellite images from 2015 available on Google Earth (Google Inc., 2015). The measurements are shown in Table 5.3.

Table 5. 3: Length of fetches at the study sites - Longest and along the direction of most common winds. (Site locations are provided in the previous chapter in Figures 4.1 to 4.7.)

Site		**Longest fetch**		**Fetch along most common winds**	
Estuary	***Sub-basin***	***Direction (°)***	***Length (km)***	***Direction (°)***	***Length (km)***
Avon	**-**	158	1.4	10	1.2
Bay of Islands	**-**	86	19	270	15
	Sub. 1		9.8	270	4.4
	Sub. 2		6.4	270	6.7

Bluff	**-**	105	8	180	6.9
Firth of Thames	**-**	166	54	290	26
Kaipara	**-**	150	46.5	180	24.7
	Sub. 1		29	50	15
Lyttelton	**-**	78	14.3	30	5.4
Mahurangi	**-**	169	5.2	200	4.1
Maketu	**-**	90	2.5	240	1.7
Manukau	**-**	116	24.2	260	22.1
	Sub. 1		7.6	260	2.1
	Pahurehure		4.3	260	3.7
	Sub. 3		9.4	220	5.3
Matakana	**-**	134	1.6	270	0.9
Okura	**-**	142	3.3	200	2.4
	Sub. 1		1.7	200	0.7
Otago	**-**	50	13.4	180	5.3
Raglan	**-**	49	5.8	180	3.4
	Waingaro		5.8	180	3.6
	Waitetuna		3.2	180	2.5
Tairua	**-**	46	2	210	0.9
Tauranga	**-**	132	20.6	240	9.0
	Sub. 1		7.2	200	5.7
	Waikaraeo		2.9	180	2
	Sub. 3		4.0	240	2.4
	Te Puna		1.6	240	1.2
Waitemata	**-**	169	9.4	210	6.1
Wellington	**-**	6	14.4	270	9.6
Whangamata	**-**	176	1.7	210	0.2
Whangarei	**-**	115	17.5	160	6.8
Whangateau	**-**	27	1.6	270	0.8
Whitford	**-**	154	3.4	230	2.5
Whitianga	**-**	37	4.5	220	4.5

5.1.2.3. Significant wave height

The height of the waves generated by winds was also calculated using the wave forecasting equation for shallow-water waves proposed by the Coastal Engineering Research

Center (CERC) in 1984. The relationship has been derived from energy considerations and more precisely includes the energy gain from wind stress and energy loss because of bottom friction and percolation. The wave height H_w is thus calculated from the wind-stress factor U_A and the length of fetch $F$with Equation 5.1 (where g is the gravitational acceleration and d is a constant water depth): Here the wind-stress factor was taken as the average speed of the most common winds (Table 5.2 and 5.3) and the corresponding fetch was used (Table 5.3). The constant depth d was taken as an average of the depth of the flats of each site. Both this value and the computed wave height are given in Table 5.4.

$$H_w = \frac{{U_A}^2}{g}\ tanh\left[0.530\left(\frac{g\,d}{{U_A}^2}\right)^{\frac{3}{4}}\right]\ tanh\left\{\frac{0.00565\left(\frac{g\,F}{{U_A}^2}\right)^{\frac{1}{2}}}{\tanh\left[0.530\left(\frac{g\,d}{{U_A}^2}\right)^{\frac{3}{4}}\right]}\right\} \quad \text{(Equation 5.1)}$$

Table 5. 4: Significant wave height at the study sites. (Site locations are provided in the previous chapter in Figures 4.1 to 4.7.)

Estuary	*Sub-basin*	*Constant depth (m)*	*Wave height (m)*
Avon	**-**		
Bay of Islands	**-**	61.1	0.84
	Sub. 1	8.2	0.48
	Sub. 2	15.7	0.59
Bluff	**-**	4.8	0.96
Firth of Thames	**-**	31.3	1.05
Kaipara	**-**	14.9	0.78
	Sub. 1	8.6	0.74
Lyttelton	**-**	16.1	0.64
Mahurangi	**-**	1.9	0.40
Maketu	**-**	1.1	0.09
Manukau	**-**	10.4	2.26
	Sub. 1	5.4	0.74
	Pahurehure	4.5	0.55
	Sub. 3	3.7	0.42
Matakana	**-**	1.8	0.21
Okura	**-**	2.1	0.41
	Sub. 1	2.6	0.23
Otago	**-**	14.8	0.53
Raglan	**-**	5.7	0.59
	Waingaro	5.5	0.60
	Waitetuna	4.4	0.50
Tairua	**-**	2.7	0.26
Tauranga	**-**	7.1	1.14
	Sub. 1	4.5	0.29
	Waikaraeo	1.9	0.26
	Sub. 3	0.6	0.44
	Te Puna	2.1	0.42
Waitemata	**-**	10	1.00
Wellington	**-**	24.3	0.84
Whangamata	**-**	4.1	0.28
Whangarei	**-**	10.7	0.73
Whangateau	**-**	3.5	0.21
Whitford	**-**	3.6	0.22
Whitianga	**-**	3.4	0.34

5.3. Potential relationships between the γ-values and the physical factors

The following section describes the statistical analysis performed in order to identify potential patterns in the factors controlling γ between the study estuaries. A first analysis was conducted using a k-means method where the potential influence of each forcing on the value of γ was assessed separately. A second analysis was done using a neural network clustering method which allows all the forcings to be considered simultaneously. Both analyses were first conducted on the dataset containing the 22 whole basins studied and then conducted on the 'extended' dataset including both the 22 study estuaries and the 13 sub-basins.

5.3.1. Clustering analysis (k-means): Forcings considered separately

In order to observe a potential influence of the physical parameters described above on the hypsometry, each of the parameters has been plotted with respect to the values of $\gamma_{3,h}$ previously estimated (cf. Chapter 4). Only the value of γ in the third model and for the part of the basin below MHWS was considered because, as established in the previous chapter, they give a relatively good representation of the hypsometry of the majority of study sites. The graphs are shown in Figure 5.1. Although no clear connection appears between $\gamma_{3,h}$ and the studied physical parameters, it seems that the highest values of the factors always correspond to relatively low γ-values (i.e. $\gamma \leq 3.5$). For instance the three sites experiencing averaged wind speeds above 6 $m.s^{-1}$, the value of $\gamma_{3,h}$ remains below 2. The *k*-means clustering was initially chosen because of its relative simplicity. It is based on an iterative, data-partitioning algorithm which assigns each studied data to one of the clusters. A data point (X on Figure 5.1) is assigned the cluster at the location for which the distance to the cluster's centroid is the smallest. The *k*-means clustering analysis was performed with MATLAB using the *kmeans* function. With this method the number of clusters k needs to be chosen by the user (The MathWorks, Inc., 2015b). Given the distribution of the data, k was set to 3. The default distance measure, namely the squared Euclidian distance, was used which means that the centroid of each cluster is defined as the mean of the data of the cluster in question. The *k*-

means analysis was performed both on the dataset containing the 22 study sites and the 'extended' dataset including the 13 sub-basins. The results of these cluster analysis are given in Figures 5.1 and 5.2 and come details are given in Tables 5.5 and 5.6.

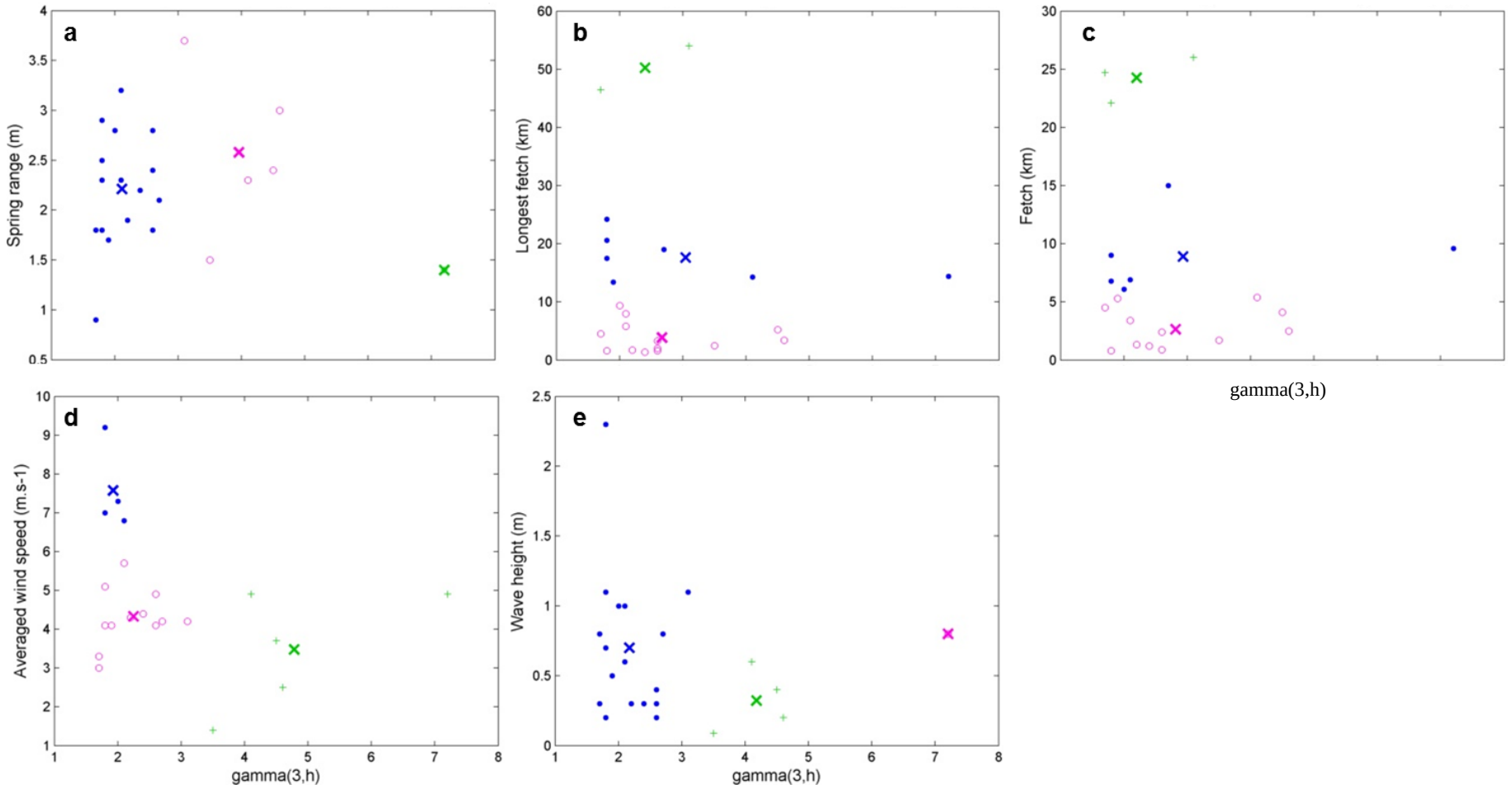

Figure 5. 1: a) Spring range, b) longest fetch, c) fetch length along direction of most common winds, d) average wind speed and e) significant wave height with respect to $\gamma_{3,h}$ for the 22 sites. Each colour (blue, pink and green) corresponds to a cluster obtained by k-means analysis (where k=3 and 25 replicates have been made)

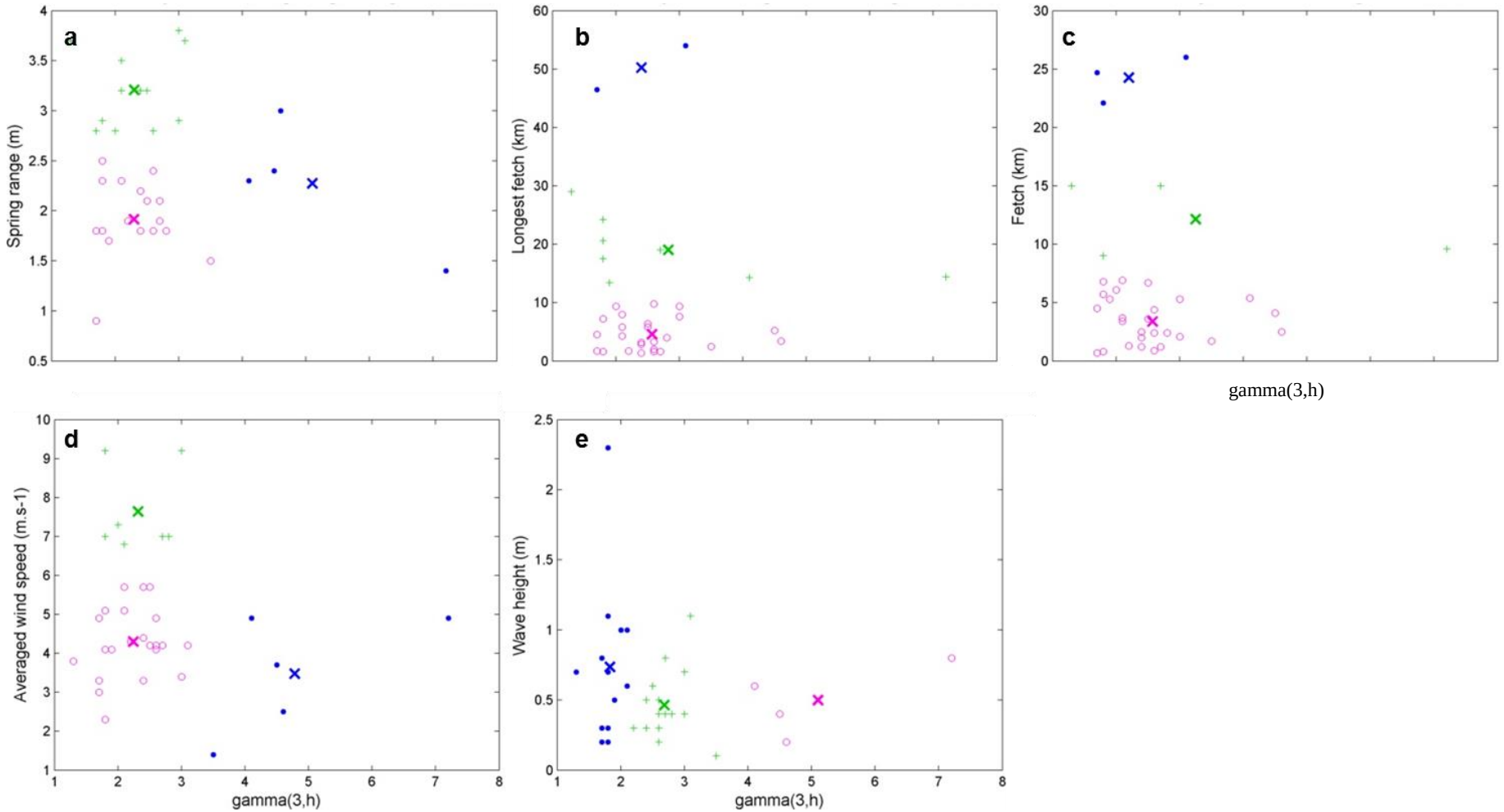

Figure 5. 2: a) Spring range, b) longest fetch, c) fetch length along direction of most common winds, d) average wind speed, e) significant wave height and f) sedimentation accumulation rates with respect to $\gamma_{3,h}$. for the 35 sites. Each colour (blue, pink and green) corresponds to a cluster obtained by k-means analysis (where k=3 and 18 replicates have been made).

Table 5. 5: Centroid location and point-to-centroid distances resulting from the k-means analysis performed on the 22 studied estuaries.

Cluster	Centroid location		Sum of point-to-centroid distance
	x	***y***	
Spring range			
1	2.1125	2.2125	6.8150
2	3.9600	2.5800	4.3800
3	7.2000	1.4000	0
Longest fetch			
1	3.0429	17.6286	117.7514
2	2.6692	3.8769	91.4308
3	2.4000	50.2500	29.1050
Fetch along direction of most common winds			
1	2.9333	8.9000	76.3533
2	2.8154	2.6485	47.5093
3	2.2000	24.2667	9.1067
Average wind speed			
1	1.9250	7.5750	3.7150
2	2.2462	4.3308	8.6200
3	4.7800	3.4800	17.4360
Wave height			
1	2.1706	0.7000	7.2153
2	7.2000	0.8000	0
3	4.1750	0.3225	0.8996
SAR			
1	2.9571	4.1714	15.3914
2	2.2000	11.0000	0
3	2.3333	0.8000	1.0667

Table 5. 6: Centroid location and point-to-centroid distances resulting from the k-means analysis performed on the 35 estuaries and sub-estuaries.

Cluster	Centroid location		Sum of point-to-centroid distance
	x	***y***	
Spring range			
1	5.1000	2.2750	7.3275
2	2.2947	1.9158	6.6347
3	2.3000	3.2083	5.1492
Longest fetch			
1	2.4000	50.2500	29.1050
2	2.8250	19.0500	233.5550
3	2.5680	4.5720	193.6448
Fetch along direction of most common winds			
1	2.1200	20.5600	113.1800
2	2.8462	6.1385	63.7431
3	2.5882	1.9588	22.8788
Average wind speed			
1	2.2391	4.3000	21.9148
2	4.7800	3.4800	17.4360
3	2.3143	7.6429	8.4457
Wave height			
1	1.8286	0.7357	4.3607
2	5.1000	0.5000	6.2200
3	2.6824	0.4647	2.5635

The first observation to be made is that the 'goodness' of the resulting clusters is uneven and depends upon the factor, i.e. some clusters are more heterogeneous than others. Indeed Tables 5.5 and 5.6 shows that the distances between the points and the centroid within each cluster is relatively low when considering the spring range and the wave height but are high for the longest fetch and the length of fetch along the direction of most common winds.

No clear trend seems to appear between the values of $\gamma_{3,h}$ and the physical parameters. Nonetheless the highest values of the forcings (spring range above 3 m, longest fetches above 40 m, fetches along direction of most common winds above 20 m, wind speed above 6 $m.s^{-1}$ and wave height above 1.5 m) seem to

always correspond to relatively low values of $\gamma_{3,h}$ ($\gamma_{3,h} < 3.5$). Since it only corresponds to a few sites (1, 2 or 3 depending on the factor) it is only a slight trend. Leaving aside those 'extreme' values, no clear influence of the spring range on the value of $\gamma_{3,h}$ can be established (Figures 5.1 (a) and 5.2 (a)). When looking at the length of fetches, the wave height and especially the average wind (Figures 5.1 (b, c, e and d) and 5-2 (b, c, e, and d)), as $\gamma_{3,h}$ gets bigger the range of the values of the parameters gets smaller and the values globally decrease. This however could be due to the fact that the amount of data decreases as $\gamma_{3,h}$ increases.

Another point is that some sites appear to group together. For example Firth of Thames and Kaipara, the two estuaries with the highest sediment loadings belong to the same cluster regarding both fetches and the wave height. In the same way Lyttelton, Mahurangi and Whitford cluster together for the 6 forcing factors.

5.3.2. Neural network clustering (SOM): Combined forcings

Another analysis was conducted on the dataset considering all the physical factors combined instead of separately. This clustering was done with 'Artificial' Neural Network (ANN) which basically consists of different algorithms working at the same time. The network can therefore be trained to give a certain output. The Neural Network Toolbox™ provided by MATLAB was used and the data were clustered with a Self-Organizing Map (SOM) setting the total number of neurons to 4 (which means the output will consist of 4 clusters). The input included six of the physical parameters, namely $\gamma_{3,h}$, the spring range, the longest fetch, the length of fetch along the direction of most common winds, the average wind speed and the significant wave height (Figure 5.3). Because the result of such an analysis can vary due to the randomness of the data, it was performed 500 times and the result (cluster combination) that was obtained the most often was chosen. As previously, the analysis was performed on both the dataset containing

the 22 study sites and the extended dataset including the sub-basins. The results are shown in Figure 5.4 and Tables 5.7 and 5.8.

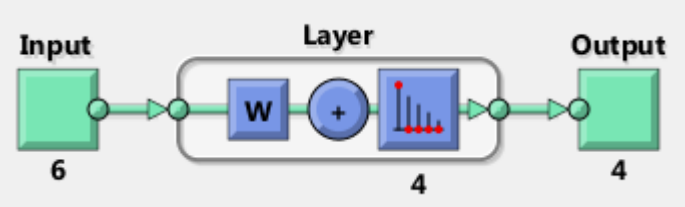

Figure 5. 3: Self-Organizing Map of the neural network clustering analysis. The input (6) indicates the number of parameters taken into account in the analysis (here being the 6 forcing factors) and the output (4) is the number of neurons (i.e. clusters) resulting from the analysis.

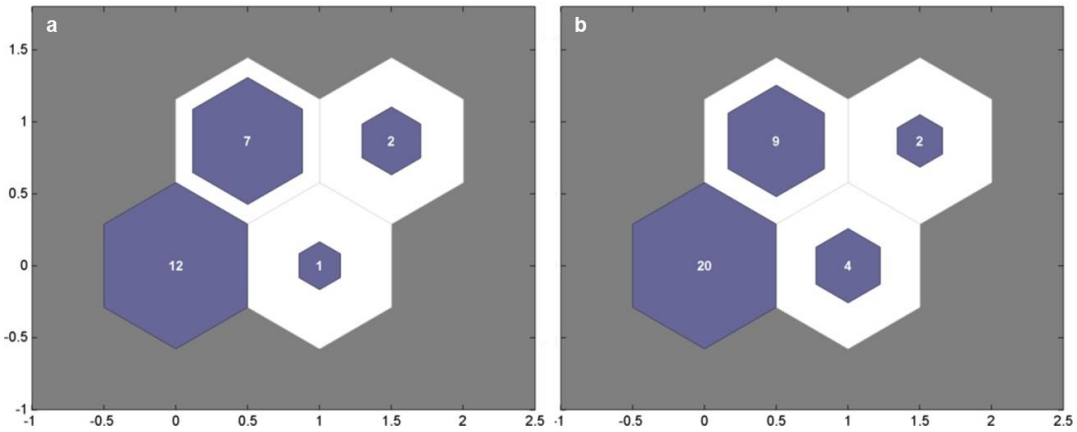

Figure 5. 4: Number of data points associated with each neuron when the analysis is performed on the a) 22 sites and b) when it includes the sub-basins.

Table 5. 7: Results of the neural network clustering performed on the 22 study estuaries.

Cluster	N1	N2	N3	N4
Site	Avon Bluff Mahurangi Maketu Matakana Okura Raglan Tairua Whangamata Whangateau Whitford Whitianga	Bay of Islands Lyttelton Otago Tauranga Waitemata Wellington Whangarei	Firth of Thames Kaipara	Manukau
Number of sites	12	7	2	1

Table 5. 8: Results of the neural network clustering conducted on the 35 sites.

Cluster	N1	N2	N3	N4
Site	Avon Bay of Islands Sub.2 Mahurangi Maketu Manukau Sub.1 Pahurehure Matakana Okura Okura Sub.1 Raglan Waingaro Waitetuna Tairua Waikaraeo Tauranga Sub.3 Tepuna Whangamata Whangateau Whitford Whitianga	**Bluff** Bay of Islands Sub.1 Lyttelton Manukau Sub.3 Otago Tauranga Sub.1 Waitemata Wellington Whangarei	Firth of Thames Kaipara	**Bay of Islands** Kaipara Sub.1 Manukau **Tauranga**
Number of sites	20	9	2	4

A first observation to be made is that the clusters are uneven: they contain from 2 to 12 sites out of 22 (Table 5.7) and from 2 to 20 sites out of 35 (Table 5.8). Moreover when adding study sites (i.e. the 13 sub-basins) 3 estuaries, namely Bluff, Bay of Islands and Tauranga, change from a cluster to another (N1 to N2 for Bluff and N2 to N4 for Bay of Islands and Tauranga). MATLAB's SOM neural network also enables visualization of the distances between adjacent neurons (Figure 5.5). The closer two neurons are to one another the more similar their elements are likely to be to each other. Figure 5.5 shows that the clusters N1 and N2 and the clusters N2 and N4 are indeed very close to one another. Conversely some basins seem to group together in any case which would mean they are more alike to one another within a same cluster. Especially the cluster N2, containing Firth of Thames and Kaipara, appear to be very different to the other (large distance to any other group).

The SOM clustering also gives the relative weight of each input factor for every cluster (Figures 5.6 and 5.7). This plot particularly shows that the bigger the cluster is, the less strongly it will be related to every input. As a matter of illustration the cluster N1, which contains the most elements, has a strong connection to the value of $\gamma_{3,h}$, a weaker one to the spring range and is weakly connected to the average wind speed, the length of the both fetches and the wave height. On the contrary the neuron N4, containing only one element, is rather strongly connected to five of the six inputs. This weight distribution of the input does not vary substantially when including the sub-basins. Similarly to the previous cluster analysis the group consisting of Firth of Thames and Kaipara (N3) is strongly connected to the longest fetch and the length of fetch along the direction of most common winds (Figures 5.1 (b and c), 5.6 (d and e) and 5.7 (d and e)). Regarding the values of $\gamma_{3,h}$, Figures 5.6 (a) and 5.7 (a) show that their influence on the way the estuaries were clustered is relatively strong for N1 (respectively N1 and N2) but very weak for N2 and N4 (respectively N4) when considering 22 sites (respectively including the 13 sub-basins). Yet when looking at the distribution of γ-values within the four clusters no correlation seems to appear (Tables 5.9 and 5.10).

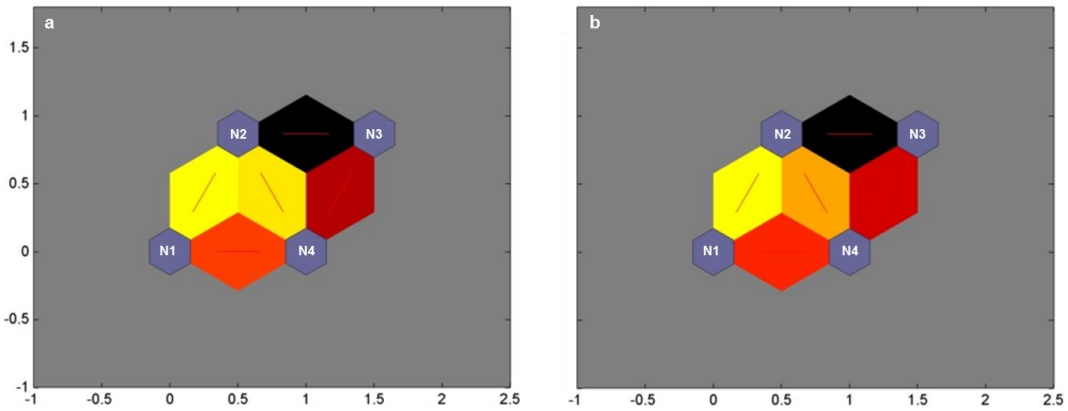

Figure 5. 5: Distances between neighbouring neurons (clusters) for the neural network analysis performed on a) 22 study sites and b) including the sub-basins. The neurons are represented by the four blue hexagons. The lighter and darker colours represent respectively smaller and larger distances between two groups.

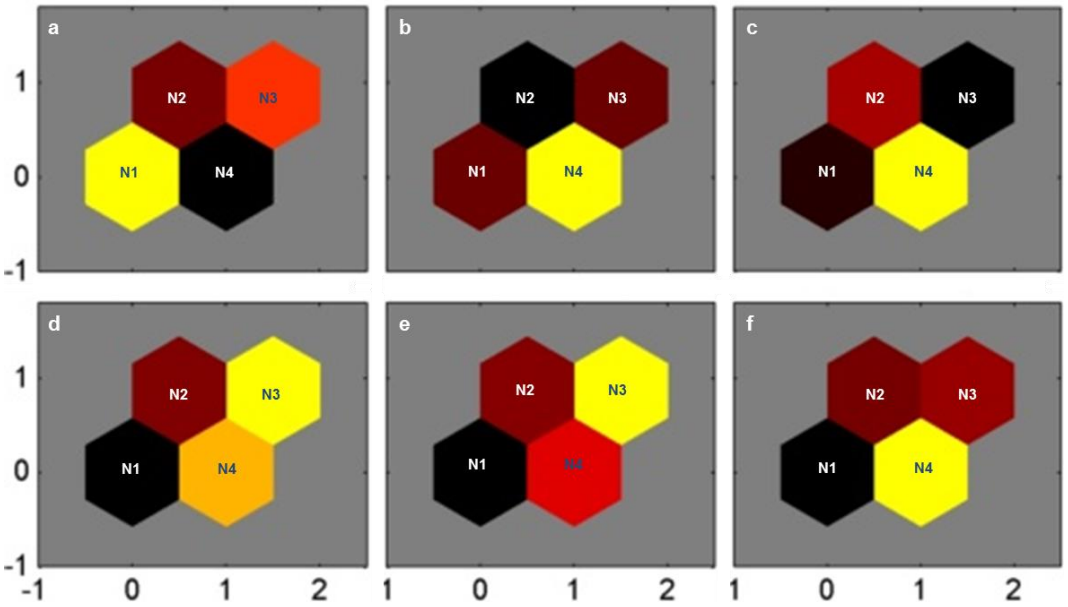

Figure 5. 6: Weight of a) $\gamma_{3,h}$, b) spring range, c) average wind speed, d) length of fetch along direction of most common winds, e) longest fetch and f) significant wave height connecting each input to each cluster defined by the neural network analysis conducted on the 22 study sites. (The lighter the colour is, the larger the input weighs.)

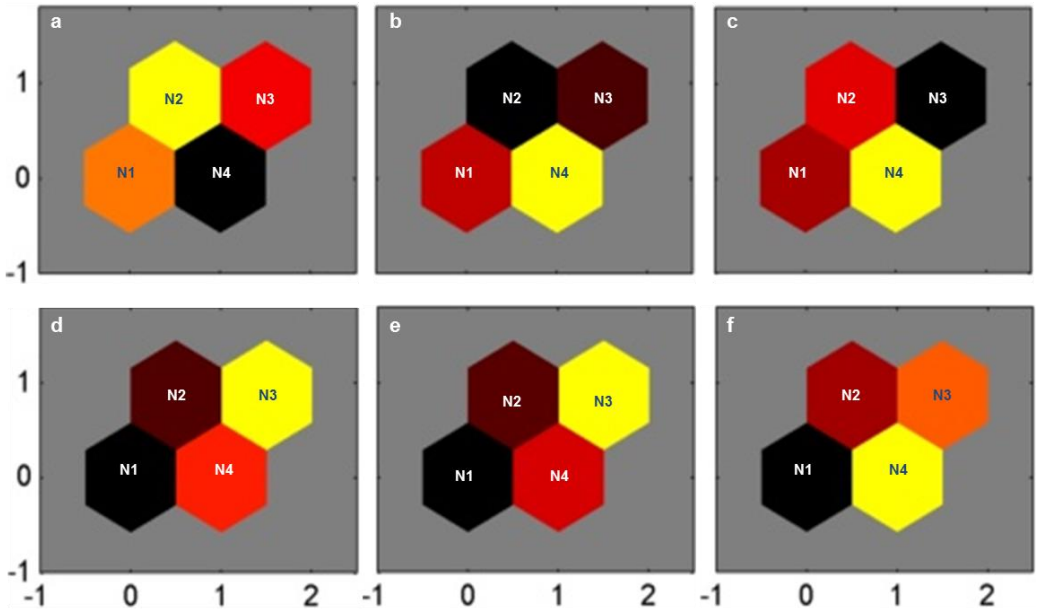

Figure 5. 7: Weight of a) $\gamma_{3,h}$, b) spring range, c) average wind speed, d) length of fetch along direction of most common winds, e) longest fetch and f) significant wave height connecting each input to each cluster defined by the neural network analysis conducted on the 35 study sites. (The lighter the colour is, the larger the input weighs.)

Table 5. 9: Distribution of $\gamma_{3,h}$ within the four clusters derived by the neural network analysis performed on the 22 study sites.

Cluster		N1	N2	N3	N4
Number of elements		12	7	2	1
$\gamma_{3,h}$	*Minimum value*	1.7	1.8	1.7	1.8
	Maximum value	4.6	7.2	3.1	1.8

Table 5. 10: Distribution of $\gamma_{3,h}$within the four clusters derived by the neural network analysis performed on the 35 sites (including sub-estuaries)

Cluster		N1	N2	N3	N4
Number of elements		20	9	2	4
$\gamma_{3,h}$	*Minimum value*	1.7	1.8	1.7	1.3
	Maximum value	4.6	7.2	3.1	2.7

5.4. Discussion

5.4.1. Established estuary classification: Estuary Environment Classification (EEC)

Environmental classifications have been widely used especially for management purposes in order to better understand large scale processes and identify patterns (Hume *et al.*, 2007). Even though the principle is common (grouping ecosystems based on their similarity to one another) the approaches can be very different and every classification will focus on different factors. Thus regarding estuaries some classifications are based on the geomorphology of the basins and others on their hydrogeology and salinity for instance (Hume *et al*., 2007; Pritchard, 1967). In 2007 Hume *et al*. introduce a classification using a controlling factor approach called Estuary Environment Classification (EEC). It contains a hierarchical component and groups estuaries at three different scales encompassing long-term interacting processes (Table 5.11).

Table 5. 11: Summary of the factors used to define the three levels of the EEC defined by Hume *et al*. (2007).

Level	Scale	Processes	Factors
1	Global scale	Climatic and oceanic	Latitude Oceanic basins Large landmasses
2	Estuary-scale	'Hydrodynamic' *(Mixing, circulation, stratification, flushing, sedimentation)*	Oceanic forcing River forcing Basin morphometry
3	Catchment	Catchment *(Variation in freshwater inflows and fluxes of terrestrial sediment and other freshwater constituents)*	Catchment geology Land cover

According to the level 2 of the EEC four of the eight categories are represented by the 22 study sites, namely D, E F and G. The description made by Hume *et al.* (2007) is given in Table 5.12. Figure 5.8 shows the values of $\gamma_{3,h}$ with respect to the study sites classified according to the EEC. Given the uneven distribution of the study sites with regard to the EEC classification no clear conclusion can be made, however it appears most of the tidal lagoons or barrier-enclosed lagoons (Category E) and most of the barrier-enclosed lagoons or drowned valleys (Category F) have a relatively low γ-value ($\gamma \leq 3$). Conversely the highest γ-values correspond to the only Category G estuary. On the one hand, although a single element does not enable derivation of a pattern, the relatively high γ-value could be attributed to the fact that Wellington is qualified as a deep, narrow and mostly sub-tidal estuary and is likely to have poor flushing. Because of its important depth the ocean and the wind do not have a great influence on the substrate (Hume *et al*., 2007). In other words Wellington seems to be the study site where tidal and wind processes are the most limited. On the other hand this site is rather special in that it is tectonically active and therefore greatly influences the morphology.

Table 5. 12: Description of classes D, E, F and G of the EEC (from Hume *et al*., 2007)

Category	Description	Study sites
D: Coastal embayments	-'Shallow, circular to slightly elongate' -Simple shorelines -Wide entrances open to the ocean -Small intertidal areas -'Hydrodynamic processes dominated by the ocean'	Firth of Thames
E: Tidal lagoons or barrier-enclosed lagoons	-'Shallow, circular to slightly elongate basins' -Simple shorelines -Narrow entrances, often constricted by a spit or sand barrier -'Extensive intertidal areas' -'Hydrodynamic processes dominated by ocean'	Lyttelton Okura Otago Whangamata
F: Barrier-enclosed lagoons or drowned valleys	-Shallow basins -Complex shorelines, often numerous arms -Narrow mouths, often spit or sand barrier at the entrance -Extensive intertidal areas -Often deep channels Hydrodynamic processes dominated by tides	Avon Bluff Kaipara Mahurangi Maketu Manukau Matakana Raglan Tairua Tauranga Waitemata Whangarei Whangateau Whitford Whitianga
G: Fjords or sounds	-Narrow, elongate basins -Very deep -Strong influence of thermohaline forcing (water circulation mainly driven by density differences between freshwater and seawater)	Wellington

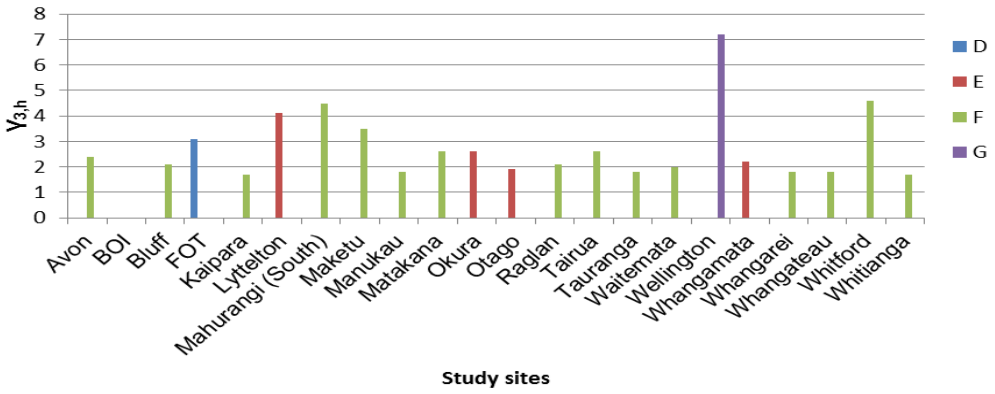

Figure 5. 8: Distribution of $\gamma_{3,h}$ with respect to study sites classified according to the EEC.

5.4.2. Influence of forcing factors on γ-values

The two statistical analyses enabled to group some estuaries together but could not show any clear influence of some forcing factors on the values of $\gamma_{3,h}$. It suggests that some study sites tend to be similar (in terms of environmental conditions) and yet have very different γ-values. This idea tends to be confirmed when looking at the distribution of the study estuaries according to the EEC defining types of estuaries particularly depending on hydrodynamic processes. However even though the EEC does not explain the values of $\gamma_{3,h}$ it has to be acknowledged that the study sites are not very varied. Indeed more than half of them are distributed within two categories which which are similar (e.g. shallow basins, narrow mouths).

Another parameter has been introduced by Friedrichs & Aubrey (1996) which is the ratio of the tidal range to wave activity. Even though they suggest that tidal range and wave activity have each an influence on the shape of the hypsometric curve they show that the relative importance of those two forcings seems to also be an important control on the shape of the curve. More precisely, they show that a high ratio (and therefore dominance of tidal currents relative to

wind waves) correlates to a more convex hypsometry whereas a small ratio corresponds to a more concave hypsometry. Thus this ratio was calculated and plotted against $\gamma_{3,h}$ for the 22 study sites (Figure 5.9). This plot shows that for most sites high ratios correspond to high values of $\gamma_{3,h}$ and as the ratio decreases the values of $\gamma_{3,h}$ decrease as well. This trend does not seem to be in agreement with Friedrichs & Aubrey's findings. Indeed for instance the hypsometric curve the two sites with the highest ratio, namely Maketu and Whitford, has a clearly concave upper part. Conversely the hypsometry of the two of the sites with the lowest ratio, namely Manukau and Tauranga, is mostly convex (Figures A.12 and A.24 in Appendix A). The trend is however not statistically significant and some sites behave as predicted by Friedrichs & Aubrey. For example Whangateau has a relatively high ratio of tide to wave and its hypsometric curve is more convex. In turn Wellington has a very low ratio and its hypsometric curve curve is clearly concave (Figure A.30 in Appendix A).

Table 5. 14: Ratio between spring range (from LINZ) and wave height (from CERC, 1984).

Site	Spring range/Wave height
Avon	7.3
BOI	2.6
Bluff	2.3
FOT	3.4
Kaipara	1.1
Lyttelton	3.8
Mahurangi	6.0
Maketu	16.7
Manukau	1.3
Matakana	12.0
Okura	7.0
Otago	3.4
Raglan	5.3
Tairua	6.0
Tauranga	1.6
Waitemata	2.8
Wellington	1.8
Whangamata	6.3
Whangarei	3.3
Whangateau	12.5
Whitford	15.0
Whitianga	6.0

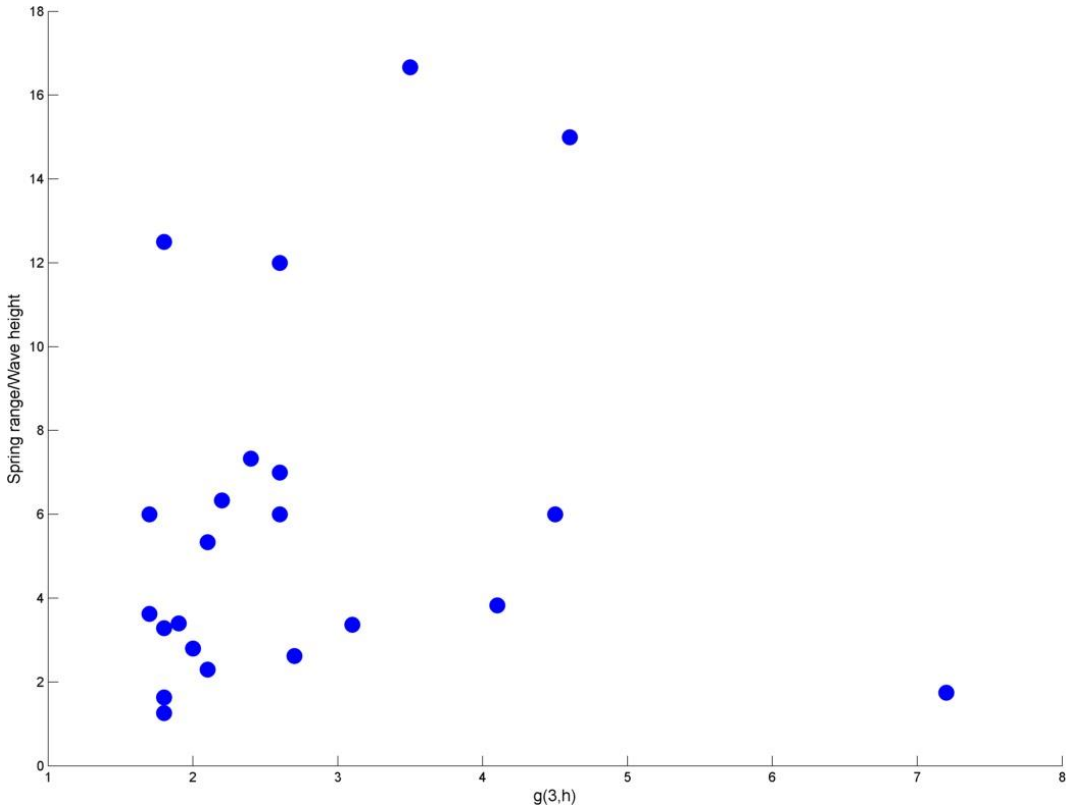

Figure 5. 9: Ratio of spring range by wave height with respect to $\gamma_{3,h}$.

5.5. Concluding remarks

The two statistical analyses (clustering by k-means and neural network) do not show any clear correlation between the values of $\gamma_{3,h}$ estimated in the previous chapter and the forcing factors (tide, fetch, wind or wave). It only shows some trends suggesting that estuaries with similar environmental conditions can have very different γ-values. This would suggest that the values of γ could not be explained and therefore predicted only by the following forcing factors: tide, length of fetch, wind and wave. The limited number of sites and especially the fact that are not very varied regarding the factors considered prevents however from drawing any clear conclusions.

Chapter 6

Non-environmental parameters: Tidal dominance and degree of infilling

This chapter presents some parameters describing the study estuaries that are not environmental (described in the previous chapter) but give some indications regarding the sediment transport in the basins and consequently regarding their infilling. More precisely, current data, collected during previous deployments, are presented for four of the study sites. Then rates of sedimentation extracted from the literature are given. The final indicator is a proposed measure of the actual 'degree' of infilling of the study sites. The observations are compared to the ones made by Boon & Byrne in 1981.

6.1. Introduction

Infilling is a natural and ongoing process which shapes the morphology of estuaries (Hume & Swales, 2003). One important driver of infilling is the tidal currents with the difference of magnitude of velocity and the difference of duration between ebb and flood being particularly important (Dronkers, 1986). Current data are described in the next section for four of the study sites. These current meter data provide particular insight regarding the net sediment transport (seaward or landward). The sedimentation accumulation rates (SAR) have also been gathered from studies of most of the study sites in order to assess a potential correlation with the values of $\gamma_{3,h}$ calculated in previous chapters. The last sub-section focuses on the maturity of the study sites. A quantitative measure of maturity is estimated as a proportion of the intertidal area compared to the area of

the whole estuary. This enables comparison of the values of $\gamma_{3,h}$ estimated in this study with the findings of Boon & Byrne (1981) and assessment of whether the γ-values can be correlated to the infilling of an estuary.

6.2. Non-environmental factors: Currents, sedimentation and degree of infilling

6.2.1. Current data

Current data have been collected for four of the study sites, Maketu, Raglan, Tairua (data collected at three different locations) and Tauranga (data from two locations) from recent work. Some details of the data collection are given in Table 6.1 along with their source. For each of them the current data have been processed with MATLAB and velocity stage plots have been made (Figures 1 to 4). Those plots show the magnitude of the velocity of the tide at different elevations. They particularly give an insight of the flood/ebb dominance. The values of the maximum velocity both during ebb and during flood are given in Table 6.2 for each velocity stage plot. At Maketu and Raglan, the velocity of the tide reaches a higher peak during the ebb than during the flood which indicates that those estuaries are overall ebb-dominant. At Tairua and Tauranga the available data seem to indicate a spatial difference in dominance within the estuary. Indeed Figures 6.3 and 6.4 show that the tide gets more and more distorted as it propagates in the estuary. However when taking an average of the three locations, it appears that Tairua estuary is overall ebb-dominant with a peak of velocity reaching 0.54 $\mathrm{m.s^{-1}}$ during the flooding tide (compared to 0.53 $\mathrm{m.s^{-1}}$ during the ebbing tide). Yet as it propagates within the estuary it seems that the tide becomes less and less ebb-dominant. When taking the average of the two locations in Tauranga the tidal stage plot indicates the site is flood-dominant with

velocities reaching 0.41 $m.s^{-1}$ during flood (compared to 0.36 $m.s^{-1}$ during ebb tide). Nevertheless beside the overall dominance (ebb dominant for 3 of the sites and flood dominant for Tauranga), the peaks of magnitude of velocities in the tidal stage plots gives more detail regarding the ebbing and flooding of the tide. Indeed it is often interesting to make a distinction between the behaviour of the tide (and especially the ebb/flood dominance) at low water and high water. Most estuaries would tend to be more ebb-dominant in the lower part and particularly in the channels and become more flood-dominant at higher elevations and particularly over the tidal flats (Hunt *et al.*, 2015). This would contribute to narrow the channels on the one hand and increase the elevation of the flats on the other. Thus at all four of the sites, low water elevations always correspond to a dominance of the ebb velocities and as the water level increases there is a 'switch' to flood dominance. The elevation of this switch varies from an estuary to the other: it occurs at about mid-tide at Maketu (Figure 6.1), Tauranga (Figure 6.3) and Tairua (Figure 6.5) and a little before the highest tide at Raglan (Figure 6.2). This would mean that, for the four estuaries, when only the lower part is under water, the intertidal part (deep intertidal) is ebb-dominant whereas as the water level increases and inundates the basin the intertidal part becomes flood-dominated. Both at Maketu and Raglan, the time of slack water is very close to high or low tide but the maximum velocity occurs before high or low tide; the tide is therefore between standing and progressive. The difference in water level during the maximum flood velocity and the maximum ebb velocity (0.15 m compared to -0.05 m at Maketu and 0.55 m compared to 0.35 m at Raglan), means that the flood-dominance of the upper part of the intertidal flats is enhanced. In Tairua and Tauranga however the slack water occurs almost at the same time as high or low tide and the maximum velocity almost at mid tide which means that in those two estuaries the tide tends to be more standing.

In terms of morphology of the basins, the tidal asymmetry described above is one of the key drivers since it has a major role in the net sediment transport and especially in the transport of the suspended fraction of the sediment. The bed load portion will not be discussed here since it is not highly affected by the tidal asymmetry. Another distinction to be made is regarding the size of the sediment. Generally, the movement of the coarser suspended sediments will tend to be more

influenced by the magnitude of the current velocities and by the difference between the velocities during ebb and flood whereas the finer suspended sediments will be more affected by the duration of slack water periods (Dronkers, 2986). Therefore the ebb-dominance in the lower part of the basin would be expected to result in a net export of sediment (especially the coarser fraction) from the channels and lower intertidal, making this intertidal part more and more flat. When the tide is high, the flood dominance would be expected to lead to a deposition of sediments. The finer sediments will only be able to deposit around high tide (around the time of slack water). Overall an increase of the intertidal flat elevation and a deepening of the channels are expected. This can be observed on the hypsometric curves of Raglan and Tauranga (Figures A.20 and A.24 in Appendix A). It is also interesting to note that the elevation at which the maximum flood velocity occurs almost corresponds to the elevation of the point of inflection of each hypsometric curve rendering the expected net deposition of sediment on the upper intertidal. The shape of the curves for Maketu and Tairua are also in accordance with the expectations (developed channel and relatively high elevation of the tidal flat but the intertidal part is less flat than at the two other sites. At Tairua the fact that the part of the curve corresponding to the intertidal flat is less flat than at Raglan and Tauranga for instance could be correlated to the change of ebb/flood dominance occurring within the estuary due to the distortion of the tide. Indeed as mentioned before the tide tends to be less ebb-dominant at high elevations as it propagates inside the estuary (Figure 6.3). This would lead to an uneven deposition of sediments hence the steeper slope of the curve corresponding to the intertidal area. This hypothesis cannot be tested at Maketu since current data at only one location could be collected for the present study.

Table 6. 1: Location of the current data recording device and source of the data.

Site	Instrument	Location	Duration of deployment	Source
Maketu	Portable FSI (Falmouth Scientific Institute) current meters	2 within main channel: -Relatively close to the estuary mouth (S1); and -Further in the estuary (S2)	2 tidal cycles (24 hours) during a spring tide	Goodhue (2007)
Raglan	S4 current meter	Main channel	About 4 weeks	Hunt *et al*. (2015)
Tairua	Argonaut ADV	3 along main channel: -1 very close to the estuary month; -1 a little further but still relatively close to the mouth; and -1 further into the estuary	-1st deployment: 40 days in July 2010	Liu (2014)
Tauranga	S4 electromagnetic current meters	Motuhou and Western sites	4 tidal cycles in February 1999	Tay *et al*. (2013)

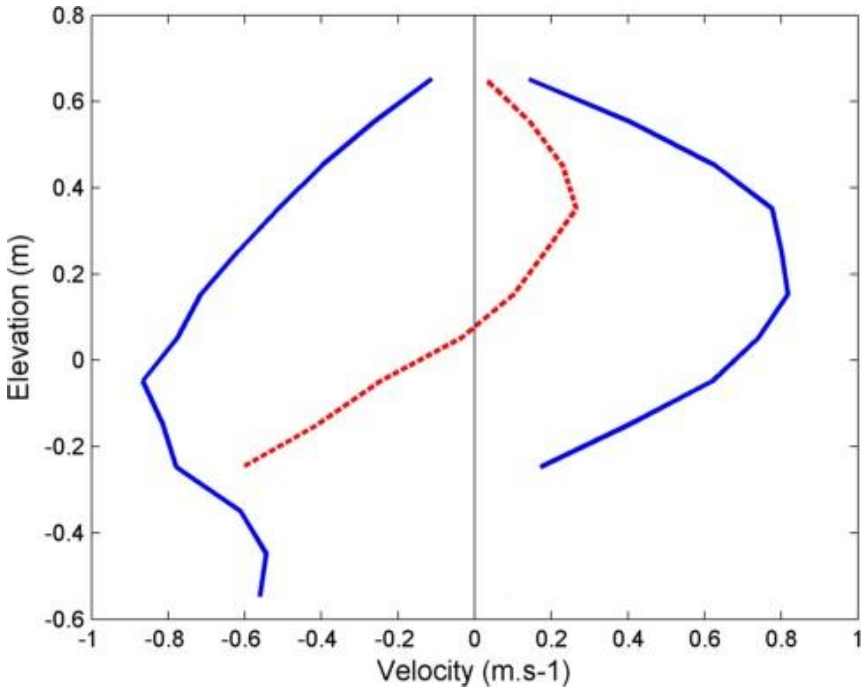

Figure 6. 1: Velocity stage plot at Maketu: Magnitude of velocity (blue line) and difference of magnitude bewteen flood and ebb (red dotted line).

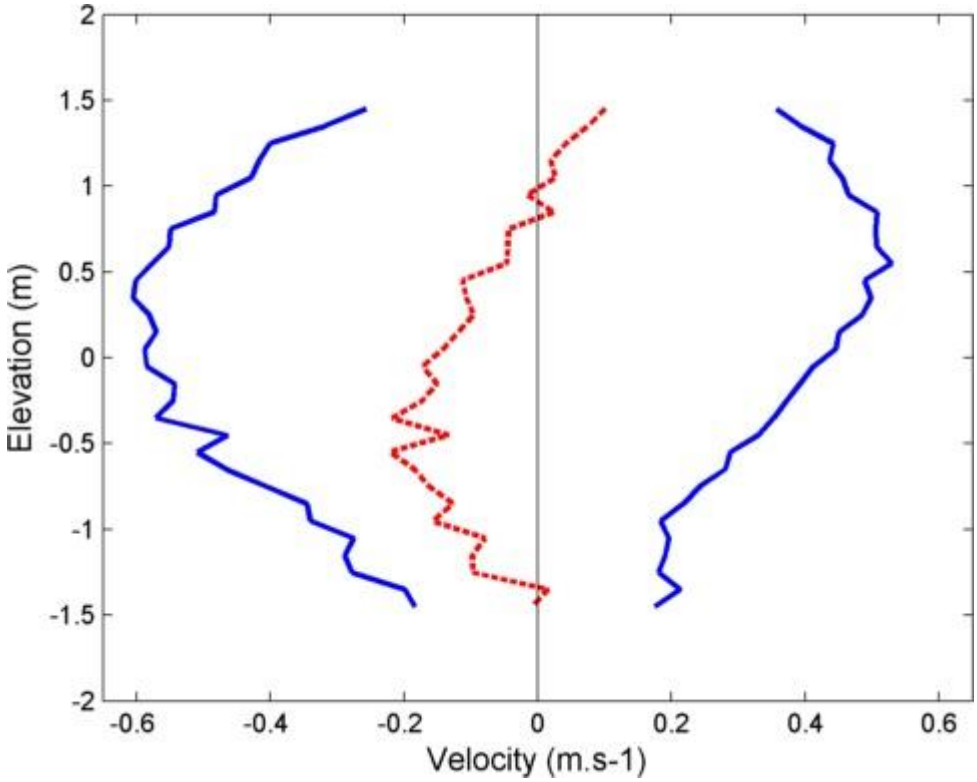

Figure 6. 2: Velocity stage plot at Raglan: Average of magnitude of velocity (blue line) and difference of magnitude between flood and ebb (red dotted line).

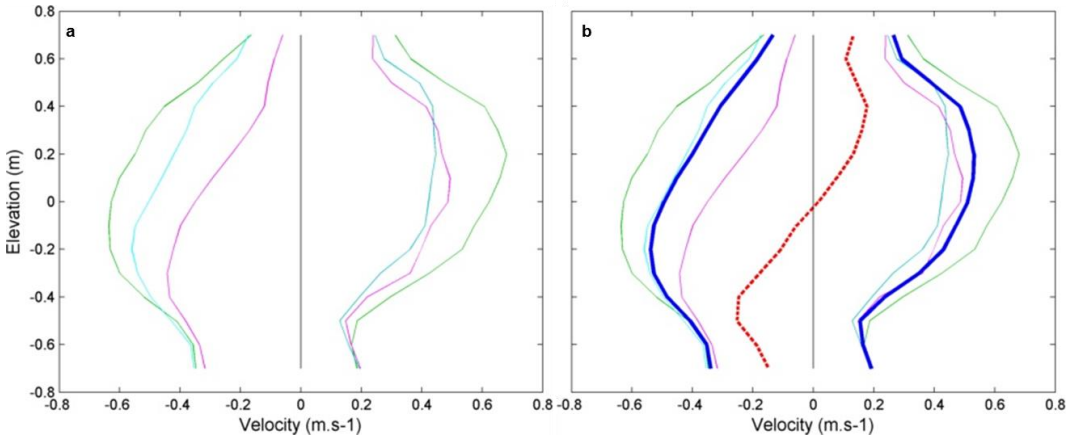

Figure 6. 3: a) Velocity stage plots at Tairua near the entrance (green and cyan) and deeper inside the estuary (magenta) and b) along with the average magnitude of velocity in the estuary (thick blue line) and difference of magnitude between flood and ebb (thick red dotted line).

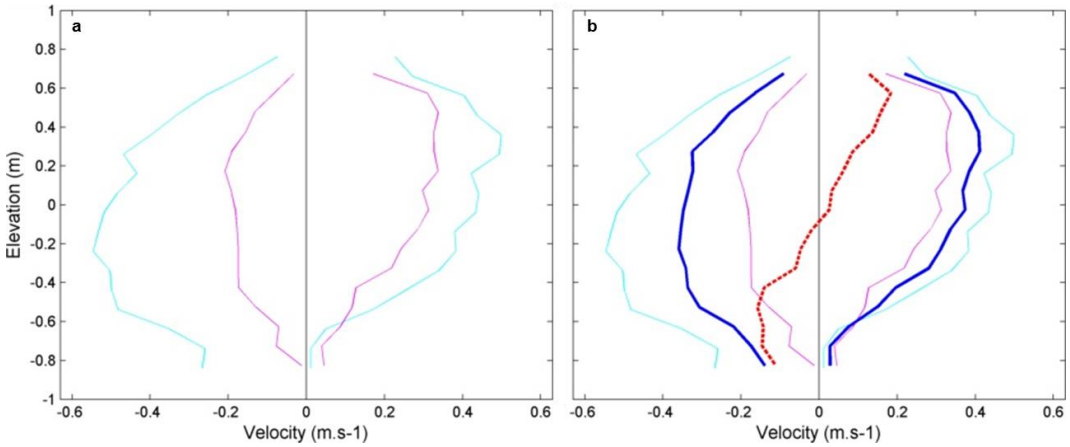

Figure 6. 4: a) Velocity stage plots at Tauranga relatively near the entrance (red) and deeper inside the harbour inside the main channel (green) and b) average velocity (blue line) and difference of magnitude between flood and ebb (red dotted line).

Table 6. 2: Maximum velocities during ebb and during flood at Maketu, Raglan, Tairua and Tauranga.

Site	Location	Ebb			Flood		
		Maximum magnitude ($m.s^{-1}$)	Elevation (m)	Area (m^2)	Maximum magnitude ($m.s^{-1}$)	Elevation (m)	Area (m^2)
Maketu		0.87	-0.05	0.72	0.82	0.15	0.57
Raglan		0.60	0.35	1.32	0.53	0.55	1.07
Tairua	ADV1	0.64	-0.1	0.68	0.68	0.20	0.65
	ADV2	0.56	-0.3	0.58	0.45	0.2	0.46
	ADV3	0.44	-0.3	0.40	0.49	0.1	0.48
	Average of three above	*0.54*	*-0.2*	*0.55*	*0.53*	*0.2*	*0.53*
Tauranga	1	0.55	-0.24	0.64	0.50	0.36	0.51
	2	0.20	0.17	0.21	0.34	0.47	0.35
	Average of two above	*0.36*	*0.23*	*0.42*	*0.41*	*0.27*	*0.42*

The maximum magnitudes of absolute velocities (which means the maximum speed reached during ebb for ebb-dominant sites and the maximum speed reached during flood for flood dominant sites) have also been plotted for each site with respect to their corresponding value of $\gamma_{3,h}$ (Figure 6.5). Given the limited number of data points, only an indication of potential trends can be derived. However two observations can be made: first the flood-dominant site (Tauranga) has the lowest value of $\gamma_{3,h}$ compared to the three ebb-dominant estuaries. Second, the value of $\gamma_{3,h}$ tends to increase with the absolute magnitude of the velocity of the tide (i.e. maximum ebb velocity for Maketu, Raglan and Tairua and maximum flood velocity for Tauranga; Table 6.7 and Figure 6.5). Yet this trend does not hold for Tairua when considering the absolute difference between the maximum velocity during ebb and during flood (Figure 6.6). Following Boon & Byrne's study (1981), the tidal duration differences between the ebb tide and the flood tide (i.e. the difference between the duration of the ebbing tide and the duration of the flooding tide) have been plotted with respect to

the values of $\gamma_{3,h}$ for the four sites studied here. A negative difference means that the ebb is longer that the flood whereas a positive difference means that the flood lasts longer than the ebb (Figure 6.7). Like Boon & Byrne's observation (1981) the sites with the smallest γ-values have positive tidal durations (which means the flood tide is longer than the ebb tide) whereas the site with the highest γ-value has a much longer ebbing tide compared to the flooding tide. Nevertheless Figure 6.7 shows that the positive tidal duration differences increase (become 'more and more positive') as $\gamma_{3,h}$ increases to 2.6. Thus at Raglan, and Tairua the tide behaves as predicted by 'traditional' theory and as described by Boon & Byrne (1981): the velocities are higher during ebb and the flooding phase is longer than the ebbing one. At Maketu however the current are stronger during ebb than during flood but the ebb lasts longer than the flood. This does not contradict Boon & Byrne (1981) since they observed that for basins with relatively high γ-values ($\gamma \geq 3.5$) the tidal duration was negative which means the ebb was longer than the flood suggesting flood dominance but the highest velocities could occur either during ebb or during flood depending on the tidal range and the location of the conveyance channel. At first glance Tauranga does not seem to completely match Boon & Byrne's study: it corresponds to a small value of $\gamma_{3,h}$ ($\gamma_{3,h} = 1.8$) and its tidal duration difference is positive (i.e. the flood is longer than the ebb) but the highest velocities are observed during flood. However this flood dominance of the magnitudes of velocities results from an average of the current data collected within the estuary. Indeed the magnitude of the velocities collected in the channel (around the middle of the basin) are higher during flood than ebb but the opposite trend is observed in the data collected nearer the entrance of the harbour(Figure 6.4a). At this second location Tauranga would therefore fit Boon & Byrne's study.

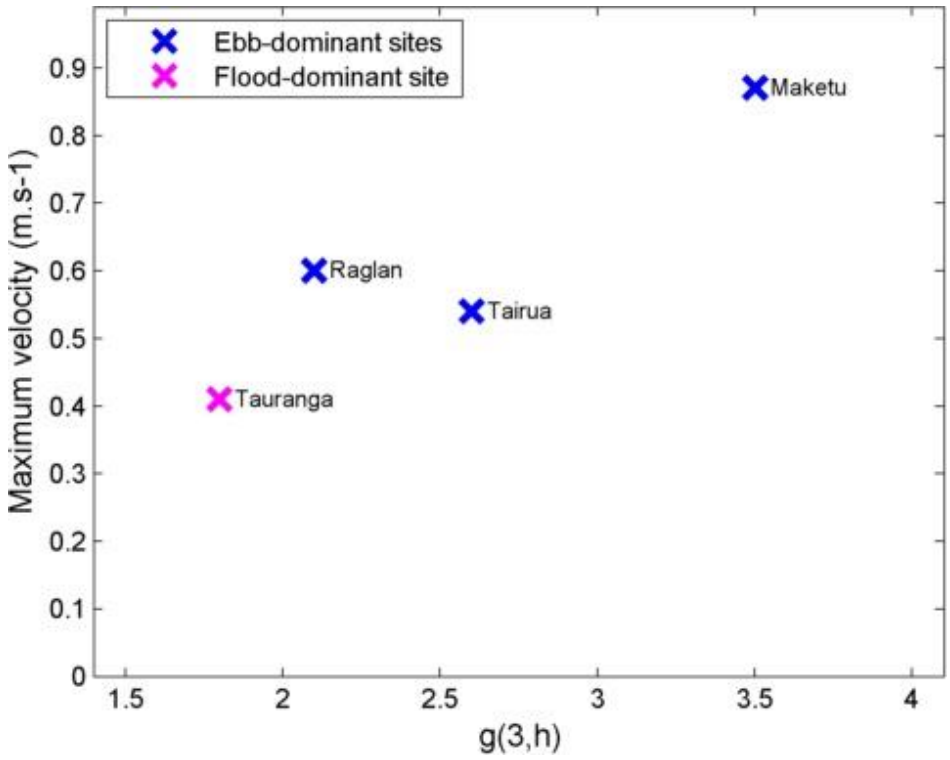

Figure 6. 5: Maximum magnitude of absolute velocity with respect to $\gamma_{3,h}$. (i.e. maximum ebb velocity for Maketu, Raglan and Tairua and maximum flood velocity for Tauranga).

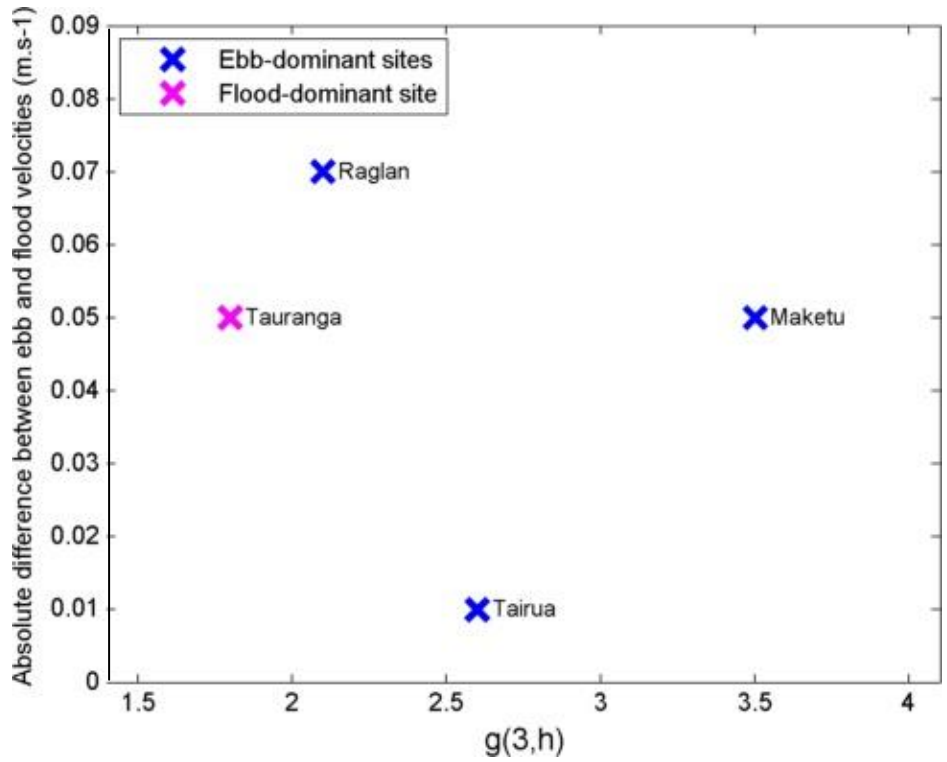

Figure 6. 6: Average difference between ebb velocities and flood velocities (in absolute values).

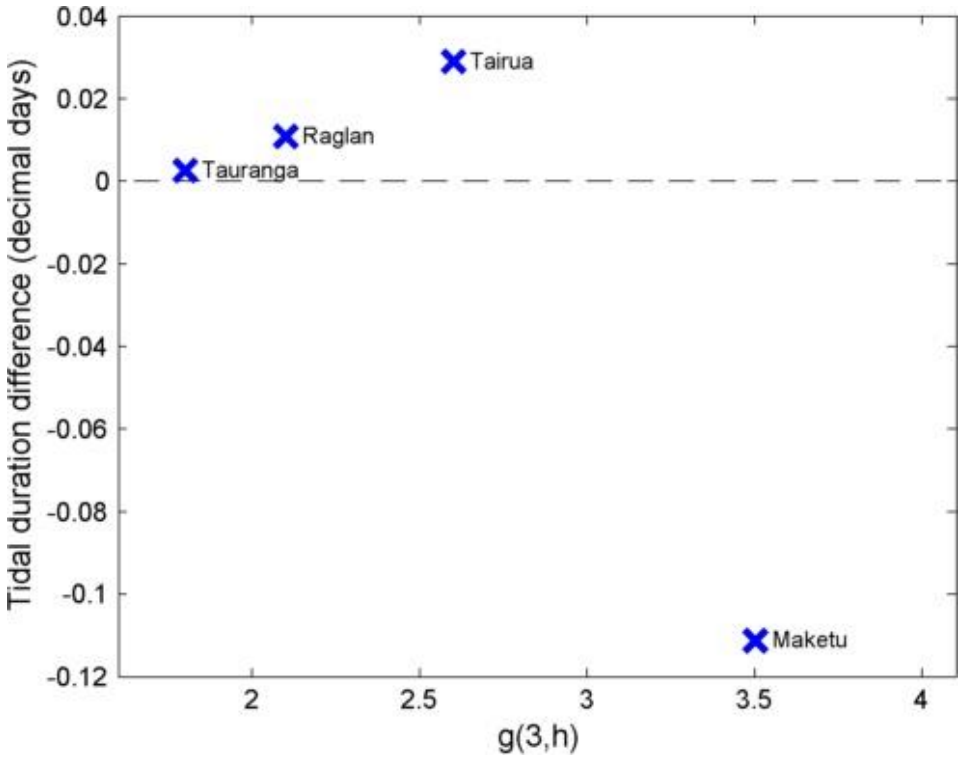

Figure 6. 7: Difference between the duration of flood and the duration of ebb.

6.2.2. Sedimentation accumulation rates

The sedimentation accumulation rates (SAR) were also considered. Sedimentation is a natural and ongoing process in estuaries which globally contributes to an increase of the elevation of the tidal flats in the long term. However this process is not constant over time and can be affected by other parameters such as sea level rise (Swales *et al.*, 2008). SAR are usually derived by measuring the thickness of sediment between layers previously dated in cores (Swales *et al.*, 2005). Deposition of sediments in estuaries is the result of the combination of a lot of different processes (driven especially by the tides and the waves). The rates in which a basin infills with sediments is therefore mainly dependent upon the relative efficiency of each process and the availability of the material sources (Mead & Moores, 2005). Although sediments accumulation is a natural process it is often disrupted by human activities. Thus in New Zealand, sedimentation has increased with human activities and more particularly deforestation, agricultural land use and the development of urbanisation (Swales,

2012). Table 6.3 summarizes the sedimentation accumulation rates observed at the study sites. For the sake of consistency and when several rates were given for a same site representing its evolution with time, only the most recent value was considered. Furthermore when rates were available at different locations of an estuary (e.g. values available for intertidal and subtidal areas) an average has been taken.

Table 6. 3: Sedimentation accumulation rates found in literature.

Site		**Average accumulation rate ($mm.year^{-1}$)**	**Method**	**Source**
Avon	-	-		
Bay of Islands	-	3.0	^{210}Pb dating of cores	Swales *et al.* (2010)
	Sub. 1	2.0	^{210}Pb dating of cores	Swales *et al.* (2010)
	Sub. 2	4.0	^{210}Pb dating of cores	Swales *et al.* (2010)
Bluff	-	-		
Firth of Thames	-	1.0	Coring	Hume & Dahm (1992) in Mead & Moores (2005)
Kaipara	-	~ 5	^{210}Pb dating of cores	Swales (2012)
	Sub. 1	-		
Lyttelton	-			
Mahurangi	-	~ 4.6	^{210}Pb dating of cores	Swales (2002)
Maketu	-	-		
Manukau	-	-		
	Sub. 1	-		
	Pahurehure	-		
	Sub. 3	-		
Matakana	-	-		

Okura	-	~ 4.2	^{210}Pb dating of cores	Swales (2002)
	Sub. 1	-		
Otago	-	-		
Raglan	-	≤ 0.5	Radiocarbon dating	Swales *et al.* (2005)
	Waingaro	-		
	Waitetuna	-		
Tairua	-	6	Inferred marker bed	Hume & Gibb (1987)
Tauranga	-	0.9	^{137}Cs and ^{210}Pb dating of cores	Hancock *et al.* (2009)
	Sub. 1	-		
	Waikareao	0.9	Presence of organochlorine coumpounds	Burggraaf *et al.* (1994)
	Sub. 3	-		
	Te Puna	-		
Waitemata	-	3.3	^{210}Pb dating of cores	Swales *et al.* (2002)
Wellington	-	-		
Whangamata	-	11	^{210}Pb dating of cores	Sheffieldt *et al.* (1995)
Whangarei	-	-		
Whangateau	-	-		
Whitford	-	3.1	^{137}Cs and ^{210}Pb dating of cores	Swales *et al.* (2002)
Whitianga	-	-		

Those SAR have been plotted with respect to $\gamma_{3,h}$ and a cluster analysis have been conducted using the k-means method (with $k = 3$) as described in the previous chapter. The result of the k-means clustering is shown in Figure 6.8 where each cluster is represented by a different colour (green, pink and blue) and the details are given in Tables 6.4 and 6.5. There is no clear correlation between the sedimentation accumulation rates and the values of $\gamma_{3,h}$ (Figure 6.8). However it might be noteworthy that the site with the highest sedimentation rates

(Whangamata) has a relatively low value of $\gamma_{3,h}$ but does not group together with any other site. Also the sites with the highest values of $\gamma_{3,h}$ have moderate to high sedimentation rates (SAR around 4 $mm.yr^{-1}$) especially if Whangamata is disregarded (due to its unusually high rates compared to the 21 other study sites). Yet this trend is not reciprocal since five of the sites with relatively low values of $\gamma_{3,h}$ also have SAR of the same order of magnitude (Table 6.3 and Figure 6.8).

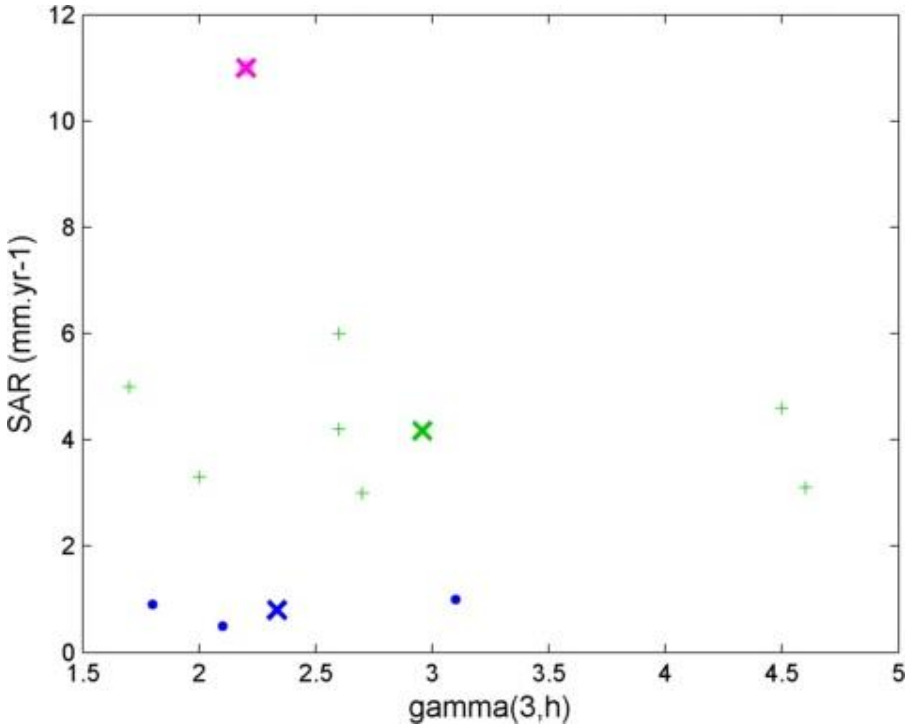

Figure 6. 8: Sedimentation accumulation rates with respect to $\gamma_{3,h}$. The color represents the 3 different clusters C1 (green), C2 (pink) and C3 (blue) and the crosses (x) are the location of the centroids.

Table 6. 4: Location of the centroids resulting from the clustering analysis.

Cluster	Centroid location		Sum of point-to-centroid distance
	x	*y*	
C1	3.0	4.2	15.4
C2	2.2	11.0	0
C3	2.3	0.8	1.1

Table 6. 5: Study sites clustered by the k-means clustering analysis given the values of $\gamma_{3,h}$ and SAR.

	C1	C2	C3
Sites	Firth of Thames Raglan Tauranga	Bay of Islands Kaipara Mahurangi Okura Tairua Waitemata Whitford	Whangamata

6.2.3. Stage of infilling

Despite variations in sedimentation rates and phases of net sediment export, on the long term, sediments accumulate until an estuary gets completely filled up. This phenomenon is sometimes referred to the aging of estuaries (Dalrymple *et al*., 1992; Hume & Swales, 2003). This infilling is rendered by an extension of the intertidal part and a reduction of the subtidal one (Swales *et al*., 2008). For this reason Swales *et al*. (2002) qualified the 'degree' of infilling of their study estuaries by comparing the extent of the intertidal area compared to the subtidal part. As an example of this is Mahurangi: they estimated the intertidal flats to be about 55% of the high tide area of the estuary and qualified the infilling 'advanced'. Within the framework of their work on the EEC (cf. chapter 5), Hume *et al.* (2007) calculated both the area at high tide and the proportion that was intertidal flats of the sites they were studying. This proportion is used here as an index of infilling and has been plotted with the values of $\gamma_{3,h}$ (Table 6.6; Figure 6.9). A k-means cluster analysis has also been conducted (with $k = 3$) as

presented in the previous chapter and the resulting clusters are given in Table 6.7. It would seem that as the proportion of intertidal area gets bigger, the value of $\gamma_{3,h}$ gets smaller, which is not surprising since both measures depend on the shape of the intertidal. Indeed the lowest γ-values correspond to the highest values of proportion of intertidal areas (ranging between 0.36 (Waitemata) to 0.85 (Whangateau) for $\gamma_{3,h} < 3$). Leaving Whitford aside, the proportion of intertidal area appears to decrease as $\gamma_{3,h}$ increases ($\gamma_{3,h}$ above 3 correspond to proportions of intertidal area below 0.58). This could however be due to the unbalanced distribution of the sites regarding their infilling: most of the estuaries are partially (proportion of intertidal above 0.40 following Swales *et al*., 2002) to substantially infilled and very few study sites are at an early stage of infilling.

Table 6. 6: Proportion of intertidal area (% of high water area) given by Hume *et al*. (2007).

Site	Intertidal area (proportion of high water area)
Avon	**0.6648**
Bay of Islands	**-**
Bluff	**0.5222**
Firth of Thames	**0.1528**
Kaipara	**0.4192**
Lyttelton	**0.1615**
Mahurangi	**0.5118**
Maketu	**0.5833**
Manukau	**0.618**
Matakana	**0.7598**
Okura	**0.7927**
Otago	**0.4532**
Raglan	**0.69**
Tairua	**0.5111**
Tauranga	**0.7701**
Waitemata	**0.3616**
Wellington	**0.0001**
Whangamata	**0.7782**
Whangarei	**0.5839**
Whangateau	**0.8544**
Whitford	**0.8152**
Whitianga	**0.7227**

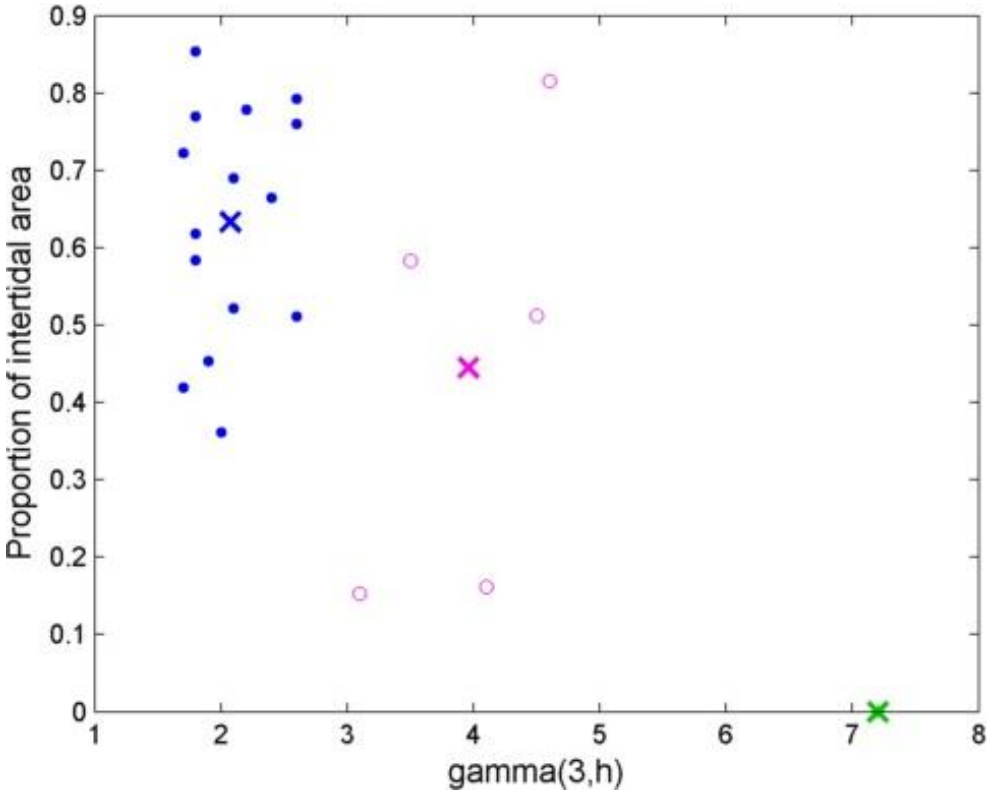

Figure 6. 9: Proportion of intertidal area with respect to $\gamma_{3,h}$. Each colour corresponds to a different cluster (C1: blue, C3: pink and C3: green) resulting from the k-means analysis and the crosses (x) give the location of the centroids.

Table 6. 7: Study sites clustered according to $\gamma_{3,h}$ and proportion of intertidal area.

Site	C1	C2	C3
Sites	Avon Bluff Kaipara Manukau Matakana Okura Otago Raglan Tairua Tauranga Waitemata Whangamata Whangarei Whangateau Whitianga	Firth of Thames Lyttelton Mahurangi Maketu Whitford	Wellington

6.3. Discussion

The current data suggest relatively good agreement with the findings of Boon & Byrne in 1981 particularly regarding the relationship between the γ-values of the sites in questions and both the tidal duration differences between ebbing and flooding and the phase during which the peak velocity occurs. Indeed, as described by Boon & Byrne, two of the sites with relatively small values of $\gamma_{3,h}$,

Raglan and Tairua (whose $\gamma_{3,h}$ is respectively equal to 2.1 and 2.6) have longer flood than ebb and stronger velocities during ebb. Also in accordance with Boon & Byrne, the site with the highest value of $\gamma_{3,h}$ (Maketu) has conversely a longer ebb than flood. The ebb dominance of the site regarding the magnitude of the velocities is not contradictory with their theory since they specify that the timing of the maximum velocities is a function of the tidal range and the location of the channel. The channel will enhance the effect of the frictional forces thus influencing the distortion of the tide. Maximum discharge would therefore be expected to be stronger during flood (phase with shorter duration) but because of the depth of the channel the velocities will be stronger during ebb especially as the water level decreases. As for Tauranga it does not appear to exactly match Boon & Byrne's findings when looking at the average of the current data. However the current data have been collected at two different locations: one inside the harbour inside the main channel and another one relatively near the entrance of the estuary but outside the main channel. The first one shows a positive tidal duration difference (longer flood than ebb) and a higher peak of velocity during ebb which matches Boon & Byrne's observations since the value of $\gamma_{3,h}$ in Tauranga have been estimated as 1.8. At the second location however there is a negative tidal duration difference (longer ebb than flood) and a higher peak of velocity during flood. This could be connected with another finding of Boon & Byrne who specify that basins with low γ-value, as it is the case here, have their tidal duration differences increasing with the cross-sectional area until the area reaches a certain value. Then the cross sectional area keeps increasing but the tidal duration differences start to decrease (Figure 6.10). Regarding Tauranga the location where the first current data have been collected being a deeper channel (with a larger cross-sectional area) the tidal duration differences are positive (longer flood) and the velocities are stronger during flood whereas the second current data have been collected in a much shallower channel (with a smaller cross-sectional area) where the tidal duration difference are much smaller (and have become negative) and where the peak of velocity occurs during flood. Applying Boon & Byrne's (1981) findings it could mean that the location corresponds to a part of the basin that is more infilled.

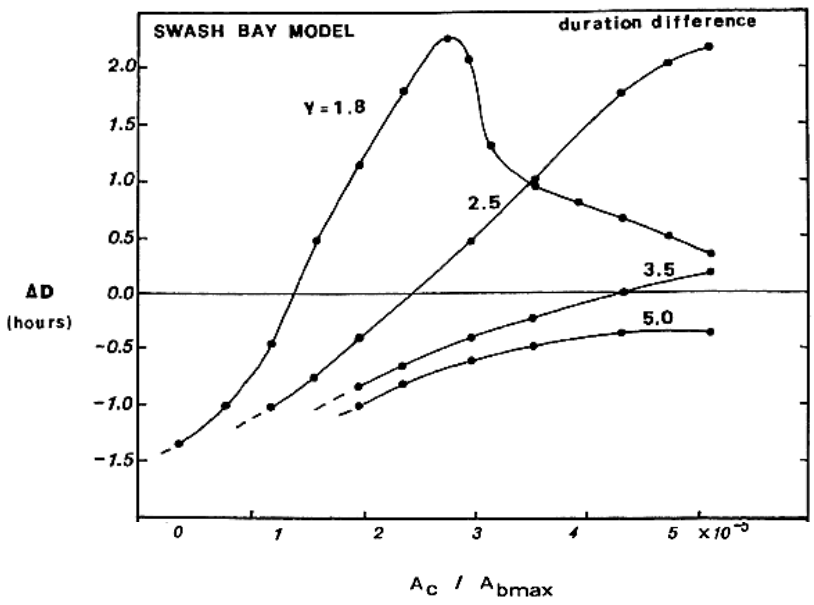

Figure 6. 10: Example of results obtained by Boon & Byrne (1981). Tidal duration differences between flood and ebb phases with respect to the cross-sectional area of the channel for basins with different values of γ ($\gamma = 1.8, 2.5, 3.5$ and 5.0; Boon & Byrne, 1981).

Sedimentation accumulation rates have also been gathered and plotted against $\gamma_{3,h}$. Given the availability of the data from previous studies for the study sites, only the most recent rates were considered. Although sedimentation is not constant over time those rates give an indication of the change in elevations of the intertidal flats (Swales *et al*., 2008). A clustering analysis was conducted but no clear correlation between the SAR and the values of $\gamma_{3,h}$ could be established. The sites with the highest values of $\gamma_{3,h}$ have relatively moderate to high sedimentation rates compared to the other study sites. This would appear to contradict Boon & Byrne's theory which relates high values of γ ($\gamma \geq 3.5$) to early basin. Indeed early basins are often expected to have relatively low SAR. Then as the basin ages (i.e. infills with sediments) the natural SAR would be expected to increase because there would be less space for sediments to deposit (Mead & Moores, 2005; Swales *et al*., 2002; Swales *et al*., 2008). The basins with low values of $\gamma_{3,h}$ do not all fit this hypothesis since they present a very wide range of sedimentation rates. Yet it is important to notice that sedimentation

accumulation rates have been influenced a lot by human activities especially in the last few centuries. Thus the very high sedimentation rate observed at Whangamata for instance takes into account the increase of deposition of material which results from the clearance of the area and the development of the forestry activity (Mead & Moores, 2005).

The third point addressed in this chapter is the stage of infilling (or maturity) of the study sites and the potential correlation with the value of $\gamma_{3,h}$. Following Swales *et al*. (2008), the degree of infilling has been quantitatively estimated by using the proportion of the intertidal area within the sites; the proportion of intertidal would therefore be all the more important that the estuary is infilled. Even though the correlation is not clear for all the study sites a trend appears: globally it would seem that the proportion of intertidal increases as the value of $\gamma_{3,h}$ decreases. This matches with Boon & Byrne's study who used the value of γ to defined the degree of infilling of their study basin setting high values ($\gamma = 3.5$ and 5.0) to simulate a basin at his early stage (young i.e. unfilled) and low values ($\gamma = 2.5$ and 1.8) to simulate its mature stage (infilled). Nevertheless although this trend appears when taking the study sites as a whole some estuaries do not follow this pattern. Especially at Whitford, the estimated value of $\gamma_{3,h}$ is relatively high ($\gamma_{3,h} = 4.6$) whereas the proportion of intertidal would suggest the basin has an advanced infilling. When looking at the hypsometric curve it appears that the elevation of the intertidal part of the basin is relatively low which is why the value of γ is high. Contrary to most of the other study sites Boon & Byrne's equation represents the hypsometry of Whitford better when the part of the below mean tide is considered (Figure A.34 in Appendix A) rather than the part below MHWS. Besides the values of $\gamma_{3,l}$ or $\gamma_{3,m}$ (2.3 and 2.9 respectively) would agree better with the proportion of intertidal. Conversely for Kaipara, Otago and Waitemata, the estimated values of $\gamma_{3,h}$ are relatively low (1.7, 1.9 and 2.0 respectively) but the proportions of intertidal indicate that the basins are at a relatively young stage of infilling. When comparing the hypsometric curves of those sites and the hypsometry predicted by Boon & Byrne's relationship given

$\gamma = \gamma_{3,h}$ it appears that Boon & Byrne's equation tends to over-estimate the extent of the flat (the observed cumulative areas corresponding to the elevations of the tidal flats are smaller than the ones predicted by the equation at the same elevations) which could explain the low values of $\gamma_{3,h}$ (Figures A.7, A.19 and A.29 in Appendix A).

6.4. Concluding remarks

This chapter presents current data for four of the study sites whose behaviour seems to be in relative accordance with Boon & Byrne's study (1981). Indeed the sites with the lowest values of $\gamma_{3,h}$ have a longer flooding tide compared to the ebbing one and the strongest magnitudes of velocities occur during the phase of shorter duration (hence the ebb-dominance of those sites). Supplementary current meters (at different locations) could help substantiate Boon & Byrne's hypothesis that ebb or flood dominance could be influenced by the cross-sectional areas of the channels by observing the behaviour of the tide inside the channels and on the tidal flats (to observe the effect of the geometry and particularly the depth of the channels). Also current data would be necessary in more estuaries in order to draw clear conclusions. The sedimentation accumulation rates do not show any clear correlation with the values of $\gamma_{3,h}$. A quantitative estimate of the degree of infilling of the study sites has also been proposed as a proportion of the intertidal part. For most of the study estuaries, the estimated values of $\gamma_{3,h}$ would behave the way Boon & Byrne expected, i.e. high values would correspond to basins at an early stage whereas low values would describe mature (infilled) estuaries. A few sites however do not match those observations which might be partly attributed to an over-estimation of the intertidal tidal flats of Boon & Byrne's model. Indeed the model sometimes predicts that the intertidal flats are larger than they actually are which leads to an under-estimation of the value of γ. In such cases considering that γ is a measure of the degree of infilling would tend to over-estimate the actual infilling of a site.

Chapter 7

General discussion and concluding remarks

7.1. General discussion: Hypsometry of New Zealand estuaries and Boon & Byrne's relationship

The hypsometry has been calculated for 22 New Zealand estuaries where the hypsometry is the distribution of the cumulative area at each elevation, following Boon & Byrne's study (1981). Apart from 2 sites, the Bay of Islands and Lyttelton, the hypsometric curves have a characteristic sigmoidal shape as described by Boon (1975) and Boon & Byrne (1981). They often show a unique point of inflection separating a concave section corresponding to the highest elevations and a convex part for the rest of the basin. Despite the global similarities, the location of the point of inflection and the area under the curve are however different for each site. The upper concave part of the curve is usually less extended than the convex one, i.e. the point of inflection is usually located near the elevation of the highest tide making the hypsometry of almost all study estuaries mostly convex. This however is not the case for Whitford and even less for Wellington for which the concavity of the upper part reaches almost half of the basin's depth at Whitford and about 70% at Wellington. The Bay of Islands' and Lyttelton's hypsometric curves seem to differ from the other sites by their wholly convex shape which even tends to come relatively close to a straight line with small variations of slope almost along the complete curve. Past studies (e.g. Dieckmann *et al.*, 1987; Friedrichs & Aubrey, 1996; Yu *et al.*, 2012) underlined the influence of the tidal range on the shape of the hypsometric curve. They observed that large tidal ranges tended to correspond to more convex curves whereas small tidal ranges could be related to more concave curves. Generally speaking all the hypsometric curves I measured were mostly convex, with small variations in the extent of the concave upper part. The spring tides of all study

sites were mesotidal or microtidal. This does not seem really consistent with previous studies. However most of the study sites with relatively high spring tidal range such as Kaipara, Manukau or Raglan for instance have an hypsometric curve which is more convex and their upper concave part is relatively small. Conversely Wellington which has the smallest spring tidal range is the site whose hypsometric curve has the largest upper concave part. In other words all the estuaries follow the pattern described by Dieckmann *et al.* (1987) and Friedrichs & Aubrey (1996) relatively well even though it does not seem that the extent of the concave upper part is correlated to the tidal range. In other words some estuaries globally follow the pattern described by Dieckmann *et al*. (1987) and Friedrichs & Aubrey (1996) in terms of concavity of the hypsometric curve but it is not applicable to all the study estuaries. Furthermore Dieckmann *et al.* who had observed the same trend in 1987 and Yu *et al.* (2012) mostly focused on the part of the curve between high water and low water. In that case a few estuaries does not seem to behave the same way such as Mahurangi and Whitford whose hypsometric curves are the ones where the concavity of the upper part is the most pronounced (apart from Wellington) and yet their tidal range is relatively large (with a spring tide of 2.4 m and 3 m respectively). In their study in 1996 Friedrichs & Aubrey (1996) also observed that the convexity of the hypsometric curve could be associated with long-term accretion and limited wave activity (with the reverse being the case for concavity). On the one hand, as before Mahurangi and Whitford seem to have the opposite behaviour compared to the one expected since they have low waves and relatively high sedimentation rates (average of about 5 $mm.yr^{-1}$ and 4 $mm.yr^{-1}$ since 1950 respectively (estimated by Swales *et al.*, 2002). Even though they suggest an influence of each one of the three parameters (tidal range, long-term net sediment transport and wave activity) Friedrichs & Aubrey (1996) note that the ratio between the tidal range and the wave activity was also important in defining the curvature of the hypsometry relating a large ratio to convex hypsometry and vice versa. In Chapter 5, only the tidal range and the wave height were considered which led to the observation that most of the study sites do not seem to behave in agreement with this pattern. Figure 7.1 gives the ratio of tide to wave with respect to the values of $\gamma_{3,h}$.and includes the SAR values. As stated in Chapter 5 a slight trend appears with higher

values of $\gamma_{3,h}$ (which usually gives more concave hypsometric curve at the highest elevations) corresponding to higher ratio of tide to wave which does not seem to follow Friedrichs & Aubrey (1996). Regarding the SAR no clear correlation appears in Figure 7.1. The highest rate (which was observed at Whangamata) does correspond to a relatively low value of γ which would agree with the fact that low values of γ characterises relatively mature (infilled) basins. In the same way, at the site with the highest values of $\gamma_{3,h}$ (Whitford and Mahurangi) the accumulation rate is relatively low which means that those sites are likely to be at a relatively early stage of infilling. However some sites such as Kaipara have low values of SAR and low values of $\gamma_{3,h}$.and vice versa. This seems to contradict Boon & Byrne's finding that the value of γ can be used as a measure of infilling for all the study sites.

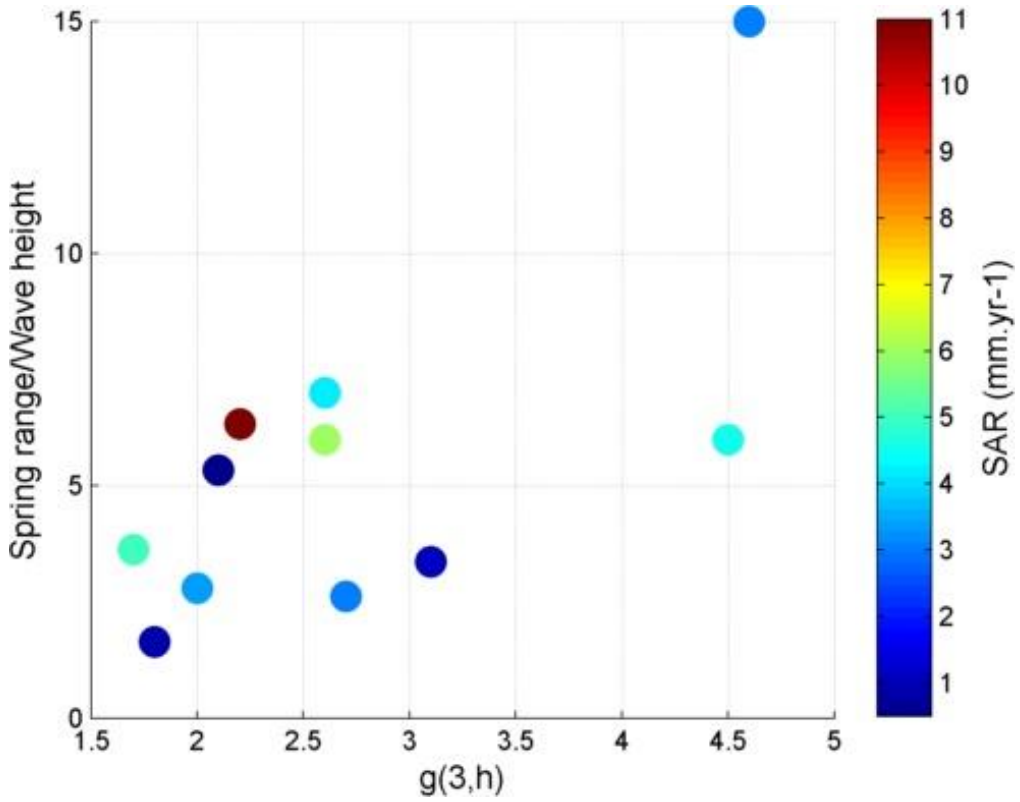

Figure 7. 1: Ratio of tidal current to wave activity with respect to $\gamma_{3,h}$ and SAR for the study sites where SAR could be collected.

In past studies, the hypsometry of basin has been modelled as a linear function (e.g. Seelig *et al.*, 1977) which has proven unsatisfactory especially when studying the geomorphology hence the development of various relationships throughout the years. Following Strahler's (1952) work, Boon (1975) and Boon & Byrne (1981) derived a formula describing the distribution of area with regard to elevation as dimensionless quantities and introducing two empirical parameters r and γ. This formula has been applied to the study sites in two different ways. First the values of r and γ were defined as the least square errors between the modelled and the observed hypsometry. The first estimation was not really satisfactory because the whole basins were considered. Indeed some studies including Dieckmann *et al.* (1987) and Friedrichs & Aubrey (1996) stressed the influence of the tide on the hypsometry. This is why a new fitting was undertaken by only considering the hypsometry below the level of the tide. When applied globally, this second estimation gave relatively good results especially when taking the level of high water during spring tides. Some sites such as Mahurangi, Matakana, Whitford and especially Wellington were however not very well represented by this model especially at the highest elevations and at the elevation at which the tidal flats stop and the channel networks starts. The lack of fit in the latter region could be because of interpolation protocols used by the researchers that developed the bathymetric grids. Secondly Boon & Byrne's formula was applied again setting the value of r to 0.01. This follows Boon & Byrne (1981), who used this value for the rest of their study, and Hunt *et al.* (2015). Using an *r* value of 0.01 is especially convenient since the present study aims at observing a potential correlation between the values of γ as defined by Boon & Byrne (1981) and the stage of infilling of the corresponding estuaries. Besides past studies and the results of the first estimation have shown that 0.01 seems to be on the right order of magnitude. This new model gave errors slightly larger compared to the observed data since there is only one free parameter left, but remains satisfactory for most of the study sites except Bay of Islands and Lyttelton. Those two sites have already been described has having a relatively different hypsometry (mostly convex and small variations of the values of the slopes all along the curve). At almost every site, there is a gap between the observed and the modelled

hypsometry when the curve drops (i.e. when the channel network begins) and at the highest elevations especially when the observed hypsometry shows a pronounced concave part as described above (e.g. Mahurangi, Maketu, Wellington, Whitford). Those gaps are especially important at Mahurangi, Wellington and Whitford where the concavity is the most marked. Thus on the whole it appears that the relationship proposed by Boon & Byrne in 1981 is relatively good at describing New Zealand estuaries' overall hypsometry (RMSE error between the observed hypsometry and the one corresponding to Boon & Byrne's equation $\varepsilon < 6\%$ for all but 4 study estuaries) but for about half of the sites the formula fails to precisely represent the hypsometric curve in the upper part of the channel network where the model tends to over-estimate the curve and/or at the highest elevations of the basin where the model tends to under-estimate the curve (below MHWS).

The estimations of the values of r and γ resulting from both considerations (r as a fitting coefficient and $r = 0.01$) in the present study are plotted on Figure 7.2 along with the values obtained in previous studies in the US (Boon, 1975; Boon & Byrne, 1981; Eiser & Kjerfve, 1986), in the UK (Townend, 2008), in New Zealand (Hunt *et al*., 2015) and considering a modelled estuary (van Maanen *et al.*, 2013). This graph shows that the estimated values of γ are globally higher in New Zealand compared to estuaries studied in the United States or the United Kingdom. According to Boon & Byrne's study in 1981 this would suggest that New Zealand estuaries are quite young compared to the ones in the UK or in the US. This could also be attributed to the various types of the estuaries developed in New Zealand. Indeed particularly because of the geology of the area basins have very different shapes which reciprocally influence the patterns of infilling (Hume & Swales, 2003).

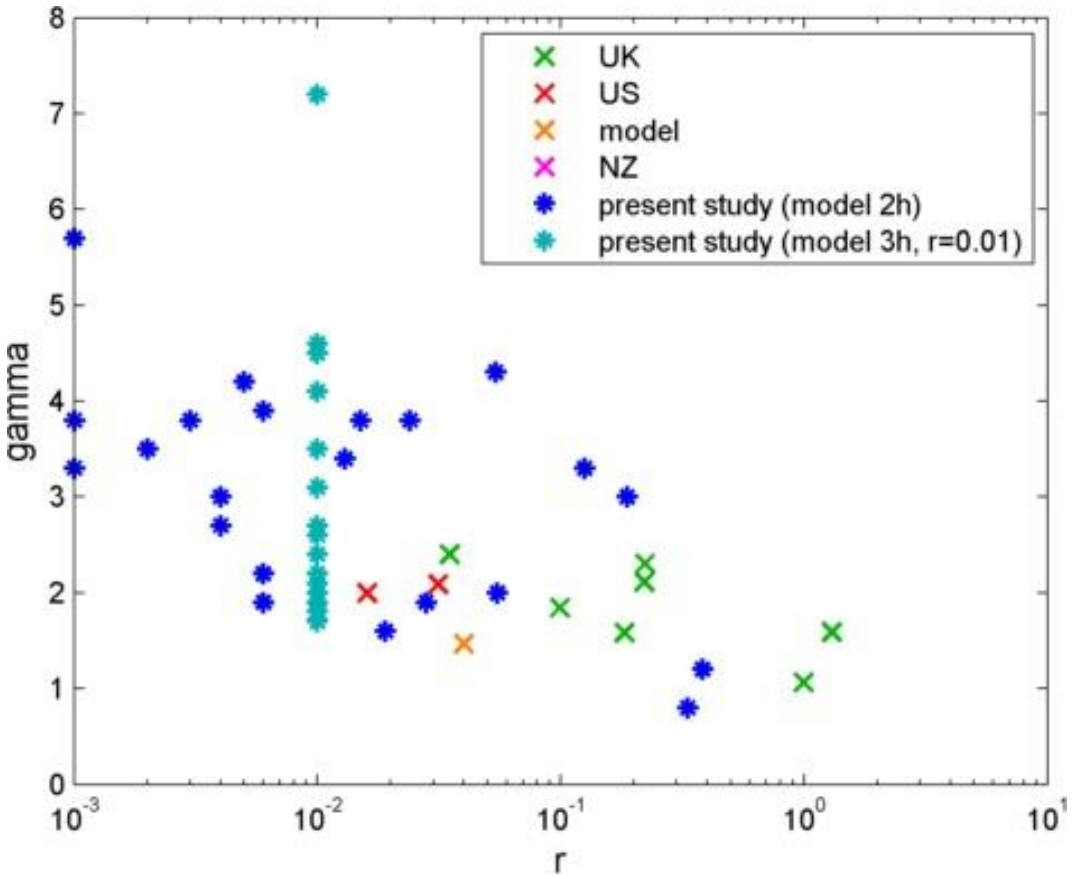

Figure 7. 2: Distribution of values of γ estimated in the present study (in dark blue for the model considering *r* as a fitting coefficient and in light blue when setting r=0.01) and found in the literature from studies conducted overseas.

Four of the study sites (Bay of Islands, Lyttelton, Waitemata and Wellington) are however not very well represented by the third model based on Boon & Byrne (1981), i.e. when considering the basin below MHWS and γ being the only fitting parameter. Firstly Bay of Islands and Lyttelton have a very different observed hypsometry compared to the other 20 sites. Indeed they show no clear drop suggesting they lack a definite channel network. Bay of Islands is a bay and can be divided into at least 2 sub-basins which could explain why Bay of Islands does not behave as the other estuary in terms of hypsometry. The sub-basins, when studied separately, do not either seem to have a typical sigmoidal shape but it might be due to the scale of the grid (the grid cell size is relatively big compared to the size of the sub-estuary). One site is not enough to define a pattern but it could be conjectured that the hypsometry of bays with very complex shoreline curvatures such as Bay of Islands cannot be represented by Boon &

Byrne's relationship if r is set to 0.01. Indeed r being an indicator of the curvature of the basins 0.01 is here an under-estimation of its value. In such cases it would therefore be worthwhile considering r as a fitting coefficient like γ. The hypsometry of Lyttelton was computed from a relatively recent bathymetric map which included a dredging of the harbour, making the resulting curve unrepresentative of natural conditions. It could be interesting to compute the hypsometry of this estuary before the dredging occurred in order to assess its impact on the curve. The third site which is not well represented by Boon & Byrne's relationship is Waitemata where a large gap is observed where the curve drops. This however might be due to the way the bathymetry was interpolated. Indeed the observed hypsometry does not have the characteristic curvature at the elevations corresponding to the upper part of the channel. A linear interpolation was likely used, which tends to over-estimate the upper part of the channel in Boon & Byrne's equation. Wellington is also not well represented by the model. One difference with the other site is that the point of inflection of its hypsometry is very low (below half of the basin's elevations) whereas at the other sites the point of inflection is very close to the most upper part. This could due to the fact that this area is tectonically active which might explain why the basin is mostly subtidal.

No clear influence of external forcing on the values of γ could be shown, but a few trends have seemed to appear. Indeed a statistical analysis has been conducted in order to observe patterns between the tidal range, the length of fetch, the wind speed and the height of the waves and the value of γ estimated at each site. There was no clear correlation but some sites seemed clustered together suggesting some external driving force. The groups are however not even with usually one or two clusters containing more than $\frac{3}{4}$ of the sites and the other two containing one or a couple of estuaries. The neural network analysis showed that the clustering is mainly driven by the value of γ and the tidal range but that their influence is not very strong. The neural network also suggested that Manukau is affected by different conditions since it constituted a cluster by itself (mainly influenced by the tidal range, average wind speed and significant wave height). In

the same way, Firth of Thames and Kaipara often grouped together and the factor with the greatest influence seemed to be the length of their fetch. Firth of Thames does have a relatively unusual shape in that the curve is steeper than others where the tidal flats should be. Yet it is a rather unusual estuary often referred to a coastal embayment (e.g. as described in the EEC, Hume *et al.*, 2007). The other two, Kaipara and Manukau, have characteristic hypsometric curves and seem to be well represented by Boon & Byrne's formula. The reason they are separated from the other sites in the neural network analysis is likely to be the length of the fetch since those three estuaries are the ones with the longest fetch along the direction of most common winds.

The last aspect of this study was to compare the values of γ and the stage of infilling of each study estuary. In 1981, Boon & Byrne used the values of γ as a measure of the infilling of their basin. Large values of γ ($\gamma = 5.0$) were used to model the basin with a young age (before infilling) and smaller values ($\gamma = 3.5, 2.5 \text{ and } 1.8$) represented older basins (as the basin gets infilled the value of γ decreases). In order to test this correlation for New Zealand estuaries, a degree of infilling of each estuary was estimated as the proportion of intertidal area of the whole estuary at high tide. The basins thus infill as the proportion of intertidal area increases. In that case the estimations of γ-values seem to globally follow the trend described by Boon & Byrne and decrease as the proportion of intertidal increases. This result is not surprising because both measures are based on the morphology of the intertidal. Nevertheless at some sites the intertidal flats are relatively deep in the basin even though the infilling is advanced (e.g. Whitford). It would also be possible that the channel network is not well developed or not well incised in an estuary which would tend to increase the value of γ but does not necessary mean that the estuary not infilled. This however is not the case for every single study estuary. For instance Whitford has a very high value of γ ($\gamma_{3,h} = 4.6$) but the proportion of intertidal area suggests that the basin is still at an early stage. Although note that Boon & Byrne's equation was not a perfect fit for Whitford. When the errors are averaged all along the curve, the

modelled hypsometric curve is globally below the observed one and the value of γ is therefore over-estimated. The opposite occurs for Kaipara and Waitemata which have a relatively low γ-value ($\gamma = 1.7$ and 2 respectively) and a relatively low degree of infilling. For those two estuaries, the modelled curve is above the observed one which likely leads to an under-estimation of the value of γ. Another thing to point out is that $2.5 \leq \gamma \leq 3.5$ are often used as the threshold values between an unfilled and an infilled basin (Boon & Byrne, 1981; Moore *et al.*, 2009; Gardiner *et al.*, 2011). Values of γ above 3.5 would correspond to early basins (little infilled) showing flood-dominance whereas estuaries with value of γ below 2.5 should be at a mature stage (infilled) and ebb-dominant. This does not really match the current data and the SAR collected for the present study. Indeed Raglan ($\gamma = 2.1$, ebb-dominant) and Tairua ($\gamma = 2.6$, ebb-dominant) follow this trend reasonably well but Maketu ($\gamma = 3.5$, ebb-dominant) and Tauranga ($\gamma = 1.8$, flood-dominant) behave the opposite way. The SAR also suggests that the value of γ cannot be correlated to the degree of infilling. Overall according to the estimations of γ for New Zealand estuaries in the present study it seems that the parameter γ cannot be used as an indicator of infilling of every basin especially since they do not seem to be in accordance with the current data in terms of ebb or flood dominance.

7.2. Limitations

A point important to acknowledge is that the study sites are not representative of all estuaries. The bathymetry of 22 estuaries has been collected within the framework of the present study which is a relatively good number in order to identify potential patterns especially considering the commercial sensitivity of such data which therefore tend to be hard to access. 13 sub-basins whose hypsometric curve had a characteristic sigmoidal shape were also included

in order to bring out the potential patterns. However even though some trends could be identified, it seems that the dataset is not very well distributed with regard to some characteristics. For instance 13 sites are of the same type (barrier-enclosed lagoon or drowned valley) according to the EEC (Hume *et al.*, 2007) whereas the categories D (coastal embayment) and G (fjord or sound) are represented by only one site each (Firth of Thames and Wellington respectively). Similarly 21 sites out of 22 are mesotidal (when considering the spring tide). For example, most of the sites follow observations from past studies regarding the tidal range. Also regarding the data, the bathymetries were collected from different sources and were computed with different methods, some of which no precise details could be obtained. This could have influenced some of the analysis. Indeed the same bathymetry from a couple of sites was collected from different sources and the resulting hypsometry was slightly different. Therefore the diversity of interpolating methods could explain some differences.

Another aspect that needs to be remembered is that most of the present study focuses on the Boon & Byrne's relationship setting the value of r to 0.01. Indeed the aim of this work was not only to assess whether the formula could be used to describe New Zealand estuaries but also to observe whether the value of the empirical parameter γ could be used as a measure of the degree of infilling of the study estuaries. Consequently following some past studies (e.g. Boon & Byrne, 1981; Hunt *et al.*, 2015) the last fitting of Boon & Byrne's formula to the observed hypsometry used the coefficient r as a constant rather than a fitting parameter. This compromise enabled a focus on the variation of the values of γ but led to a less satisfactory model.

In their study in 2012, Yu *et al.* (2012) observed that hypsometry was influenced by the area of the basin and the tidal range. They used numerical modelling to determine whether the scale of the basin and the tidal range had an influence on the hypsometry and especially on the part of the curve representing the tidal flats. They considered the hypsometric integral, namely the area below the hypsometric curve, and the hypsometric curve itself. Their study showed that both the integral hypsometry and the area hypsometry depended upon the scale of the basin and the tidal range. More precisely, clearly concave hypsometries correspond to large basins where the tidal range is low, and vice versa. However

the scale does not seem to have an influence on the hypsometry of the study sites in the present work. Indeed the largest estuaries (study sites with the largest cumulative area) are Kaipara, Firth of Thames and Manukau. Firth of Thames has indeed a rather unusual hypsometry but it is the only coastal embayment studied in the present study. Its relatively different shape could therefore be due its size but also to its wide opening to the sea and/or the dominance of the ocean processes (rather than the tidal or river ones). Kaipara and Manukau are in turn well represented by Boon & Byrne's equation. Thus the present study does not seem to have any evidence of the scale-dependence of the hypsometry when expressed in terms of area which is in accordance with Boon (1975) and Boon & Byrne (1981).

7.3. Concluding remarks

- The bathymetry of 22 New Zealand estuaries has been collected and used to compute the hypsometry as the distribution of the areas above given elevations. When represented in the form of hypsometric curves most of them have a characteristic sigmoidal shape with a point of inflection relatively close to the upper surface of the basin separating a concave and a convex parts.

- The relationship defined by Boon & Byrne in 1981 was then applied to the data using one fitting parameter, γ, to find the best fit with the observed hypsometry. It has appeared that the model proposed by Boon & Byrne was reasonably satisfactory for most of the study sites provided the part of the basin below high tide was considered (the RMSE between Boon & Byrne's equation and the observed hypsometric curves is below 5% for more than half of the sites and exceeds 10% for only 3 estuaries out of 22). This is in agreement with previous works which assessed the influence of the tide on the hypsometry. The main gaps were observed on the upper parts of the curve (highest elevations) and at the upper part of the channel network (where the curve changes quickly). The equation however did not work for Wellington which might be due its type (fjord) or because it is still tectonically active. It also could not represent Bay of Islands when γ was the only fitting coefficient. This might be because of the complex shoreline of this estuary. The equation could however fit the data when the coefficient r was also made variable suggesting that setting its value to 0.01 is only reasonable when the shoreline curvature is rather simple. It is important to realize that those are only hypotheses since each of those sites behaving differently have some unusual features they do not share with any other of the study sites.

- No clear influence of physical parameters (tide, length of fetch, speed of wind or wave height) on the values of γ could be shown.

- When comparing the values of γ obtained in the present study and previous studies conducted overseas it appears that the values estimated for New Zealand estuaries are globally higher. Following Boon & Byrne (1981) this could be correlated to the fact that New Zealand basins are relatively younger ecosystems than in the United Kingdom or the United States. The values of γ were then compared to the degree of infilling of the study sites. On the one hand it seems that the values of γ match the proportion of intertidal of the high water area of each basin. Indeed for most of the sites it seems that high values of γ correspond to a small proportion of intertidal whereas low values of γ to high ones. On the other hand it does not however work for all the sites and especially it globally does not match the current data or the sedimentation accumulation rates. Practically the present study would suggest that the value of γ does not give a very good indication of infilling of New Zealand estuaries and considering other parameter such as current data or accumulation rates would be needed in order to draw a clear conclusion.

References

Boon, J. D. (1975). Tidal discharge asymmetry in a salt marsh drainage system. *Limnol. Oceanogr*, *20*(1), 71-80.

Boon III, J. D., & Byrne, R. J. (1981). On basin hyposmetry and the morphodynamic response of coastal inlet systems. *Marine Geology*, *40*(1), 27-48.

Burggraaf, S.; Langdon, A.G. & Wilkins, A.L. (1994). Organochlorine contaminants in sediments of Tauranga Harbour, New Zealand. NZJMFR 28(3): 291-298.

CERC. 1984. Shore Protection Manual, Volume 1. Waterways Experiment Station, Corps of Engineers, Coastal Engineering Research Center (CERC)

Dalrymple, R. W., Zaitlin, B. A., & Boyd, R. (1992). Estuarine facies models: conceptual basis and stratigraphic implications: perspective. *Journal of Sedimentary Research*, *62*(6). pp. 1130-1146

Davies, J.L. (1964). A morphogenic approach to world shorelines: Zeit. f. Geomorph., v. 8., p. 27-42.

Dieckmann, R., Osterthun, M., & Partenscky, H. W. (1987). Influence of water-level elevation and tidal range on the sedimentation in a German tidal flat area.*Progress in oceanography*, *18*(1), 151-166.

Dronkers, J. (1986). Tidal asymmetry and estuarine morphology. Netherlands Journal of Sea Research, 20, 117-131.

Eiser, W. C., and Kjerve B. (1986), Marsh topography and hypsometric characteristics of a South Carolina salt marsh basin, Estuar. Coast. Mar. Sci., 23, 331 – 345.

Friedrichs, C. T. (2011). Tidal flat morphodynamics: a synthesis. *Treatise on estuarine and coastal science*, *3*, 137-170.

Friedrichs, C. T. & Aubrey, D. G. (1988). Non-linear tidal distortion in shallow well-mixed estuaries: a synthesis. Estuarine, Coastal and Shelf Science, 27, 521-545.

Friedrichs, C. T. & Aubrey, D. G. (1996). Uniform bottom shear stress and equilibrium hyposometry of intertidal flats. In: Pattiaratchi, C. B. (ed.) Mixing in Estuaries and Coastal Seas. Washington, DC: AGU.

Gardiner, S., Nicholls, R., & Tanton, T. (2011). Management Implications of Flood/Ebb tidal dominance: its influence on saltmarsh and intertidal habitat stability in Poole Harbour. In *Littoral 2010–Adapting to Global Change at the Coast: Leadership, Innovation, and Investment* (p. 06004). EDP Sciences.

Glaze, M. (1998). *The design and implementation of a GUI-based control allocation toolbox in the MATLAB® environment* (Master's thesis, Faculty of the Virginia Polytechnic Institute and State University).

Goodhue, N. (2007). *Hydrodynamic and water quality modelling of the lower Kaituna river and Maketu estuary* (Master's thesis, University of Waikato, Hamilton, New Zealand). Retrieved from http://researchcommons.waikato.ac.nz/handle/10289/2375

Google Inc. (2015). Google Earth (Version 7.1.5.1557) [Software]

Green, M. O., Black, K. P., & Amos, C. L. (1997). Control of estuarine sediment dynamics by interactions between currents and waves at several scales. *Marine Geology*, *144*(1), 97-116.

Green, M. O., & Coco, G. (2007). Sediment transport on an estuarine intertidal flat: measurements and conceptual model of waves, rainfall and exchanges with a tidal creek. *Estuarine, Coastal and Shelf Science*, *72*(4), 553-569.

Hancock, N.; Hume, T. & Swales, A. (2009). Tauranga Harbour Sediment Study, Harbour Bed Sediments. NIWA Client Report HAM2008–123, prepared for Environment Bay of Plenty, March 2009. 65 pp.

Harris, P. T. (1988). Large-scale bedforms as indicators of mutually evasive sand transport and the sequential infilling of wide-mouthed estuaries. *Sedimentary Geology*, *57*(3), 273-298.

Hayes, M.O. (1975). Morphology of sand accumulations in estuaries, in L.E. Cronin, ed., Estuarine Research: v. 2, p. 3-22. Academic Press, New York.

Hume, T.M. and Gibb, J.G. (1987). The "wooden-floor" marker bed – a new method of determining historical sedimentation rates in some New Zealand estuaries. Journal of the Royal Society of New Zealand, 17 (1): 1-7

Hume, T.M. and Dahm, J. (1992). An Investigation of the Effects of Polynesian and European Land Use on Sedimentation in Coromandel Estuaries. Prepared for the Department of Conservation, Hamilton Regional Office

Hume, T., & Swales, A. (2003). How estuaries grow old. *NIWA Water and Atmosphere*, *11*(1).

Hume, T. M., Snelder, T., Weatherhead, M., & Liefting, R. (2007). A controlling factor approach to estuary classification. *Ocean & Coastal Management*, *50*(11), 905-929.

Hunt, S., Bryan, K. R., & Mullarney, J. C. (2015). The influence of wind and waves on the existence of stable intertidal morphology in meso-tidal estuaries. *Geomorphology*, *228*, 158-174.

Keulegan, G. H. (1967). *Tidal flow in entrances; water-level fluctuations of basins in communication with seas* (No. CTH TECHNICAL BULLETIN-14). COMMITTEE ON TIDAL HYDRAULICS (ARMY) WASHINGTON DC.

Kirby, R. (1992). Effects of Sea-Level Rise on Muddy Coastal Margins. *Dynamics and exchanges in estuaries and the coastal zone*, 313-334.

Kirby, R. (2000). Practical implications of tidal flat shape. *Continental Shelf Research*, *20*(10), 1061-1077.

Langbein, W. B. (1947). *Topographic characteristics of drainage basins* (pp. 125-157). US Government Printing Office.

Land Information New Zealand (LINZ) (2015). Tide predictions. Available at: http://www.linz.govt.nz/sea/tides/tide-predictions.

LINZ (2014). *Land Information New Zealand (LINZ)*. Retrieved from www.linz.govt.nz.

Liu, Z. (2014). Hydrodynamic and sediment transport numerical modelling and applications at Tairua Estuary, New Zealand (Doctoral thesis, University of Waikato, Hamilton, New Zealand). Retrieved from: http://researchcommons.waikato.ac.nz/handle/10289/8672

Lyttelton Port of Christchurch (LPC) (2012). *Capital & Maintenance Dredging Consents* [Fact sheet]. Retrieved from: http://ecan.govt.nz

Luo, W. (1998). Hypsometric analysis with a geographic information system. *Computers & Geosciences*, *24*(8), 815-821.

Masek, J. G., Isacks, B. L., Gubbels, T. L., & Fielding, E. J. (1994). Erosion and tectonics at the margins of continental plateaus. *Journal of Geophysical Research: Solid Earth (1978–2012)*, *99*(B7), 13941-13956.

Masselink, G., Hughes, MG, & Knight, J. (2011). Introduction to Coastal Processes and Geomorphology, 2nd edn. London: Hodder Education.

The MathWorks, Inc. (2015a). *MATLAB® Creating Graphical User Interfaces: User's Guide* (R2015b).

The MathWorks, Inc. (2015b). *K*-means Clustering [Webpage]. Retrieved from: http://au.mathworks.com/help/stats/k-means-clustering.html.

Mead, S. & Moores, A. (2005). Estuary sedimentation: A review of estuarine sedimentation in the Waikato region. Environment Waikato Technical Report Series 2005/13

Monahan, B.J., Pilditch, C.A., Bryan, K.R., Brockhuizer, N. 7 Ellis, J.I. Transport and retention of benthic invertebrate larvae in a large semi-enclosed meso-tidal estuary (in preparation)

Moore, R. D., Wolf, J., Souza, A. J., & Flint, S. S. (2009). Morphological evolution of the Dee Estuary, Eastern Irish Sea, UK: a tidal asymmetry approach. *Geomorphology*, *103*(4), 588-596.

National Institute of Water and Atmospheric Research (NIWA) (2015). Tide forecaster. Available at: https://www.niwa.co.nz/services/online-services/tide-forecaster.

NIWA (n.d.). CliFlo: NIWA's National Climate Database on the Web. Retrieved from: http://cliflo.niwa.co.nz/

Nordstrom, K. F., & Roman, C. T. (1996). *Estuarine shores: evolution, environments, and human alterations*. John Wiley & Sons.

Oertel, G. F. (2001). Hypsographic, hydro-hypsographic and hydrological analysis of coastal bay environments, Great Machipongo Bay, Virginia. *Journal of Coastal Research*, 775-783.

Pethick, J.S. (1994). Estuaries and wetlands: function and form. In: Wetland Management, Thomas Telford, London, pp. 75-87.

Perillo, G. M. (Ed.). (1995). *Geomorphology and sedimentology of estuaries* (Vol. 53). Elsevier.

Potter, B. (NIWA) (2001). *Estuaries* [Website page]. Retrieved from: https://www.niwa.co.nz/.

Pritchard, D.W. (1967). Observations of circulation in coastal plain estuaries. In: G.H. Lauff (Editor), Estuaries. Am. Soc. Adv. Sci., Publ., 83: 3-5.

Ridderinkhof, H. (1997). The effect of tidal asymmetries on the net transport of sediments in the Ems Dollard estuary. *Journal of Coastal Research*, 41-48.

Seelig, W.N., Harris, D.L. and Herehenroder, B.E. (1977). A spatially integrated numerical model of inlet hydraulics. Coastal Eng. Res. Cent., Fort Belvoir, Va., GITI Rep., 14: 99 pp.

Seelig, W. N., & Sorensen, R. M. (1978). Numerical model investigation of selected tidal inlet-bay system characteristics. *Coastal Engineering Proceedings*, *1*(16).

Sheffield, A.T., Healy, T.R., McGlone, M.S. (1995). Infilling Rates of a Steepland Catchment Estuary, Whangamata, New Zealand. In Journal of Coastal Research. 11(4) pp 1294-1308. 1995

Strahler, A. N. (1952). Hypsometric (area-altitude) analysis of erosional topography. *Geological Society of America Bulletin*, *63*(11), 1117-1142.

Swales, A., Hume, T.M., McGlone, M.S., Pilvio, R., Ovenden, R., Zviguina, N., Hatton, S., Nicholls, P., Budd, R., Hewitt, J., Pickmere, S. & Costley, K. (2002). Evidence for the physical effects of catchment sediment runoff preserved in estuarine sediments: Phase II (field study). Technical publication 221 prepared for Auckland Regional Council. NIWA Report HAM2002-067.

Swales, A., Ovenden, R., McGlone, M.S., Hermanspahn, N., Budd, R., Okey, M.J., Hawken, J. (2005). Whaingaroa (Raglan) Harbour: sedimentation rates and the effects of historical catchment landcover changes. NIWA technical report for Environment Waikato. Technical report 2005/36.

Swales, A.; Bell, R.G.; Gorman, R.; Oldman, J.W.; Altenberger, A. ; Hart, C.; Claydon, L.; Wadhwa, S.; Ovenden, R. (2008). Potential future changes in mangrove-habitat in Auckland's east-coast estuaries. Prepared by NIWA for Auckland Regional Council. Auckland Regional Council Technical Publication Number TR 2009/079.

Swales A., Ovenden R., Wadhwa S. & Rendle D. (2010). Bay of Islands OS20/20 survey report. Chapter 4: Recent sedimentation rates (over the last 100–150 years [pdf]. *In*: Bay of Islands OS20/20 survey report. Prepared by NIWA. Report WLG2010-38, 48 p.

Swales, A. (2012). Sedimentation in New Zealand [Website page]. Retrieved from: https://www.niwa.co.nz/freshwater-and-estuaries/research-projects/sedimentation-in-new-zealand-estuaries

Tay, H. W., Bryan, K. R., de Lange, W. P., & Pilditch, C. A. (2013). The hydrodynamics of the southern basin of Tauranga Harbour. *New Zealand Journal of Marine and Freshwater Research*, *47*(2), 249-274.

Townend, I. H. (2008). Hypsometry of estuaries, creeks and breached sea wall sites. In *Proceedings of the Institution of Civil Engineers (ICE)-Maritime Engineering*, *161*(1), 23-32.

Van Maanen, B., Coco, G., & Bryan, K. R. (2013). Modelling the effects of tidal range and initial bathymetry on the morphological evolution of tidal embayments. *Geomorphology*, *191*, 23-34.

Wang, Z. B., Jeuken, M. C. J. L., Gerritsen, H., De Vriend, H. J., & Kornman, B. A. (2002). Morphology and asymmetry of the vertical tide in the Westerschelde estuary. *Continental Shelf Research*, *22*(17), 2599-2609.

Wells, J. T., & Park, Y. A. (1992). Observations on shelf and subtidal channel flow: implications of sediment dispersal seaward of the Keum River Estuary, Korea. *Estuarine, Coastal and Shelf Science*, *34*(4), 365-379.

Yu, Q., Wang, Y., Flemming, B., & Gao, S. (2012). Modelling the equilibrium hypsometry of back-barrier tidal flats in the German Wadden Sea (southern North Sea). *Continental Shelf Research*, *49*, 90-99.

Appendix A

Bathymetric map and comparison between observed and modelled hypsometries

Figures A.1 to A.35 show the bathymetric map, the observed hypsometric curves (blue line) and the curve corresponding to Boon & Byrne's relationship (red dotted line) for all seven considerations (model 1 (r and γ used as fitting coefficients; whole basin), model 2 (r and γ used as fitting coefficients; part of the basin below MHWS, below MLWS and below the average tidal level) and model 3 ($r = 0.01$ and γ used as a fitting coefficient; part of the basin below MHWS, below MLWS and below the average tidal level) made in the present study. The corresponding estimated values of *r* and γ are given in Chapter 4.

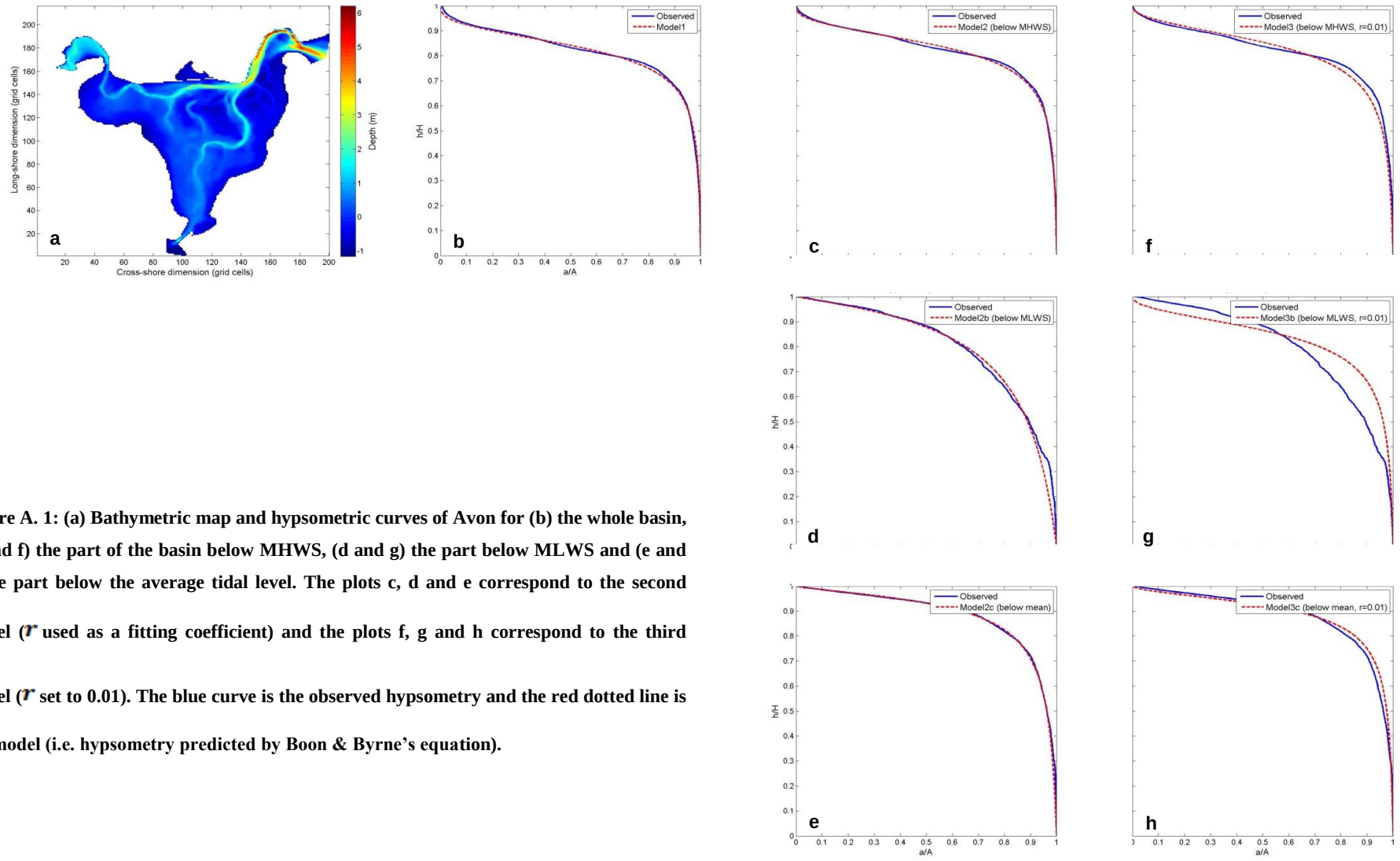

Figure A. 1: (a) Bathymetric map and hypsometric curves of Avon for (b) the whole basin, (c and f) the part of the basin below MHWS, (d and g) the part below MLWS and (e and f) the part below the average tidal level. The plots c, d and e correspond to the second model (T used as a fitting coefficient) and the plots f, g and h correspond to the third model (T set to 0.01). The blue curve is the observed hypsometry and the red dotted line is the model (i.e. hypsometry predicted by Boon & Byrne's equation).

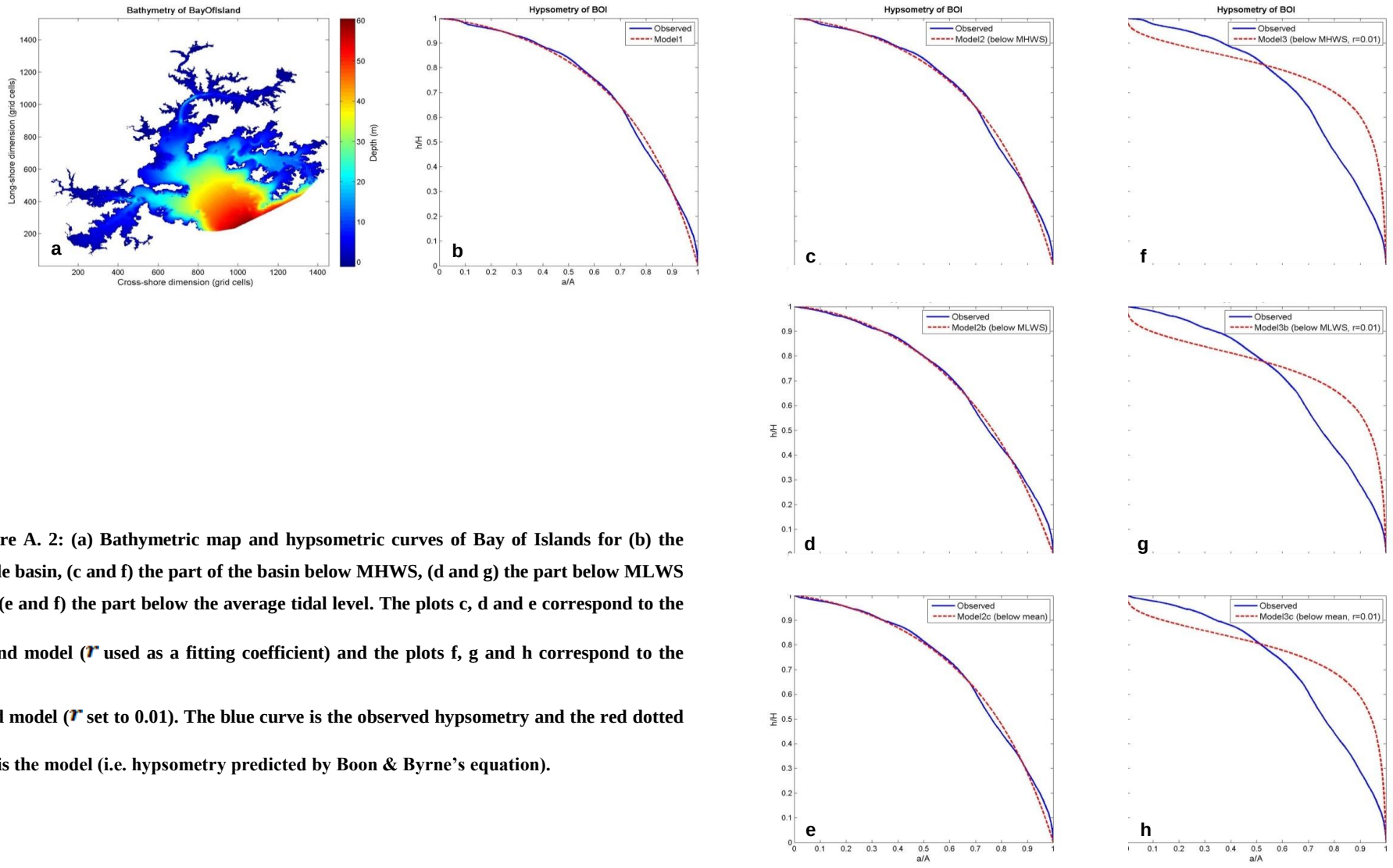

Figure A. 2: (a) Bathymetric map and hypsometric curves of Bay of Islands for (b) the whole basin, (c and f) the part of the basin below MHWS, (d and g) the part below MLWS and (e and f) the part below the average tidal level. The plots c, d and e correspond to the second model (r used as a fitting coefficient) and the plots f, g and h correspond to the third model (r set to 0.01). The blue curve is the observed hypsometry and the red dotted line is the model (i.e. hypsometry predicted by Boon & Byrne's equation).

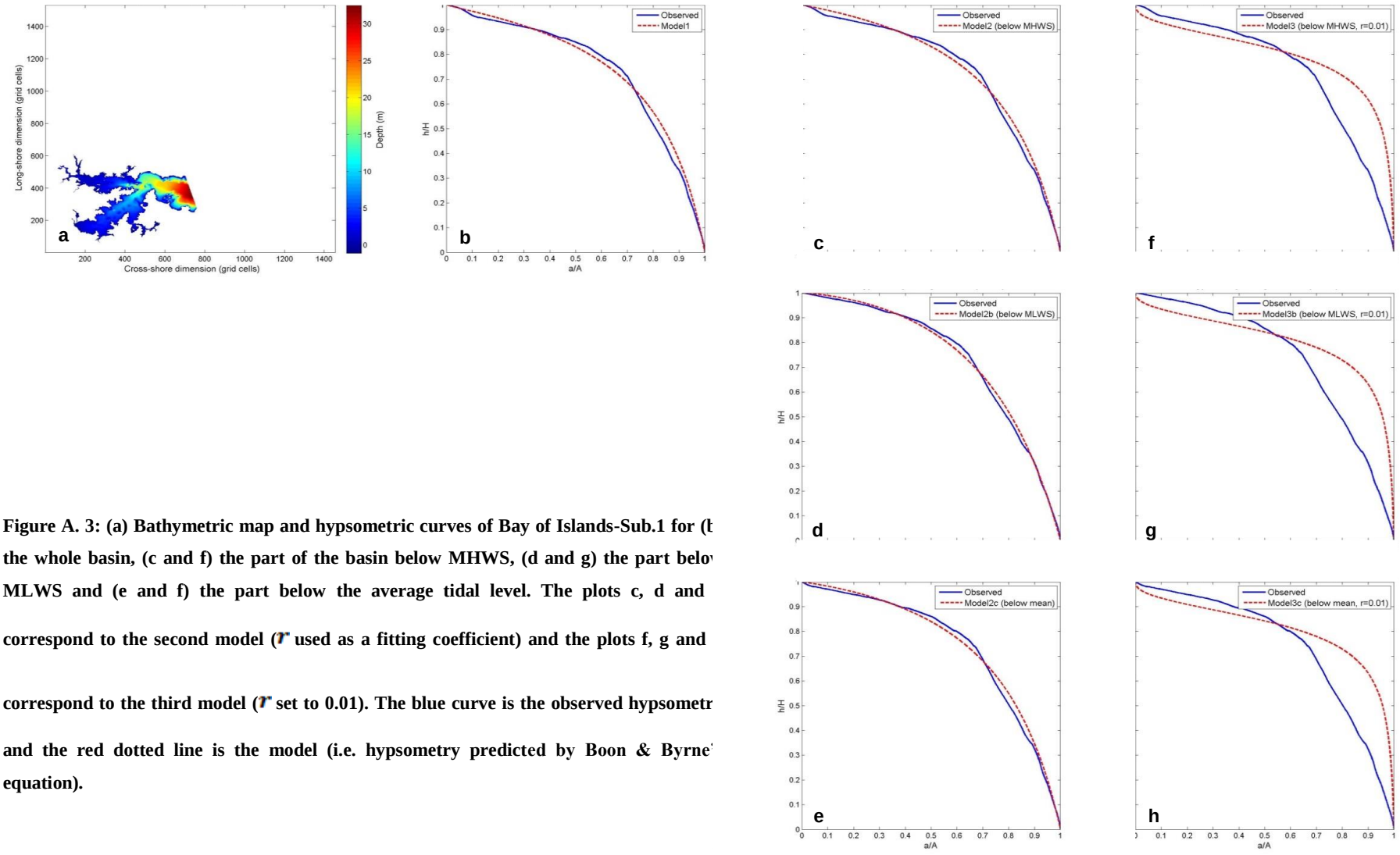

Figure A. 3: (a) Bathymetric map and hypsometric curves of Bay of Islands-Sub.1 for (b the whole basin, (c and f) the part of the basin below MHWS, (d and g) the part belo MLWS and (e and f) the part below the average tidal level. The plots c, d and correspond to the second model (r used as a fitting coefficient) and the plots f, g and correspond to the third model (r set to 0.01). The blue curve is the observed hypsometr and the red dotted line is the model (i.e. hypsometry predicted by Boon & Byrne' equation).

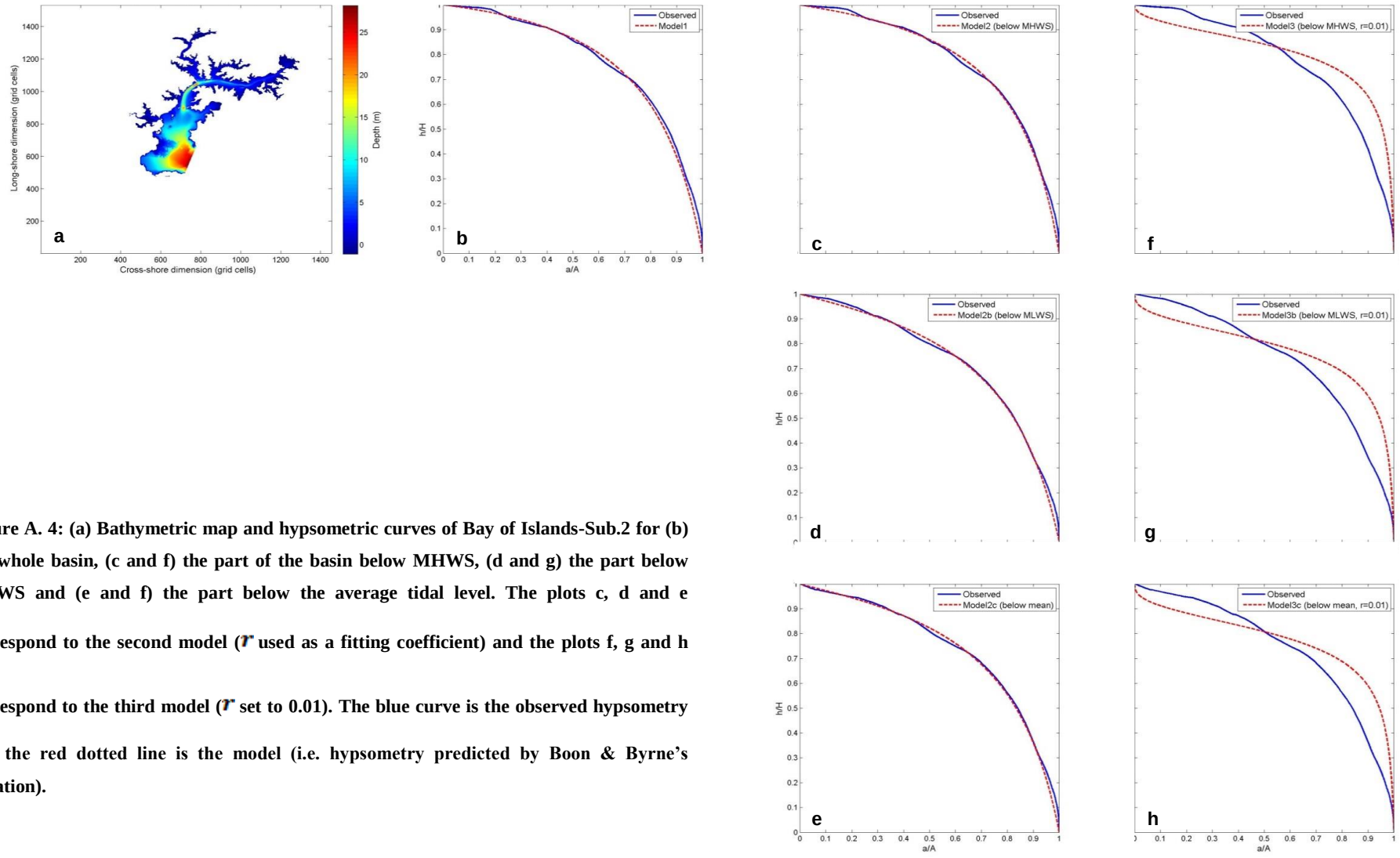

Figure A. 4: (a) Bathymetric map and hypsometric curves of Bay of Islands-Sub.2 for (b) the whole basin, (c and f) the part of the basin below MHWS, (d and g) the part below MLWS and (e and f) the part below the average tidal level. The plots c, d and e correspond to the second model (r used as a fitting coefficient) and the plots f, g and h correspond to the third model (r set to 0.01). The blue curve is the observed hypsometry and the red dotted line is the model (i.e. hypsometry predicted by Boon & Byrne's equation).

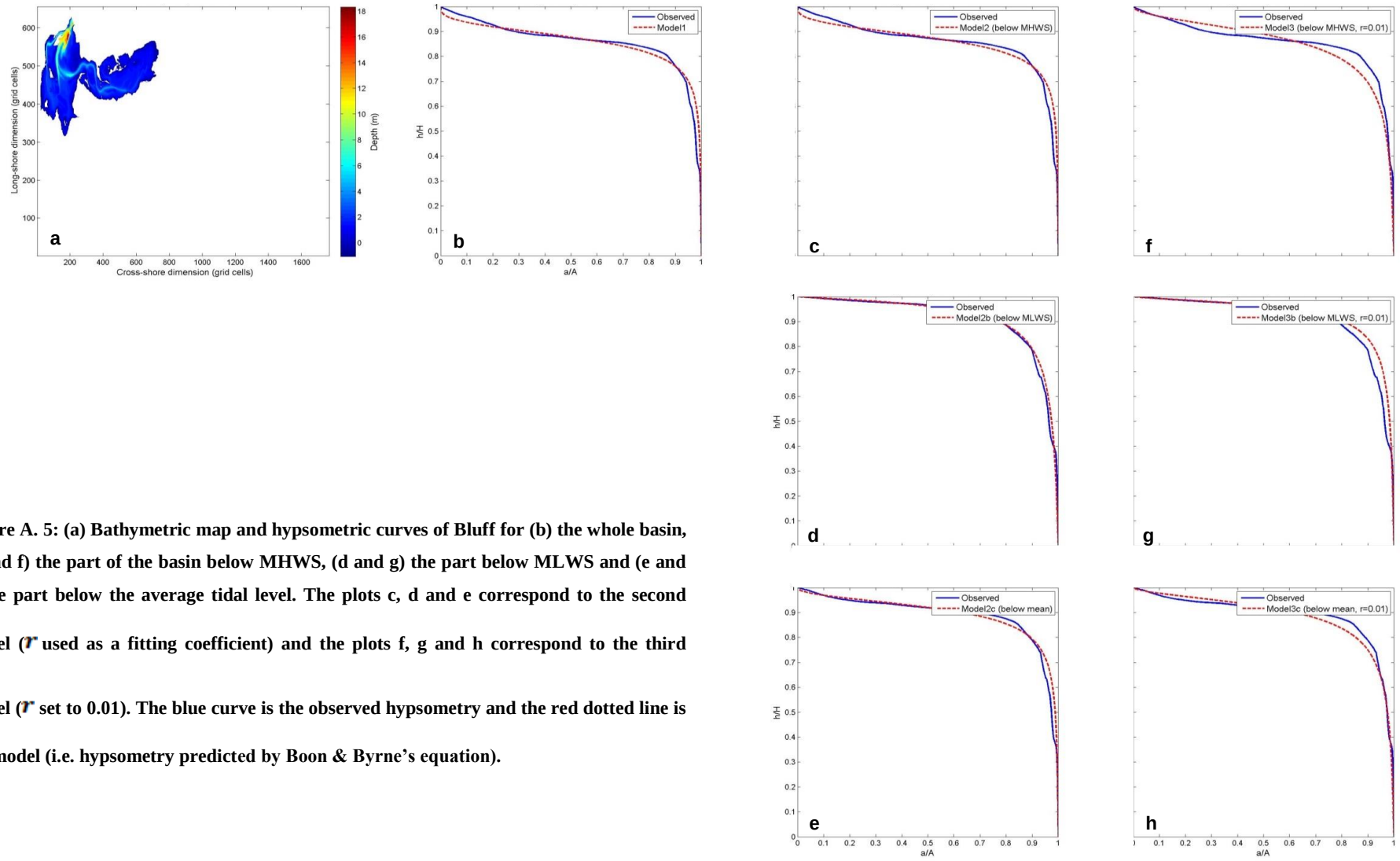

Figure A. 5: (a) Bathymetric map and hypsometric curves of Bluff for (b) the whole basin, (c and f) the part of the basin below MHWS, (d and g) the part below MLWS and (e and f) the part below the average tidal level. The plots c, d and e correspond to the second model (r used as a fitting coefficient) and the plots f, g and h correspond to the third model (r set to 0.01). The blue curve is the observed hypsometry and the red dotted line is the model (i.e. hypsometry predicted by Boon & Byrne's equation).

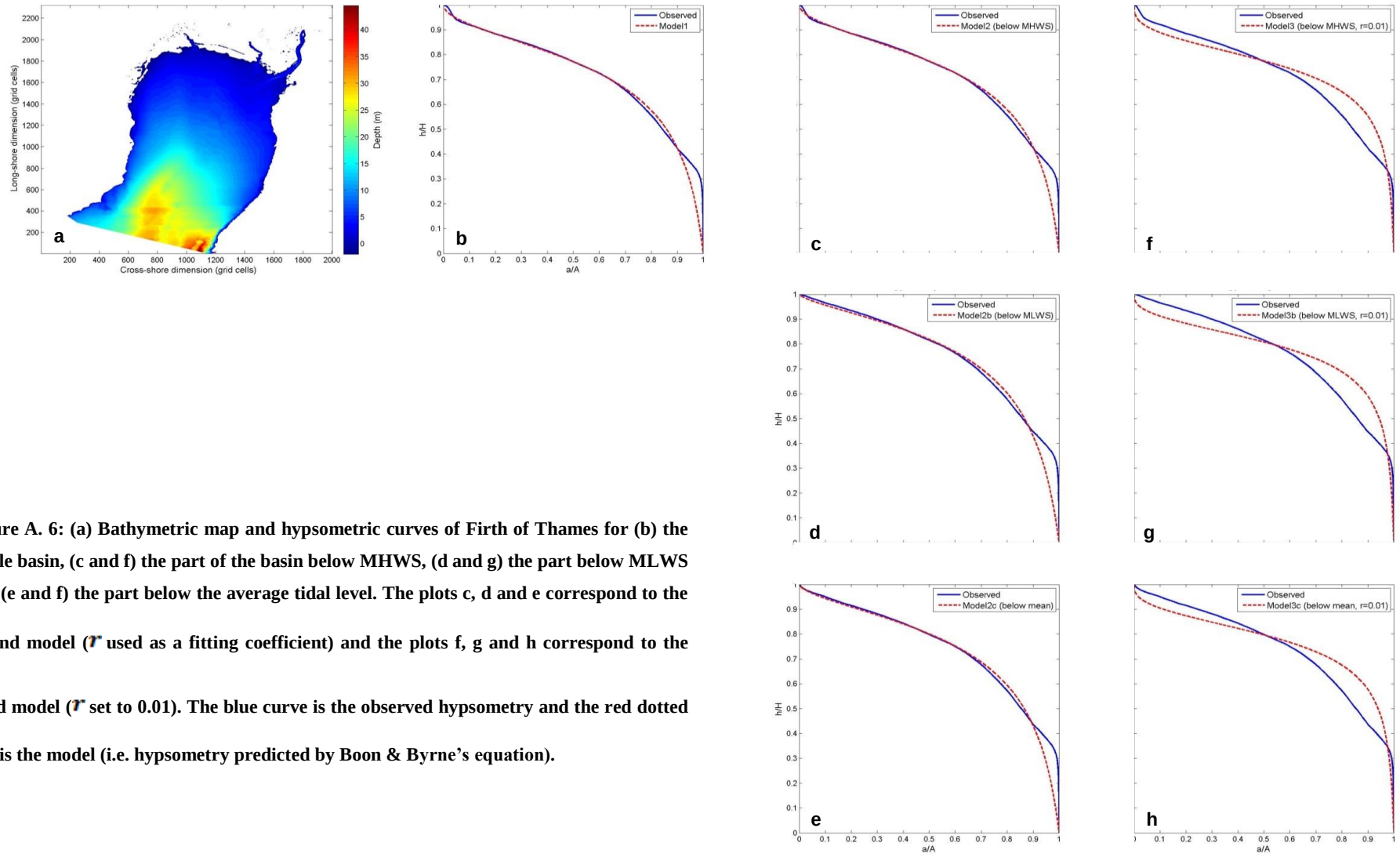

Figure A. 6: (a) Bathymetric map and hypsometric curves of Firth of Thames for (b) the whole basin, (c and f) the part of the basin below MHWS, (d and g) the part below MLWS and (e and f) the part below the average tidal level. The plots c, d and e correspond to the second model (r used as a fitting coefficient) and the plots f, g and h correspond to the third model (r set to 0.01). The blue curve is the observed hypsometry and the red dotted line is the model (i.e. hypsometry predicted by Boon & Byrne's equation).

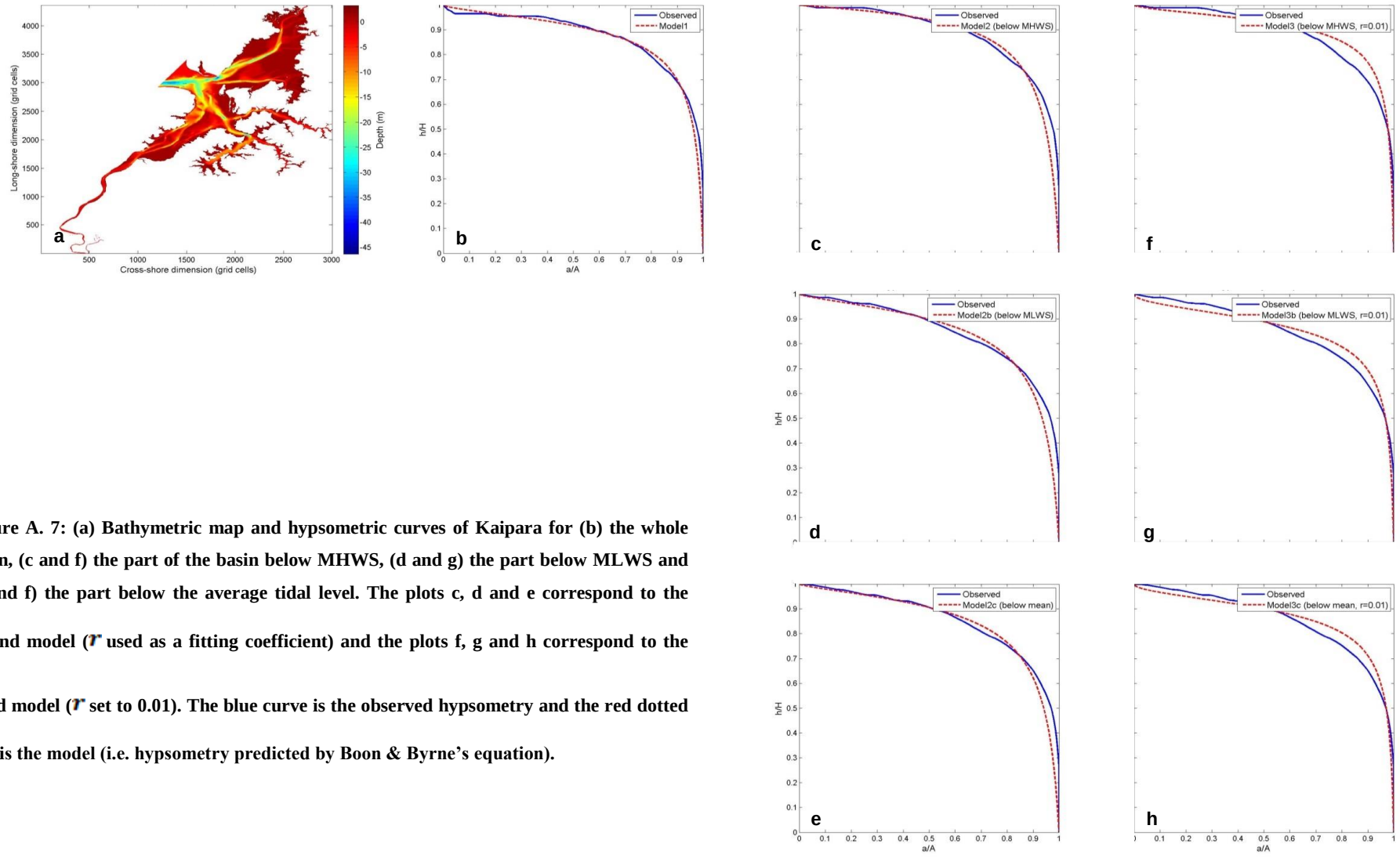

Figure A. 7: (a) Bathymetric map and hypsometric curves of Kaipara for (b) the whole basin, (c and f) the part of the basin below MHWS, (d and g) the part below MLWS and (e and f) the part below the average tidal level. The plots c, d and e correspond to the second model (r used as a fitting coefficient) and the plots f, g and h correspond to the third model (r set to 0.01). The blue curve is the observed hypsometry and the red dotted line is the model (i.e. hypsometry predicted by Boon & Byrne's equation).

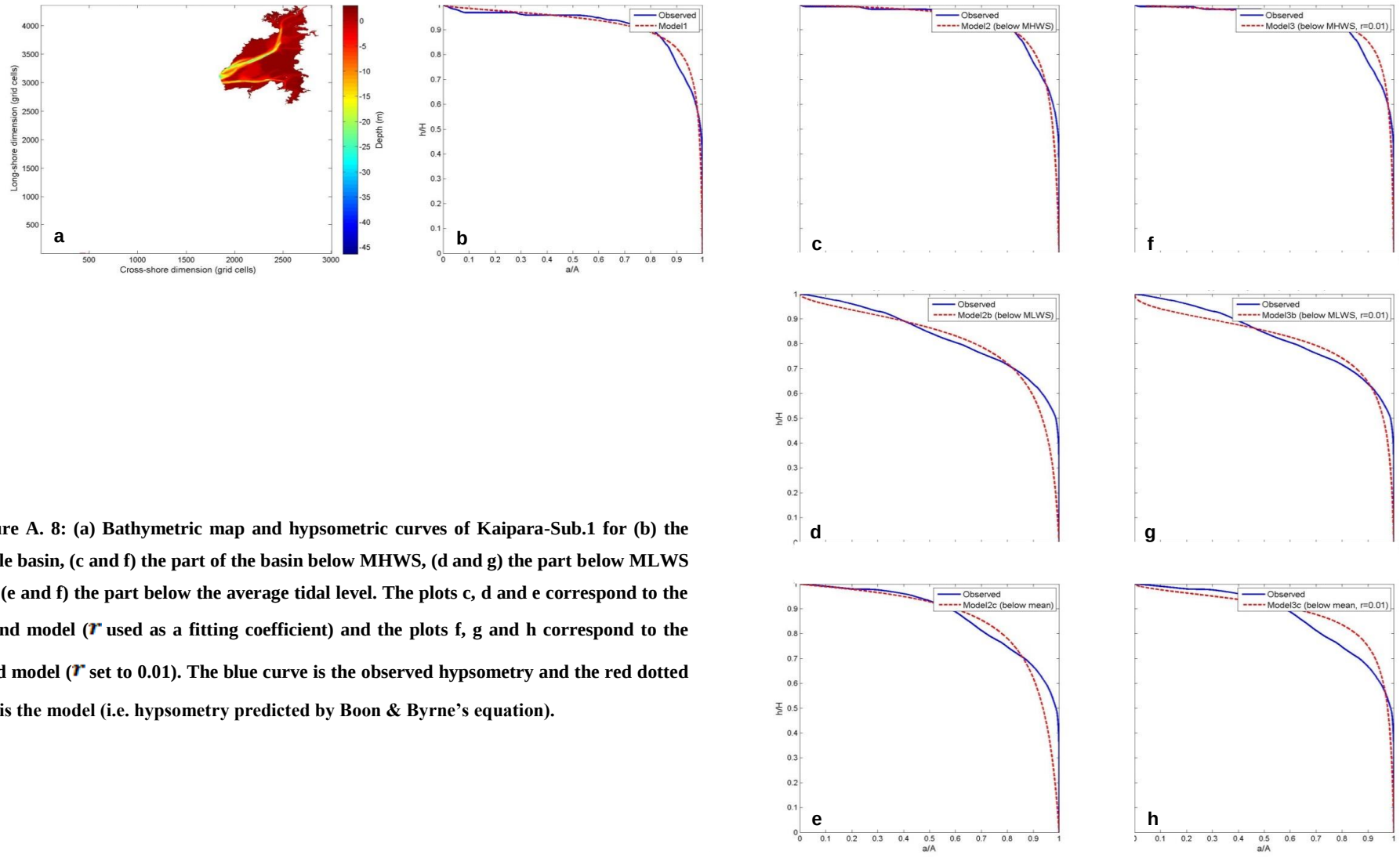

Figure A. 8: (a) Bathymetric map and hypsometric curves of Kaipara-Sub.1 for (b) the whole basin, (c and f) the part of the basin below MHWS, (d and g) the part below MLWS and (e and f) the part below the average tidal level. The plots c, d and e correspond to the second model (r used as a fitting coefficient) and the plots f, g and h correspond to the third model (r set to 0.01). The blue curve is the observed hypsometry and the red dotted line is the model (i.e. hypsometry predicted by Boon & Byrne's equation).

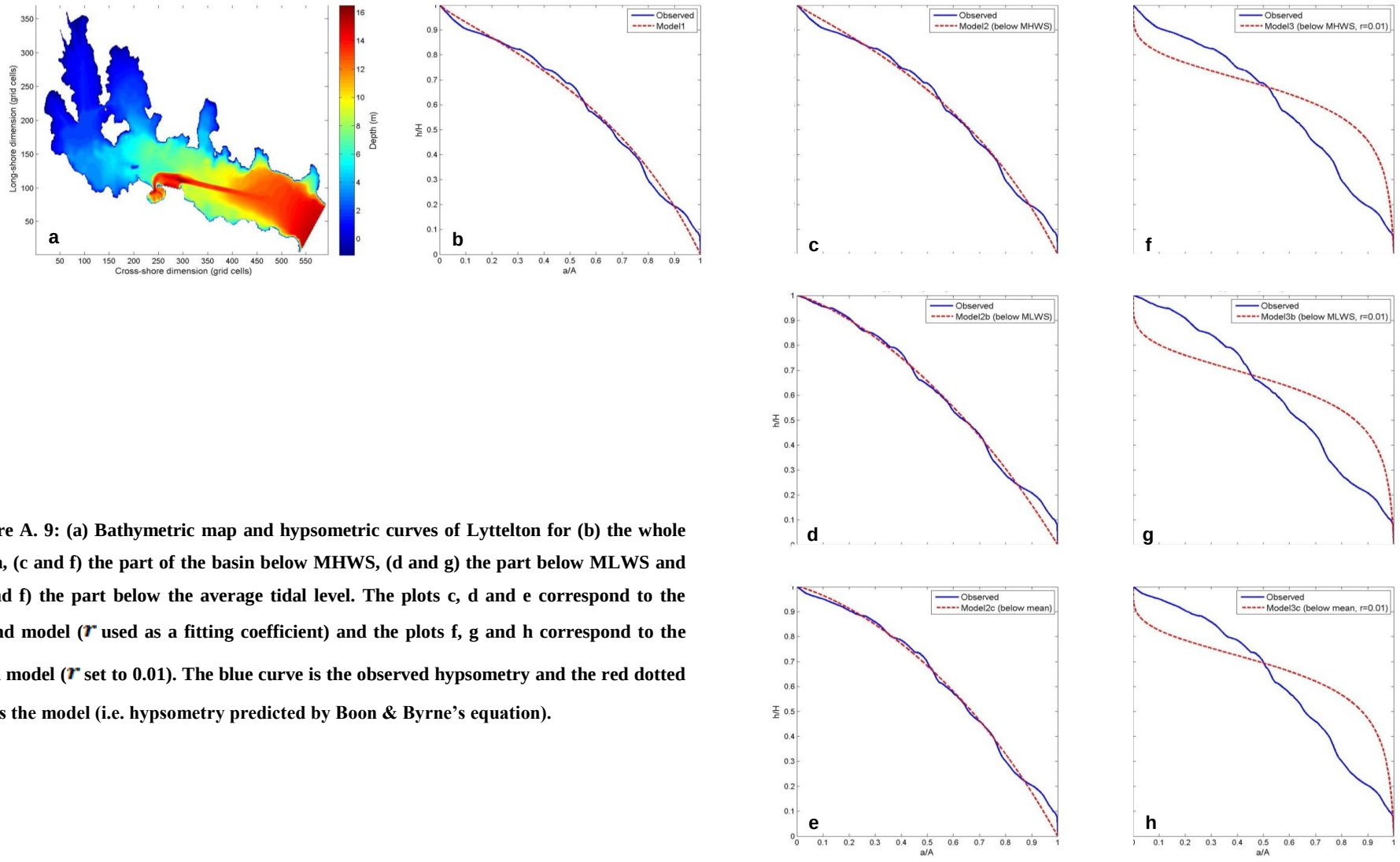

Figure A. 9: (a) Bathymetric map and hypsometric curves of Lyttelton for (b) the whole basin, (c and f) the part of the basin below MHWS, (d and g) the part below MLWS and (e and f) the part below the average tidal level. The plots c, d and e correspond to the second model (r used as a fitting coefficient) and the plots f, g and h correspond to the third model (r set to 0.01). The blue curve is the observed hypsometry and the red dotted line is the model (i.e. hypsometry predicted by Boon & Byrne's equation).

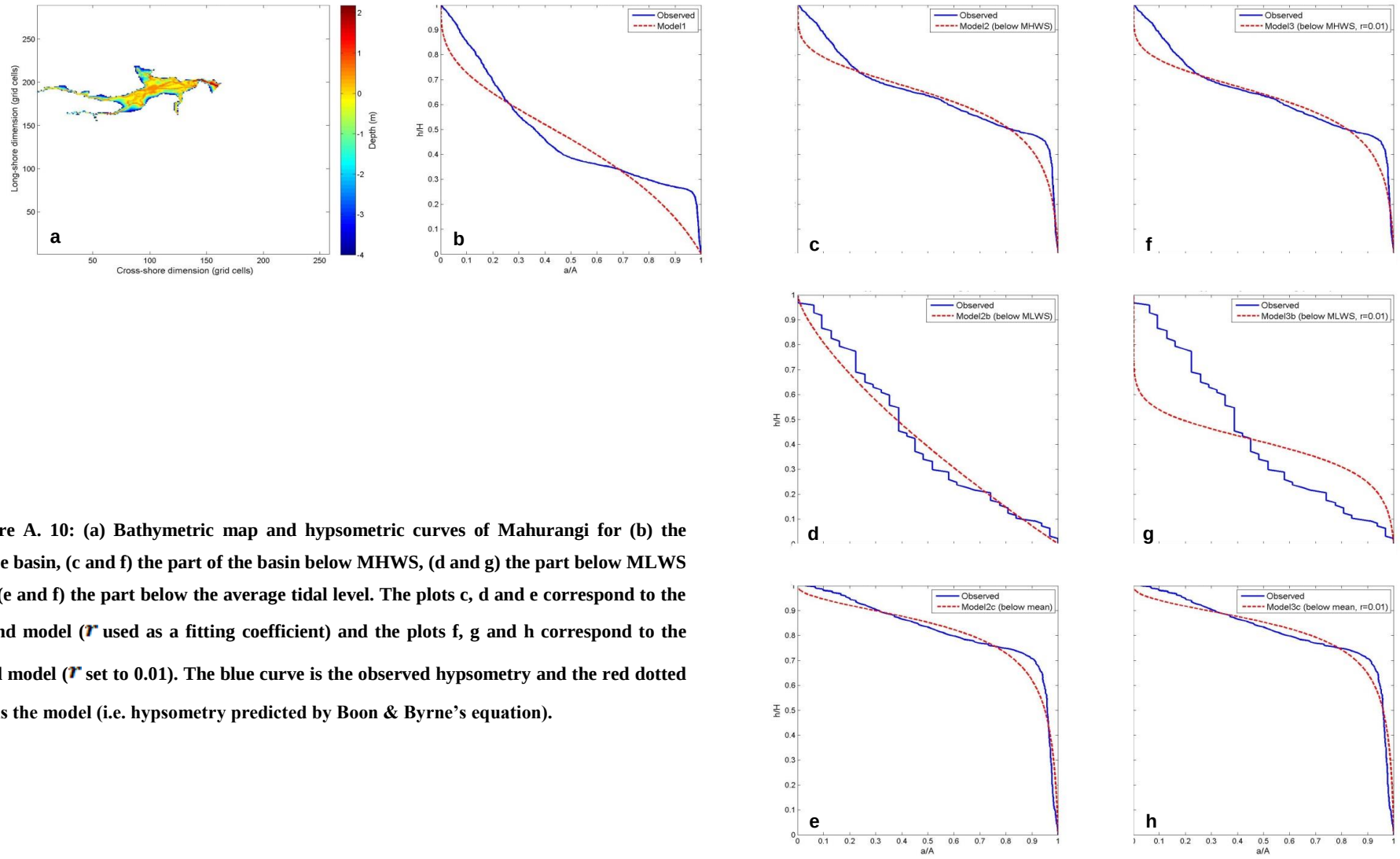

Figure A. 10: (a) Bathymetric map and hypsometric curves of Mahurangi for (b) the whole basin, (c and f) the part of the basin below MHWS, (d and g) the part below MLWS and (e and f) the part below the average tidal level. The plots c, d and e correspond to the second model (r used as a fitting coefficient) and the plots f, g and h correspond to the third model (r set to 0.01). The blue curve is the observed hypsometry and the red dotted line is the model (i.e. hypsometry predicted by Boon & Byrne's equation).

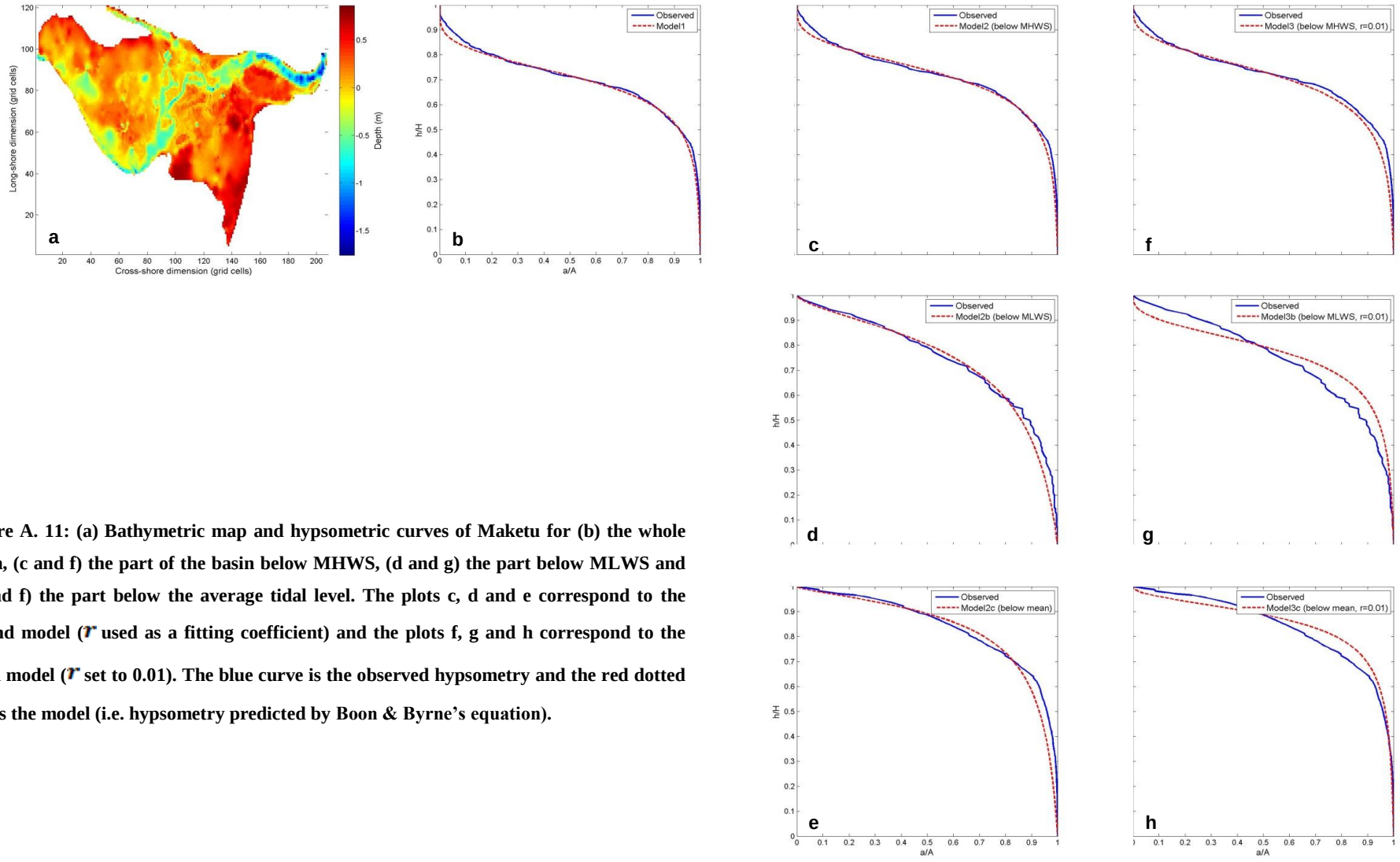

Figure A. 11: (a) Bathymetric map and hypsometric curves of Maketu for (b) the whole basin, (c and f) the part of the basin below MHWS, (d and g) the part below MLWS and (e and f) the part below the average tidal level. The plots c, d and e correspond to the second model (r used as a fitting coefficient) and the plots f, g and h correspond to the third model (r set to 0.01). The blue curve is the observed hypsometry and the red dotted line is the model (i.e. hypsometry predicted by Boon & Byrne's equation).

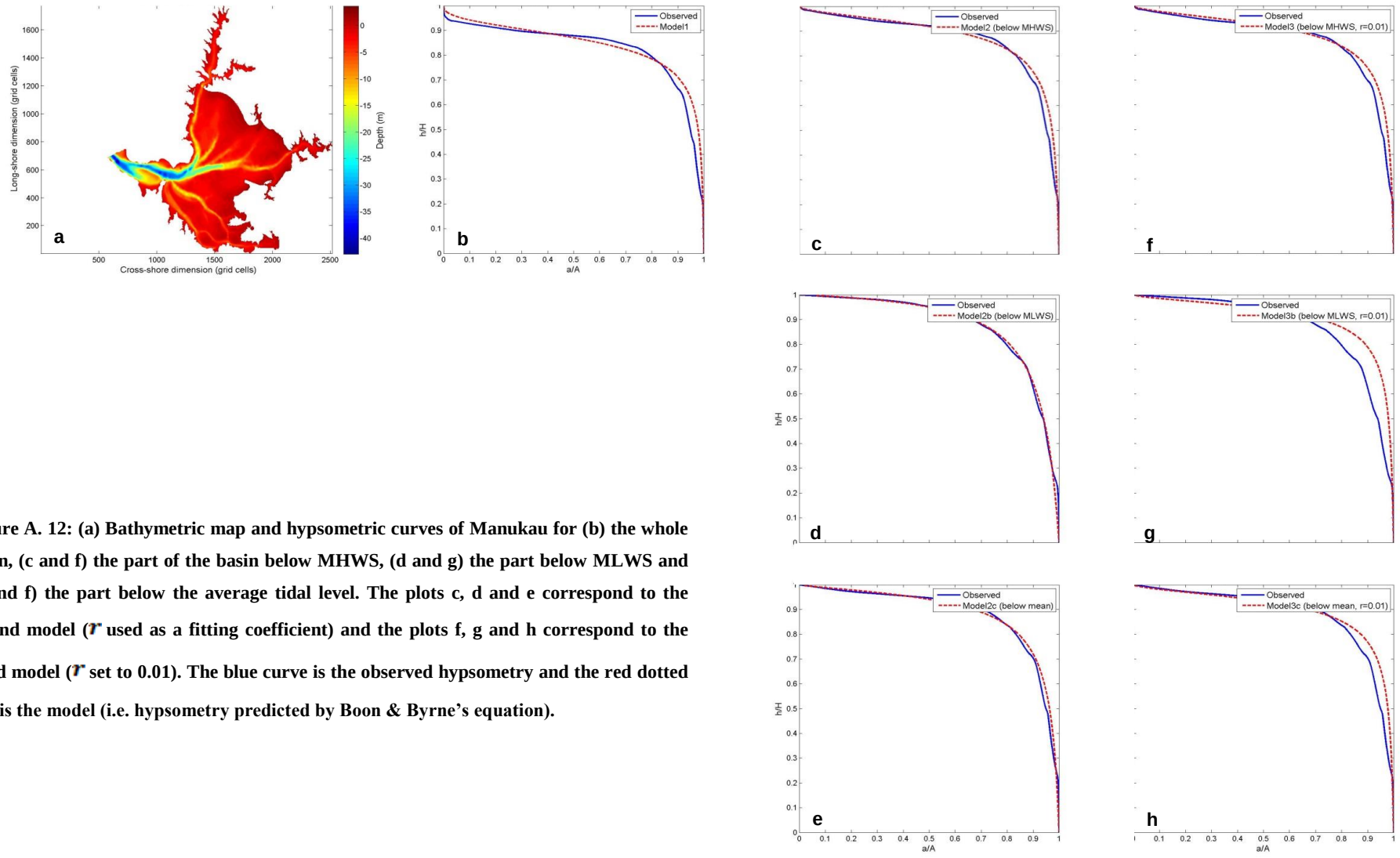

Figure A. 12: (a) Bathymetric map and hypsometric curves of Manukau for (b) the whole basin, (c and f) the part of the basin below MHWS, (d and g) the part below MLWS and (e and f) the part below the average tidal level. The plots c, d and e correspond to the second model (r used as a fitting coefficient) and the plots f, g and h correspond to the third model (r set to 0.01). The blue curve is the observed hypsometry and the red dotted line is the model (i.e. hypsometry predicted by Boon & Byrne's equation).

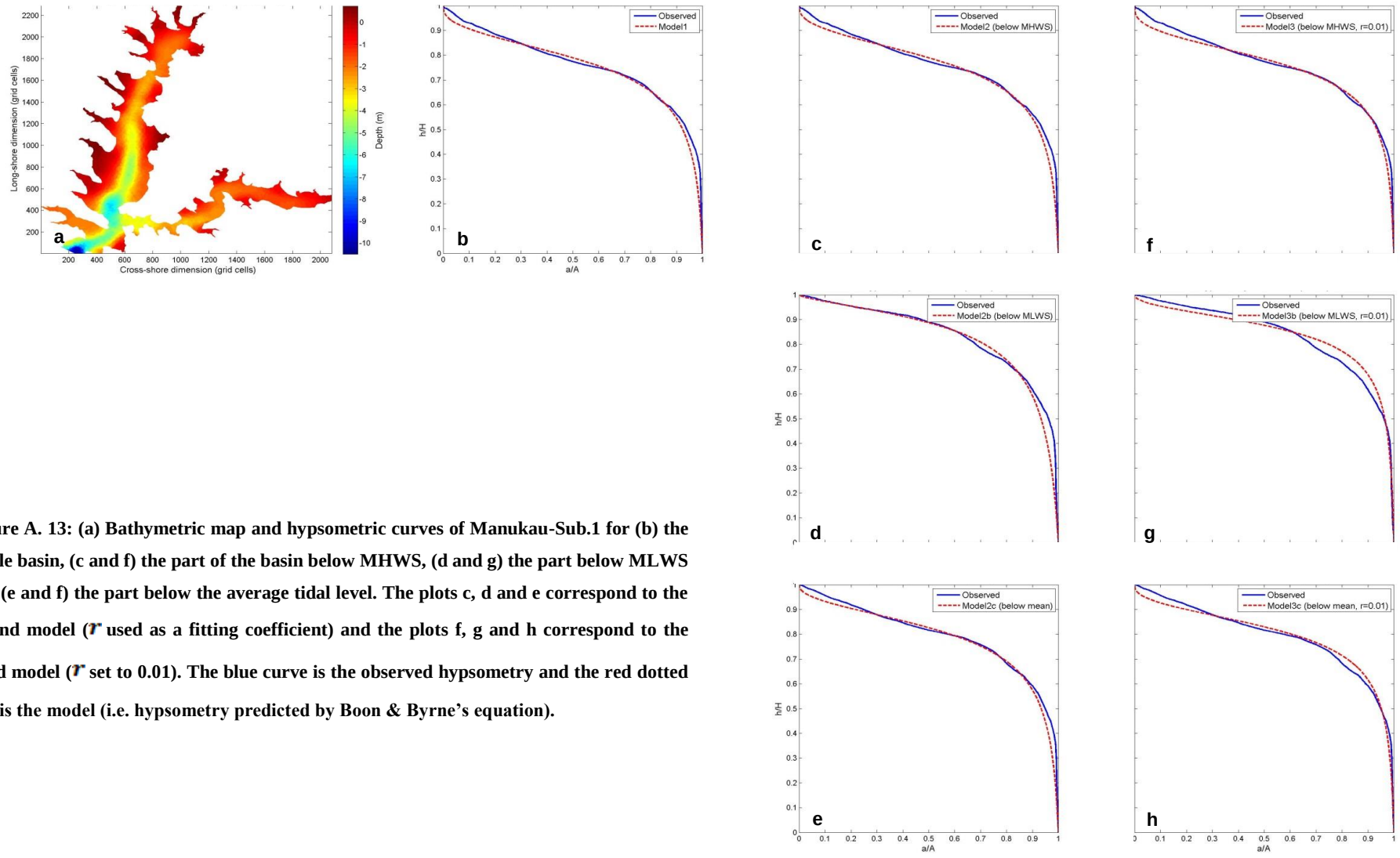

Figure A. 13: (a) Bathymetric map and hypsometric curves of Manukau-Sub.1 for (b) the whole basin, (c and f) the part of the basin below MHWS, (d and g) the part below MLWS and (e and f) the part below the average tidal level. The plots c, d and e correspond to the second model (r used as a fitting coefficient) and the plots f, g and h correspond to the third model (r set to 0.01). The blue curve is the observed hypsometry and the red dotted line is the model (i.e. hypsometry predicted by Boon & Byrne's equation).

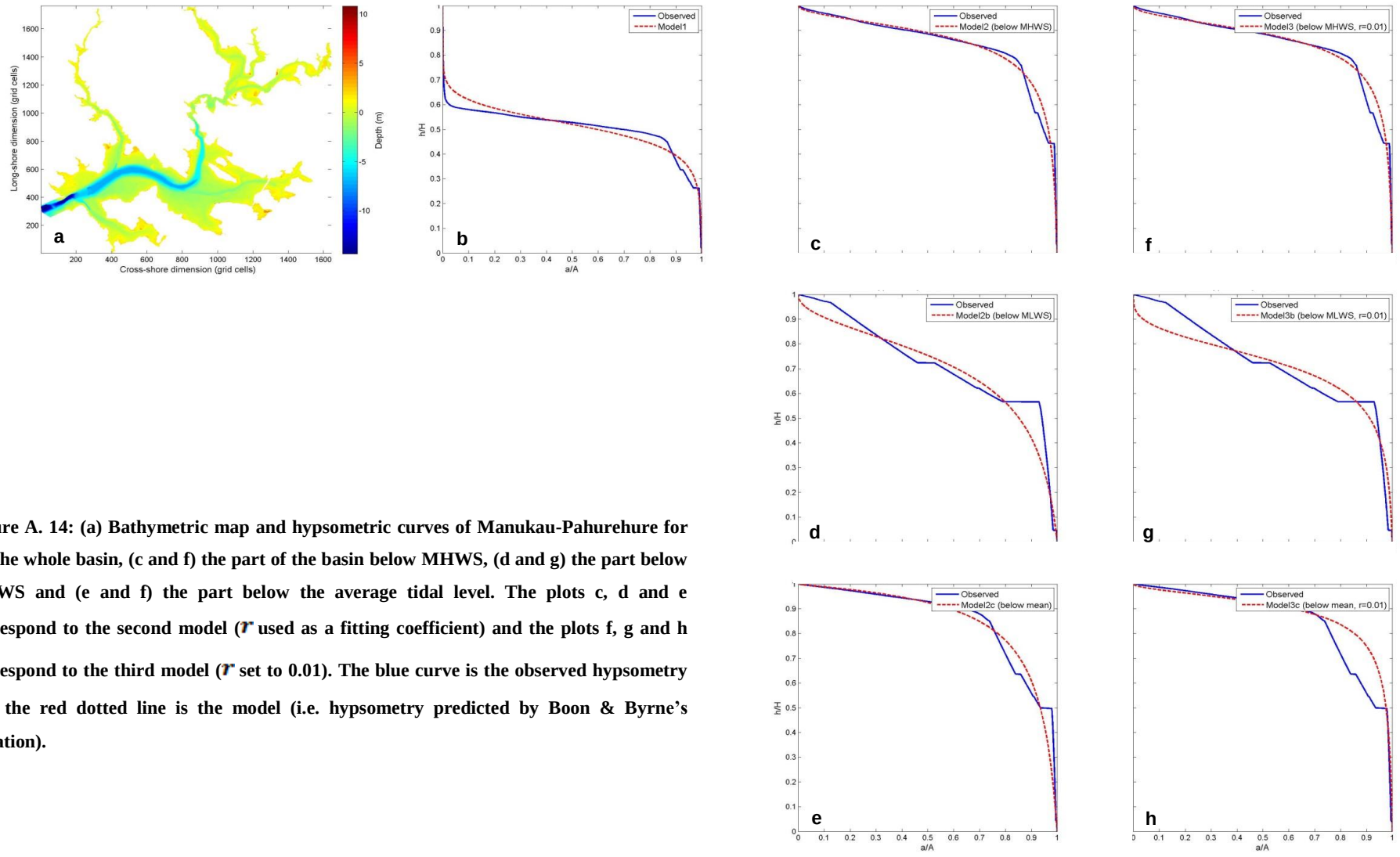

Figure A. 14: (a) Bathymetric map and hypsometric curves of Manukau-Pahurehure for (b) the whole basin, (c and f) the part of the basin below MHWS, (d and g) the part below MLWS and (e and f) the part below the average tidal level. The plots c, d and e correspond to the second model (r^* used as a fitting coefficient) and the plots f, g and h correspond to the third model (r^* set to 0.01). The blue curve is the observed hypsometry and the red dotted line is the model (i.e. hypsometry predicted by Boon & Byrne's equation).

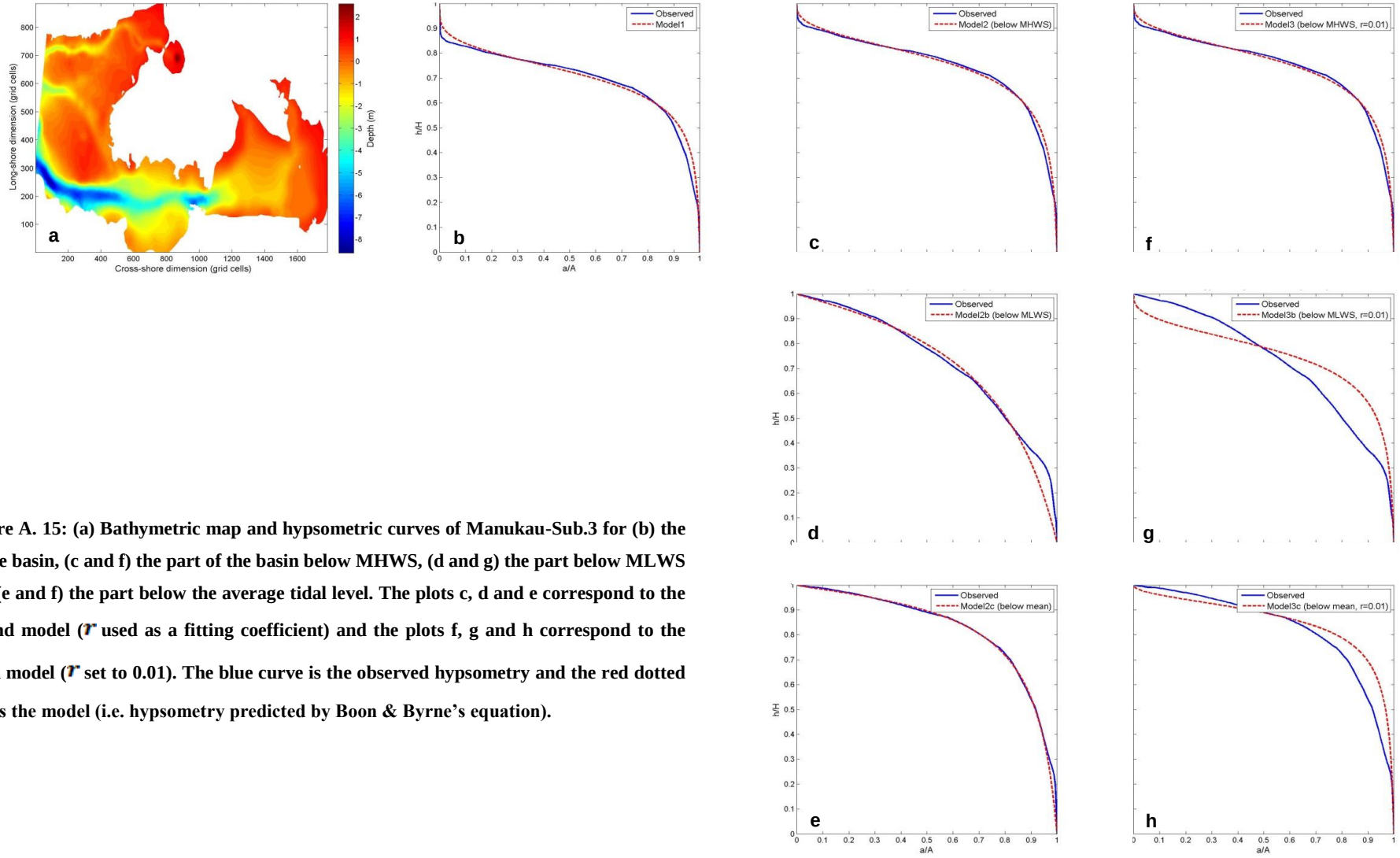

Figure A. 15: (a) Bathymetric map and hypsometric curves of Manukau-Sub.3 for (b) the whole basin, (c and f) the part of the basin below MHWS, (d and g) the part below MLWS and (e and f) the part below the average tidal level. The plots c, d and e correspond to the second model (r used as a fitting coefficient) and the plots f, g and h correspond to the third model (r set to 0.01). The blue curve is the observed hypsometry and the red dotted line is the model (i.e. hypsometry predicted by Boon & Byrne's equation).

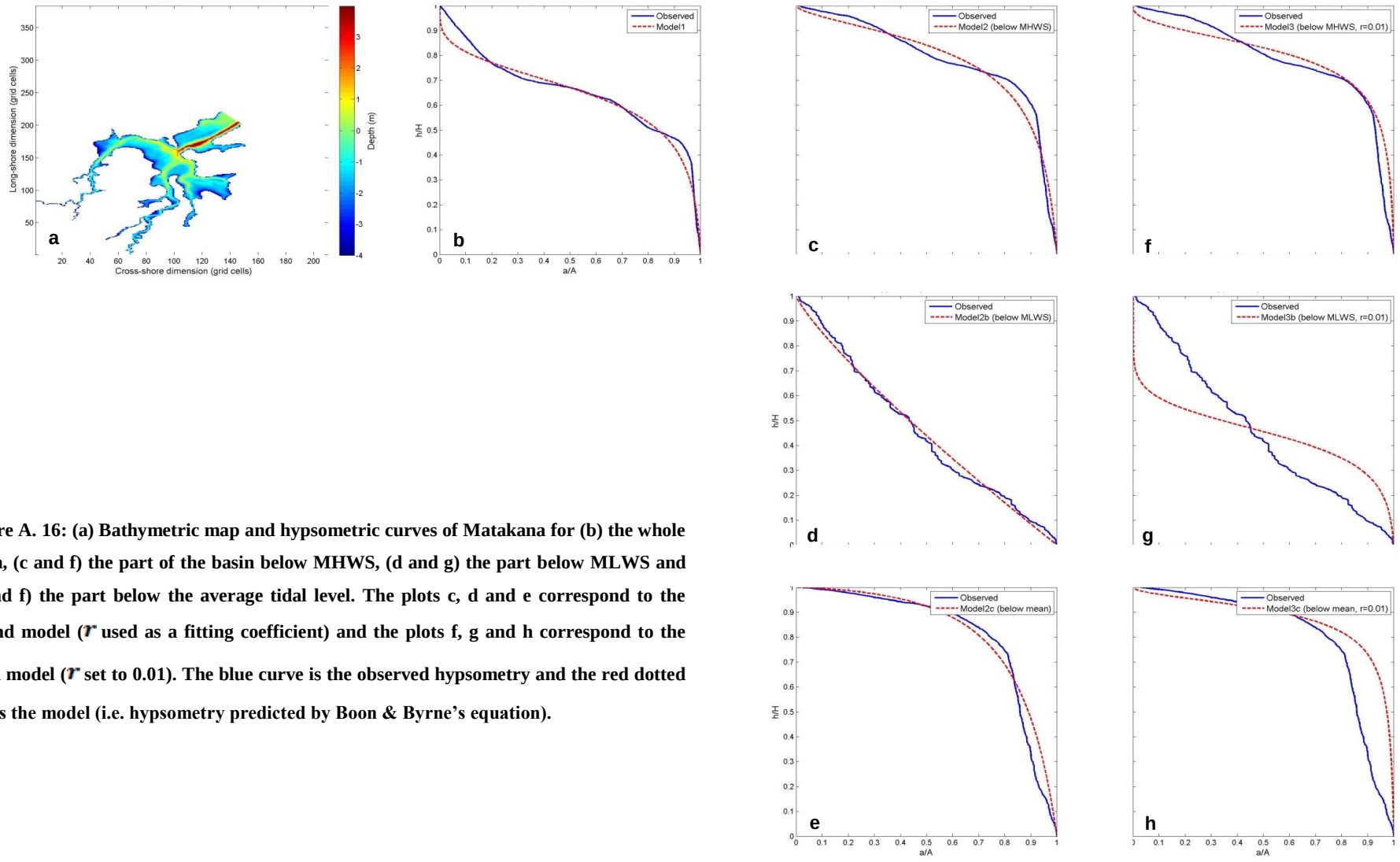

Figure A. 16: (a) Bathymetric map and hypsometric curves of Matakana for (b) the whole basin, (c and f) the part of the basin below MHWS, (d and g) the part below MLWS and (e and f) the part below the average tidal level. The plots c, d and e correspond to the second model (r used as a fitting coefficient) and the plots f, g and h correspond to the third model (r set to 0.01). The blue curve is the observed hypsometry and the red dotted line is the model (i.e. hypsometry predicted by Boon & Byrne's equation).

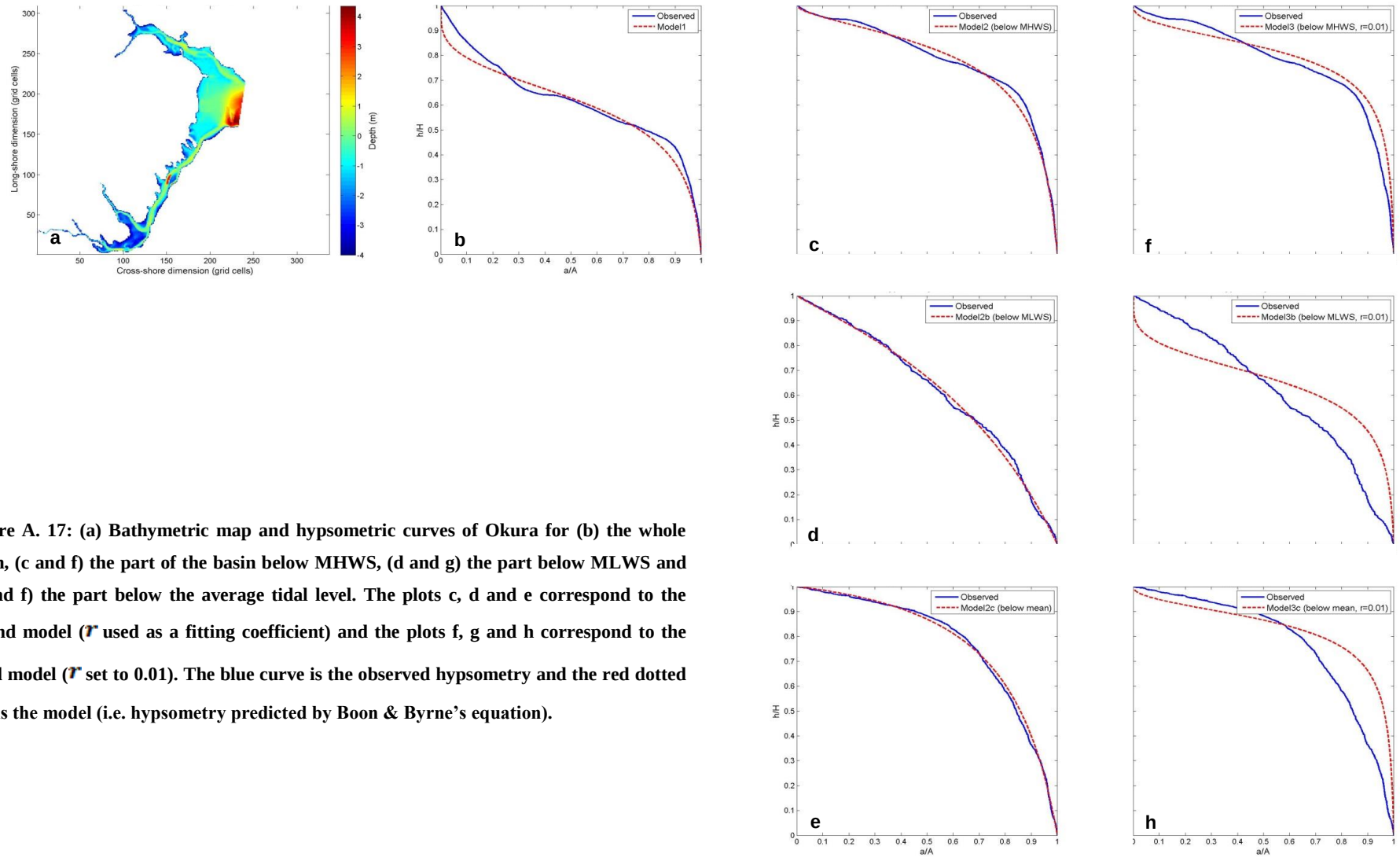

Figure A. 17: (a) Bathymetric map and hypsometric curves of Okura for (b) the whole basin, (c and f) the part of the basin below MHWS, (d and g) the part below MLWS and (e and f) the part below the average tidal level. The plots c, d and e correspond to the second model (r used as a fitting coefficient) and the plots f, g and h correspond to the third model (r set to 0.01). The blue curve is the observed hypsometry and the red dotted line is the model (i.e. hypsometry predicted by Boon & Byrne's equation).

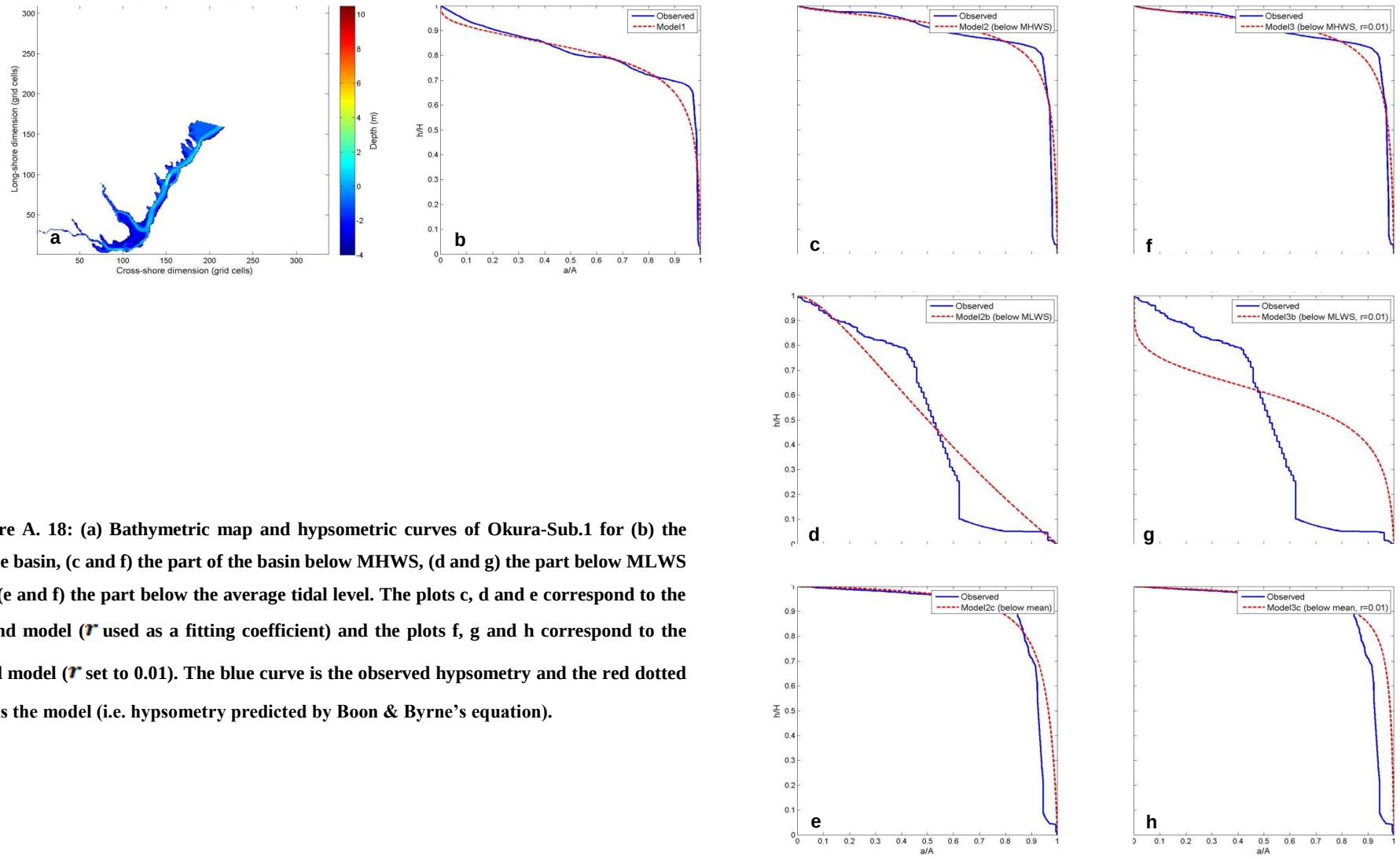

Figure A. 18: (a) Bathymetric map and hypsometric curves of Okura-Sub.1 for (b) the whole basin, (c and f) the part of the basin below MHWS, (d and g) the part below MLWS and (e and f) the part below the average tidal level. The plots c, d and e correspond to the second model (r used as a fitting coefficient) and the plots f, g and h correspond to the third model (r set to 0.01). The blue curve is the observed hypsometry and the red dotted line is the model (i.e. hypsometry predicted by Boon & Byrne's equation).

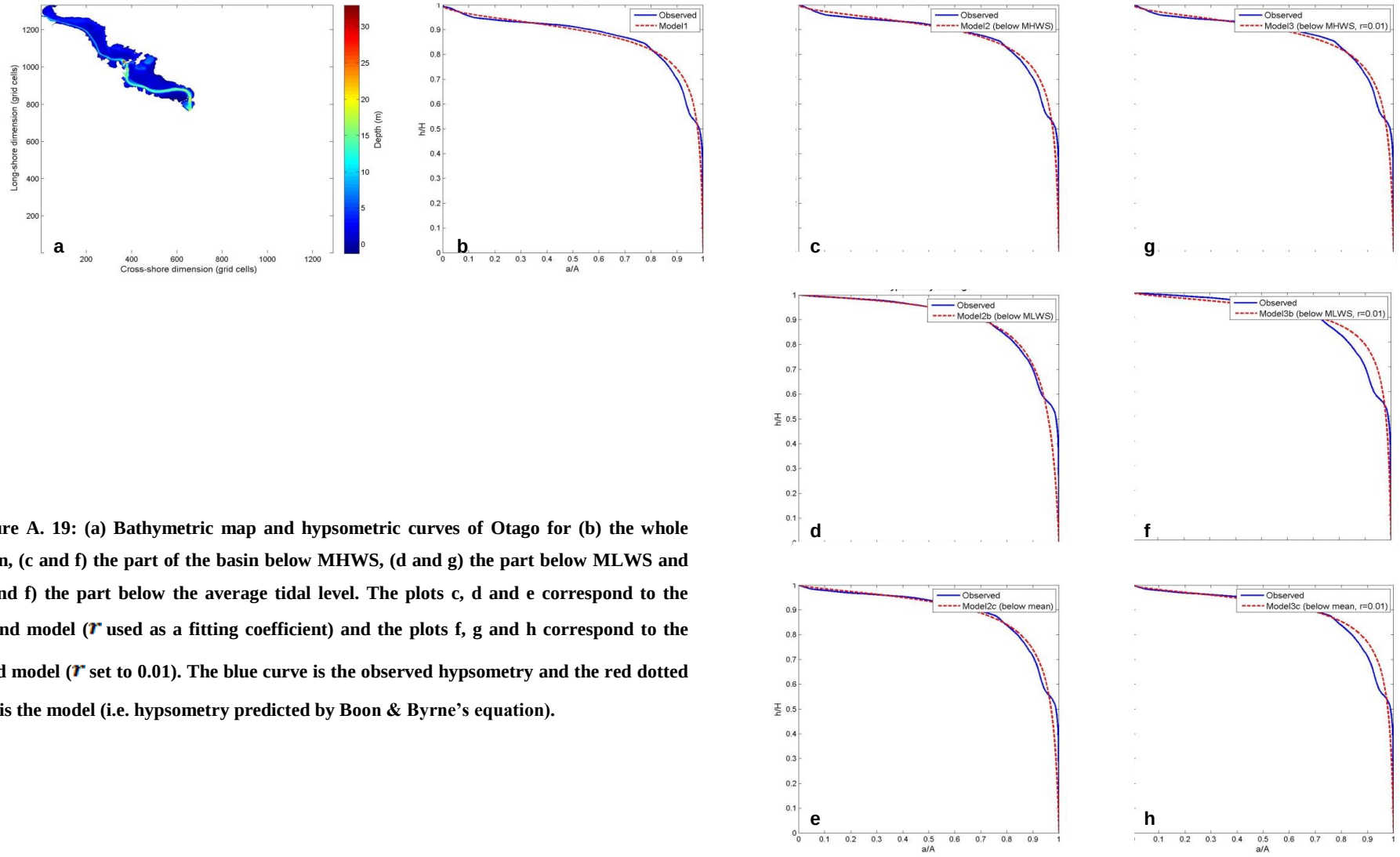

Figure A. 19: (a) Bathymetric map and hypsometric curves of Otago for (b) the whole basin, (c and f) the part of the basin below MHWS, (d and g) the part below MLWS and (e and f) the part below the average tidal level. The plots c, d and e correspond to the second model (r used as a fitting coefficient) and the plots f, g and h correspond to the third model (r set to 0.01). The blue curve is the observed hypsometry and the red dotted line is the model (i.e. hypsometry predicted by Boon & Byrne's equation).

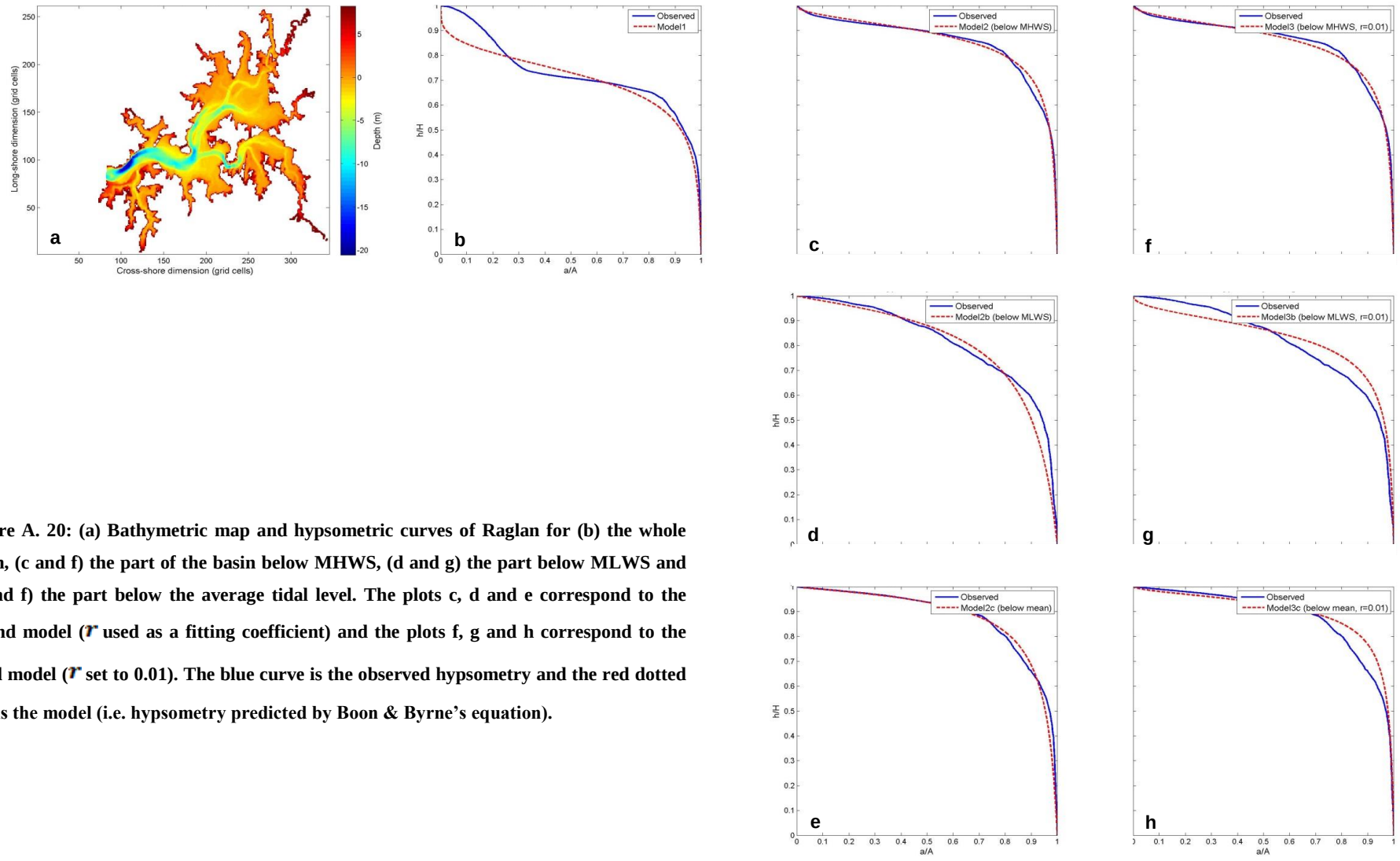

Figure A. 20: (a) Bathymetric map and hypsometric curves of Raglan for (b) the whole basin, (c and f) the part of the basin below MHWS, (d and g) the part below MLWS and (e and f) the part below the average tidal level. The plots c, d and e correspond to the second model (r used as a fitting coefficient) and the plots f, g and h correspond to the third model (r set to 0.01). The blue curve is the observed hypsometry and the red dotted line is the model (i.e. hypsometry predicted by Boon & Byrne's equation).

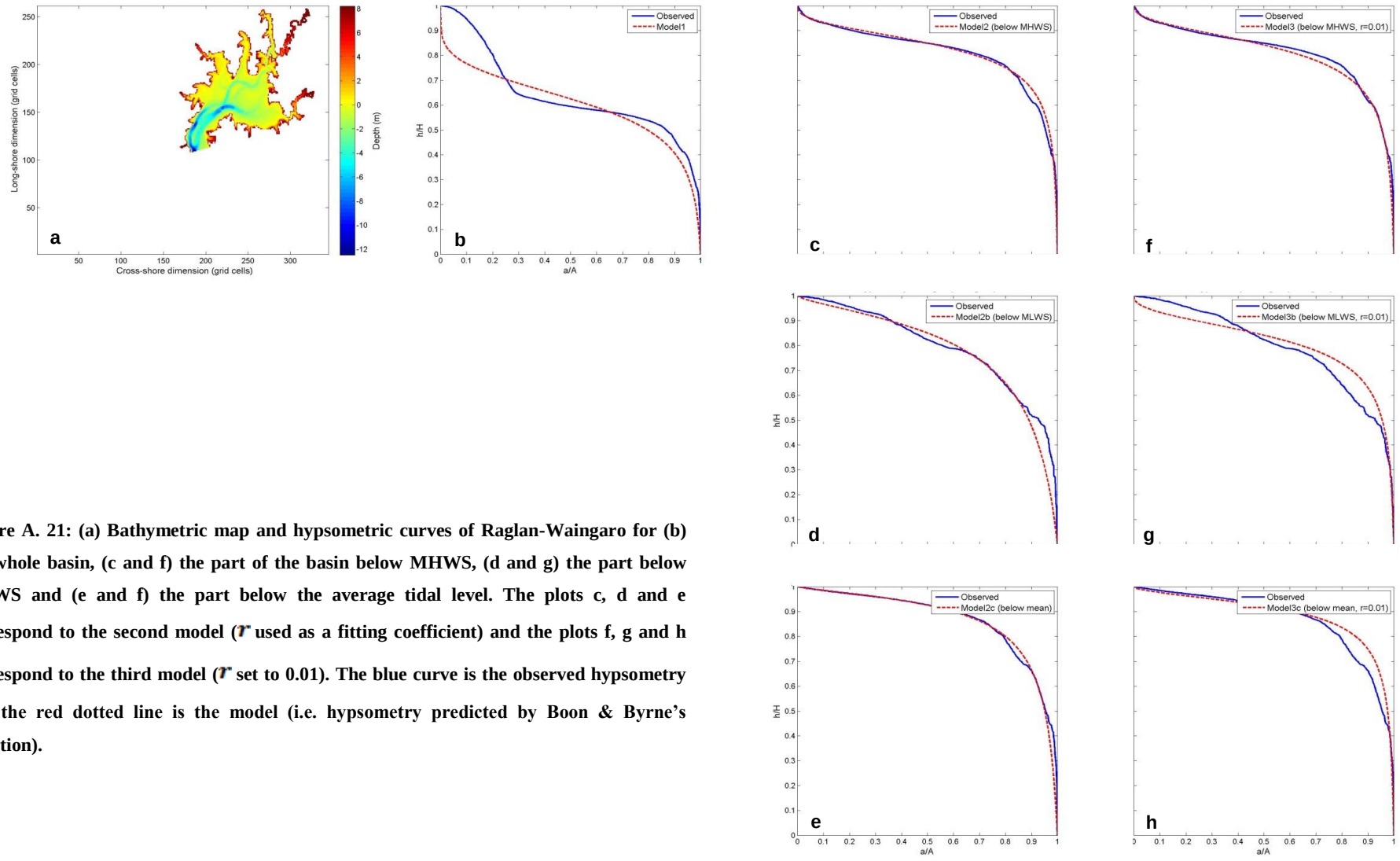

Figure A. 21: (a) Bathymetric map and hypsometric curves of Raglan-Waingaro for (b) the whole basin, (c and f) the part of the basin below MHWS, (d and g) the part below MLWS and (e and f) the part below the average tidal level. The plots c, d and e correspond to the second model (r' used as a fitting coefficient) and the plots f, g and h correspond to the third model (r' set to 0.01). The blue curve is the observed hypsometry and the red dotted line is the model (i.e. hypsometry predicted by Boon & Byrne's equation).

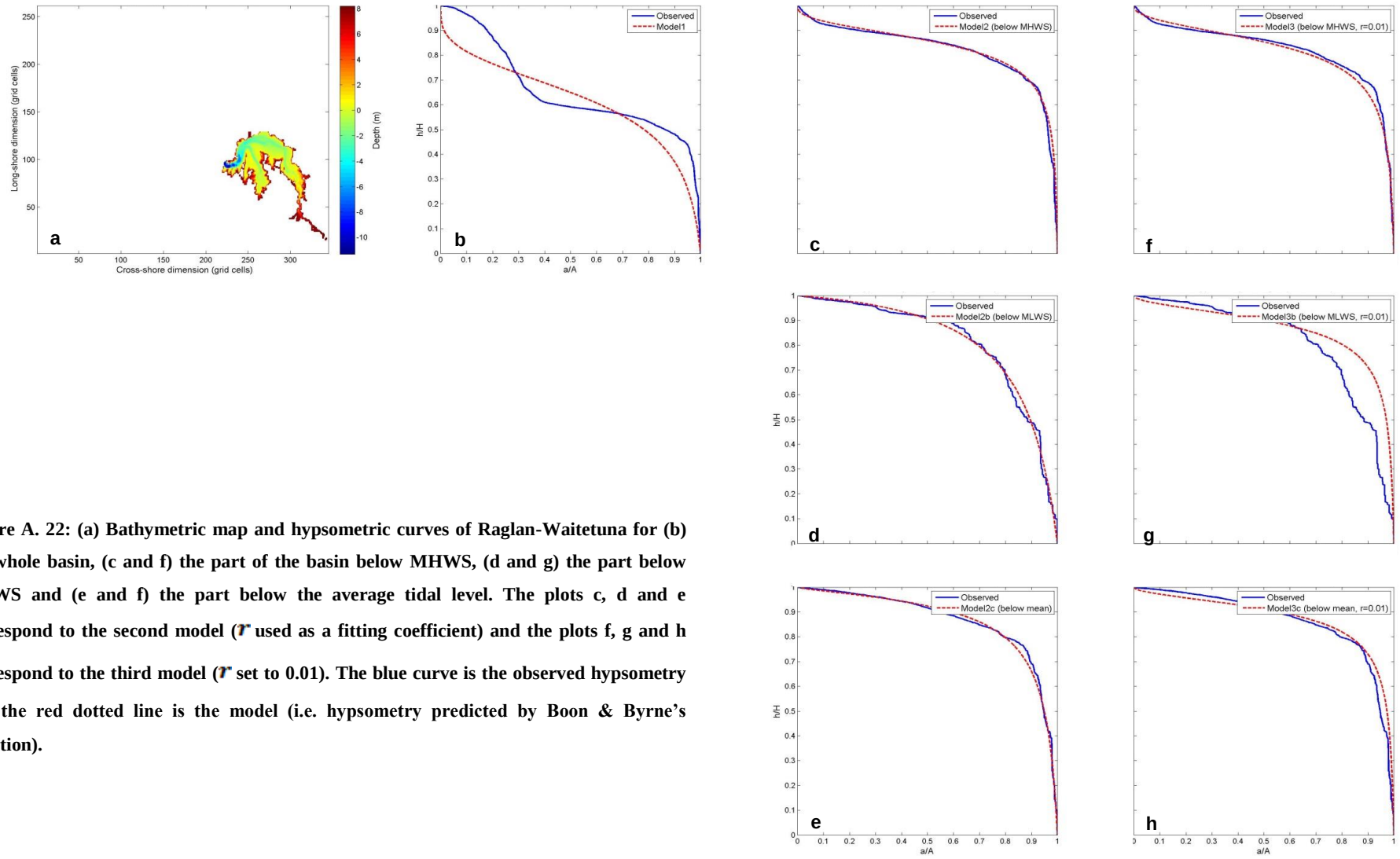

Figure A. 22: (a) Bathymetric map and hypsometric curves of Raglan-Waitetuna for (b) the whole basin, (c and f) the part of the basin below MHWS, (d and g) the part below MLWS and (e and f) the part below the average tidal level. The plots c, d and e correspond to the second model (r' used as a fitting coefficient) and the plots f, g and h correspond to the third model (r' set to 0.01). The blue curve is the observed hypsometry and the red dotted line is the model (i.e. hypsometry predicted by Boon & Byrne's equation).

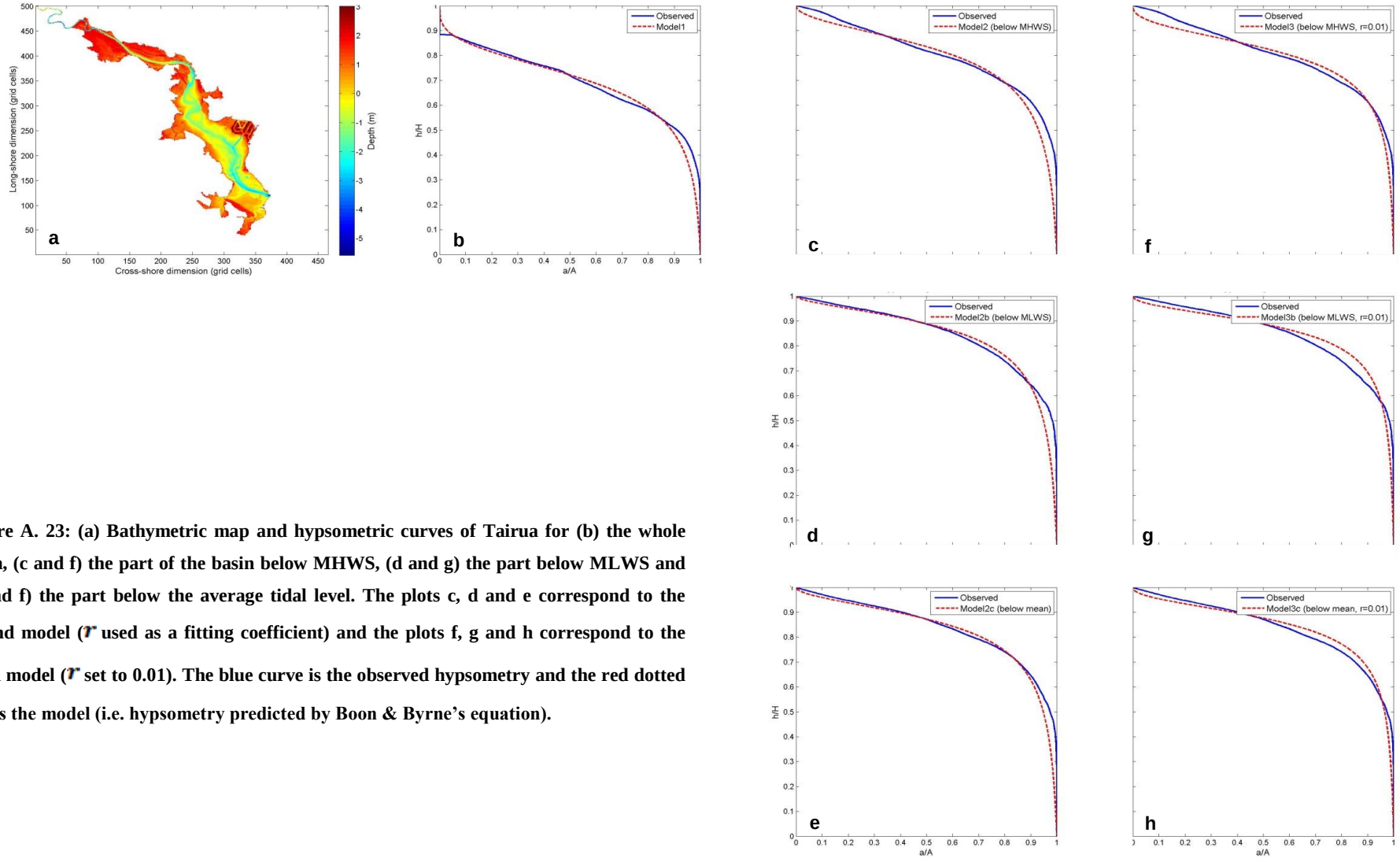

Figure A. 23: (a) Bathymetric map and hypsometric curves of Tairua for (b) the whole basin, (c and f) the part of the basin below MHWS, (d and g) the part below MLWS and (e and f) the part below the average tidal level. The plots c, d and e correspond to the second model (r used as a fitting coefficient) and the plots f, g and h correspond to the third model (r set to 0.01). The blue curve is the observed hypsometry and the red dotted line is the model (i.e. hypsometry predicted by Boon & Byrne's equation).

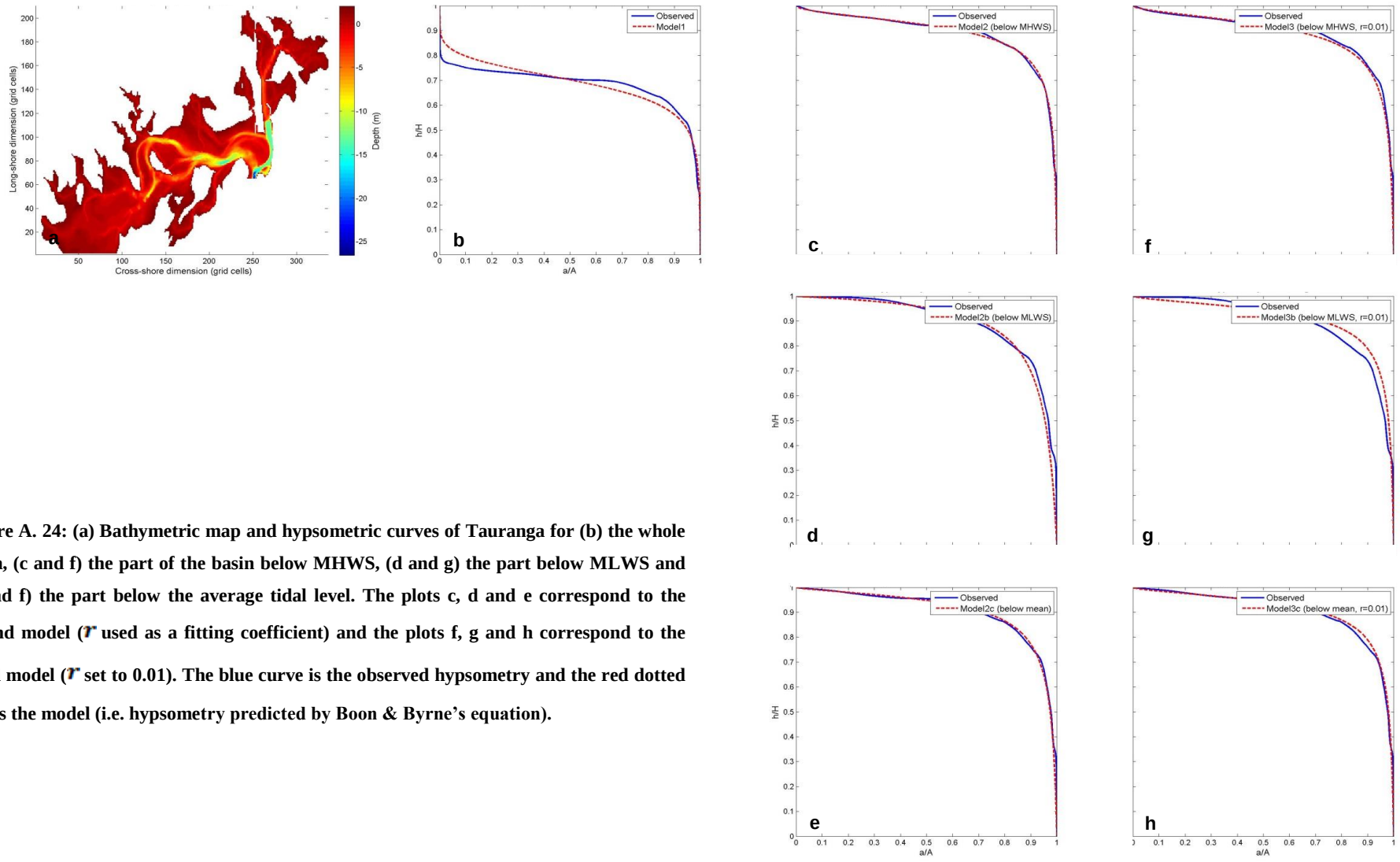

Figure A. 24: (a) Bathymetric map and hypsometric curves of Tauranga for (b) the whole basin, (c and f) the part of the basin below MHWS, (d and g) the part below MLWS and (e and f) the part below the average tidal level. The plots c, d and e correspond to the second model (r used as a fitting coefficient) and the plots f, g and h correspond to the third model (r set to 0.01). The blue curve is the observed hypsometry and the red dotted line is the model (i.e. hypsometry predicted by Boon & Byrne's equation).

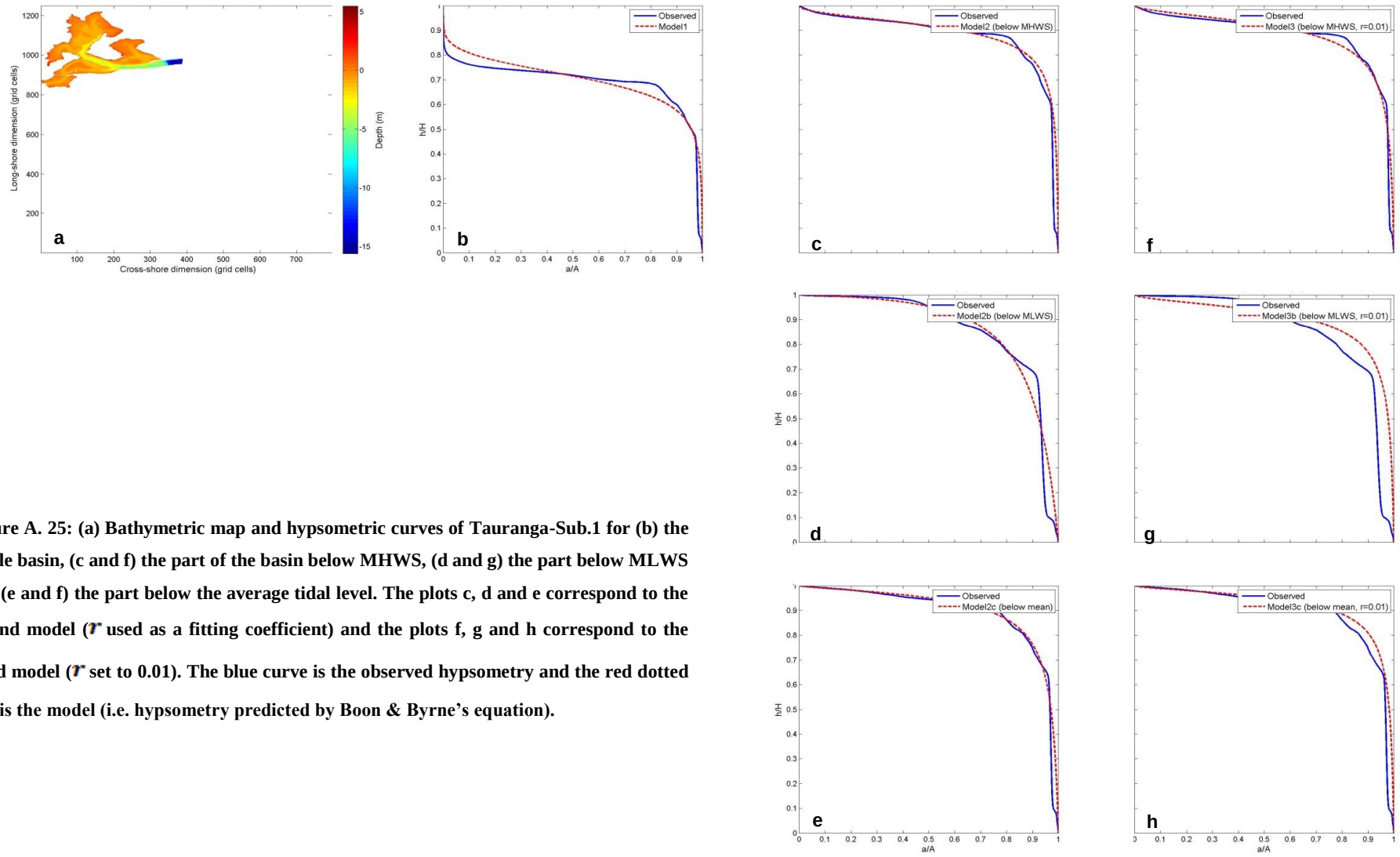

Figure A. 25: (a) Bathymetric map and hypsometric curves of Tauranga-Sub.1 for (b) the whole basin, (c and f) the part of the basin below MHWS, (d and g) the part below MLWS and (e and f) the part below the average tidal level. The plots c, d and e correspond to the second model (r used as a fitting coefficient) and the plots f, g and h correspond to the third model (r set to 0.01). The blue curve is the observed hypsometry and the red dotted line is the model (i.e. hypsometry predicted by Boon & Byrne's equation).

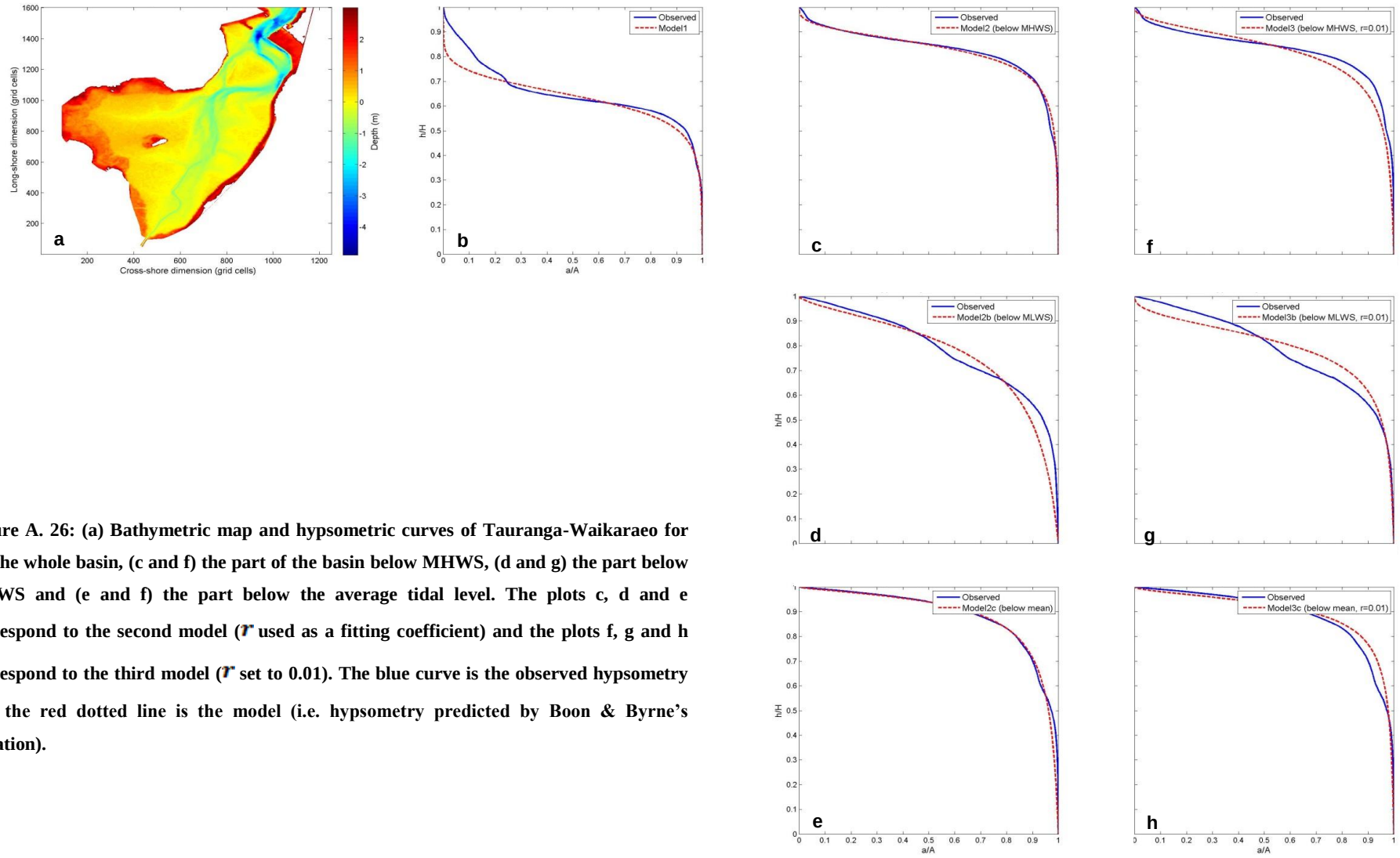

Figure A. 26: (a) Bathymetric map and hypsometric curves of Tauranga-Waikaraeo for (b) the whole basin, (c and f) the part of the basin below MHWS, (d and g) the part below MLWS and (e and f) the part below the average tidal level. The plots c, d and e correspond to the second model (r^* used as a fitting coefficient) and the plots f, g and h correspond to the third model (r^* set to 0.01). The blue curve is the observed hypsometry and the red dotted line is the model (i.e. hypsometry predicted by Boon & Byrne's equation).

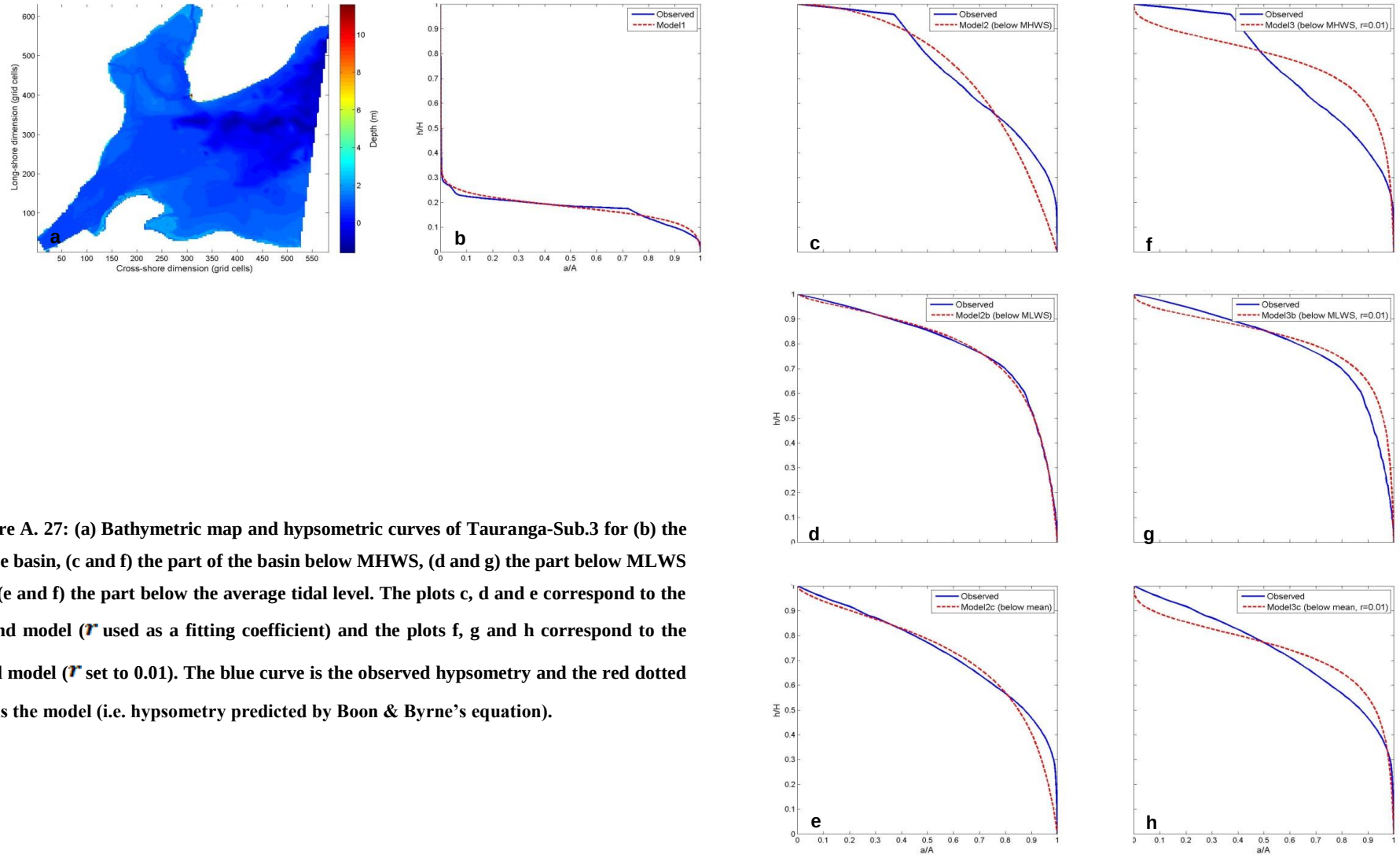

Figure A. 27: (a) Bathymetric map and hypsometric curves of Tauranga-Sub.3 for (b) the whole basin, (c and f) the part of the basin below MHWS, (d and g) the part below MLWS and (e and f) the part below the average tidal level. The plots c, d and e correspond to the second model (r used as a fitting coefficient) and the plots f, g and h correspond to the third model (r set to 0.01). The blue curve is the observed hypsometry and the red dotted line is the model (i.e. hypsometry predicted by Boon & Byrne's equation).

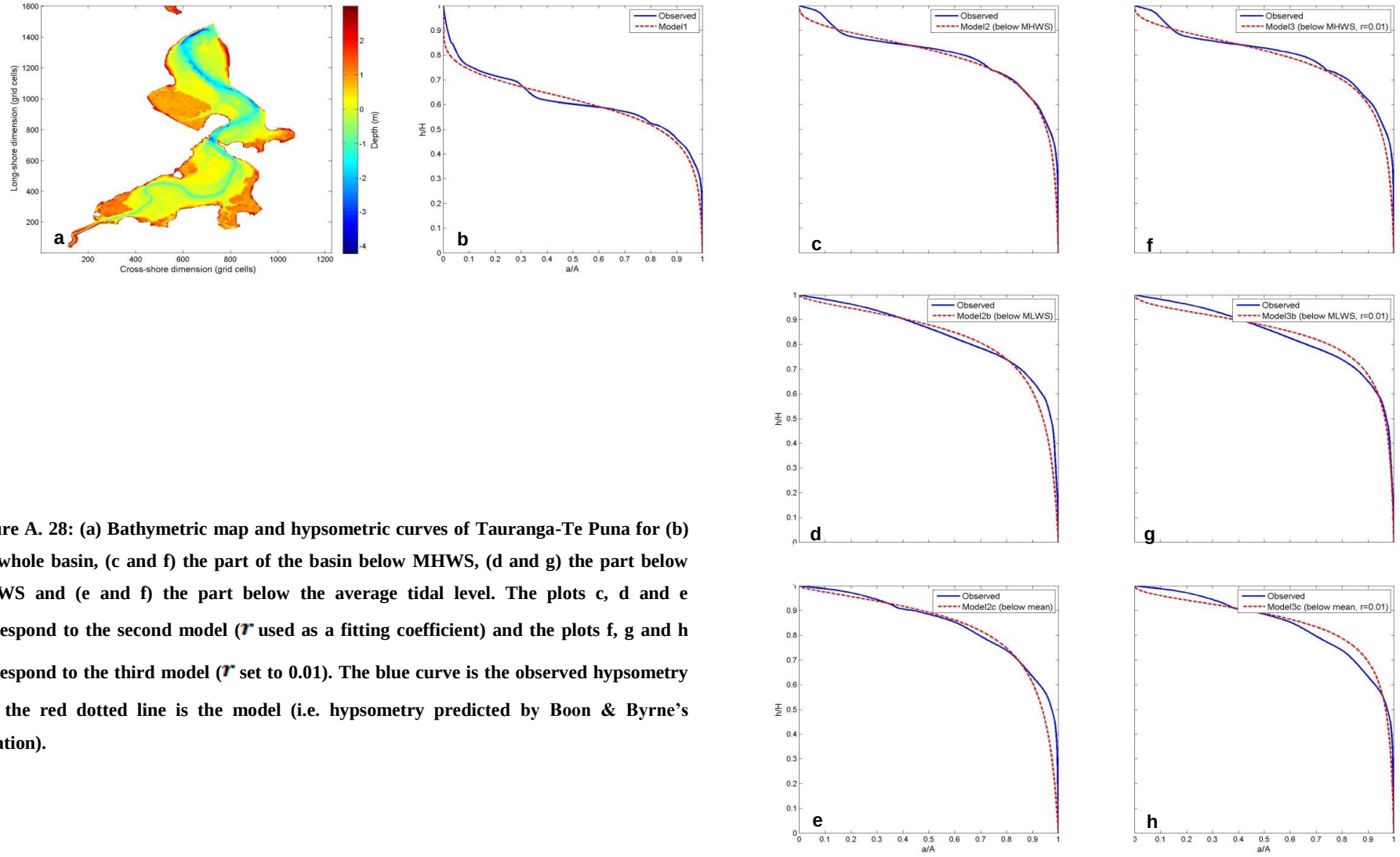

Figure A. 28: (a) Bathymetric map and hypsometric curves of Tauranga-Te Puna for (b) the whole basin, (c and f) the part of the basin below MHWS, (d and g) the part below MLWS and (e and f) the part below the average tidal level. The plots c, d and e correspond to the second model (r^* used as a fitting coefficient) and the plots f, g and h correspond to the third model (r^* set to 0.01). The blue curve is the observed hypsometry and the red dotted line is the model (i.e. hypsometry predicted by Boon & Byrne's equation).

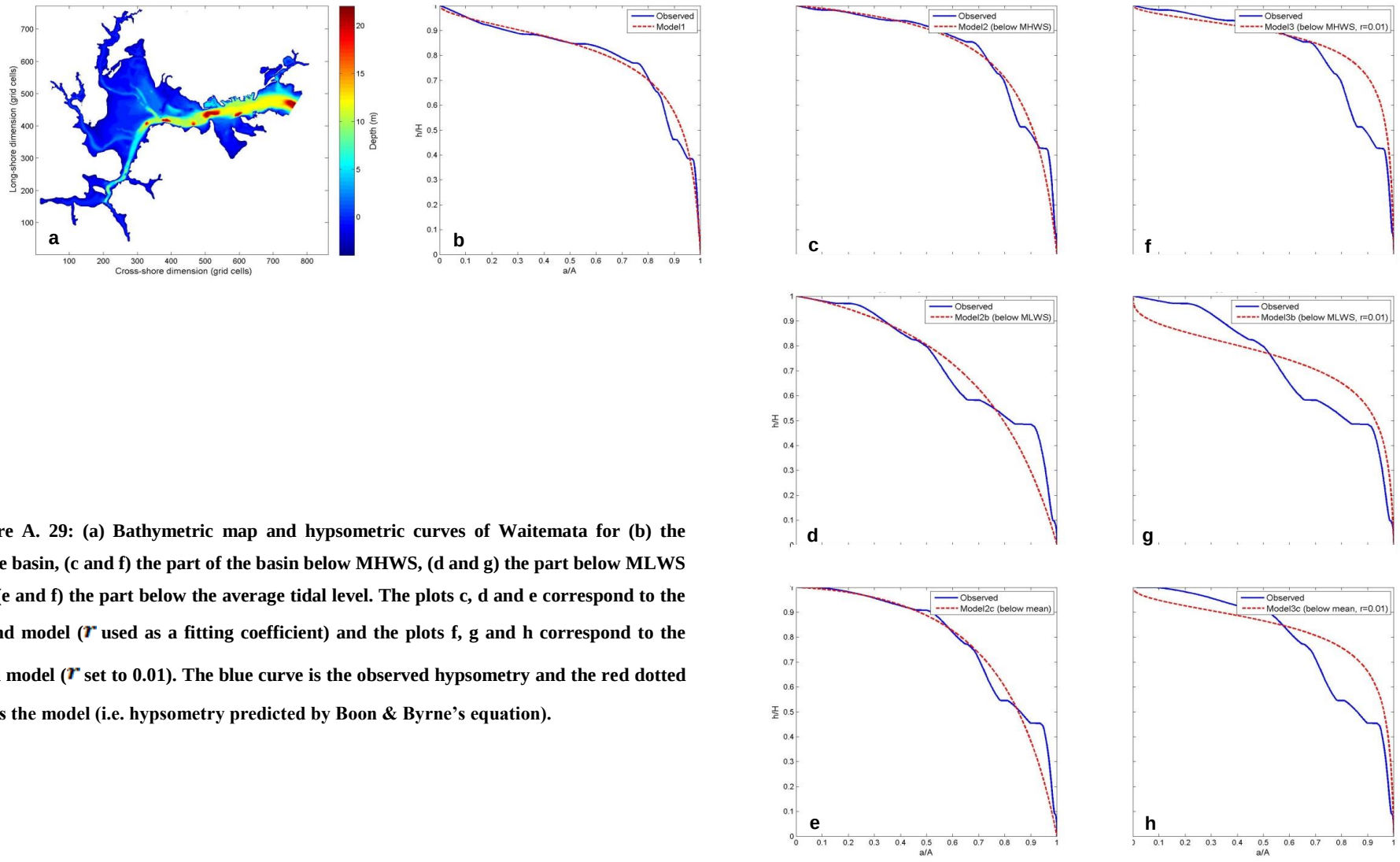

Figure A. 29: (a) Bathymetric map and hypsometric curves of Waitemata for (b) the whole basin, (c and f) the part of the basin below MHWS, (d and g) the part below MLWS and (e and f) the part below the average tidal level. The plots c, d and e correspond to the second model (r used as a fitting coefficient) and the plots f, g and h correspond to the third model (r set to 0.01). The blue curve is the observed hypsometry and the red dotted line is the model (i.e. hypsometry predicted by Boon & Byrne's equation).

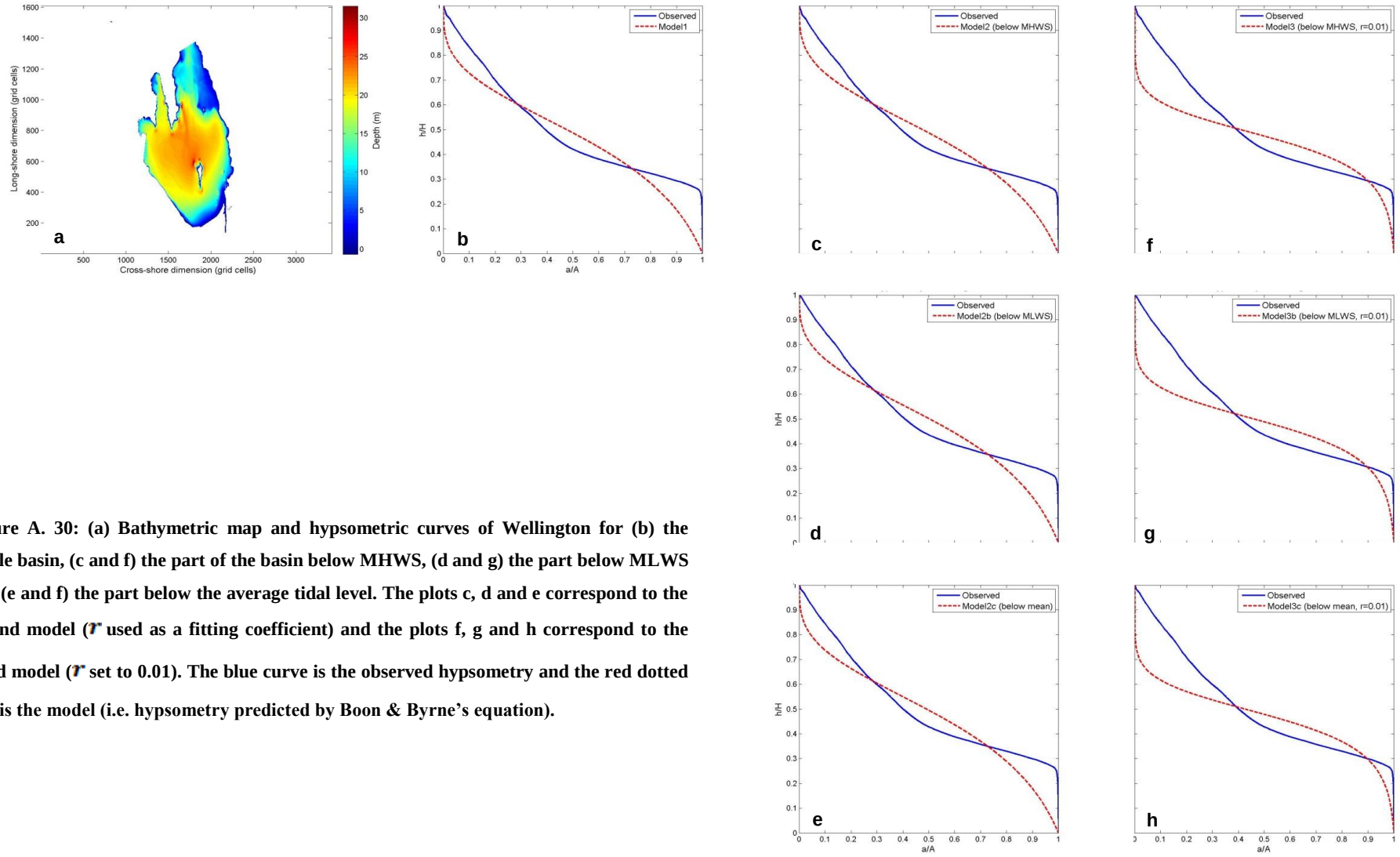

Figure A. 30: (a) Bathymetric map and hypsometric curves of Wellington for (b) the whole basin, (c and f) the part of the basin below MHWS, (d and g) the part below MLWS and (e and f) the part below the average tidal level. The plots c, d and e correspond to the second model (r used as a fitting coefficient) and the plots f, g and h correspond to the third model (r set to 0.01). The blue curve is the observed hypsometry and the red dotted line is the model (i.e. hypsometry predicted by Boon & Byrne's equation).

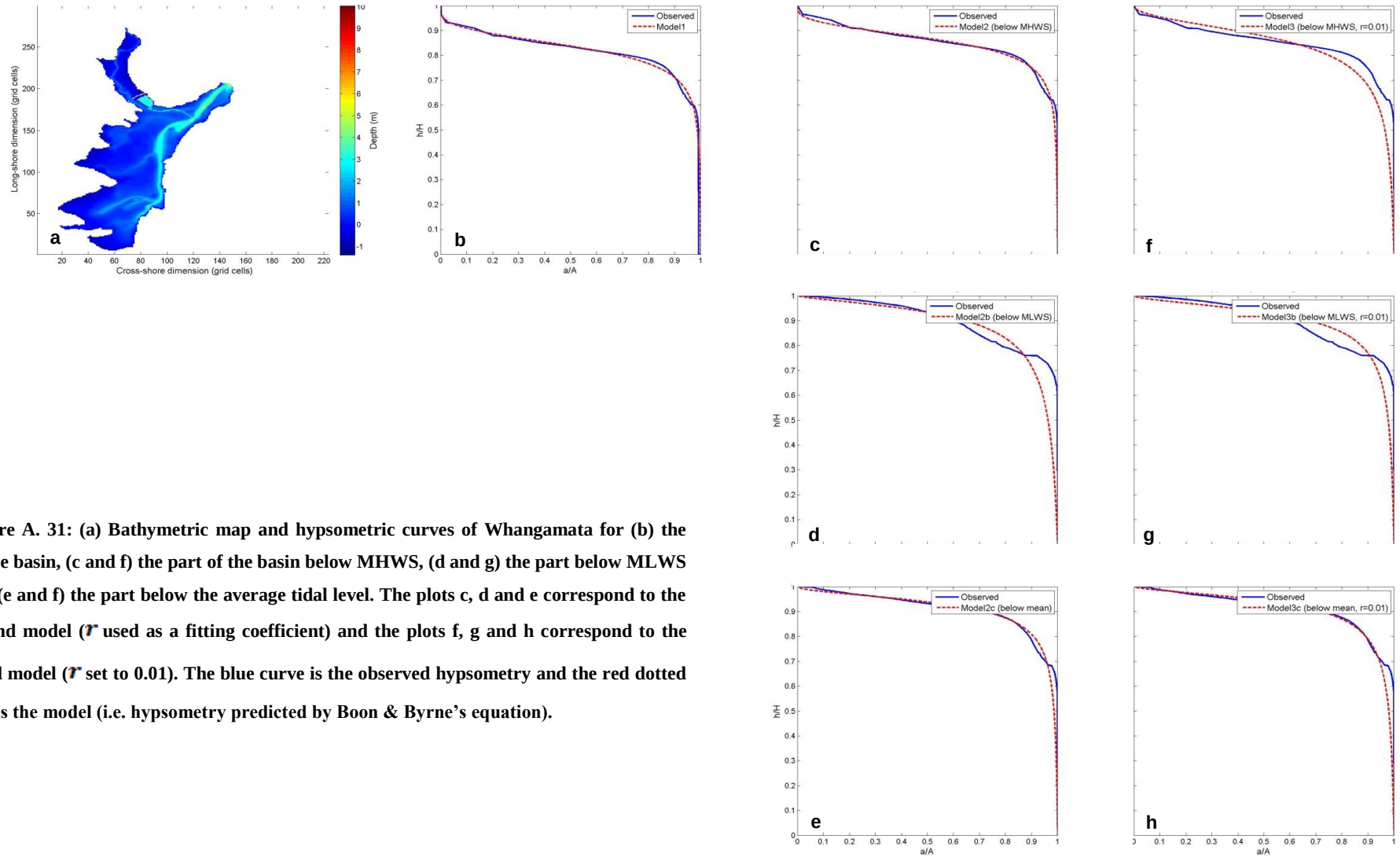

Figure A. 31: (a) Bathymetric map and hypsometric curves of Whangamata for (b) the whole basin, (c and f) the part of the basin below MHWS, (d and g) the part below MLWS and (e and f) the part below the average tidal level. The plots c, d and e correspond to the second model (r used as a fitting coefficient) and the plots f, g and h correspond to the third model (r set to 0.01). The blue curve is the observed hypsometry and the red dotted line is the model (i.e. hypsometry predicted by Boon & Byrne's equation).

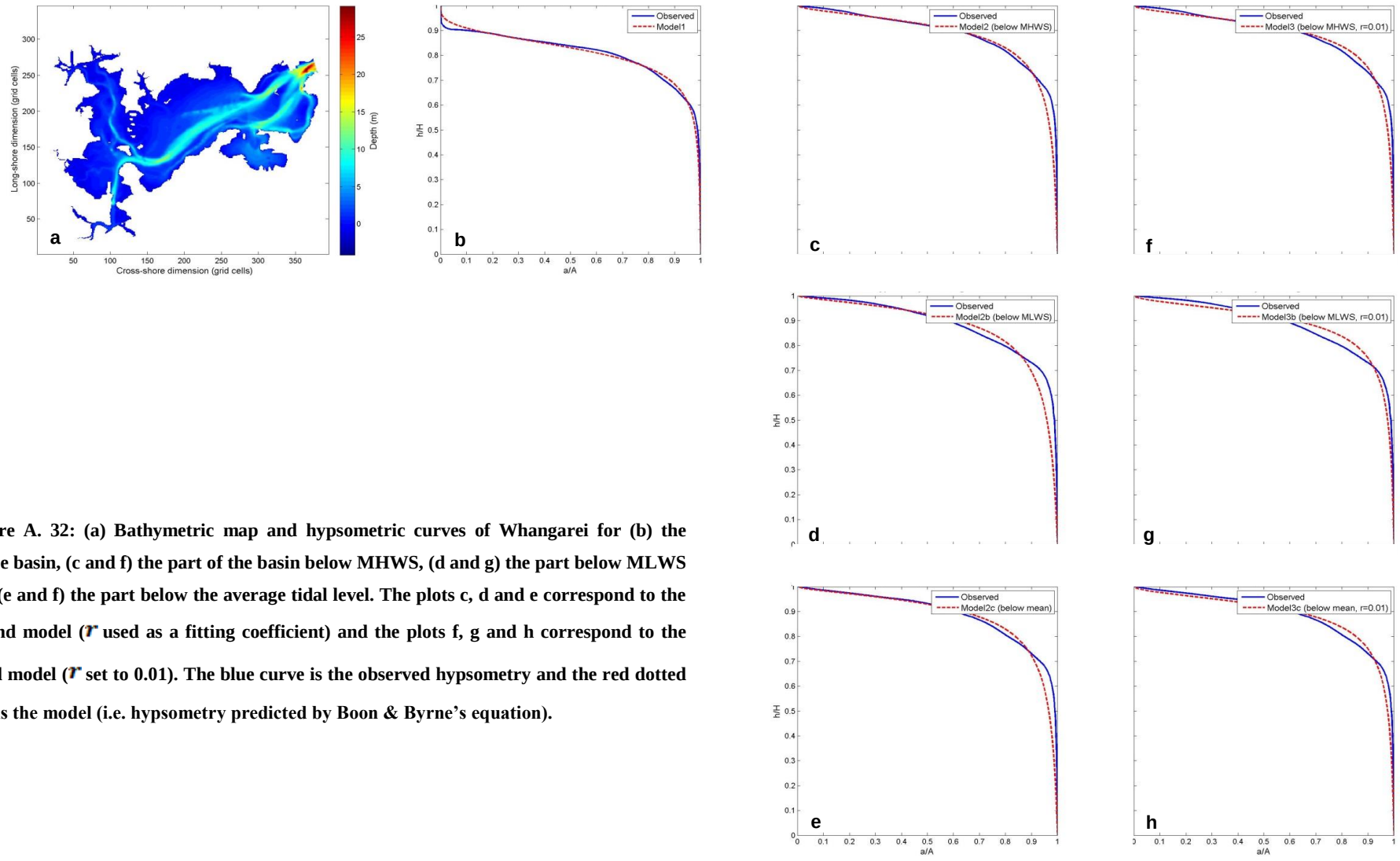

Figure A. 32: (a) Bathymetric map and hypsometric curves of Whangarei for (b) the whole basin, (c and f) the part of the basin below MHWS, (d and g) the part below MLWS and (e and f) the part below the average tidal level. The plots c, d and e correspond to the second model (r used as a fitting coefficient) and the plots f, g and h correspond to the third model (r set to 0.01). The blue curve is the observed hypsometry and the red dotted line is the model (i.e. hypsometry predicted by Boon & Byrne's equation).

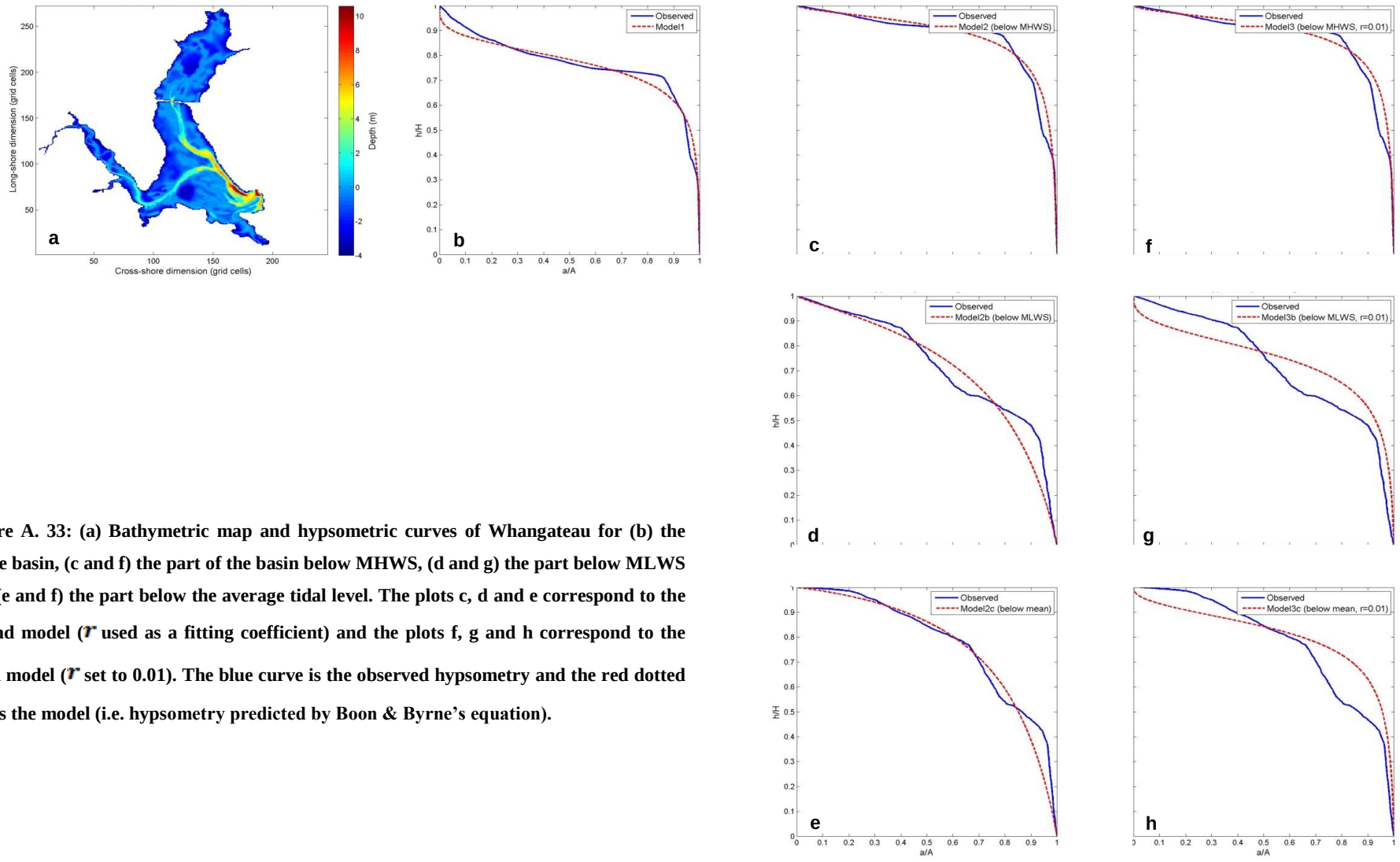

Figure A. 33: (a) Bathymetric map and hypsometric curves of Whangateau for (b) the whole basin, (c and f) the part of the basin below MHWS, (d and g) the part below MLWS and (e and f) the part below the average tidal level. The plots c, d and e correspond to the second model (r used as a fitting coefficient) and the plots f, g and h correspond to the third model (r set to 0.01). The blue curve is the observed hypsometry and the red dotted line is the model (i.e. hypsometry predicted by Boon & Byrne's equation).

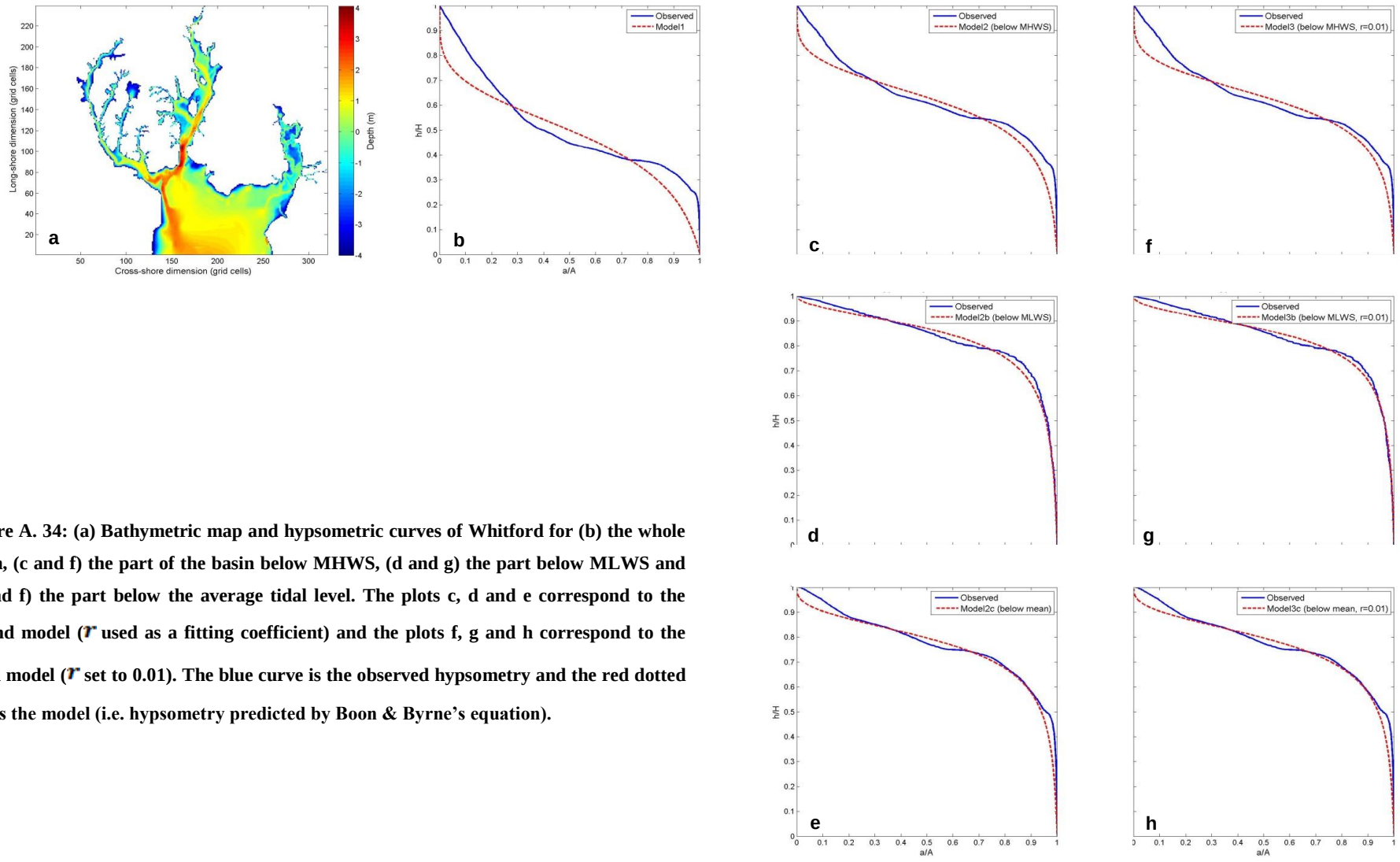

Figure A. 34: (a) Bathymetric map and hypsometric curves of Whitford for (b) the whole basin, (c and f) the part of the basin below MHWS, (d and g) the part below MLWS and (e and f) the part below the average tidal level. The plots c, d and e correspond to the second model (r used as a fitting coefficient) and the plots f, g and h correspond to the third model (r set to 0.01). The blue curve is the observed hypsometry and the red dotted line is the model (i.e. hypsometry predicted by Boon & Byrne's equation).

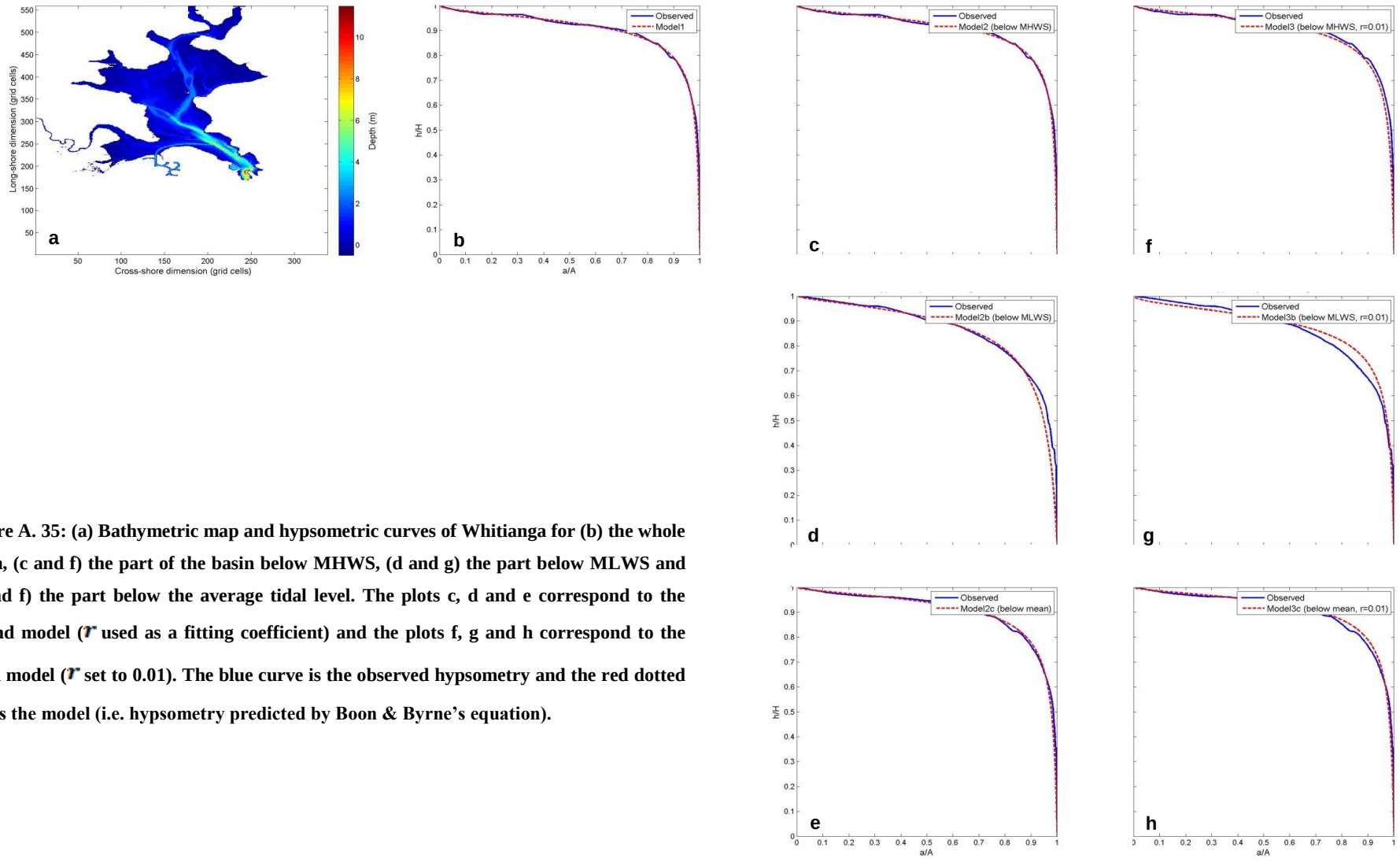

Figure A. 35: (a) Bathymetric map and hypsometric curves of Whitianga for (b) the whole basin, (c and f) the part of the basin below MHWS, (d and g) the part below MLWS and (e and f) the part below the average tidal level. The plots c, d and e correspond to the second model (r used as a fitting coefficient) and the plots f, g and h correspond to the third model (r set to 0.01). The blue curve is the observed hypsometry and the red dotted line is the model (i.e. hypsometry predicted by Boon & Byrne's equation).

Appendix B

Water levels for each study estuary and sub-estuary

The water levels have been obtained from LINZ's website (Land Information New Zealand (LINZ), 2015). The tidal terms are illustrated in Figure B.1 and the tidal levels are given in Table B.1. They correspond to predictions of the height of high and low waters occurring during a spring (MHWS and MLWS respectively) and during a neap (MHWN and MLWN) tide. The values given by LINZ correspond to heights relative to chart datum (CD) and have been converted to heights relative to mean sea level (MSL; Figure B.1). This was done by subtracting the height of MSL relative to CD to the tidal levels relative to CD. Both heights (relative to CD and relative to MSL) are given in Table B.1. The water levels at Whangamata and Whitford were not available on the LINZ website and were therefore obtained from NIWA's predictions available online (National Institute of Water and Atmospheric Research (NIWA), 2015).

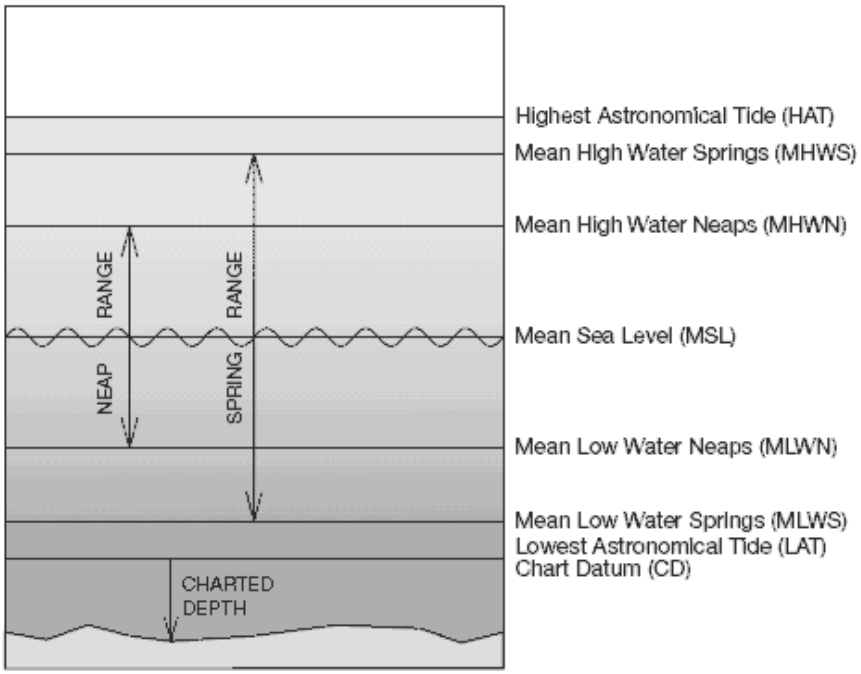

Figure B. 2: Definition of tidal terms (Land Information New Zealand (LINZ), 2015)

Table B. 1: Tidal levels predicted by LINZ at the study estuaries and sub-estuaries.

Study site		Relative to Chart Datum (m)					Relative to MSL (m)		
Site	**Sub-basins**	**MHWS**	**MHWN**	**MLWS**	**MLWN**	**MSL**	**MHWS**	**MLWS**	**Mean tidal level**
Avon	-	2.4	1.9	0.2	0.6	1.3	1.1	-1.1	0
Bay of Islands	-	2.4	2.0	0.3	0.8	1.4	1.0	-1.1	-0.05
	Sub. 1	2.4	2.2	0.6	0.8	1.5	0.9	-0.9	0
	Sub. 2	2.5	2.1	0.4	0.8	1.4	1.1	-1	0.05
Bluff	-	2.8	2.4	0.5	1.0	1.74	1.06	-1.24	-0.09
Firth of Thames	-	4.0	3.1	0.3	1.2	2.2	1.8	-1.9	-0.05
Kaipara	-	3.2	2.7	0.3	0.8	1.7	1.5	-1.4	0.05
	Sub. 1	3.8	3.1	0.1	0.8	2.0	1.8	-1.9	-0.05
Lyttelton		2.5	2.0	0.2	0.6	1.41	1.09	-1.21	-0.06
Mahurangi	-	2.7	2.3	0.3	0.8	1.5	1.2	-1.2	0
Maketu	-	2.0	1.7	0.5	0.7	1.2	0.8	-0.7	0.05
Manukau	-	3.2	2.6	0.3	0.9	1.8	1.4	-1.5	-0.05
	Sub. 1	3.2	2.6	0.3	0.9	1.8	1.4	-1.5	-0.05
	Pahurehure	3.9	3.2	0.4	1.1	2.1	1.8	-1.7	0.05
	Sub. 3	4.2	3.4	0.4	1.3	2.42	1.78	-2.02	-0.12
Matakana	-	2.7	2.3	0.3	0.8	1.5	1.2	-1.2	0
Okura	-	3.0	2.5	0.2	0.8	1.7	1.3	-1.5	-0.1
	Sub. 1	3.0	2.5	0.2	0.8	1.7	1.3	-1.5	-0.1
Otago	-	2.0	1.7	0.3	0.5	1.1	0.9	-0.8	0.05
Raglan	-	3.3	2.6	0.1	0.9	1.8	1.5	-1.7	-0.1
	Waingaro	3.3	2.6	0.1	0.9	1.8	1.5	-1.7	-0.1
	Waitetuna	3.3	2.6	0.1	0.9	1.8	1.5	-1.7	-0.1
Tairua	-	1.9	1.6	0.1	0.4	1.0	0.9	-0.9	0
Tauranga	-	1.9	1.6	0.1	0.4	1.08	0.82	-0.98	-0.08
	Sub. 1	1.9	1.6	0.1	0.4	1.08	0.82	-0.98	-0.08
	Waikareao	1.9	1.6	0.1	0.4	1.08	0.82	-0.98	-0.08
	Sub.3	1.9	1.6	0.1	0.4	1.08	0.82	-0.98	-0.08
	Te Puna	1.9	1.6	0.0	0.3	1.0	0.9	-0.9	0
Waitemata	-	3.2	2.7	0.4	0.9	1.8	1.4	-1.4	0
Wellington	-	1.8	1.4	0.4	0.7	1.1	0.7	-0.7	0
Whangamata	-						1.0*	-1.0*	0*
Whangarei	-	2.7	2.3	0.4	0.8	1.58	1.12	-1.18	-0.03
Whangateau	-	2.7	2.3	0.2	0.6	1.5	1.2	-1.3	-0.05
Whitford	-						1.5*	-1.5*	0*
Whitianga	-	2.1	1.8	0.3	0.6	1.2	0.9	-0.9	0

*Tidal levels estimated from NIWA(National Institute of Water and Atmospheric Research (NIWA), 2015)

Appendix C

Wind data of the study estuaries and sub-estuaries

The wind data are from NIWA's database CliFlo which can be accessed online (National Institute of Water and Atmospheric Research (NIWA), n.d.). The station number and the years when the observations started and when they ended are given in Table C.1. When available the hourly observations were downloaded; otherwise observations with a three hour frequency were selected. Therefore for the sake of consistency the wind speed and direction were averaged for every day at each station before plotting the wind roses. The wind roses of each site were plotted with MATLAB and are given in Figures C.1 to C.4.

Table C. 1: Station ID where the wind data come from for each site along with the year when the observations started and the year when they ended. The observations are available online on the CliFlo website.

Site		Station agent number	Start time	End time
Estuary	**Sub-estuary**			
Avon	-	37654	2009	2011
Bay of Islands	-	1196	1983	1996
	Sub. 1	1196	1983	1996
	Sub. 2	1196	1983	1996
Bluff	-	5830	1978	1986
Firth of Thames	-	38619	2010	2015
Kaipara	-	1369	1982	1986
	Sub. 1	1380	1966	1967
Lyttelton	-	4903	1978	1986
Mahurangi	-	1374	1972	1990
Maketu	-	12428	1996	2001
Manukau	-	1500	1978	1984
	Sub. 1	1500	1978	7984
	Pahurehure	1965	1945	1983
	Sub. 3	22719	2002	2006
Matakana	-	1358	1971	1972
Okura	-	1400	1986	1995
	Sub. 1	1400	1986	1995
Otago	-	24851	2003	2008
Raglan	-	2027	1991	1994
	Waingaro	2027	1991	1994
	Waitetuna	2027	1991	1994
Tairua	-	31827	2005	2010
Tauranga	-	1610	1964	2004
	Sub. 1	1614	1989	2003
	Waikaraeo	1611	1970	1991
	Sub. 3	1610	1964	2004
	Te Puna	1610	1964	2004
Waitemata	-	1436	1986	1987
Wellington	-	3446	1980	1988
Whangamata	-	1534	1971	1991
Whangarei	-	1301	1969	1973
Whangateau	-	1358	1971	1972
Whitford	-	22167	2001	2007
Whitianga	-	1520	1990	1998

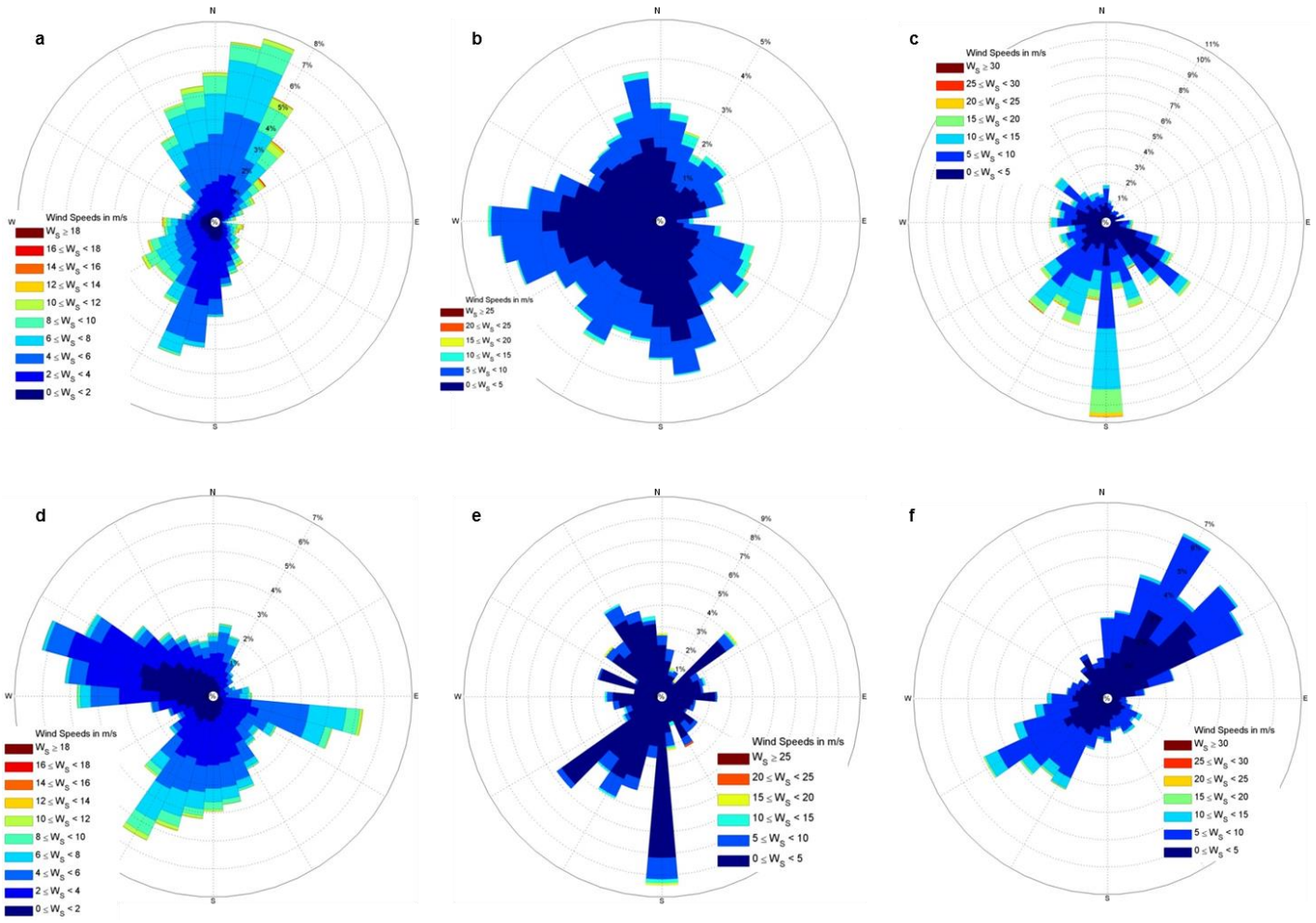

Figure C. 1: Wind rose of a) Avon, b) Bay of Islands, c) Bluff, d) Firth of Thames, e) Kaipara and f) Lyttelton computed from the wind observations available on CliFlo.

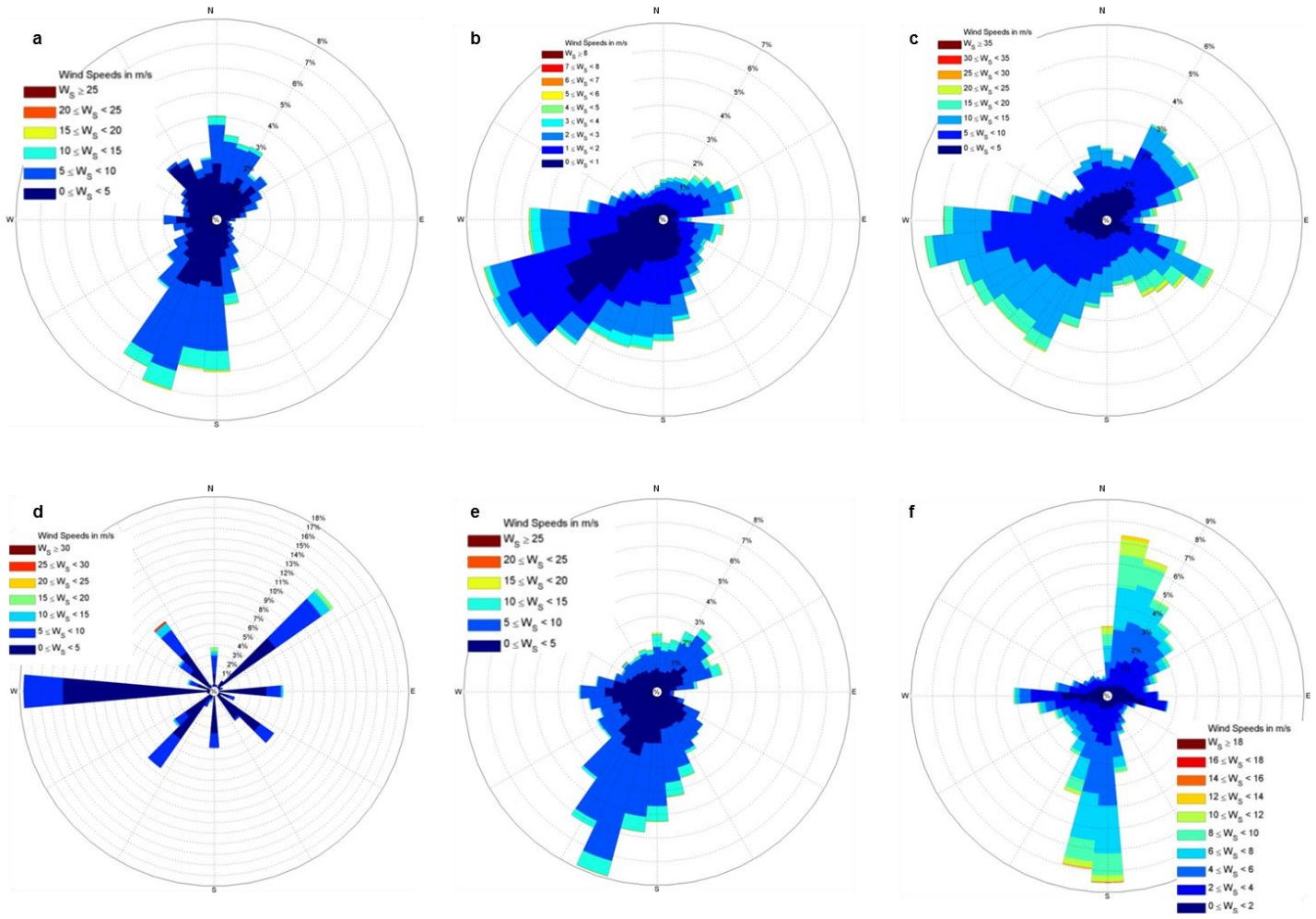

Figure C. 2: Wind roses of a) Mahurangi, b) Maketu, c) Manukau, d) Matakana, e) Okura and f) Otago computed from the wind observations available on CliFlo.

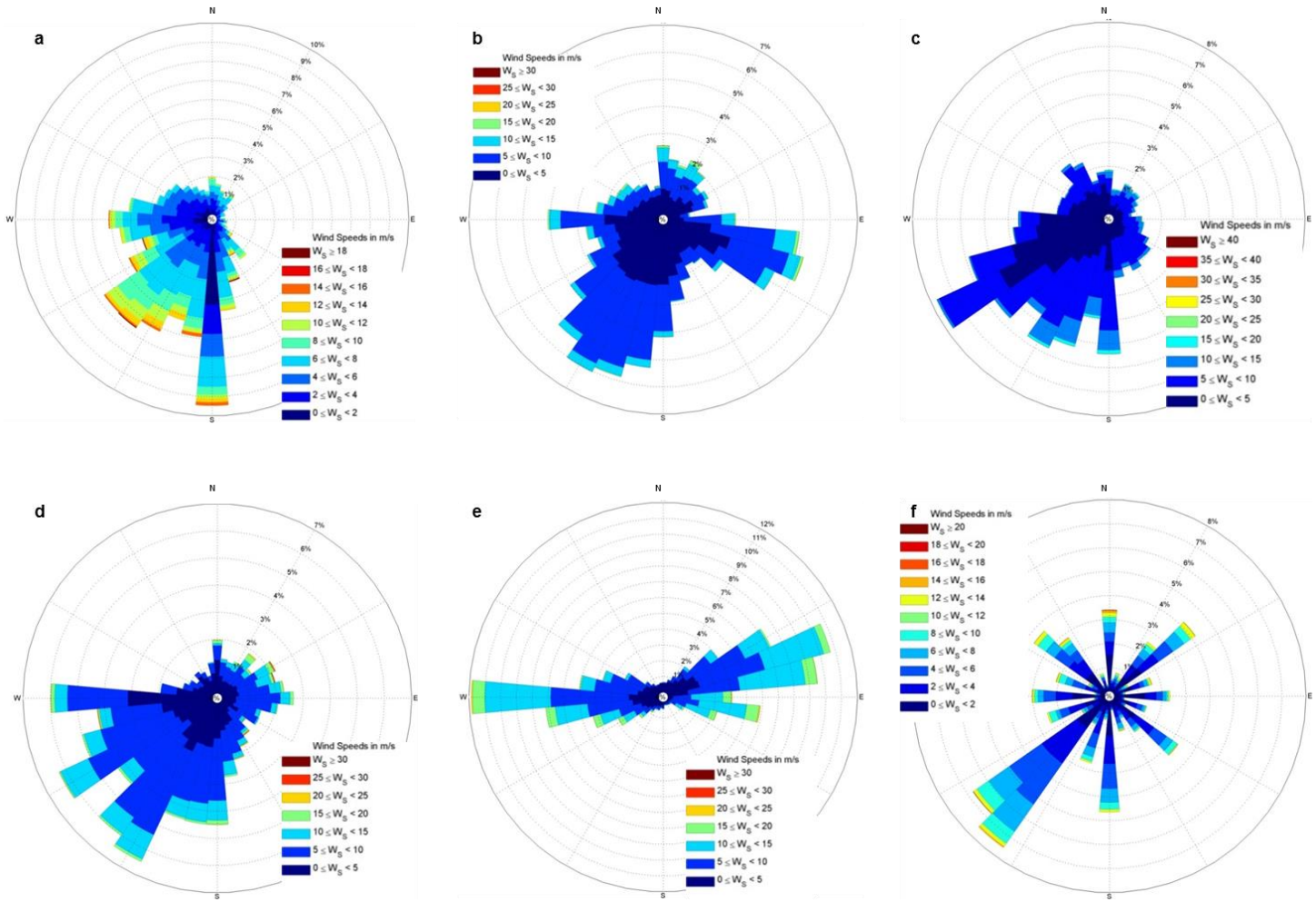

Figure C. 3: Wind roses of a) Raglan, b) Tairua, c) Tauranga, d) Waitemata, e) Wellington and f) Whangamata computed from the wind observations available on CliFlo.

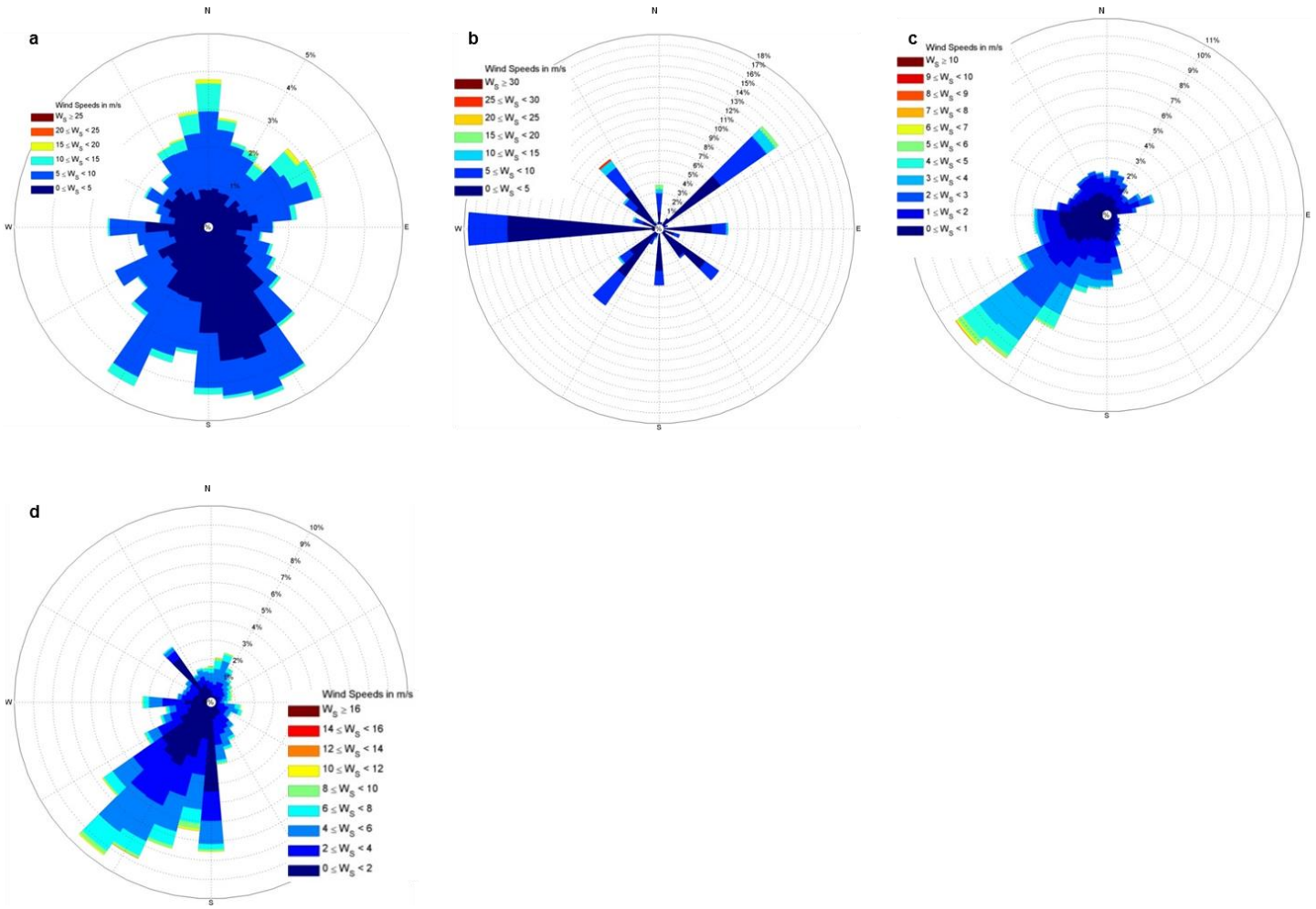

Figure B. 4: Wind roses of a) Whangarei, b) Whangateau, c) Whitford and d) Whitianga computed from the wind observations available on CliFlo.